Acta Pharmaceutica Sinica B 2026;16(8):4898−4977

Chinese Pharmaceutical Association
Institute of Materia Medica, Chinese Academy of Medical Sciences

Acta Pharmaceutica Sinica B

www.elsevier.com/locate/apsb
www.sciencedirect.com

REVIEW

Nanocarrier-based delivery of Pt(IV) compounds for chemoimmunotherapy and theranostics: Advances, challenges, and prospects

Daniil Spector[†], Roman Akasov[†], Vladislav Bykusov, Georgy Karetnikov, Anastasia Zharova, Elena Beloglazkina, Olga Krasnovskaya[†,*]

Chemistry Department, Lomonosov Moscow State University, Moscow 119991, Russia

Received 28 November 2025; received in revised form 4 March 2026; accepted 20 May 2026

KEY WORDS

Cisplatin;
Platinum(IV) prodrug;
Stimuli-responsive activation;
Chemoimmunotherapy;
ICD;
NPs;
Theranositcs drug resistance

Abstract Nanocarrier-based delivery of platinum compounds represents the next generation of platinum-based chemotherapy, which is a first-line treatment for many types of tumors. Despite the significant success of Pt(IV) prodrugs as effective antitumor agents, the therapeutic efficacy of most of the reported prodrugs is limited due to rapid biodegradation in the bloodstream and limited accumulation in the tumor. To overcome these limitations, various types of nanomedicines have been developed as drug delivery systems for Pt(IV) prodrugs, with those demonstrating significantly enhanced antitumor effects due to passive and active tumor targeting, stimulus-responsive drug release, effective synergistic therapy, the ability to induce immunogenic cell death, stimulate native and adaptive immunity, and preventing tumor recurrence. Also, the design of Pt(IV)-based theranostic nanoagents opens up photothermal, fluorescent, and photoacoustic imaging modalities for real-time monitoring of drug delivery and therapeutic response. The ability to harness photocontrolled chemotherapy along with immunotherapy, PDT, and PTT holds immense promise for synergistic anticancer effects. In the present review, we highlighted recent advances in the design of Pt(IV)-based NPs reported in 2022−2025 with the focus on the further development of this fast-growing research area.

*Corresponding author.
E-mail address: Krasnovskayao@gmail.com (Olga Krasnovskaya).
[†]These authors made equal contributions to this work.

Peer review under the responsibility of Chinese Pharmaceutical Association and Institute of Materia Medica, Chinese Academy of Medical Sciences.

https://doi.org/10.1016/j.apsb.2026.05.026

1. Introduction

Platinum-based anti-cancer drugs, including cisplatin, carboplatin, and oxaliplatin are clinically approved worldwide and are the first choice for malignant tumor treatment. Cisplatin (*cis*-diamminedichloroplatinum, CDDP) is one of the most widely used and clinically important therapeutic agents worldwide. As the first generation of the platinum anti-cancer drug, CDDP has evident therapeutic effects on many malignant tumors, such as breast, ovarian, testicular, lung, gastric, colorectal, and head and neck cancers[1−5]. Second-generation drug carboplatin possesses improved biosafety compared to CDDP due to its a lower hydration rate due to the presence of bidentate cyclobutanedicarboxylic acid ligand[6]. Third generation of platinum clinical drug is represented by oxaliplatin (OXA) with less toxicity and better tolerability, which is also capable of immune response stimulation[7−9]. In addition, other Pt(II)-based drugs such as nedaplatin, heptaplatin, lobaplatin, miriplatin and dicycloplatin have been approved for use in Japan (1995), Korea (1999), China (2003), Japan (2009) and China (2012) (Fig. 1)[10]. However, Pt(II)-based drugs are commonly associated with high toxicity and resistance, which forces increases in chemotherapy doses and significantly worsens the quality of life of patients[11].

Given the limitations of Pt(II) complexes in cancer therapy, the development of alternative platinum-based anticancer therapeutics is currently a great challenge. Among these, Pt(IV) prodrugs are one of the most promising classes of Pt-based compounds for further development in preclinical and clinical settings. Traditionally, Pt(IV) prodrugs are oxidized forms of clinically used Pt(II) drugs, into the axial position of which an easily modifiable hydroxyl group is introduced. Subsequently, one or two axial hydroxyl groups are conjugated with pharmacophores that can enhance, complement, or target the action of platinum therapy[12−15]. Due to the ease of chemical modification of axial hydroxyl groups, the desired biological action of the resulting Pt(IV) prodrugs become easily achievable[10,16]. Thus, Pt(IV) prodrugs can exert several anticancer effects through the simultaneous release of Pt(II) drug and bioactive ligands when they are exposed to internal or external reducing agents after entering cancer cells. Pt(IV) prodrugs capable of inducing immunogenic cell death (ICD) in addition to chemotherapeutic action has been an extremely attractive topic for research in the last few years[17−20]. Also, stimuli-responsive Pt(IV) prodrugs, which are stable and non-toxic until influenced by an external stimuli, such as light, ultrasound, or X-ray is of great interest[14,21,22]. Thus, in recent decades, significant efforts have been directed toward developing Pt(IV) complexes as next-generation platinum-based anticancer agents[15,16,23−27].

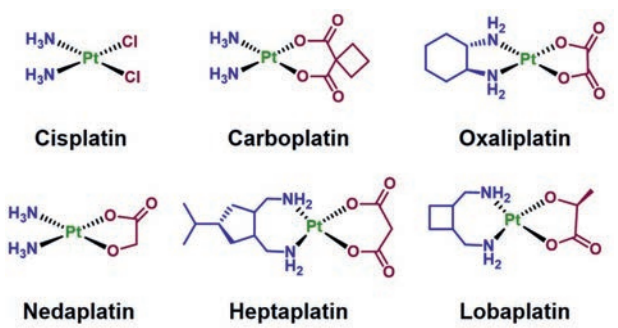

Figure 1 Pt(II) chemotherapeutic drugs used in clinical practice.

Despite the obvious advantages of Pt(IV) prodrugs over clinically used Pt(II) agents, several critical limitations stand in the way of their clinical application. These critical drawbacks include poor drug solubility and rapid biodegradation in the bloodstream, which results in high toxicity of prodrugs and the fact that their therapeutic efficacy does not exceed that of the parent Pt(II) drug[16,28,29]. The use of nanoformulations of Pt(IV) prodrugs can resolve both issues, increasing the water stability and biocompatibility of prodrugs. Also, nanoscale drug delivery enables a combination of Pt(IV) prodrug with another anticancer drug or imaging agents in one nanoplatform, thus allowing the design of prodrugs with combined synergistic action, as well as theranostic agents. The use of nanoformulations of Pt(IV) prodrugs allows the design of theranostic agents for fluorescent, photothermal, and ultrasound visualization of tumors, in addition to highly effective antitumor therapy[30,31]. Also, the design of nanoformulations instead of low-molecular Pt(IV) prodrugs allows more opportunities to control the release of the active drug at the tumor site. Stimuli-sensitive release of several drugs from the nanoformulation under the influence of such factors as intracellular acidic pH, light, or the presence of reducing agents allows localizing the site of drug release and minimizing the impact on healthy tissues (Fig. 2)[32−34].

To date, different types of nanomedicines have been developed as drug delivery systems for Pt(IV) prodrugs, including those that demonstrate significant antitumor effects, far exceeding those of the low-molecular Pt(IV) prodrug and the parent Pt(II) drug, due to passive and active targeting, stimulus-responsive drug release, effective synergistic therapy, and also an ability to induce ICD[30,35,36]. The escalating volume of high-impact publications dedicated to the design of Pt(IV)-based therapeutic and theranostic nanoagents prompted us to sum up this comprehensive review.

Since nanotherapeutics based on Pt(IV) prodrugs is an extensively developing field of medicinal chemistry, the advances in this area of research are regularly reviewed by leading experts. In 2023, Wang et al.[37] published a review on stimuli-responsive nanoparticles (NPs) as delivery systems for Pt(IV) prodrugs, with the focus on the various approaches to the nanoparticle design and the mechanisms to controllably release Pt-based chemotherapeutics in tumors. In 2024, Zhou et al.[36] published a comprehensive review on the nanoscale delivery of Pt(IV) prodrugs from 2020 to 2024 and described in details multiple methods to encapsulate a Pt(IV) prodrug into a nanosized vehicle, from carbon nanotubes to lipid micelles. While these reviews provide a thorough overview of the advances in the design of Pt-based nanodrugs, they focus primarily on the various approaches to the assembly of nanoscale Pt-based drugs. Thus, the goal of our review is to provide a detailed overview of the recent advances (2022−2025) in the design of Pt(IV) nanodrugs based on their mechanism of antitumor activity, the ability to overcome the resistance of tumors to CDDP or stimulate antitumor immune response. In Section 2, we summarize general information about Pt(IV) prodrugs, necessary for a basic understanding of their chemical and biological properties. In Section 3, we summarize general information about NPs, namely their basic physicochemical properties, barriers to their clinical application, and the main synthetic approaches for obtaining Pt(IV) prodrug nanoformulations. In Section 4, we discuss the biological aspects of developing Pt(IV)-based nanoprodrugs, highlighting five key interrelated avenues that could significantly enhance the therapeutic effect of Pt(IV)-based NPs compared to clinically used Pt(II) drugs.

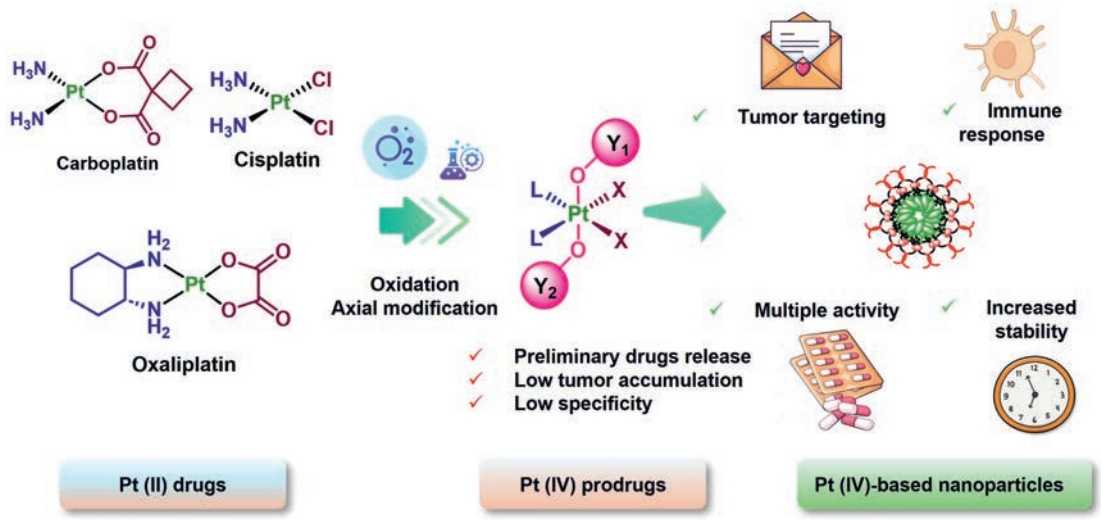

Figure 2 Synthesis pathway of Pt(IV) prodrugs and their assembly into Pt(IV)-based nanoparticles; comparison of advantages of Pt(IV) prodrugs and Pt(IV)-based NPs properties.

We honestly believe that this review is useful not only for the development of Pt(IV) prodrugs and their nanoformulations, but also for researchers interested in medicinal chemistry and the development of effective platinum-containing drugs for chemotherapy, immunotherapy and theranostic.

2. Pt(IV) prodrugs: Synthesis, reduction and nanocarrier-based delivery

2.1. Pt(IV) prodrugs: From the laboratory to the clinic

Despite the apparent simplicity of synthesis and the potential for easy tuning of their therapeutic efficacy, only a few Pt(IV) prodrugs have reached clinical trials, including ormaplatin, iproplatin, satraplatin, and LA-12 (Fig. 3, Table 1). Ormaplatin, also known as Tetraplatin [tetrachlorido(1,2-diaminocyclohexane)platinum(IV)], is one of the first Pt(IV) prodrugs tested in clinical trials. Due to the high reactivity of chloride ligands, ormaplatin is rapidly reduced to dicholoro-1,2-(diaminocyclohexane)platinum (II). Accordingly, clinical trials of ormaplatin were terminated in Phase I, and Phase II trials were not initiated due to its pronounced neurotoxicity which is a consequence of it's extremely rapid reduction rate[38]. Iproplatin (*cis*-dichloro-trans-dihydroxy-bis-isopropylamine platinum IV), with two chlorine axial ligands, showed acceptable toxicity in Phase I and II clinical trials. However, the lack of significant superiority in therapeutic efficacy compared to CDDP or carboplatin led to the termination of Phase III[39]. Satraplatin (JM216), with two axial acetato groups, demonstrated high stability which made it suitable for oral administration. The combination of satraplatin and prednisone reached Phase III clinical trials in castration-resistant prostate cancer, but due to the lack of an overall survival benefit, further Phase III studies were terminated[40,41]. A structurally similar Pt(IV) prodrug LA-12 with lipophilic adamantylamine moiety was developed; LA-12 participated in phase I clinical trials, but no additional information has been reported since (Fig. 3)[42–44].

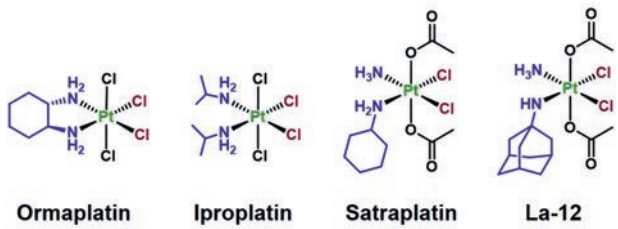

Figure 3 Pt(IV) prodrugs participated in clinical trials.

Thus, to successfully complete clinical trials, Pt(IV) prodrugs should not only overcome the shortcomings of clinically used Pt(II) complexes but also demonstrate significantly improved therapeutic efficacy compared to them. To meet these criteria, Pt(IV) prodrug should be sufficiently stable, accumulate well in tumor cells, exhibit at least some selectivity for tumor tissue and possess an additional therapeutic effect in addition to Pt-induced DNA damage.

2.2. Pt(IV) prodrugs: Synthesis and chemical properties

According to the theory of hard and soft acids and bases, Pt(II) center is a soft acid which prefer to bind with soft bases. d8 Pt(II) complexes have a square planar geometry, and ligand substitution reactions occur through the formation of pentacoordinate intermediate (Fig. 4)[45]. Therefore, Pt(II) complexes possess reduced stability, and their leaving group can be easily displaced by nucleophiles. For example, CDDP readily exchanges chloride anions for water, or other solvent, and forms covalent adducts with DNA or sulfur-containing biomolecules; this is one of the main reasons for the deactivation of Pt(II) drugs in the blood and the development of drug resistance[10]. The ligand exchange reaction between Pt(II) compounds and nucleophiles occurs *via* coordination of the nucleophile to the soft center of Pt(II) *via* an empty p_z orbital, forming a square-pyramidal transition state. Since the hard d_6 center of Pt(IV) does not have an empty p_z orbital, attack by nucleophiles on the Pt(IV) center is hindered, making Pt(IV) prodrugs more stable compared to Pt(II) drugs.

2.3. Oxidation of Pt(II) coordination compounds

The most common synthetic approach to the preparation of Pt(IV) prodrugs is two-electron oxidation of a Pt(II) drug *via* oxidizing

Table 1 Multi-action Pt(IV)-based nanoparticles (NPs), summarized in this review.

Ref.	NPS	Pt(IV) prodrug	Synthesis of NPs Size of nanoparticles (NPs), drug loading (DL, %), and encapsulation efficiency (EE, %) Drug release mode	Mechanism of action	Tumor model, type, *in vivo* antitumor efficacy
	Pt(IV)−based NPs to overcome multidrug resistance				
	Regulating cholesterol metabolism				
202	1(a−d)-NP FSPNPs (5NPs, 6NPs, 7NPs, 8NPs)	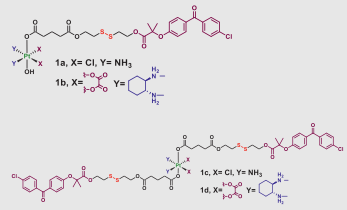	Self-assembly of amphiphilic prodrug CMC: no data ζ ~20 mV 1a = 168.18 ± 0.49 nm 1b = 185.96 ± 3.31 nm 1c = 174.42 ± 2.83 nm 1d = 186.71 ± 3.23 nm PDI: ~0.22 Rod structure Drug release: pH, GSH	DNA damage: γ-H2AX↑ Mitochondria damage: ROS↑ Apoptosis: Bax↑, Bcl2↓, p53↑ Ferroptosis: GPX4 ↓ GSH↓	Subcutaneous A2780 ovarian tumor (3.5 mg Pt/kg): TIR: 1a-NP ~78.92%, Cisplatin ~9.24%
	Endoplasmic reticulum stress induction				
211	2-NP-m (PPD NPs) 2-NP (IPD NPs)	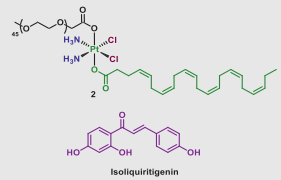	2-NP-m: Self-assembly of Pt(IV) prodrug 179.03 ± 4.22 nm, PDI: 0.14 ± 0.02 CMC: no data 2-NP Self-assembly of Pt(IV) prodrug with isoliquiritigenin, 10:1 CMC: no data EE = 33.1% DL = 3 % d = 155.47 ± 0.46 nm, PDI = 0.19 ± 0.04 ζ = −3.86 mV Drug release: GSH, ROS	DNA damage: γ-H2AX↑ Apoptosis: Bax↑, Bcl2↓, caspase-12↑ ER stress: GRP78↑, CHOP↑	Subcutaneous patient-derived xenograft ovarian tumor (2.5 mg Pt/kg): Tumor volume, mm^3: PBS ~1450, Cisplatin ~550 2-NP-m ~550 2-NP ~200
	Cyclin-dependent kinases 4 and inhibition				
216	3-NP (BioPt^{IV}@Rib)	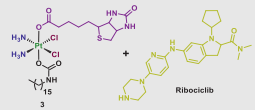	Self-assembly of amphiphilic prodrug with ribociclib 4:1 CMC = 2.75 μg/mL LE = 17% (Rib), 29% (Cis) d ~73 nm ζ = 8.18 mV PDI = 0.12 Drug release: GSH	Apoptosis	Subcutaneous MB49 bladder tumor (3.5 mg Pt/kg): Relative tumor volume, V/V_0: Saline ~10 Cisplatin ~10 3 ~14 3-NP ~5
	HO-1 inhibition				
220	4-NP (15-NPs)	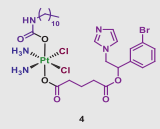	Self-assembly of amphiphilic Pt(IV) prodrug 4 CMC: no data d = 97.61 nm Zeta n.d.	DNA damage: γ-H2AX↑. Mitochondrial damage: MMP↓, ROS↑. Metastasis: migration&invasion↓,	Subcutaneous Hepa1−6 syngeneic hepatoma tumor (2.5 mg Pt/kg): TIR: Cisplatin: 43.21%,

(*continued on next page*)

Table 1 (*continued*)

Ref.	NPS	Pt(IV) prodrug	Synthesis of NPs Size of nanoparticles (NPs), drug loading (DL, %), and encapsulation efficiency (EE, %) Drug release mode	Mechanism of action	Tumor model, type, *in vivo* antitumor efficacy
			PDI = 0.084 Drug release: GSH	Apoptosis: p53↑, Bax↑, Bcl2↓. HO1 pathway: HO-1↓, HIF1α↓ VEGFA↓, p38↓ MMP9↓ MDR: P-gp↓, p-ATM↓, p-ATR↓, GST-π↓ Antitumor immunity: T cell proliferation *in vitro*↑, macrophage polarization↑ T cells in tumor: $CD4^+$↑, $CD8^+$↑, $CD3^+$↑	4: 58.23%, 4-NP: 65.88%, 4-NP-high-dose (5 mg-Pt/kg): 80.35%
	Pt(IV)-based NPs for tumor microenvironment remodeling Hypoxia overcoming				
233	5-NP-Hb (Hb@$BTOPt^{IV}$) 5-NP (Without hemoglobin) ($BTOPt^{IV}$)	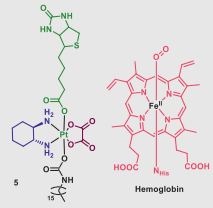	5-NP Self-assembly of amphiphilic prodrug 5. CMC = 2.15 μg/mL d = 86.9 ± 1.4 nm PDI = 0.08 ± 0.03 ζ = +13.23 mV 5-NP-Hb Self-assembly with Hemoglobin, 6:1 DL = 29.58 ± 2.64% EE: no data 133.1 ± 2.7 nm PDI = 0.18 ± 0.06 ζ = 3.82 mV Release: Ascorbic acid	ICD: DAMPs release↑ Cytokines: IFN-γ↑, IL-10↑, TNF-α↑ T cells in tumor: $CD4^+$↑, $CD8^+$↑, $CD3^+$↑ DC maturation ↑ Hypoxia treatment: HIF-1α↓	Subcutaneous 4T1 triple-negative breast tumor (3.5 mg Pt/kg) Tumor inhibition rate: 5-NP-Hb: 78%, 5-NP (Without hemobgobin): 51%, OXA: 16%, OXA + Biotin: 15% An increase in the population of mature DCs: OXA: 3.46%, PBS: 2.60%, 5-NP-Hb: 9.78%, 5-NP (Without hemobgobin): 6.94% Proportion of regulatory T cells at the tumor site: 5-NP-Hb: 12.69%, 5-NP (Without hemobgobin): 15.5%, OXA: 18.82%, OXA + Biotin: 19.25%

	Nitric oxide delivery				
153	6-NP (T-SPNA$_{Pt/NO}$)	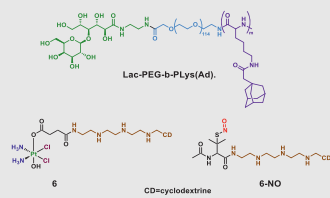	"Guest−Host" supramolecular self-assembly, from 1:1 (6:6-NO) to 1:20 d = 82.6 nm DL, EE: no data PDI = 0.2 Drug release: ascorbic acid (Pt), GSH (NO)	Intracellular ROS: $ONOO^-$↑, Glutathione production: GR↓, GSH↓ DNA damage: Pt-DNA adducts↑. Activity *in vivo*: $ONOO^-$↑, GSH ↓, DNA adducts ↑, γ-H2AX↑ Cisplatin resistance: XPA↓	Subcutaneous LM3 hepatoma tumor, (3 mg Pt/kg): Relative tumor volume, V/V_0 6-NP: 2.9 Cisplatin: 4.6 Orthotopic cisplatin-resistant luc-LM3/CDDP hepatoma tumor (3 mg Pt/kg): Luminescence, p/s/cm^2/sr 6-NP ∼4 Cisplatin ∼20 Subcutaneous patient-derived hepatoma tumor (3 mg Pt/kg): Relative tumor volume, V/V_0 6-NP: 2.2 Cisplatin: 3.8
140	7-NP (EA-Pt@M$_{DBCO}$)	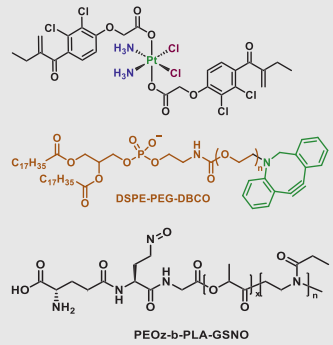	Self-assembly of 7:PEOz-*b*-PLA-GSNO:DSPE-PEG2000-DBCO 1:6:1 *via* film dispersion method EE = 82.40 ± 2.87% DL = 7.92 ± 0.27% d = 122.2 nm PDI: no data ζ = −20 mV Release: pH, GSH	DNA damage: γ-H2AX↑ GSH synthesis: P-gp↓, GST↓, NO release↑ Mitochondria damage: MMP↓	Orthotopic cisplatin-resistant A549/DDP-luc lung tumor (inhalation of1.5 mg Pt/kg, 7 times for 3 days) Relative tumor radiance: Control ∼14, Cisplatin ∼12.5, 7-NP ∼5, Ac4ManNAz+7-NP ∼1.25
	Reducing MDSCs				
244	8-NP-RA (PRA@Oxa-c16) 8-NP (without retinoic acid) (P@Oxa-c16)	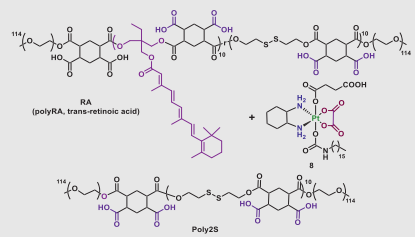	PRA: self-assembly of polyRA d = 51.6 nm ζ = −23.0 mV CMC: no data 8-NP-RA: Encapsulation of 8 (1 mg) in the amphiphilic PRA polymer (10 mg) DL, EE: no data d = 74.3 nm PDI ∼0.1 ζ = −46.3 mV 8-NP: Encapsulation of 8 in the amphiphilic polymer poly2S DL, EE: no data Poly2s (10 mg) and Oxa-c16 (1 mg) Drug release: GSH	ICD: DAMPs release↑ Antitumor immunity: Macrophage polarization ↑, DC maturation↑, MDSC↓ $CD8^+$ ↑, $CD4^+$↑ T cells in tumor: $CD8^+$↑	Subcutaneous MC38 colon cancer tumor (dose not stated): TGI: 8-NP-RA: 70.1% 8-NP (without retinoic acid): 58.7% PRA: 19.5% Survival rate after 60 days: 8-NP (without retinoic acid): 20% 8-NP-RA: 60% PBS: 0% Subcutaneous MC38 colon cancer tumor (8-NP dose not stated, 150 μg aCD8 per dose):

(*continued on next page*)

Table 1 (*continued*)

Ref.	NPS	Pt(IV) prodrug	Synthesis of NPs Size of nanoparticles (NPs), drug loading (DL, %), and encapsulation efficiency (EE, %) Drug release mode	Mechanism of action	Tumor model, type, *in vivo* antitumor efficacy
					Ratio of tumor volume V/V_{PBS}: 8-NP-RA + αCD8 ~100%, 8-NP ~27% Subcutaneous MC38 colon cancer tumor (8-NP dose not stated, 150 μg αPD-L1 per dose): Ratio of tumor volume V/V_{PBS}: 8-NP-RA+ αPD-L1: 5.5% (2/5 tumors eradicated) 8-NP-RA: 36% αPD-L1 ~81% Subcutaneous 4T1-luc recurrent model (8-NP dose not stated, 150 μg αPD-L1 per dose): Tumor recurrence: PBS: significant tumor recurrence 8-NP: tumor recurrence, 8-NP-RA+ αPD-L1: negligible tumor recurrence 8-NP-RA: poor therapeutic effect
249	Inflammation reduction 9-NP (Tf-NPs@CPF2-Pt(IV)) 9-NP-m (without transferrin) (NPs@CPF2-Pt(IV))	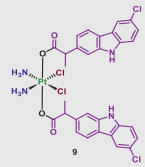 9	9-NP-m Encapsulation of prodrug 9 into DSPE-PEG_{2000} $d = 97.2 \pm 1.4$ nm PDI $= 0.11 \pm 0.01$ $\zeta = -15.24 \pm 0.45$ mV EE ~94%, DL: no data 9-NP Co-incubation of DSPE-PEG2000-Tf with 9-NP-m $d = 123.2 \pm 3.5$ nm PDI $= 0.32 \pm 0.02$ $\zeta = -17.03 \pm 0.52$ Drug release: Passive diffusion	Mitochondrial damage: MMP↓, ROS↑. Apoptosis: p53↑, Bax↑, Bcl-2↓, caspase-3↓, *c*-caspase-3↑. DNA damage: γ-H2AX↑. Inflammation: COX-2↓, MMP-9↓, IL-1β↓, TNF-α↓ EMT inhibition: E-cadherin↑, N-cadherin↓, vimentin↓, Snail1↓, β-catenin↓, cyclin D1↓, c-Myc↓ Antitumor immunity: PD-L1↓ T cells in tumor: $CD3^+$↑,	Subcutaneous triple-negative 4T1 breast tumor (2 mg Pt/kg): TGI: Cisplatin: 25.7%, 9-NP: 80.4% Tumor volume, mm^3 Cisplatin ~600, 9-NP ~300 4T1 metastasis model, (2 mg Pt/kg): TGI Cisplatin: 25.5%, 9-NP: 79.2%

143	10-NP (NP/OXA-ASP$_2$)	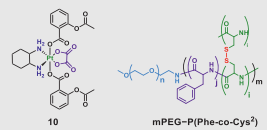	Encapsulation of prodrug 10 in polymer DL = 4.70% EE: no data d = 85,2 ± 53,6 PDI, ζ = no data Drug release: GSH	CD8$^+$↑, Apoptosis: cl-caspase-3↑ Oxidative stress: GSH↓, ROS↑ Glycolysis inhibition: glucose uptake↓, lactate efflux↓, ATP↓, Mapks↓, Cdks↓ Pkm↓ Apoptosis: Aifm1↑, Cycs↑, Bax↑, Itpr3↓, Actg1↓ ICD: DAMP↑, HSPs↑ Glycolysis *in vivo*: HK2↓, Pkm2↓ Antitumor immunity: CD8$^+$↑, MDSC↓, Tregs↓ Cytokines: TGF-β↓, IL-10 ↓, TNF-α↑, IL-1β↑, IL-6↑	Subcutaneous CT-26 colon tumor (5 mg oxaliplatin/kg): TIR 10-NP ∼85.2% oxaliplatin ∼57.6%
	Pt(IV)-based NPs to induce immunogenic cell death cGAS−STING pathway activation				
275	11-NP (NPs)	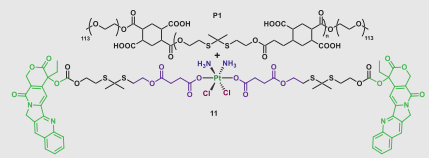	11-NP: Ultrasonic method with ROS-sensitive polymer P1, mPEG$_{2k}$-DSPE and prodrug EE = 62.9% DL = 12.6% d = 97.47 nm PDI = 0.127 ζ = −20 mV Drug release: H_2O_2	DNA damage: γ-H2AX↑, p53↑ cGAS−STING pathway: p-STING↑, p-IRF3↑, p-TBK-1↑. Apoptosis induct'ion Cytokines: IL-6↑, IFN-β↑, IFN-γ↑ Antitumor immunity: memory T cells↑, DC maturation↑ (CD80$^+$CD86$^+$ ↑). T cells in tumor: CD8$^+$↑, CD4$^+$↑	Subcutaneous murine colon CT-26 tumor (3 mg Pt/kg): Tumor weight, g: CDDP: 0.842, 11-NP: 0.271
276	12-NP (NP-Pt-IDOi)	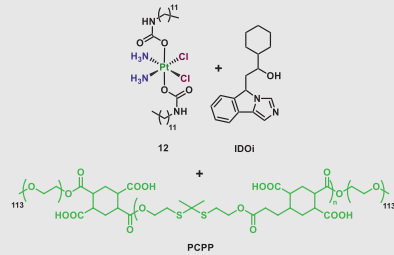	Nanoprecipitation of prodrug 12 with ROS-sensitive polymer PHPM and IDO inhibitor NLG91 2:5:1 DL: no data EE = 8.5% d = 113.2 ± 3.6 nm PDI = 0.157 ζ = −10.1 mV Drug release: ROS	DNA damage: Pt-DNA adducts↑, γ-H2AX↑. cGAS−STING pathway: p-STING↑, p-IRF3↑, p-TBK-1↑. IDO↓ Antitumor immunity: memory T cells↑, macrophage polarization↑, DC maturation ↑, Tregs↓ (Foxp3↓) T cells in tumor: CD8$^+$↑, CD4$^+$↑	Orthotopic K7M2-LUC osteosarcoma tumor (3.5 mg Pt/kg) Average bioluminescence, p/s/cm^2/sr: 12-NP: 3.50 × 10^9 CDDP: 11 × 10^9
280	13a-NP (NPPt) 13b-NP (NPMn)		13a-NP: Sonification of complex 13a (5 mg), ROS-sensitive polymer PCPP, and DSPE-PEG$_{2000}$ DL = 38.9% EE = 82.7% d = 122 nm	DNA damage: γ-H2AX↑, mtDNA in cytoplasm↑. Gas-STING pathway: cGAS↑, p-STING↑, p-TBK1↑, p-IRF3↑. ICD: DAMPs release↑	Subcutaneous patient-derived ovarian tumor (1 mg Pt/kg, 3.5 mg Mn/kg): TIR Cisplatin: 35.2%, 13a-NP + 13b-NP: 92.9%

(*continued on next page*)

Table 1 (*continued*)

Ref.	NPS	Pt(IV) prodrug	Synthesis of NPs Size of nanoparticles (NPs), drug loading (DL, %), and encapsulation efficiency (EE, %) Drug release mode	Mechanism of action	Tumor model, type, *in vivo* antitumor efficacy
		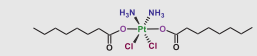 13a  13b 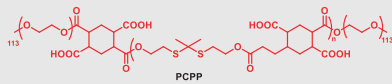 PCPP	PDI = 0.18 ζ = −19.6 mV 13b-NP: Sonification of 13b (5 mg), PCPP (5 mg), and DSPE-PEG2000 (100 mg) DL = 50.8% EE = 82.3% d = 133 nm PDI = 0.18 ζ = −18.7 mV Drug release: ROS	Cytokines: IL-2↑, IL-6↑, TNF-α↑ Antitumor immunity: Macrophage polarization ↑, DC maturation ↑, memory T cells↑, PD-L1↑, Tregs↓ T cells in tumor: $CD8^+$↑	ID8-Luc Ovarian Cancer Peritoneal Metastatic Model (3.5 mg Pt/kg): Average bioluminescence, p/s/cm^2/sr: PBS: 2.3 × 10^6, 13a-NP+13b-NP: 6.1 × 10^5, 13a-NP + 13b-NP + α-PD-1: 2.2 × 10^5
283	14-NP (NP2) 14-NP-m (without MK1775) (NP1)	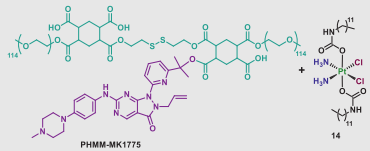 PHMM-MK1775 14 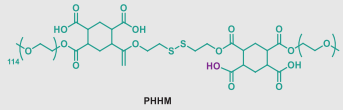 PHHM	14-NP: Self-assembly *via* nanoprecipitation of prodrug 14 with GSH-sensitive polymer PHMM-MK1775 DL, EE: no data d = 137.3 nm PDI = 0.080 ζ = −9.6 ± 2.32 mV 14-NP-m: Self-assembly *via* nanoprecipitation of prodrug 14 with GSH-sensitive polymer PHMM d = 61.8 nm PDI = 0.171 ζ = −16.2 ± 1.59 DL, EE: no data Drug release: GSH	DNA damage: Pt-DNA adducts↑, γ-H2AX↑. cGAS-STING pathway: dsDNA↑, p-STING↑, DNA repair inhibition: WEE1↓, CDK-1↓ Cytokines: IFN-α ↑, IFN-β↑. PD-L1↑ Antitumor immunity: NK cells↑, macrophage polarization↑, MSDCs↓, memory T cells↑, DC maturation↑ T cells in tumor: $CD8^+$↑ Cytokines *in vivo*: IFN-γ↑, TNF-α↑	Subcutaneous Mb49 bladder tumor (3 mg Pt/kg): TSR: Cisplatin: 63.6%, 14-NP: 86.4% Bilateral subcutaneous Mb49 tumor (3 mg Pt/kg): TSR, Primary tumor: αPD-L1: 45.3% 14-NP: 75.7% 14-NP+αPD-L1: 95.8% Tumor volume, mm^3, Distant tumor: PBS: 335 14-NP: 180 αPD-L1: 28 14-NP + αPD-L1: 0
144	15-NP (NP(3S)s)	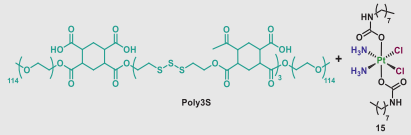 Poly3S 15	Nanoprecipitation of prodrug 15 with reduction-responsive trisulfide polymer Poly3S, 1:10 EE = 64.60 ± 6.02% DL = 1.78 ± 0.17% d = 136 nm PDI = 0.11 ζ = no data CMC: no data Drug release: GSH	H_2S↑, GSH↓ DNA damage: Pt-DNA adducts↑, γ-H2AX↑ cGAS-STING pathway: p-STING↑, p-IRF3↑ T cells in tumor: $CD4^+$↑, $CD8^+$↑ Antitumor immunity: macrophage polarization↑, DC maturation ↑	Subcutaneous 4T1 triple-negative breast tumor (1.5 mg Pt/kg): Relative tumor volume (V/V_0) PBS ∼15, Cisplatin ∼10, 15-NP ∼1 Tumor weight, mg PBS: 564, Cisplatin: 340, 15-NP: 114

	Phosphatidylserine exposure inhibition Pyroptosis induction				
288	16-NP (PDO NPs)	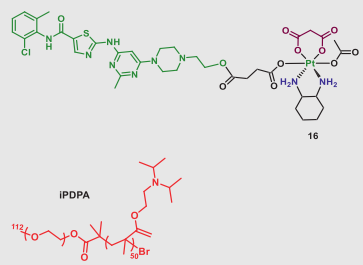	Encapsulation of prodrug 16 into pH sensitive polymer iPDPA CMC: no data DL = 6.7% EE = 38.08 % d = 27.52 nm PDI = 0.4 ζ = −0.7 mV Drug release: pH	Pyroptosis: bubbles↑, LDH↑, HMGB1↑, p-Src↓, GSDME-N↑ T cells in tumor: $CD4^+$↑, $CD8^+$↑ Antitumor immunity: MSDC↓, memory T cells in DLNs↑	Subcutaneous head and neck squamous cell carcinoma tumor (5 mg OXA/kg): Tumor volume, mm^3 OXA ∼380, 16-NP ∼220 Orthotopic HNSCC tumor (5 mg OXA/kg): Tumor volume, mm^3 OXA ∼34, 16-NP ∼10
290	17-NP (Pt-In NP) 17-NP-m (without indomethacin) (Pt NP)	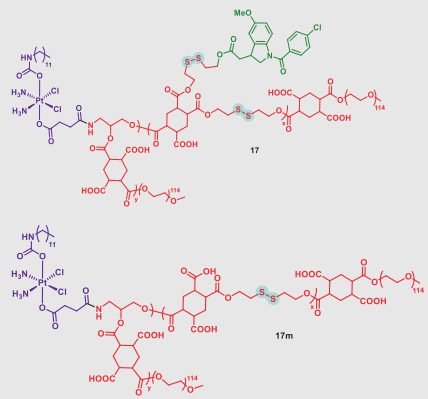	17-NP: Self-assembly of prodrug 17 *via* nanoprecipitation d = 113.9 nm PDI = 0.09 ζ = −11.8 mV CMC: no data 17-NP-m: Self-assembly of prodrug 17m *via* nanoprecipitation d = 84.6 nm PDI = 0.19 ζ = −10.9 mV CMC: no data Drug release: GSH	DNA damage: γ-H2AX↑ COX-2↓, PGE_2↓ Pyroptosis: cell swelling, membrane bubbles lactate dehydrogenase (LDH) ↑ adenosine triphosphate (ATP) ↑ GSDME-N↑ Caspase-3↑ Cytokines: IL-18, IL-1β, IL-6↑, TNF-α↑ ICD: CRT↑, HMGB1↑	Subcutaneous Pan02 pancreatic tumor (3 mg Pt/kg): TGI: 17-NP: 81%, 17-NP (without indomethacin): 59%, Cisplatin: 30% Tumor weight, g: 17-NP: 0.27, 17-NP (without indomethacin): 0.65, Cisplatin: 0.99, PBS: 1.4 Bilateral subcutaneous Pan02 pancreatic tumor, number of mice with distant tumor, mm^3 (3 mg Pt/kg): PBS: 5/5, ∼300, αPD-L1 (50 mg/kg): 5/5, ∼206, 17-NP: 4/5, ∼30, 17-NP + αPD-L1 (50 mg/kg): 0/5 αPD-L1 (50 mg/kg): 5/5, ∼206, 17-NP: 4/5, ∼30, 17-NP + αPD-L1 (50 mg/kg): 0/5
	Ferroptosis induction				
156	18a−NP (Pt(IV)-2SH@$CaCO_3$@Biotin) 18b−NP (Pt(IV)-2SS@$CaCO_3$@Biotin)	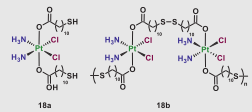 18a-NP: no *in situ* polymerization of Pt(IV) prodrug 18b-NP: after *in situ* polymerization of Pt(IV) prodrug	Loading of Pt(IV) prodrug into $CaCO_3$-based nanoparticles, then coating with DSPE-PEG_{2000}-Biotin 18a-NP DL = 21.4% d = 108 ± 3.2 nm	Intracellular Ca^{2+}↑ Mitochondrial damage: MMP↓, ATP↓, ROS↑. Ferroptosis: GPX4↓, GSH↓, lipid peroxides↑,	Subcutaneous A549 lung tumor (5 mg/kg) Tumor volume, mm^3 Cisplatin ∼1400, 18a-NP ∼300, (*continued on next page*)

Table 1 (*continued*)

Ref.	NPS	Pt(IV) prodrug	Synthesis of NPs Size of nanoparticles (NPs), drug loading (DL, %), and encapsulation efficiency (EE, %) Drug release mode	Mechanism of action	Tumor model, type, *in vivo* antitumor efficacy
			PDI = no data ζ = −20 mV 18b-NP *in situ* oxidative polymerization with I_2 and DMSO DL = 19.8% d = 115 ± 5.7 nm PDI = no data ζ = −25 mV Drug release: pH, GSH	malondialdehyde↑ Apoptosis: caspase-3↑, caspase-7↑. ICD: DAMPs release↑ Antitumor immunity: DC maturation↑, Tregs↓, Memory T cells↑ T cells in tumor: $CD4^+$↑, $CD8^+$↑,	18b-NP ∼25 Tumor weight, g Cisplatin ∼0.62, 18a-NP ∼0.27, 18b-NP ∼0.12 Lewis lung carcinoma, vaccination (1.95 mg/kg Pt^{4+} 18a-NP & 18b-NP, 5.95 mg/kg cisplatin): Tumor volume, mm^3 (after vaccination): Cisplatin ∼1300, 18a-NP ∼500, 18b-NP ∼40
151	19-NP (Abplatin$^{(iv)}$)	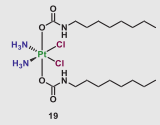 19	Encapsulation of prodrug 19 in HSA EE = 58.45 ± 1.64% DL = 3.89 ± 0.11% d = 190.9 nm PDI = 0.109 ζ = no data Drug release: pH, GSH	Ferroptosis: NOX3↑, HMOX1↑, CYBB↑, 4-HNE↑, lipid ROS↑, GPX4↓ Tumor damage: γ-H2AX ↑, cleaved-PARP↑	Orthotopic ES2-luc-derived tumor (1.5 mg Pt/kg): Tumor reduction, compared to cisplatin 19-NP: 65.97% Subcutaneous SKOV-3-derived cancer stem cell tumor, (1.5 mg Pt/kg): Tumor volume, mm^3 19-NP: 83.4 Cisplatin: 179.8
	Targeted Pt(IV)−based nanoparticles Tissue level targeting				
130	20-NP (APt^{IV})	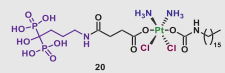 20	Self-assembly of amphiphilic prodrug CMC = 0.78 μg/mL d = 31.22 nm PDI = 0.196. ζ = no data Drug release: GSH	Intracellular Ca^{2+}↑	Orthotopic osteosarcoma K7M2 tumor (3.5 mg Pt/kg): Tumor volume, mm^3: PBS ∼1500, Cisplatin ∼600, 20-NP ∼200
131	21-NP (ALN-OXA)	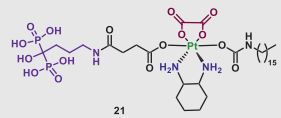 21	Self-assembly of amphiphilic prodrug 21 CMC = 8.71 μg/mL d = 22.87 nm PDI = 0.26 ζ = no data Drug release: pH, GSH	Intracellular Ca^{2+}↑ ICD & cytokines: DAMPs release↑, IL-6↑, TNF-α↑, IL-1β↑ Antitumor immunity: Macrophage polarization ↑, DC maturation↑, Tregs↓ T cells in tumor: $CD8^+$↑	Orthotopic osteosarcoma K7M2 tumor (3 mg Pt/kg): Relative tumor volume, V/V_0: Saline ∼8, OXA ∼4, 21-NP ∼2

301	22a-NP (cationic, without ALE) (NP) 22-NP (anionic, with ALE) (Ale NP)	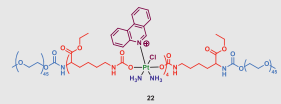 22 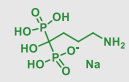 Alendronate	22a-NP: Nanoprecipitation of prodrug 22 CMC: no data d = 86 nm ζ = +25,33 mV PDI: no data 22-NP: ALE conjugation with 22a-NP d = 116 nm PDI = no data ζ = −5.09 mV Drug release: GSH	DNA damage: γ-H2AX↑ Gas-STING pathway: TBK1↑, p-TBK1↑, IRF3↑, p-IRF3↑, STING↑, p-STING↑ Cytokines: IF-1β↑, IL-6↑, IFN-β↑ Antitumor immunity: Macrophage polarization ↑, DC maturation ↑, memory T cells↑, PD-L1↑ T cells in tumor: $CD8^+$↑	Orthotopic osteosarcoma K7M2 tumor (3 mg Pt/kg): TIR Cisplatin: 36.5%, 22a-NP: 54.1%, 22-NP: 76.3%, Orthotopic osteosarcoma K7M2 tumor (combination therapy with 230 mg/kg αPD-L1, 3.5 mg Pt/kg) Tumor volume, mm^3: PBS ∼1300 (Day 16) αPD-L1 ∼1300 (Day 22) 22-NP ∼700 (Day 30) 22-NP + αPD-L1 ∼200 (Day 30) Patient-derived osteosarcoma tumor: Tumor volume, mm^3 (3.5 mg OXA/kg): Cisplatin: 527, 22a-NP: 381 22-NP: 197
	Cell level targeting Gene therapy				
306	23-NP ($NP_{CSPt/pEZH2}$)	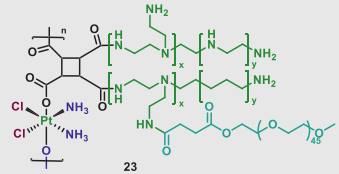 23	Self-assembly of prodrug 23 into NPs with subsequent coating with pEZH2 plasmid CMC: no data d = 140 nm PDI ≈ 0.13 ζ ≈ 30 mV Drug release: GSH	Gene editing: EZH2↓, H3K27me3↓	Subcutaneous PC-3 prostate tumor (2.56 mg Pt/kg) Tumor volume, mm^3 Control: 2050 23a-NP: 1200 Cisplatin: 570 23-NP: 310
309	24-NP ($CNP_{PtCP/si(c\text{-}fos)}$)	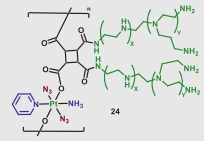 24	Self-assembly of prodrug 24 into NPs with subsequent si(c-fos) loading and coating with HA-PEG CMC: no data d = 220 nm PDI = 0.25 ζ = −12 mV Drug release: 450 nm light (20 mW/cm^2)	ROS: N_3•↑ DNA damage: Pt-DNA adducts↑ c-fos *in vitro*↓ Activity *in vivo*: c-fos↓, γ-H2AX↑,	Subcutaneous cisplatin-resistant A2780/CDDP ovarian tumor (2.77 mg Pt/kg): Tumor volume, mm^3: 24-NP: 185 Cisplatin: 1060
311	25-NP (NPt^{IV}@siXkr8)	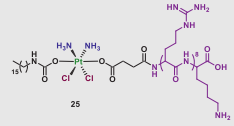 25	Self-assembly of prodrug 25, then siXkr8 loading (N/P = 6:1) CMC = 0.048 μmol/L d = 101 nm PDI = 0.12 ζ = 2 mV	DNA damage: Pt-DNA adducts↑. Cell membrane phosphatidylserine↓, *XKR8* mRNA ↓ DC maturation:	Subcutaneous 4T1 triple-negative breast tumor (3.5 mg Pt/kg): Relative tumor volume, V/V_0 PBS ∼13, Cisplatin ∼11, Complex 8

(*continued on next page*)

Table 1 (*continued*)

Ref.	NPS	Pt(IV) prodrug	Synthesis of NPs Size of nanoparticles (NPs), drug loading (DL, %), and encapsulation efficiency (EE, %) Drug release mode	Mechanism of action	Tumor model, type, *in vivo* antitumor efficacy
			Drug release: pH, NaAsc	$CD80^{+}CD86^{+}$ ↑ Antitumor immunity: Macrophage polarization ↑, DC maturation ↑ Cytokines: IFN-γ↑, TNF-α↑, IL-10↑ T cells in tumor: $CD4^{+}$↑, $CD8^{+}$↑	~7, 25-NP ~2.5 Recurrent subcutaneous 4T1 tumor model Relative volume of recurrent tumor V/V_0: PBS ~10, Cisplatin ~8, 25 ~6, 25-NP ~0
139	26-NP (Pt LNPs)	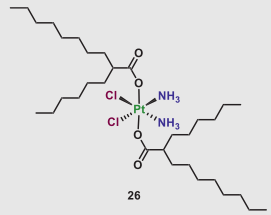 26	Microfluidic mixing of SM-102. DSPC, Cholesterol, DMG-PEG with prodrug 26 and siXkr8 and mANX5 DL = 20% EE = 90.9% d = 116.5 nm PDI = 0.09 ζ ~5 mV Drug release: GSH	Antitumor immunity: PS externalization↓, phagocytosis *in vitro*↓, PS exposure↓, DC maturation↑ Cytokines: TGF↓, IL-10↓. TNF-α↑, IL-1β↑, IL-26, Activity *in vivo*: γ-H2AX↑, DC maturation↑, $CD8^{+}$↑,	Subcutaneous 4T1 triple-negative breast tumor (1.35 mg Pt(IV)/kg): Tumor volume, mm^3 26-NP ~78 Cisplatin ~780 Bilateral subcutaneous 4T1 (1.35 mg Pt(IV)/kg): Secondary tumor volume, mm^3 26-NP ~100 Cisplatin ~400
	Nuclei targeting				
312	27-NP ($NTPt^{IV}$) 27-NP-m (without nuclei targeting) ($NOPt^{IV}$@Cy7)	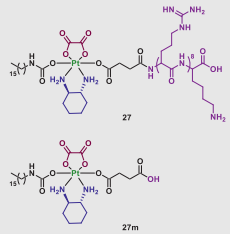 27 27m	27-NP: Self-assembly of prodrug 27 CMC = 0.07 μmol/L d = 86 nm PDI = 0.17 ζ = no data Drug release: Ascorbic acid 27-NP-m: C16-OPtIV-Suc, DSPE-mPEG2000, and Cy7	DNA damage: Pt-DNA adducts↑ ICD: DAMPs release↑ Antitumor immunity: Macrophage polarization ↑, DC maturation↑ Tregs↓ Cytokines: IFN-γ↑, TNF-α↑, IL-10↑ T cells in tumor: $CD4^{+}$↑, $CD8^{+}$↑, $CD3^{+}$↑	Subcutaneous triple-negative 4T1 breast tumor, (3.5 mg Pt/kg): Relative tumor volume V/V_0 PBS ~15 (Day 12) OXA ~9 (Day 12) 27−NP ~2 (Day 18)
	Mitochondria targeting				
313	28-NP (Gal−NP@TPt)		Encapsulation of prodrug 28 into self-assembled GSH-sensitive disulfide polymer P1 CMC (P1) = 0.028 mg/mL DL = 9% EE = no data	DNA damage: γ-H2AX↑ Apoptosis: p53↑, Bax↑, Bcl2↓, c-PARP↑, c-caspase-3↑, GSH depletion Mitochondrial damage:	Subcutaneous patient-derived tumor xenograft of hepatocellular carcinoma (2 mg Pt/kg) Tumor volume, mm^3: PBS: 2200

		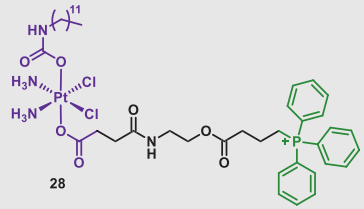	d = 129.5 nm PDI = 0.078 ζ = no data Drug release: GSH	ATP↓, MMP ↓, ROS ↑ Autophagy: autophagosomes↑, LC3-II↑, p62↓	Cisplatin: 1800 28-NP: 600 Tumor weight, g: 28-NP: 0.41, PBS: 1.81, Cisplatin: 1.32
314	29-NP (TPP-Pt-acetal-CA)	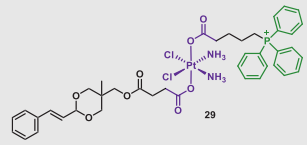	Self-assembly of prodrug 29 CMC = 1.28 μmol/L d = 109.8 nm PDI = 0.067 ζ = 8.4 mV Drug release: pH, GSH	Apoptosis Cell cycle arrest in S-phase DNA damage: γ-H2AX↑ Mitochondria damage: MMP↓, ROS↑	Subcutaneous cisplatin-resistant A549/DDP tumor (3 mg Pt/kg): Tumor volume, mm^3: PBS ∼880, Cisplatin ∼720, 29-NP ∼200
318	30-NP (LPT/HA-CD) 30-NP-m (LPT)	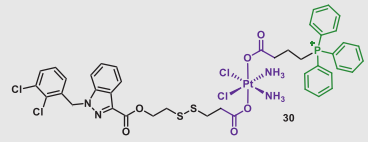	Loading of prodrug 30 into HA-CD NPs 30-NP-m (without prodrug 30) d = 119.2 nm PDI = 0.187 ζ = −30.18 mV 30-NP EE = 81.44% DL = 3.97% d = 154.8 nm PDI = 0.127 ζ = −32.90 mV Drug release: GSH	Mitochondrial damage: MMP ↓, ROS ↑, ATP content↓, Cyto C↑ Glycolysis inhibition: lactate glucose uptake↓ HK II↓ Autophagy: p62↓, LC3-II↑ Apoptosis: caspase-9↑, caspase-3↑, Bax↑	Subcutaneous cisplatin-resistant A549/DDP tumor (2 mg Pt/kg): Tumor volume, mm^3: PBS ∼660, Cisplatin ∼400, LND ∼580 30 ∼250, 30-NP ∼90 Orthotopic cisplatin-resistant A549/DDP tumor (2 mg Pt/kg): Tumor volume, mm^3 PBS ∼25, Cisplatin ∼10, 30 ∼5, 30-NP ∼2
319	31-NP (PDDN)	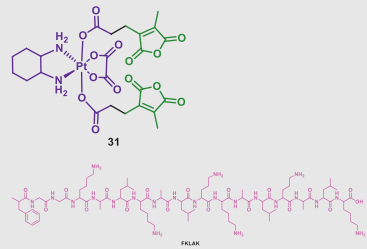	Polymerization of 31 and FKLAK at the emulsion interface EE ≈ 100% d = 112 nm PDI = no data ζ = −36.4 ± 0.04 mV Drug release: pH, GSH	Inhibition of the DNA repair Intracellular GSH↓ Mitochondrial disruption: ATP↓ Lactate dehydrogenase (LDH)↓	Subcutaneous A549 tumor (3.5 mg Pt/kg): TIR 31-NP: 74.5% FKLAK: 19.0%, Oxaliplatin: 12.6% Subcutaneous lung cancer PDX (3.5 mg Pt/kg): TIR 31-NP: 78.8% FKLAK: 14%, Oxaliplatin: 58.9%

(*continued on next page*)

Table 1 (*continued*)

Ref.	NPS	Pt(IV) prodrug	Synthesis of NPs Size of nanoparticles (NPs), drug loading (DL, %), and encapsulation efficiency (EE, %) Drug release mode	Mechanism of action	Tumor model, type, *in vivo* antitumor efficacy
	Endoplasmic reticulum targeting				
150	32-NP (HSA@C4F7-Pt(IV)	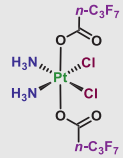 32	Loading of prodrug 32 on HSA DL, EE: no data d = 91 nm PDI = 0.155 ζ = no data Drug release: GSH	Apoptosis DNA damage: Pt-DNA adducts↑, γ-H2AX↑. Mitochondrial damage: MMP↓, ROS↑. ER stress: BiP↑, eIF2α↑, CHOP↑ ICD: DAMPs release↑ Antitumor immunity: DC maturation↑ T cells in tumor: $CD8^+$↑	Orthotopic K7M2 osteosarcoma tumor (3 mg Pt/kg): Tumor volume reduction compared to control: Cisplatin: 43%, 32: 69%, 32-NP: 85% Subcutaneous K7M2, after vaccination: Tumor volume, mm^3 PBS: 1200, 32-NP: 500
	Theranostics and stimuli-sensitive nanoparticles based on Pt(IV) prodrugs Endogenous activation				
323	33-NP (Pt^{IV}NPs)	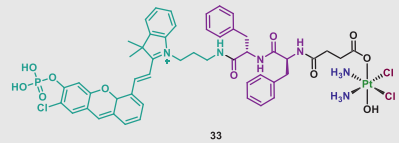 33	Self-assembly of prodrug 33 after ALP-triggered dephosphorylation d = 160 nm (for NPS formed *in vitro*) Drug release: GSH	Intracellular GSH↓	Subcutaneous HeLa cervical tumor (2.25 mgPt/kg): Relative tumor volume (V/V_0) PBS ~21, Cisplatin ~16, 33-NP ~13 33 (self-assembly of NPs *in vivo*) ~1 Orthotropic hepatocellular carcinoma HEPG2 tumor (2.25 mgPt/kg): Luminescence intensity (10^5 photons): PBS ~13.0 Cisplatin ~10.7 33-NP ~5.7 33 (self-assembly of NPs *in vivo*) ~1
324	34-NP ($Nanoplatin^{DTR}$)	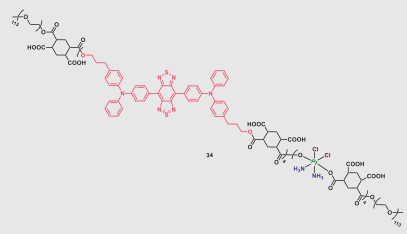	Self-assembly of prodrug 34, then coating with apoptosis probe (5′-FAM-DEVD-dabcyl), then with RGD peptide DL, EE: no data d = 110 nm PDI = no data ζ = no data Drug release: GSH	Apoptosis: caspase-3↑	Murine model of advanced stage III/IV HGSOC (4 mg Pt/kg): Impressive tumor inhibition: no quantitative analysis

121	35-NP (1-NM)	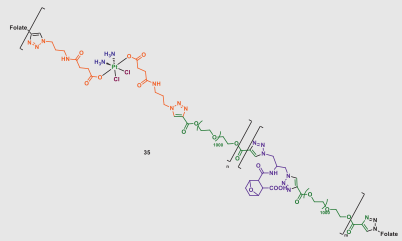	Self-assembly of prodrug 35 into micelles CMC = 37.4 mg/L DL (Pt) = 4.3% d = 180 nm PDI = 1.51 ζ = −10 mV Drug release: pH, NaAsc	Activity *in vitro*: PP2A↓, p-Akt↑, γ-H2AX↑	Subcutaneous SKOV-3 ovarian tumor (2 mg Pt/kg): Tumor volume, mm^3 35-NP: 395 Cisplatin: 375
	Exogenous activation Ultrasound-activated NPs				
32	36-NP (NP^s)	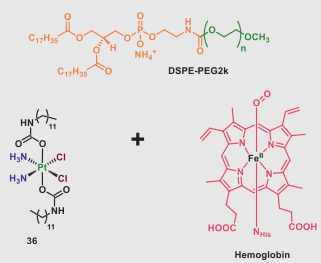	Nanoprecipitation of prodrug 36 with HGB, and DSPE-PEG_{2k} d = 174 nm PDI = 0.25 ζ = −12.9 mV Drug release: US, (1.5 W/cm^2, 10 min), NaAsc	ROS DNA damage: γ-H2AX↑	Subcutaneous CT26 murine colon tumor (1.5 mg Pt/kg): Tumor volume, mm^3: PBS ∼1800, Cisplatin ∼450, 36-NP + US ∼100
327	37-NP (OXA-Ce6 NP) 37-NP-m (without Ce6) (OXA NP)	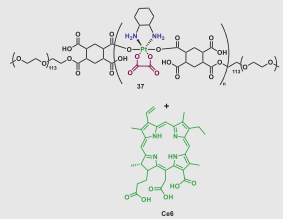	Nanoprecipitation of prodrug 37 with Ce6 37-NP-m DL, EE: no data d ≈ 130 nm PDI ≈ 0.05 ζ ≈ −5 mV 37-NP DL, EE: no data d = 149.8 nm PDI ≈ 0.12 ζ ≈ −3 mV Drug release: US (1.5 W/cm^2, 10 min)	DNA damage: Pt-DNA adducts↑. SDT: ROS↑ ICD: DAMPs release↑ Antitumor immunity: DC maturation↑, macrophage polarization↑ T cells in tumor: $CD8^+$↑, TCM in spleen↑	Subcutaneous CT-26 tumor (3.5 mg Pt/kg): Tumor volume, mm^3: PBS ∼1500, Oxaliplatin ∼1000, 37-NP + US (1 MHz, 1.5 W/cm^2, 5 min) ∼150
	Light-activated NPs UCNP				
157	38-NP (UCNP/Pt(IV)-RGD) 38-NP-m (without RGD coating) (UCNP/Pt(IV))	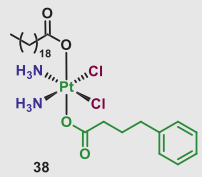	Loading of Pt(IV) prodrug 38 into UCNP DL = 16% EE: no data 38-NP-m d = 156.0 nm PDI = 0.142 ζ = −15.2 mV 38-NP d = 246.3 nm PDI = 0.116 ζ = 13.3 mV Drug release: 980 light, GSH	Pt(IV) prodrug: DNA damage: nucleolar stress↑, HDAC↓ NPs: DNA damage: γ-H2AX↑	Subcutaneous U14 squamous cell carcinoma (2.0 mg Pt/kg): Tumor volume, mm^3: Control ∼1500 38-NP ∼560 38-NP + 980 nm (0.48 W/cm^2) ∼180 Fluorescent tumor visualization

(*continued on next page*)

Table 1 (*continued*)

Ref.	NPS	Pt(IV) prodrug	Synthesis of NPs Size of nanoparticles (NPs), drug loading (DL, %), and encapsulation efficiency (EE, %) Drug release mode	Mechanism of action	Tumor model, type, *in vivo* antitumor efficacy
		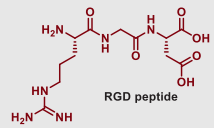			
	Pt(IV) prodrug conjugated with photo-responsive polymer				
148	39-NP (NPsT) 39m-NP (NPs)	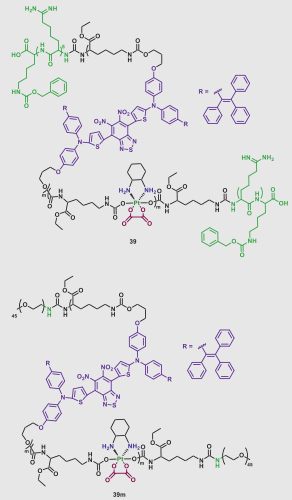	39-NP: Self-assembly of Pt(IV)-based polymer 39 d = 80 nm PDI = 0.09 ζ = 5.5 mV 39m-NP (without nuclei targeting) d = 84 nm PDI = 0.16 ζ = −0.6 mV Drug release: 808 nm light (1 W/cm^2, 10 min)	DNA damage: Pt-DNA adducts↑. PDT: ROS↑ ICD: DAMPs release↑ Antitumor immunity: DC maturation↑	Orthotopic triple-negative 4T1 breast tumor (3.5 mg Pt/kg): Ratio of tumor volume, V/V_0: PBS ~14 (Day 12) OXA ~11 (Day 12) 39-NP ~3 (Day 18) 39-NP + irradiation (808 nm, 1 W/cm^2, 10 min) ~1 (Day 18)
335	40-NP (NP^{PSP-Pt})	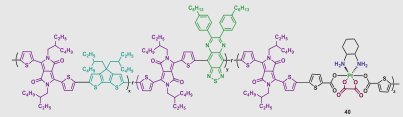	Self-assembly of prodrug 40 with hydrophilic polymer mPEG$_{2k}$-DSPE d = 115 nm PDI = 0.2 ζ = no data Drug release: 1064 nm light (1 W/cm^2, 10 min), NaAsc	ICD: DAMP release↑ Antitumor immunity: DC maturation↑ T cells in tumor: CD4$^+$↑, and CD8$^+$↑ PCE = 43.2%	Subcutaneous CT26 colon tumor (1 mg Pt/kg) Tumor volume, mm^3: PBS ~1000, OXA ~750, 40-NP ~480, 40-NP + 1064 nm, 1 W/cm^2, 10 min irradiation ~0 Subcutaneous 4T1 triple-negative breast tumor Tumor volume, mm^3 (1 mg Pt/kg): PBS ~600, OXA ~350, 40-NP ~220,

					40-NP + irradiation 1064 nm, 1 W/cm^2, 10 min ~0
	Pt(IV) prodrug co-assembled with dye Into drug carrier				
336	41-NP (BITT@BSA-DSP NPs)	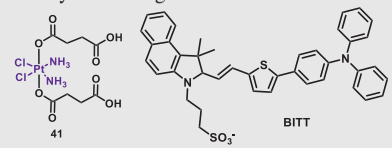	Loading of BIIT and Pt(IV) prodrug 41 into BSA EE (BITT) = 35% d = 70.2 nm PDI = 0.13 ζ = −21.50 mV	PDT: ROS↑ PCE = 26.35%	Subcutaneous MB49 bladder tumor Relative tumor volume, V/V_0 PBS ~22 41-NP ~21 41-NP + 660 nm (0.3 mW/cm^2, 10 min) ~7
337	42-NP (DSe@POC)	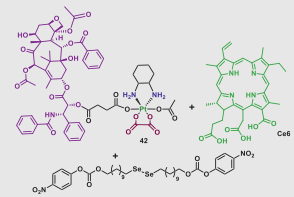	Self-assembly of prodrug 42 with Ce6 chlorine, diselenide cross-linker, and mPEG Ce6 EE = 77 ± 4.18% DL = 3.88 ± 0.21% Prodrug 31: EE = 90.27 ± 5.43% DL = 14.39 ± 0.87% d = 59.29 nm PDI = 0.315 ζ = −18 mV Drug release: H_2O_2, DTT	Pyroptosis: GSDME-N↑, c-caspase 3↑, LDH↑ ICD: DAMPs release↑ PDT: ROS↑ Antitumor immunity: DC maturation↑, MDSCs↓, Tregs↓ T cells in tumor: $CD4^+$↑, $CD8^+$↑, DLN DCs↑	Subcutaneous triple-negative 4T1 breast cancer tumor (5 mg OXA/kg) Tumor volume, mm^3 PBS ~360, OXA ~180, Complex 60 ~150, 42-NP ~120, 42-NP + irradiation 660 nm, 0.5 W/cm^2, 5 min ~40 Orthotopic MOSC2 oral tongue carcinoma tumor (5 mg OXA/kg): Tumor volume, mm^3: PBS ~28, OXA ~20, 42 ~17, 42-NP ~14, 42-NP + irradiation 660 nm, 0.5 W/cm^2, 5 min ~10 Bilateral subcutaneous 4T1: 42-NP + irradiation + αPD-1: distant tumor growth suppression 4T1 tumor recurrence: 42-NP + irradiation + αPD-1: recurrent tumor growth suppression 4T1 tumor recurrence: 31-NP + irradiation + αPD-1: recurrent tumor growth suppression
338	43-NP (NTSB)		Encapsulation of prodrug 43 into DSPE-PEG_{2K}-IR780 EE = 40.61%	Ki67↓ ROS↑ Intracellular GSH↓	Orthotopic K7M2 osteosarcoma tumor (3 mg Pt/kg):

(*continued on next page*)

Table 1 (*continued*)

Ref.	NPS	Pt(IV) prodrug	Synthesis of NPs Size of nanoparticles (NPs), drug loading (DL, %), and encapsulation efficiency (EE, %) Drug release mode	Mechanism of action	Tumor model, type, *in vivo* antitumor efficacy
		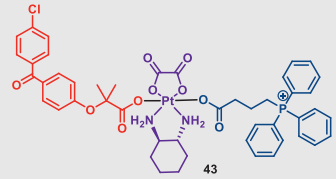 43 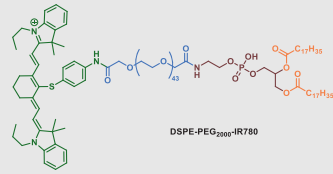 $DSPE\text{-}PEG_{2000}$-IR780	DL = 15.23% d = 74 nm PDI = no data ζ = −7 mV Release: 808 nm light, GSH	ETC↓ Ca^{2+}↑	Tumor volume reduction compared to control: Cisplatin: 43%, 32: 69%, 32-NP: 85% Subcutaneous K7M2, after vaccination: Tumor volume, mm^3: PBS: 1200, 32-NP: 500
	Self-assembly of photoactive prodrug				
339	44-NP (Pt-NPs)	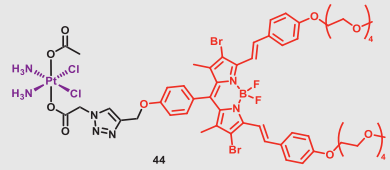 44	Loading of prodrug 44 into F127 EE = 82.7% DL = 18.3% d = 186 ± 4 nm PDI = no data ζ = no data Drug release: light (660 nm)	ROS↑ PTT ↑	No antitumor efficiency data
341	45-NP 45-NP-m (Pt-free)	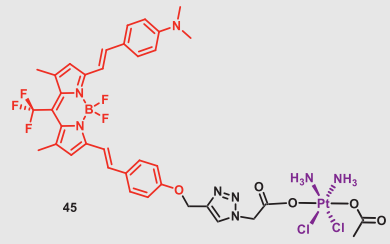 45 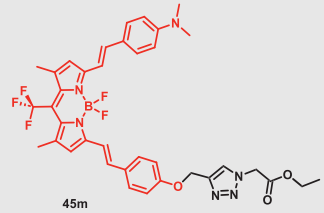 45m	Loading of prodrug 45 into F127 45-NP d = 88 nm PDI = 0.21 ζ = −25.1 mV 45-NP-m d = 83 nm PDI = 0.20 ζ = −18.4 mV Drug release: 740 nm light (0.2 W/cm^2), NaAsc		No antitumor efficiency data

	Radiation-activated NPs				
342	46-NP (Pt STNA)	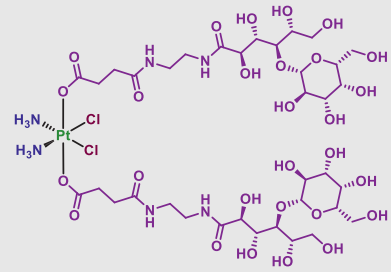	Self-assembly of prodrug 46 into nanoparticles CMC = 0.039 g/L d = 120 nm PDI ≈ 0.2 ζ = −14.9 mV Drug release: NaAsc	ROS↑ DNA damage: γ-H2AX↑ Cell cycle arrest: p-Chk1↑,	Subcutaneous hepatoma Hepa1-6 tumor (15 mg Pt/kg 46-NP, 2 mg Pt/kg cisplatin, 4 Gy): Tumor volume, mm^3: 46-NP + X-ray ∼130 Cisplatin + X-ray ∼210
343	47-NP (OXA/Fe NPs)	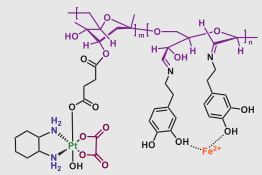	Self-assembly of prodrug 47 into nanoparticles CMC: nd d = 85.3 nm PDI = 0.067 ζ = −3.6 mV Drug release: pH, GSH	ROS in solution: OH•↑, O_2↑ Intracellular ROS: H_2O_2↓, OH•↑, lipid ROS↑ Hypoxia: HIF-1α↓ DNA damage: γ-H2AX↑ ICD: DAMPs release↑, DC maturation↑, IL-12p40↑, TNF-α↑, IFN-γ↑ Antitumor immunity: DAMP↑, DC maturation↑ T cells in tumor: $CD4^+$↑, $CD8^+$↑ Long-term immunity: $CD3^+CD8^+CD62L^-CD44^+$↑, IL-12p40↑, TNF-α↑, IFN-γ↑	Bilateral subcutaneous CT-26 colon tumor (2.5 mg Pt/kg, 6 Gy): Tumor volume, mm^3 Primary tumor: Oxaliplatin + X-ray ∼380 47-NP + X-ray ∼200 Abscopal tumor: Oxaliplatin + X-ray ∼240 47-NP + X-ray ∼100 B16-luc lung metastasis model (2.5 mg Pt/kg, 6 Gy): oxaliplatin: high luc signal 2/4 survival (Day 15) 47-NP + X-ray low luc signal, 4/4 survival (Day 15) Subcutaneous 4T1 recurrent model, Rechallenge study (Treatment (2.5 mg Pt/kg, 6 Gy), then rechallenge of a second tumor): Secondary tumor volume, mm^3: Surgery ∼720 Oxaliplatin + X-ray ∼350 47-NPs + X-ray ∼140

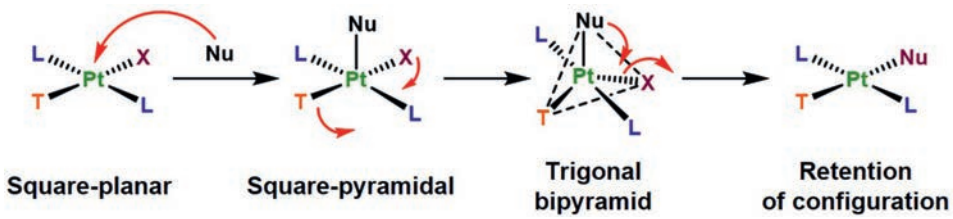

Figure 4 Ligand exchange in Pt(II) complexes.

agents, such as hydrogen peroxide or chlorine. The mechanism of Pt(II) oxidation to Pt(IV) complexes is generally accepted as a three-component reaction between the Pt(II) complex, the oxidizing agent, and the solvent (Fig. 5)[46].

Oxidation typically results in the formation of *trans*-oxidative addition products, where the four initial ligands in the square-planar Pt(II) complexes become four equatorial ligands, and their configuration is generally retained in the resulting Pt(IV) complexes[47].

Oxidation of Pt(II) complexes with hydrogen peroxide generally yields *trans*-dihydroxy complexes, in which one of the hydroxyl groups derives from the peroxide and the other from water; oxidation of Pt(II) drugs with halogens initially forms a solvent-coordinated intermediate, followed by the halogen anion displacing with the solvent to form the final *trans*-dihalogenated product. Water, alcohols, and acetic acid can be used as solvents, forming the corresponding unsymmetrical disubstituted Pt(IV) prodrugs[23,48].

2.4. *Modification of axial hydroxyl group in Pt(IV) prodrugs*

The axial OH ligand in Pt(IV) prodrugs possesses chemical properties similar to that of the alcohol hydroxyl group and can be modified with different electrophilic agents. Generally, a modification of the hydroxyl group can be accomplished *via* common acylation reactions, *via* carboxylic acids or their derivatives[16,49]. The conjugation of axial ligands with amino group with Pt(IV)−OH is possible by turning amine into isocyanates or carbamic acid esters, which readily react with OH-group forming carbamates. Similarly, the axial ligands with OH-groups can be conjugated with Pt(IV)−OH *via* using a CO bond donor, such as disuccinimidyl carbonate, with the formation of a carbonate bond (Fig. 6)[50].

2.5. *Hydrolysis of Pt(IV) complexes*

The hydrolytic stability of Pt(IV) prodrugs under physiological conditions significantly impacts their biological applications. Maintaining the integrity of the axial ligands of Pt(IV) prodrugs until they reach the tumor site is crucial for therapeutic efficacy. When hydrolysis or other ligand exchange reactions occur, the pharmacokinetic profile of Pt(IV) prodrug inevitably changes. Hydrolysis of Pt(IV) complexes can occur in both the axial and equatorial positions, depending on the nature of the ligands (Fig. 7)[29].

The hydrolytic stability of Pt(IV) complexes is closely related to the properties of the axial ligands: the greater the electron-withdrawing strength of axial ligand, the higher the tendency of Pt(IV) prodrug to hydrolysis and the faster the detachment of two axial ligands from the Pt(IV) center occurs. In 2021, Xu et al.[51]. demonstrated that the hydrolytic stability of one axial ligand of the Pt(IV) prodrug significantly depends on five other ligands around the Pt(IV) center. In unsymmetrical Pt(IV) prodrugs, with a hydroxyl or halogen substituent on one side and a carboxylate axial ligand on the other, a decrease in the electronegativity of the halogen leads to a weakening of the Pt(IV)−acetate trans interaction and an acceleration of halide hydrolysis due to a decrease in the cationic charge density at the Pt(IV) center. On the contrary, in fluoride-acetato-substituted Pt(IV) prodrugs, the acetate ligand undergoes hydrolysis instead of fluoride, since oxygen (in AcO) has a higher electronegativity than chlorine and bromine, but not fluorine. Thus, the tendency for hydrolysis of the *trans*-acetate axial ligand in Pt(IV) prodrugs increases as follows: OH $\geq$ acetate $>$ F $>$ Cl $>$ Br; this tendency was also observed by Zhou et al.[52]

Two possible pathways for hydrolysis of axial ligands in Pt(IV) prodrugs are the attack of water on the electrophilic center in the axial ligand, or the direct attack of water on the Pt(IV) center followed by Pt−O bond cleavage. Several studies confirmed that hydrolysis of Pt(IV) prodrugs occurs *via* direct attack of H_2O on the Pt(IV) center[53].

The rate of hydrolysis of Pt(IV) prodrugs is governed by the nature of the parent Pt(II) drug; thus, when all ligands being equal, carboplatin-based complexes are more stable than their CDDP- and OXA-based analogs, which can be explained by the chelating effect and σ-donor ability[54,55]. In addition, an increase in the number of substituents on the ammine ligands increases the δ-donating ability of the amino group, which leads to an increase in

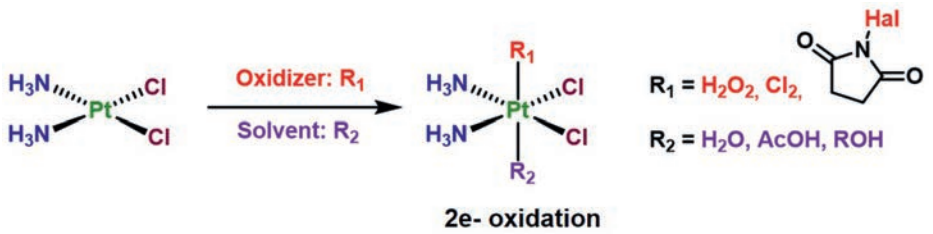

Figure 5 Oxidation of Pt(II) complexes.

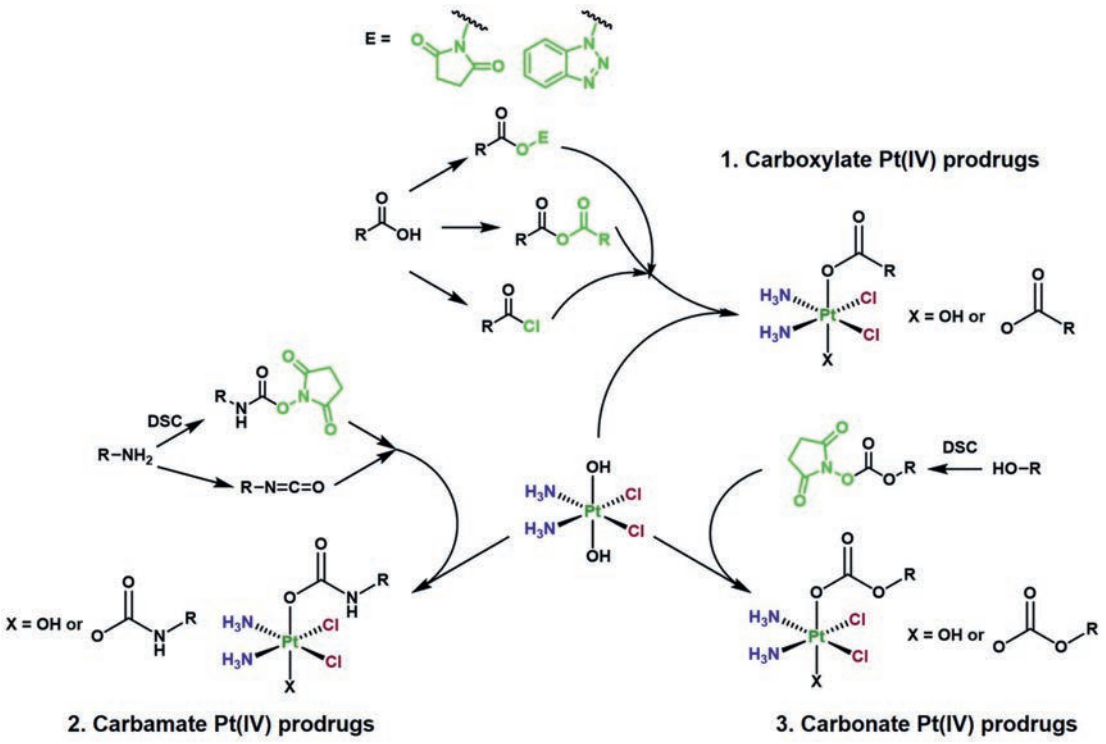

Figure 6 Synthetic approaches to the modification of axial OH ligands in Pt(IV) prodrugs.

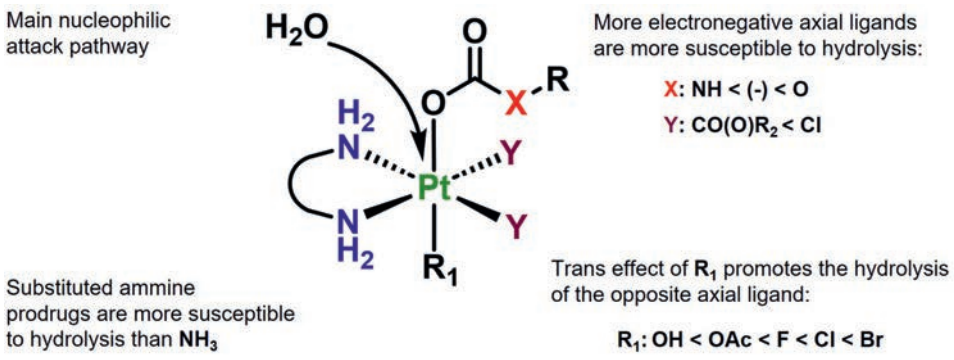

Figure 7 Factors affecting the hydrolysis of Pt(IV) prodrugs.

the rate of hydrolysis of the trans ligands; thus, the increased tendency of OXA-based Pt(IV) prodrugs to hydrolysis is associated with the replacement of the oxalate ligand with a hydroxyl group[29].

The nature of the modification of the axial hydroxyl group also affects the hydrolytic stability of Pt(IV) prodrugs. Thus, a comparison of the hydrolytic stability of Pt(IV) prodrugs with carbonate, carboxylate, and carbamate bonds in axial positions revealed the following hydrolytic stability order: Carbamate > Carboxylate > Carbonate[56,57].

2.6. *Reduction of Pt(IV) complexes*

The biological activity of Pt(IV) prodrugs is based on a reductive elimination process that converts inert Pt(IV) prodrugs into square-planar Pt(II) complexes. Typically, during reduction, the axial ligands are released and the parent Pt(II) complex is forming; however, in some cases, the formation of more than one product during reduction has been demonstrated[58].

Hydrolysis and reduction are competing reactions that can occur simultaneously. In general, the rate of Pt(IV) prodrug's reduction depends on two key parameters: the rate of electron transfer from the reducing agent to the Pt(IV) center and the ease of cleavage of the bond between Pt(IV) center and the oxygen of the axial ligand[59]. Monitoring the reduction reactions of Pt(IV) prodrugs and studying the resulting products has been widely discussed[60–62].

Initially, the cathodic peak potential (Epc) was considered as the quantitative standard of the propensity of Pt (IV) complexes to reduction. The general trend was as follows: the more negative the Ep value of a Pt(IV) complex, the more difficult it is to reduce, and the more stable the Pt(IV) prodrug. However, a significant number of studies have demonstrated a discrepancy between the reduction potential and the rate of the reduction reaction in Pt(IV) complexes[63–65]. One possible reason for this discrepancy may be

that the measurement of the reduction potential does not take into account the prodrug's hydrolysis reactions, which can occur in parallel, changing the coordination environment of the Pt(IV) center and thereby changing the overall electrochemical potential. Since the formation of electron transfer bridge greatly facilitates the reduction, kinetic factors also influence Pt(IV) prodrug's reduction susceptibility. As a result, Pt(IV) prodrugs with same ligands but different geometry can have drastically different reduction rates[66].

The process of electron transfer from the reducing agent to the Pt(IV) center occurs stepwise; after the first electron is received, a six-coordinate metastable Pt(III) intermediate is formed; the elimination of two axial ligands occurs only upon the addition of a second electron, forming an active square-planar Pt(II) complex[15,67].

The electron transfer mechanisms for the reduction of Pt(IV) complexes are classified as inner-sphere, which involve direct contact with the reducing agent, and outer-sphere. Inner-sphere mechanisms are divided into four types: (a) electron transfer through an axial ligand bridge; (b) hydride transfer through an axial ligand[68]; (c) nucleophilic attack of the enolate β-carbon of AscH on the axial ligand[69]; (d) Pt(II)-catalyzed electron transfer mechanism (Fig. 8A)[70].

The most important mechanism for the reduction of Pt(IV) prodrugs is inner-sphere electron transfer through an axial ligand bridge. Theoretically, halides and OH ligands decrease the reduction potential E_p and thus the propensity of the complexes to undergo reduction. However, halides and OH ligands also serve as an electron bridge, that facilitates electron transfer from the reducing agent to Pt(IV) center. Logically, electron transfer through an axial fluoride bridge occurs most actively. On the other hand, carbamate and carboxylate ligands are not as capable of forming an electron transfer bridge as hydroxide and halogen ligands[64].

Outer-sphere mechanisms involve direct electron transfer from the environment to the Pt(IV) center, which is what is typically determined by cyclic voltammetry. Variations involving external species have also been proposed, namely, either proton abstraction from the reducing agent or protonation of the axial ligand, accompanied by the transfer of two electrons to the Pt(IV) center (Fig. 8B).

The observed discrepancy between the rate of reduction of Pt(IV) prodrugs with axial hydroxyl groups in a living system and their electrochemical potential may be explained by the fact that Epc measurement represents a direct outer-sphere transfer of electrons from the cathode to the Pt(IV) center, whereas prodrug reduction in a biological environment occurs *via* a fundamentally different pathway, namely, in the presence of reducing agents, *via* an inner-sphere mechanism.

2.7. *Reduction of Pt(IV) complexes with external stimuli*

Activation of conventional Pt(IV) prodrugs occurs *via* the reaction with intracellular reductants, such as ascorbate and reactive cysteines, which cannot be localized exclusively in tumor tissue. To address this issue, Pt(IV) prodrugs could be designed as chemotherapeutics with controllable mode of activation. Use of external

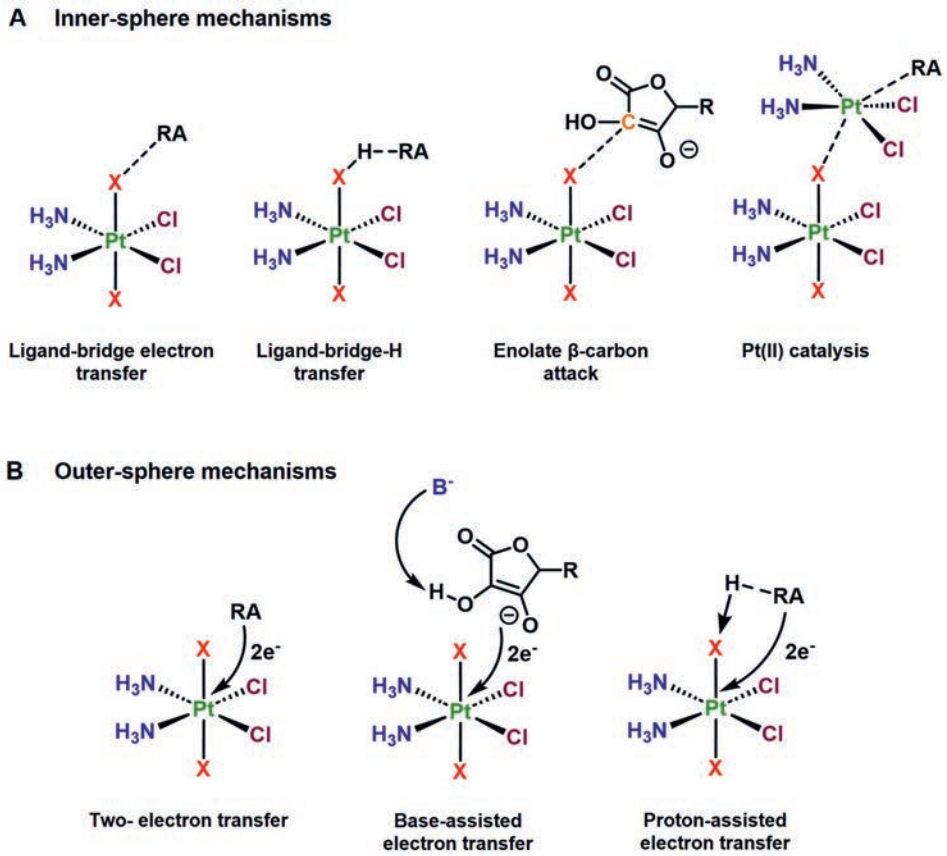

Figure 8 Mechanisms of Pt(IV) complexes reduction. (A) Inner-sphere mechanisms of reduction by general reducing agent or by ascorbate anion. (B) Outer-sphere reduction mechanisms. Reproduced from[61], licensed under a Creative Commons Attribution-NonCommercial 3.0 Unported Licence.

stimuli to induce Pt(IV)/Pt(II) transformation is highly attractive since it allows for precise spatiotemporal control over the activation site and thus could minimize side-effects of therapy with Pt(IV)-based therapeutics (Fig. 9)[14,15].

One of such external stimuli for controllable activation of Pt(IV) is light irradiation. Photoactivatable Pt(IV) prodrugs reported to date could be divided into two groups. The first group are Pt(IV) prodrugs with equatorial diiodo- and diazido axial ligands[71]. Equatorial diiodo Pt(IV) complexes were first to be considered for as light-activated prodrugs, however, their significant dark toxicity due to high reactivity towards biothiols prevented further research[72]. Pt(IV) prodrugs with equatorial *trans*-diazido ligands exhibit increased stability and undergo reductive elimination with release of azidyl radical $N_3\cdot$ under blue-light irradiation, with the substituent release of cytotoxic *trans*-Pt(II) species, which results in a significant increase in cytotoxicity when exposed to 450 nm blue light[71,73].

Photoactivated Pt(IV) prodrugs in the second group are conventional Pt(II) drugs (CDDP, carboplatin, etc.) conjugated with light-sensitive axial ligands. Light excitation of those ligands induces electron transfer from the axial ligand to the Pt(IV) center, resulting in photoreduction and release of Pt(II) complex[74,75]. Approaches to the design of Pt(IV) prodrugs with photoactive axial ligands, and the photobiology of those complexes has been the subject of multiple reviews[15,20,76,77]. In 2023, Deng et al.[78] reported Pt(IV) prodrug with coumarin-based photosensitive ligand which released Pt(II) complex carboplatin and oxidized biomolecules in an oxygen-independent manner upon two-photon activation with 880 nm light. Light-controlled activation of Pt(IV) prodrugs can also occur when the light-sensitive compound is employed as a photocatalyst and is not covalently linked to the Pt(IV) prodrug. Thus, a biorthogonal catalytic activation of Pt(IV) prodrugs *via* small-molecule riboflavin derivatives and flavoproteins was reported[79–81].

The crucial limitation of light-activated therapeutics is low penetrating ability of light in biological tissues[82–84]. On the contrary, ultrasound (US) possesses extraordinary penetration depth up to 15 cm and beyond, which allows it to reach deep tumors[85,86]. In liquid media, ultrasound induces the formation of cavitation bubbles, which collapses with rapid increase in local pressure and temperature, and generates light *via* sonoluminescence process[87,88]. Thus, light-sensitive axial ligands of Pt(IV) prodrugs could be employed as sonosensitizers to promote controlled activation of Pt(IV) prodrugs under ultrasound[89,90]. In 2023, Liu et al.[91] utilized carbocyanine axial ligand as a sonosensitizer in the design of ultrasound-activatable Pt(IV) prodrug cyaninplatin, capable of controlled carboplatin release and ROS formation, which demonstrated high therapeutic efficacy on 4T1 tumor-bearing mice.

Controlled activation of prodrugs by ionizing radiation is a novel therapeutic modality, which has recently emerged as an active area of scientific research[92]. The advantage of activating prodrugs with radiation lies in the high penetrating power of ionizing radiation, as well as in its own strong anticancer therapeutic effect[93,94]. Notably, ionizing radiation induces water radiolysis, which produces highly active hydrated electrons e_{aq}, capable of Pt(IV) reduction[95]. Two approaches towards radiotherapy-induced Pt(IV) prodrugs activation have been recently demonstrated[96,97]. X-ray-induced Pt(IV) reduction in aqueous media, or activation of Pt(IV) prodrugs in tumors in the presence of β-emitting radionuclide[96,97]. Thus, Fu et al.[96] reported rapid and efficient reduction of OXA-based Pt(IV) complex by X-ray in water *via* hydrated electrons e_{aq}. from water radiolysis. In 2024, Wang et al.[98] studied Pt(IV) complex reduction *via* [^{18}F]FDG (2-[^{18}F]- fluoro-2-deoxy-D-glucose), which is also attributed to hydrated electrons generated by water radiolysis resulting from the decay of radionuclide ^{18}F. Also in 2024, Guo et al.[97] reported an elegant and effective therapy of 4T1 tumor with Pt(IV)-gemcitabine prodrug and radiolabeled antibody [^{177}Lu]Lu-PKU525 as a β-ray emitter, which suppressed subcutaneous tumor growth with no significant adverse effects.

3. Nanocarrier-based delivery of Pt(IV) prodrugs: Key points

Generally, NPs are expected to accumulate in tumor tissue *via* enhanced permeability and retention (EPR) effect, which is driven

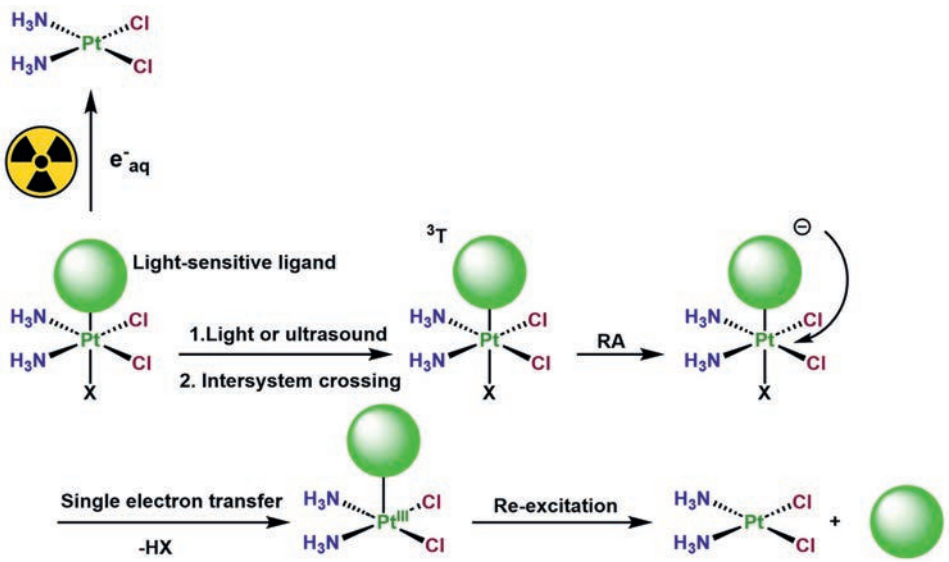

Figure 9 Controlled activation of Pt(IV) prodrugs by light, ultrasound or X-ray. RA: general reducing agent (only at this Figure RA is Reducing Agent). Activation of Pt(IV) prodrugs by radiation is independent of the nature of the axial ligand.

by structural features of solid tumors, such as hypervascularization, altered vascular architecture, and impaired lymphatic drainage[99]. However, the EPR effect is counteracted by fluid shear stress, which causes vascular compression and blood outflow, which can wash NPs out of tumor. Except at the tumor edges, transvascular and intravascular gradients in tumors are virtually zero, and pressure gradient-dependent transport of NPs is hampered. As a result, only ∼0.67% of the administered NPs dose is delivered to tumors[100].

Chemotherapeutic agents are most often administered intravenously (i.v.). After i.v. administration, the drug is exposed to blood components, such as proteins, lipids, reducing agents, radicals, enzymes, and others[101]. This is the "Achilles' heel" of low-molecular Pt(IV) prodrugs, which usually undergo rapid hydrolysis and deactivation at this step; thus, an encapsulation of Pt(IV) prodrugs in nanocarriers is expected to protect them from premature degradation and rapid elimination from the bloodstream. However, low-reactive NPs circulating in the blood are easily recognized and opsonized by opsonin, making NPs more susceptible to phagocytic clearance from blood by the mononuclear phagocyte system (MPS). MPS is responsible for the degradation and removal of exogenous substances from the blood, such as foreign pathogens and therapeutic NPs[102].

Ideally, NPs should avoid clearance from blood by the MPS[103], remain in the circulation for a long time to ensure sufficient accumulation in tumor tissues[104,105]. Small changes in the physico-chemical properties of NPs may have a significant impact on their therapeutic effectiveness[106]. Since the physical properties of NPs, such as size, shape, and surface charge and coating are dramatically affecting drug delivery efficiency, we will briefly discuss each of these parameters below.

3.1. Physico-chemical properties of NPs

3.1.1. Shape

The shape of NP can influence its fluidity and tissue accumulation. Thus, Shaw et al.[107] demonstrated that the uptake efficiency of magnetic NPs of various shapes in tumor lesions follows a descending order of spherical, elliptical, cylindrical, disc-shaped, conical, tubular, hollow core, spiral, etc. Rod-shaped NPs can be more efficiently taken up by breast cancer cells and accumulate in the brain and lungs than spherical NPs[108]. Also, stimulus-responsive change of NP's shape to improve tumor accumulation is possible[109].

3.1.2. Size

The size of NPs critically determines their biodistribution and therapeutic efficacy. Generally, NPs with ∼100 nm size are able to penetrate the endothelial layer in the peripheral vascular wall, allowing them to participate in blood circulation. Smaller NPs (<100 nm) tend to exhibit enhanced cellular uptake and prolonged circulation time, while larger NPs (>100 nm) may offer higher drug loading capacity but reduced cellular uptake[110−112]. Since the size of NPs is larger than the capillary pore diameter, their volume of distribution is limited by the route of administration. When administered i.v., NPs remain confined to the bloodstream, thereby demonstrating poor organs and tissues penetration. Since the capillaries supplying tumors with blood are typically highly perforated, NPs are prone to intratumoral accumulation *via* passive targeting[113]. NP's average size also influences their biodistribution. Thus, NPs larger than 1 μm tend to be filtered or excreted by the liver tissue, while NPs larger than 200 nm but smaller than 1 μm generally accumulate in the spleen[114].

3.1.3. Charge (Zeta-potential)

The quantitative characteristic of the charge of NPs is zeta potential (ζ), a measure of the electrical potential at the slipping plane of a particle in a colloidal system[115]. ζ close to zero suggests a low surface charge and a higher tendency of NP for aggregation[116]. A charge of NPs can significantly influence their fate after i.v. administration. The inner surface of blood vessels and the surface of cells possess numerous negatively charged components, which leads to a large number of nonspecific interactions with cationic NPs and repulsion of anionic ones[117]. The positive surface charge of NPs is a key factor in adsorption-mediated transcytosis; thus, cationic NPs can significantly accumulate in tissues due to the high rate of transvascular penetration; however, cationic NPs are easily recognized by the MPS system and are quickly cleared from the bloodstream. In contrast, NPs with a neutral and negative charge are generally demonstrate low intracellular accumulation, but possess a long bloodstream circulation[118]. Thus, cationic NPs act as "cell magnets" for rapid adhesion to the mucosa, while anionic NPs serve as "long-range travelers", avoiding detection by the immune system and improving systemic transport. Given this "charging dilemma", NPs that can change their surface charge from negative in the bloodstream to positive upon reaching tumor tissues have shown great promise for targeted drug delivery and improved tumor penetration[119−121]

3.1.4. Surface modification

One of the main obstacles for NPs to achieve a significant tumor accumulation is their rapid removal from the bloodstream by the MPS[122,123]. Most NPs under physiological conditions are coated with a wide range of proteins, the so-called "protein corona", which alters their properties, masking their surface characteristics. Opsonins can enhance the uptake of NPs by the MPS because adsorption of opsonins on the particle surface makes them more palatable to phagocytes[124]. Surface biomodification of NPs offers several benefits[125,126]. Modification of the NP's surface with polyethylene glycol (PEG), carbohydrates, acetyl groups, or protein moieties (arginine-glycine-aspartate (RGD) peptide, albumin) may significantly enhance the retention time[127]. Hoverer, despite PEG coatings is beneficial for stability and stealthiness, it can also hinder interactions of NPs with target cells, leading to decreased cellular uptake, inefficient endosomal escape, and ultimately reduced intracellular delivery; this phenomenon is also known as the "PEG dilemma"[128].

3.2. Structural types of nanocarriers for Pt(IV) prodrugs

To date, various nanotherapeutic agents based on Pt(IV) prodrugs have been developed. Multiple design paradigms to obtain nanoformulations of Pt(IV) prodrugs have been utilized, including polymeric NPs, lipid-based NPs, inorganic NPs, biological NPs, etc. Each type of NPs possesses specific characteristics that can be employed for various drug delivery purposes[129]. Pt(IV) prodrugs can be encapsulated into nanocarriers by various methods, including physical encapsulation, coordination interactions, electrostatic adsorption, self-assembly, chemical conjugation, etc[36].

While most nanocarriers used for Pt(IV) prodrugs are lipid and polymer NPs, other approaches have also demonstrated great potential, including self-assembly of Pt(IV) prodrugs into micelles, NPs based on host−guest interactions, etc. The following

subsection discusses key strategies towards synthesis of nanoformulations of Pt(IV) prodrugs, including brief overviews of selected examples (Fig. 10). Most synthesis methods involve loading the active Pt(IV) drug into an external carrier using various methods. To discuss this, two parameters need to be clarified, namely:

Encapsulation efficiency (EE%): Defines how effectively the formulation entraps the drug.

$$\mathrm{EE}\,(\%) = \left(\frac{\text{Weight of drug in NPs}}{\text{Total weight of drug added}}\right) \times 100 \quad (1)$$

Drug loading (DL or LC, %): Indicates the percentage of the nanoparticle's mass that is actually the drug.

$$\mathrm{DL}\,(\%) = \left(\frac{\text{Weight of encapsulated drug}}{\text{Total weight of drug-loaded NPs}}\right) \times 100 \quad (2)$$

3.2.1. *Self-assembly of Pt(IV) prodrugs*

One of the most straightforward approaches to NPs design is their self-assembly from the monomer drug into micelles. Amphiphilic molecules consisting of hydrophilic and hydrophobic groups can typically be assembled into NPs in aqueous solution when critical micelle concentration (CMC) is reached[130,131]. The micelle formation usually takes place in aqueous solution *via* solvent exchange approach The formation of micelles is driven by π-interactions between the drug's molecules in polar solvents[132], which sharply decreases the free energy of the solution by declining the interaction between the hydrophobic groups and surfactant[133,134] This widely-used synthetic approach is beneficial due to its simplicity and high reproducibility[135]. One significant limitation of this method is that the drug should contain both polar and non-polar moieties to form stable micelles. In 2024, Sun et al.[130] and in 2025 Yan et al.[131] reported amphiphilic Pt(IV) prodrugs with non-polar lipid tail and polar alendronate axial ligands, which self-assembled into NPs **20-NP** and **21-NP**. Due to the presence of osteosarcoma-targeting alendronate moiety, **20-NP** and **21-NP** selectively accumulated in osteosarcoma cells *in vitro* and in orthotopic osteosarcoma tumor *in vivo*.

3.2.2. *Pt(IV)prodrugs incapsulated in lipid NPs*

Synthesis of lipid NPs is a widespread method of drug delivery, which have found clinical success with FDA approval of liposomal formulation of doxorubicin (Doxil) in 1995[136]. Advantages of lipid NPs are biocompatibility, biodegradability and good EE[137]. Hydrophobic Pt(IV) prodrugs can be encapsulated in block copolymers, such as distearoyl phosphatidyl ethanolamine-PEG (DSPE-PEG2000), thereby forming micelles, liposomes, solid lipid NPs, and microemulsions[138]. In 2026, Zhang et al.[139] reported lipid nanoparticle formulation based on FDA-approved lipid combination SM-102:DSPC:cholesterol:DMG-PEG together with lipid-modified Pt(IV) prodrug for efficient encapsulation of siXkr8 and *ANX5* mRNA. Furthermore, ratio of Pt(IV) prodrug **26** to the lipids in the formulation was optimized to achieve maximized mRNA transfection efficiency. Tang et al.[140] used the same approach in an elegant design of **7-NP** nanomicelles capable of efficiently releasing Pt and NO while

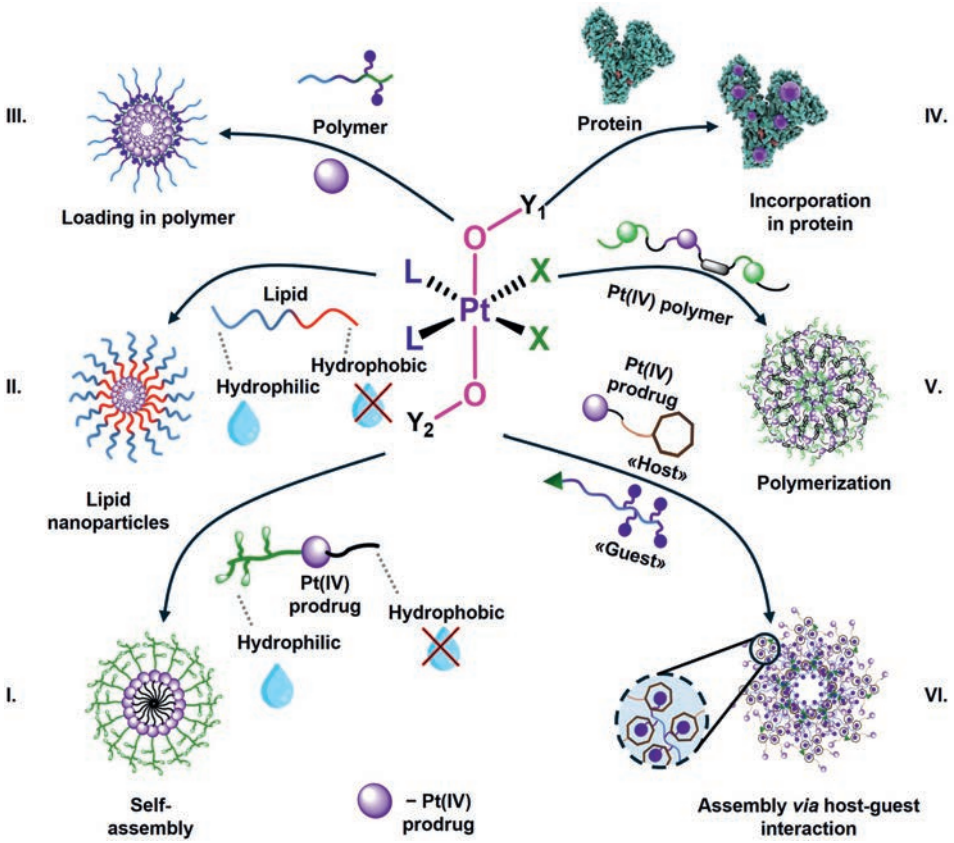

Figure 10 Design strategies for various nanoparticle platforms for Pt(IV) prodrugs. (I) Self-assembly of amphiphilic prodrug (II) Encapsulation in lipids (III) Loading in polymers; (IV) Polymerization (V) Encapsulation in protein (VI) Guest−Host interactions.

overcoming CDDP resistance. DBCO-modified DSPE-PEG polymer used for encapsulation enabled active targeting of orthotopic lung tumor and administration of the nanomicelles *via* inhalation.

3.2.3. Loading of Pt(IV) prodrugs in polymers

Loading Pt(IV) prodrugs into polymers is a versatile approach, since the size, ζ, and DL can be tuned by varying the structure of the polymer carrier[141]. The drug release profile can also be controlled by incorporating cleavage sites into the polymers that are sensitive to the tumor microenvironment, such as low pH (<6.0) or high glutathione (GSH) levels[142]. In addition, the antiproliferative activity profile of the resulting NPs can be modified by co-encapsulating multiple drugs into one polemer carrier, or by functionalizing the polymer with tumor-targeting moieties.

Yang et al.[143] encapsulated Pt(IV) prodrug **10** into GSH-responsive polymer mPEG−P(Phe-co-Cys^2) to overcome poor solubility of the complex **10** and to increase tumor selectivity of **10-NP** since polymer cleavage and prodrug **10** release was expected to occur only in GSH-rich tumor tissues. In 2024, Li et al.[144] reported nanoformulation of the Pt(IV) prodrug **15** with octyl axial ligands, encapsulated into polymer with GSH-responsive S−S−S groups. The resulting **15-NP** demonstrated high EE of prodrug **15**, GSH-triggered Pt release, and GSH consumption in tumor cells *in vitro,* along with the release of H_2S.

3.2.4. Polymerization of Pt(IV) prodrugs

Despite high flexibility of polymers as drug nanocarriers, such nanocarriers are suffer from several disadvantages, such as low EE and "burst release" of the encapsulated drug post-administration[145,146]. Instead of loading Pt(IV) prodrug in polymer, Pt(IV) complex itself can be utilized as a monomer chain. Such approach drastically improves EE when compared to co-encapsulation of polymer with small-molecule Pt(IV) prodrug, while retaining the versatility that is inherent to the polymer design[147]. In addition, Pt(IV) monomer chain serve as reduction-responsive chain of polymer, which opens up opportunities for GSH-triggered drug release.

In 2022 Wei et al.[148] reported a polymeric chain with Pt(IV) complex with photosensitizer and nucleus-targeted peptide as monomer for combined photodynamic (PDT) and photoactivated chemotherapy. The resulting polymeric **38-NP** was capable of photocontrolled Pt release and accumulated in the nucleus of 4T1 cells. Wang et al.[121] utilized this approach to obtain charge-reversing NPs **35-NP** based on Pt(IV)-containing polymer.

3.2.5. Encapsulation of Pt(IV) prodrugs in proteins

A perspective approach to deliver Pt(IV) prodrugs to tumor tissue is a loading of a small-molecule complexes into biological proteins, like human serum albumin (HSA). Generally, biological proteins are biocomparable, and biological protein-based NPs demonstrate high loading efficiency, long bloodstream circulation and increased tumor accumulation[149]. In 2024, Xie et al.[150] encapsulated Pt(IV) prodrug **32** with perfluorocarbon axial ligand into HSA and the resulting **32-NP** demonstrated great accumulation in orthotopic osteosarcoma tumor as well as enhanced tumor inhibition rate compared to CDDP and HSA-free prodrug **32**. In 2022, Wang et al.[151] reported two distinct methods for the encapsulation of Pt(IV) prodrugs **19a−d** into HSA. Pt(IV) prodrugs **19a** and **19b** with lipid axial ligands were loaded in HAS non-covalently, while **19c** and **19d** were conjugated with HSA covalently *via* maleimide moiety. **19a-NP** with non-covalently loaded Pt(IV) prodrug **19a** demonstrated the most optimal *in vitro* activity and tumor-targeting ability.

3.2.6. Pt(IV)-based nanoparticle assembly via host−guest interaction

Cyclodextrins (CDs) possess a hydrophilic exterior surface and hydrophobic interior cavity which makes them optimal for the design of supramolecular host−guest systems[152]. NPs based on cyclodextrins are a versatile platform capable of controlled release of loaded drugs and tumor-targeted delivery. A significant advantage of host−guest systems compared to conventional co-delivery approach is precise control over the composition of NPs. In 2021, Deng et al.[153] used cyclodextrin-modified Pt(IV) prodrug and NO-releasing moiety in the design of **7-NP** based on host−guest interaction with adamantine-modified PEG-*b*-Plys. The ratio between NO-donor and Pt(IV) prodrug could be tightly controlled, which allowed optimization of the ratio for maximized antiproliferative activity.

3.2.7. Other methods

A variety of alternative approaches to nanoparticle design are also utilized. Thus, inorganic NPs are being extensively utilized as carriers for antitumor drugs[154]. Furthermore, *in situ* nanoparticle assembly and interfacial polymerization have emerged as a promising methods for developing nanoformulations[155].

In 2023, Wei et al.[156] reported $CaCO_3$-based NPs with adsorbed Pt(IV) prodrug with axial 11-mercaptoundecanoic acid. The terminal SH groups of Pt(IV) prodrug **18** were then covalently linked in an oxidation polymerization reaction forming a polymer Pt(IV) complexes with S−S linker. Such design prevented leakage of the Pt(IV) complex from the NPs when outside tumor tissue, while low pH and high GSH content in tumor environment prompted release of Ca^{2+} and Pt(IV) prodrug from **18a-NP**, which leads to GSH consumption and an increase in intracellular ROS.

In 2024, Liu et al.[157] used upconversion NPs (UCNP) as a nanocarrier of Pt(IV), capable of NIR light-controlled Pt(II) release. The Pt(IV) prodrug **44** was loaded into the $NaYF_4$:Yb,Tm@$NaYF_4$ NPs, which exhibit 475 nm fluorescence when irradiated with 980 nm laser. The resulting **44-NP** demonstrated almost complete release of axial phenylbutyrate ligand and Pt after only 15 min of irradiation with 980 nm laser (0.48 W/cm^2), while in the dark in the presence of 10 mmol/L GSH 50% Pt release was achieved in around 5 h.

4. Pt(IV)-based NPs reported in 2022−2026

Considering the superior advantages of using Pt(IV) prodrug nanocarriers instead of small-molecule therapeutic agents, numerous Pt(IV)-based nanomedicines have been developed to date. Pt(IV)-based nanomedicines differ in their production method, surface modifications, active targeting, and the method of active component release. The main achievements in the development of Pt(IV)-based nanomedicines, reported in 2022−2025, are summarized in Table 1. We have classified the developed NPs by their mechanism of biological action, which achieves the maximum therapeutic effect. Five main interrelated approaches to the development of NPs based on Pt(IV) prodrugs were segregated: NPs capable of overcoming resistance to CDDP, NPs acting on the tumor microenvironment, NPs stimulating the immune response, NPs directed to tissue or cellular organelles, and NPs

capable of exerting a therapeutic effect under the influence of an external stimulus.

4.1. Pt(IV)-based NPs to overcome multidrug resistance

Tumor resistance to CDDP arises through multiple mechanisms, including enhanced drug efflux (*e.g.*, *via* P-glycoprotein (P-gp) or ATP7A/B), increased GSH-mediated antioxidant mechanisms, improved DNA damage repair, reduced intracellular accumulation (*e.g.*, *via* CTR1 downregulation), biochemical and epigenetic alterations, leading to therapeutic failure. The development of chemotherapeutic drugs capable of overcoming resistance to CDDP is an urgent task of modern medicinal chemistry[158,159]. CDDP's main molecular mode of action consists of five key steps: cellular uptake, activation, DNA binding, formation of DNA cross-links, and apoptosis-inducing protein cascade[10]. CDDP can enter the cancer cell both through passive diffusion and through organic cation transporters, such as copper transporter CTR1[160,161]. Upon entering the cell CDDP undergoes ligand exchange of one of its chloride ligands to water, and the resulting negatively charged mono-aquated form can enter the nucleus and bind to the nuclear DNA[162,163]. It should be noted that CDDP can also target mitochondria, which alco contain DNA, leading to cell death[164−166]. CDDP induces DNA damage by forming a variety of intra- and interstrand crosslinks which inhibit DNA replication and transcription[167,168]. CDDP-induced DNA damage leads to the activation of the p53 protein, which in turn activates a cascade of pro-apoptotic proteins, including PUMA, BAX, and BAK, while suppressing the anti-apoptotic Bcl-2 protein[169,170]. Activated BAX and BAK translocate to mitochondria, leading to the permeabilization of their membrane and release of cytochrome *c* into the cytoplasm, which activates the caspase cascade, ultimately leading to cell death[171−173].

To combat the cytotoxic activity of CDDP, tumor cells utilize a variety of mechanisms that negate or prevent DNA damage and subsequent apoptosis. Mechanisms of CDDP resistance are generally classified according to the specific step within the CDDP mode of action that is affected: pre-target, on-target, and post-target[174]. A generalized mechanism of CDDP mode of action along with the pathways of cell resistance to CDDP is shown in Fig. 11.

Pre-target resistance mechanisms include a number of ways to prevent CDDP from reaching the nuclear DNA. CDDP treatment induces degradation of the CTR1 transporter, which contributes to resistance[175,176]. A variety of membrane transporters, including P-gp and adenosine triphosphate ATP7A/B, contribute to the CDDP resistance by increasing its efflux from the tumor cells[177−179]. In the cytoplasm, CDDP is scavenged by nucleophiles like GSH, which is catalyzed by the glutathione *S*-transferases (GST) enzyme[180,181].

A significant contribution to cell resistance to CDDP is due to the high activity of on-target resistance mechanisms of DNA repair in response to CDDP-induced DNA damage. CDDP lesions are removed from the DNA by repair systems, mostly nucleotide excision repair, a protein complex that replaces the damaged nucleotides[182]. Recent studies suggest that defective base excision repair activity contributes to the removal of platinum adducts from the DNA[183]. Mismatch repair system is another system of DNA reparation, which detects CDDP lesions and transmits a proapoptotic signal upon failure to repair CDDP crosslinks[184−186].

Post-target mechanisms of CDDP resistance include alterations in the transduction of pro-apoptotic signals in response to DNA damage. Mutations in the p53 protein result in loss of its ability to induce apoptosis, which occurs in approximately half of human neoplasms[174,187,188]. Another way for tumor to prevent apoptosis is an overexpressing the key regulator of p53, MDM2, which binds with p53, leading to its degradation[189,190]. MDM2 overexpression is associated with the hyperactivated PI3K/Akt pathway, which also promotes upregulation of survivin, a protein that inhibits caspase activity and thus promotes chemo resistance[191−193]. Additionally, CDDP resistance is also associated with the increased expression of antiapoptotic proteins of the Bcl-2 family, which prevents Bax from translocating into mitochondria[194].

4.1.1. Regulating cholesterol metabolism

Chemotherapy resistance was found to be related to cholesterol metabolism, since cholesterol accumulation allows cancer cells to evade apoptosis and keep dividing and proliferating, which may be regulated by inhibiting the biosynthesis of cholesterol or depleting its cellular excess[195,196]. Alterations in lipid metabolism are a well-known hallmark of cancer[197] and cholesterol accumulation is attributed to the drug resistance of prostate, pancreatic, bladder, and breast cancer[198]. Regulation of cholesterol metabolism may affect cellular architecture and signaling processes in cancer cells; furthermore, it may induce ferroptosis, a programmed necrotic cell death characterized by intracellular iron accumulation and lipid peroxidation[199] and pyroptosis[200,201].

In 2025, Guo et al.[202] reported a series of NPs based on Pt(IV) prodrugs **1a−d** with fenofibrate acid (FA) in an axial position, capable of regulating cholesterol metabolism and inducing cell death by increasing reactive oxygen species (ROS) level and depleting GSH, thereby contributing to overcoming CDDP resistance (Fig. 12). For NPs design, the authors proposed OXA, a third generation platinum drug that often causes tumor cells to become resistant to therapy, and CDDP[203,204]. **1a−d NPs** released OXA/CDDP and FA in the presence of GSH, NaAsc, and under acidic pH 5.5. Also, CDDP-based **1a-NPs** activated lipid regulator peroxisome proliferator-activated receptors alpha (PPARα) which reduced cholesterol level and increased membrane permeability. In addition to causing cell death *via* mitochondrial damage and apoptosis, **1a-NPs** induced ferroptosis of ovarian cancer A2780 cells, as indicated by decreased intracellular GSH level, reduced glutathione peroxidase 4 (GPX4) expression, and elevated lipid peroxidation level. The biodistribution of **1a-NP** was generally similar to that of CDDP, however, **1a-NP** showed increased accumulation in the tumor. On the A2780 xenograft tumor, **1a-NP** inhibited tumor growth significantly more than CDDP, with tumor growth inhibition (TGI) rate of 8.5-fold greater, which was accompanied by a reduction in mice body mass compared to that of CDDP group; also H&E staining as well as BUN, UA, and creatinine (CR) levels evaluation demonstrated no damage to the relevant organs caused by **1a-NP**.

4.1.2. Endoplasmic reticulum stress induction

Endoplasmic reticulum (ER) stress generally occurs in tumors due to stressful extracellular environmental challenges, such as hypoxia, nutrient deprivation, and pH changes. Tolerance to CDDP-induced ER stress inhibits apoptosis, prevents an imbalance in ER and mitochondrial calcium homeostasis, and maintains cell survival, thus leading to CDDP resistance[205,206]. Therefore, moderate ER stress contributes to cancer cell survival and chemotherapeutic resistance; however, excessive and prolonged ER stress results in apoptosis, which can be used in antitumor therapy[207,208].

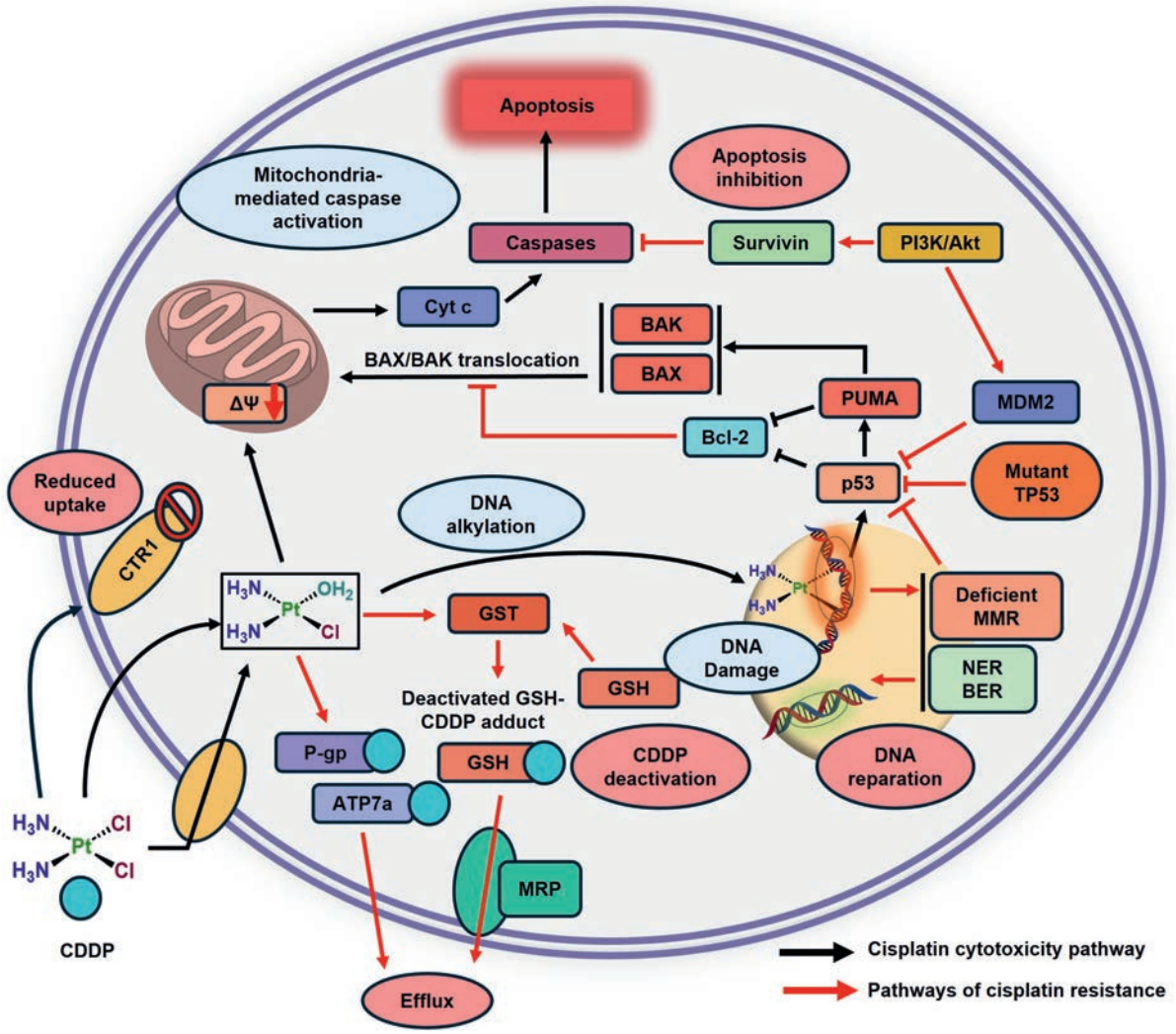

Figure 11 Cisplatin main molecular mode of action (black arrows) and main resistance pathways (red arrows). Cisplatin enters the cell *via* passive diffusion or *via* active transport, where it exchanges chloride ligand into water and binds the DNA with the formation of DNA crosslinks. Damaged DNA results in the formation of pro-apoptotic signal, which activates pro-apoptotic proteins, resulting in programmed cell death. Main mechanisms of resistance to cisplatin include reduced uptake, deactivation and increased efflux (pre-target), enhanced DNA repair (on-target) and suppression of pro-apoptotic signal (post-target).

Natural flavonoid isoliquiritigenin (ISL) is reported to exhibit an antitumor effect on breast and colon cancers *via* several signaling pathways, including ER stress induction[209,210]. In 2024, Yang et al.[211] reported NPs based on Pt(IV) prodrug **2** with PEG and docosahexaenoic acid, in axial positions, with was prone to self-assembly with co-encapsulated ISL in 10:1 ratio (Fig. 13). The release of both ISL and CDDP from **2-NP** in the presence of GSH and H_2O_2 was confirmed. **2-NP** accumulated specifically in the ER of ovarian adenocarcinoma SKOV-3 cells and induced ER stress accompanied by GSH depletion, ROS formation (including DHA peroxides), ER swelling, an increased expression of caspase 12, C/EBP homologous protein (CHOP), and its upstream glucose-regulated protein (GRP78). Cy5-labeled **2-NP** demonstrated high intratumoral accumulation in the patient-derived ovarian cancer model of BALB/c mice according to fluorescence data and inductively coupled plasma mass spectrometry (ICP-MS).

An antitumor activity study demonstrated the ability of **2-NP** to significantly inhibit the growth of patient derived xenograft (PDX) tumors, with tumor volume 2.5-fold lower than in the CDDP-treated group, with no substantial change in weight and no damage to main organs. It is important to note that ISL-free **2-NP-m** showed a therapeutic efficacy lower than that with ISL-loaded **2-NP**, which obviously indicates the effectiveness of co-therapy. Importantly, despite the high therapeutic efficacy of the equimolar mixture of CDDP and ISL, drug mixture therapy was accompanied by significant weight loss during therapy. This clearly indicates the greater safety of using nanoformulations that include several drugs instead of a mixture of low-molecular drugs.

4.1.3. Cyclin-dependent kinases 4 and 6 (CDK4/6) inhibition

Cyclin-dependent kinases 4 and 6 (CDK4/6) are fundamental drivers of the cell cycle, which are required for the initiation and progression of various malignancies[212]. CDK 4/6 inhibitors effectively halt cell proliferation by preventing cancer cells from transitioning from the G1 phase to the S phase[213], and an inhibition of CDK4/6 is a quite promising therapeutic approach[212].

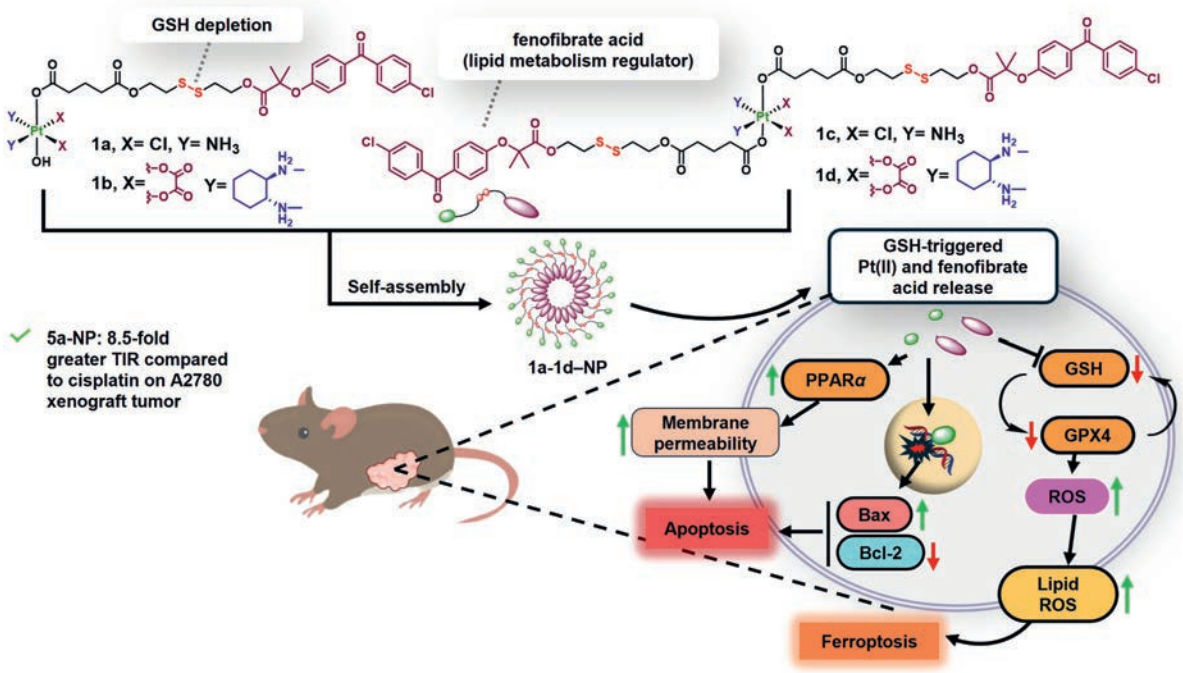

Figure 12 Series of Pt(IV) prodrugs **1a−1d** containing the lipid metabolism regulator fenofibrate acid and their self-assembly into nanoparticles **1a-NP−1d-NP**. The intracellular mechanism of **1-NP**: induction of apoptosis and ferroptosis[202].

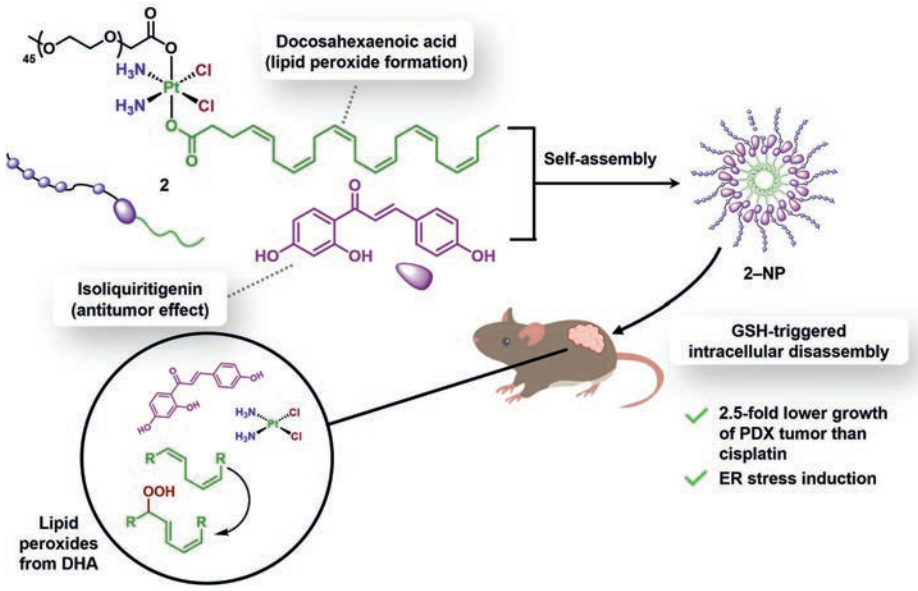

Figure 13 Pt(IV) prodrug **2** functionalized with ROS-producing ligand docosahexaenoic acid and its self-assembly with isoliquiritigenin into **2-NP**[211].

Also, CDK4/6 inhibitors are able to increase cell sensitivity to CDDP by lowering the cell proliferation rate, keeping cancer cells in a phase that is more sensitive to CDDP, thereby reducing drug resistance[214].

In 2025, Zhu et al.[215] reported an amphiphilic Pt(IV) prodrug **3** with biotin and a lipid chain as axial ligands, capable of self-assembly onto Pt(IV) NPs **3-NP** with a biotin outer shell, which also served as a carrier of ribociclib (Rib), a highly effective CDK inhibitor (Fig. 14)[216]. **3-NP** showed the ability to release both Rib and CDDP in the reducing environment. **3-NP** showed higher intracellular accumulation than CDDP, as well as greater toxicity due to the presence of CDK inhibition. A significant tumor-specific accumulation of **3-NP** was proved using the BALB/c mouse model of bladder cancer with the biotin + B49 cell line *via* both the fluorescence detection of Cy7-labeled **3-NP** and post-mortem ICP-MS. A high antitumor efficacy of **3-NP** was demonstrated on the same tumor model; a significant TGI compared to CDDP, with reduced toxicity and less weight loss

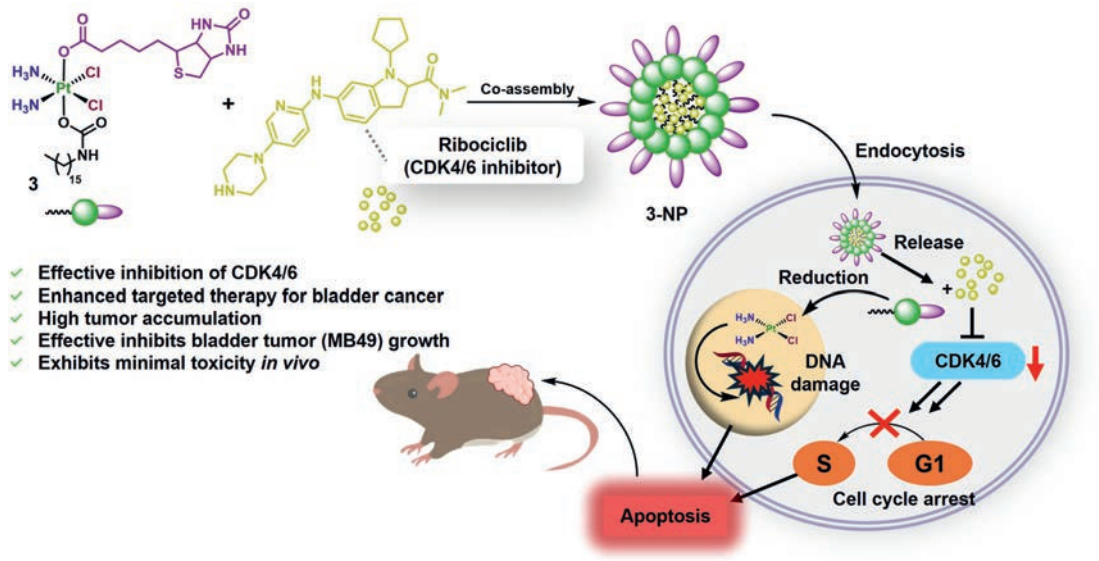

Figure 14 Lipophilic Pt(IV) prodrug **3** functionalized with hydrophilic targeting ligand biotin and its co-assembly with CDK4/6 inhibitor ribociclib into nanoparticles **3-NP**. The intracellular mechanism of **3-NP**: apoptosis of cancer cells induced by DNA damage and enhanced by cell cycle arrest in G1 phase[216].

were revealed. A comparison of a therapeutic efficacy of equimolar mixture of CDDP with Ribociclib with the corresponding nanoformulation **3-NP** clearly indicates a preference for using the latter, due to greater efficiency in cytotoxicity, apoptosis, and delivery of Pt to tumor tissues. Even though weight loss during **3-NP** therapy was comparable to that during CDDP therapy, the high survival rate after **3-NP** therapy also confirms its greater biocompatibility.

4.1.4. Heme oxygenase inhibition

Heme oxygenase (HO) is an enzyme that catalyzes the degradation of heme into biliverdin, carbon monoxide (CO), and free iron (Fe^{2+}) in the presence of molecular oxygen (O_2) and reduces nicotinamide adenine dinucleotide phosphate (NADPH)[217]. HO-1 is involved in the adaptive response to cellular stress and in attenuating inflammation. An overexpression of HO-1 in cancer cells correlates with tumor growth, aggressiveness, metastatic and angiogenetic potential, and immune escape[218]. Additionally, HO-1 may counteract the effects of certain chemotherapeutic drugs, including CDDP[219]; therefore, inhibition of HO-1 could be promising for antitumor research.

In 2025, Liu et al.[220] reported an amphiphilic Pt(IV) prodrug **4** with HO-1 inhibitor (HO-1i) in the axial position, which self-assembled into Pt(IV)-based NPs **4-NP,** capable of exhibiting CDDP-sensitizing, anti-resistant, and immune-regulating action (Fig. 15). **4-NP** showed the ability to release Pt and HO-1i under an acidic pH in the presence of GSH. **4-NP** retained the potent cytotoxicity of prodrug **4** with the increase in the selection index between HepG2 and normal liver cells. Also, **4-NP** induced a strong S-phase cell cycle arrest, further promoting significant cell apoptosis. Both prodrug **4** and **4-NP** significantly suppressed HO-1 activity *in vitro*, which led to the inhibition of the CO-mediated p38/MAPK pathway, accompanied by downregulation of p38 and MMP-9 proteins. **4-NP** showed the ability to suppress HIF-1α and VEGF-A expression. Both prodrug **4** and **4-NP** proved to target three major mechanisms of drug resistance: drug efflux mediated by P-gp, enzymatic system-related detoxification, and DNA damage repair. Also, both prodrug **4** and **4-NP** showed an ability to promote T-cell proliferation and macrophage polarization. *In vivo* antitumor efficacy **4-NP** was demonstrated on murine hepatoma Hepa1−6 syngeneic tumor model, **4-NP** exhibited more pronounced tumor inhibition than CDDP and prodrug **4**, along with promotion of T cell tumor infiltration and significantly reduced toxicity. High-dose **4-NP** demonstrated significantly superior therapeutic efficacy to CDDP but caused significant weight loss. At low doses, the therapeutic effect was weakened but still greater than that of CDDP, along with minor weight loss. Significant tumor necrosis was also observed in the free **4** and **4-NP** groups, with no obvious damage observed in major organs.

One of the important factors in favor of using NPs is high biocompatibility of ones, as well as lower toxicity in comparison with traditional Pt(II)-based drugs. Thus, the much lower toxicity of **4-NP** in comparison with CDDP clearly demonstrates less side binding in the case of using NPs instead of "naked" chemotherapy. Also, a significant decrease in toxicity of **4-NP** in comparison with CDDP can be associated with disturbances in the mechanism of resistance to CDDP, allowing to reduce the outflow of the drug from the cell and reduce the therapeutic dose, which in combination allows to reduce the toxicity. In general, the use of nanoformulations in combination with the ability to increase the sensitivity of cells to CDDP at the molecular level allows to achieve significant success in therapy.

In summary, co-therapy with Pt(IV) prodrugs and resistance-reducing agents undoubtedly allows for overcoming various mechanisms of CDDP resistance and enhancing therapeutic action. The therapeutic efficacy of the **NP-1-4** nanoparticle confirms the advantages of using nanoformulations of Pt(IV) prodrugs instead of a mixture of a "platinum agent + resistance-reducing drug", given the typically high toxicity of such a mixture compared to the use of nanoformulations. It should also be noted that the **NP-1-4** nanodrug was obtained by the simple self-assembly of amphiphilic prodrugs, without the use of additional carriers. This simple approach to nanoparticle design, on the one

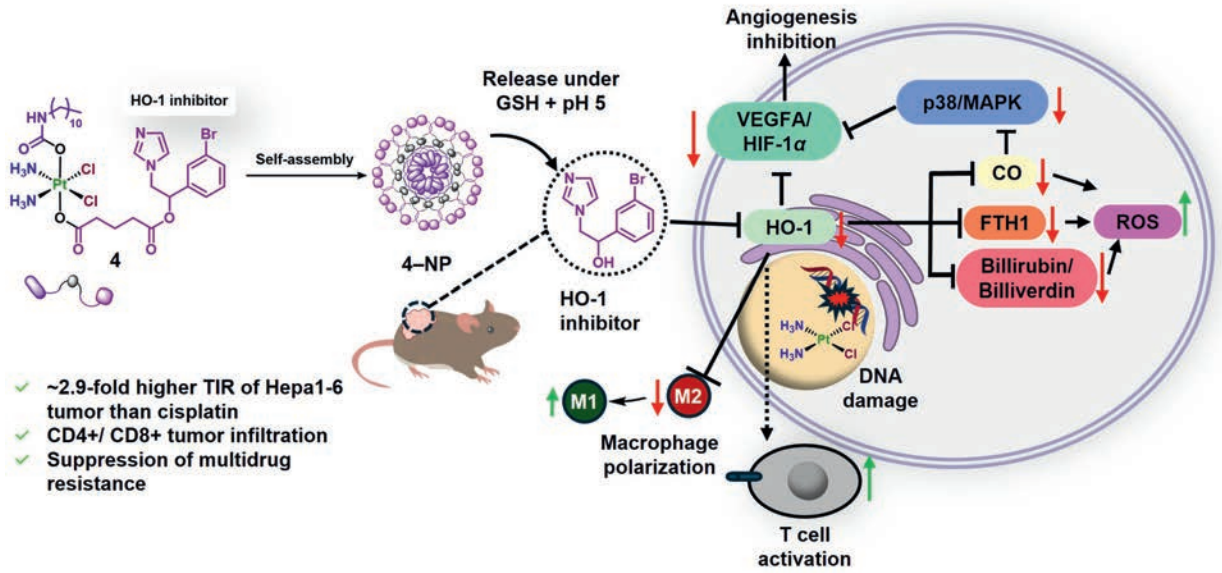

Figure 15 Pt(IV) prodrug **4** with HO-1 inhibitor as axial ligand and its assembly into **4-NP**. The intracellular mechanism of **4-NP**: MDR and TME reversal by inhibition of HO-1[220].

hand, enables high drug loading capacity into the nanomaterial; on the other hand, the resulting NPs are "naked" for the MPS, which seeks to eliminate them. Thus, NPs **1-** − **4-NP** demonstrate significant accumulation in important organs such as the liver, kidneys, and spleen, with the exception of **3-NP**, which contains tumor-targeting biotin on its surface. Overall, the therapeutic approach described in this section is quite promising; however, NPs require greater accumulation in the tumor to maximize their therapeutic effect.

4.2. Pt(IV)-based NPs for tumor microenvironment (TME) remodeling

Cancer is a complex ecosystem whose maintenance of homeostasis requires alteration of a number of metabolic pathways and the involvement of a large number of non-cancerous cells[221]. The major components of the tumor microenvironment (TME) are blood vessels, lymphatic vessels, fibroblasts, immune cells and an extracellular matrix[222]. TME cells and their secreted molecules play critical roles in tumor progression and thus represent attractive therapeutic targets, since the changes in TME may regulate growth, invasion, and metastasis of solid tumor[223,224]. TME includes maintaining a proinflammatory microenvironment, avoiding immune response, and maintaining tumor life support in conditions of altered metabolic functions, such as hypoxia and acidification of the pH of the environment[225].

Hypoxia is an important feature of the tumor microenvironment and a well-known hallmark of cancer that present in 90% of solid tumors[226]. Altering hypoxia level may regulate drug metabolism and significantly enhance both chemotherapy and immunotherapy efficacy. Thus, hypoxia tracers, hypoxia-activated prodrugs, drugs targeting hypoxia-inducible factors and downstream factors are of great interest[227].

The key players in immunosuppressive TME are regulatory T cells (Tregs), myeloid-derived suppressor cells (MDSCs), and cancer-associated fibroblasts, which contribute to immune cell dysfunction. Targeting these elements can completely reverse previously ineffective immunotherapy and enhance the action of chemotherapeutic agents[228,229].

Since TME remodeling has become an effective task for development of effective chemotherapeutic and immune stimulating agents; several Pt(IV) based-nanoagents capable of affecting TME have been reported and summarized below.

4.2.1. Hypoxia overcoming

Hypoxia that occurs in solid tumors due to poor vascularization, limited oxygen supply, and fast cell growth often hinders the efficacy of Pt(II)-based therapy. Hypoxia also activates survival pathways in cancer cells, such as HIF-1α signaling, which promotes DNA repair, resistance to apoptosis, and upregulation of drug efflux pumps, further diminishing CDDP's cytotoxic effects[230,231]. Additionally, the acidic and oxidative stress-resistant microenvironment in hypoxic tumors can alter CDDP's chemical reactivity, reducing its DNA-binding capacity and overall therapeutic impact[232]. Therefore, increasing oxygen concentrations in tumors could be a promising therapeutic strategy.

In 2025, Sun et al.[233] reported a Pt(IV) prodrug **5** with a hydrophobic lipid and a hydrophilic biotin as axial ligands in order to enhance drug accumulation in tumor cells that overexpress biotin receptor (Fig. 16). Upon self-assembly of prodrug **5**, nanodrug **5-NP** was obtained, and further encapsulation with hemoglobin (Hb) yielded **5-NP-Hb**, which were supposed to release oxygen in tumor cells, thereby mitigating hypoxia-induced immunosuppression. Biotin-mediated accumulation of **5-NP-Hb** in murine triple negative breast cancer (4T1) cells was demonstrated, as well as increased intracellular accumulation and DNA platinization compared to OXA and an OXA-biotin mixture. Tumor-specific accumulation was confirmed with fluorescently labeled **5-NP-Hb**; the maximum fluorescence was achieved after 48 h and was maintained after 72 h. Although **5-NP** demonstrated accumulation in main organs similar to OXA, tumor accumulation of both **5-NP and 5-NP-Hb** significantly increased ~3-fold compared to OXA. Importantly, hypoxia in tumor tissues was reduced, which was confirmed *via* both fluorescence staining and

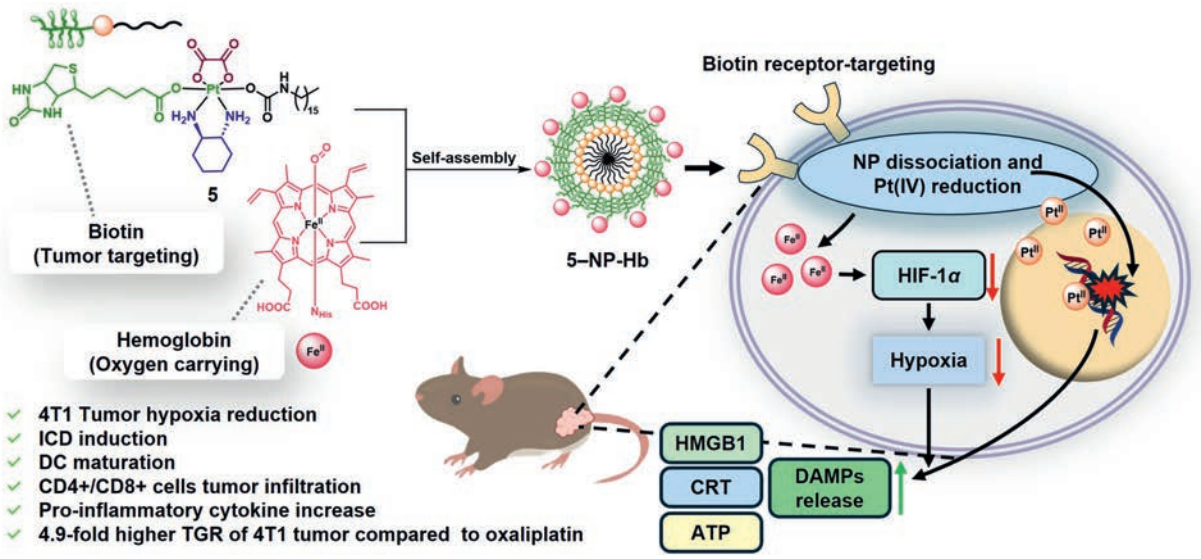

Figure 16 Pt(IV) prodrug **5** with tumor targeting biotin axial ligand and its assembly with hemoglobin into **5-NP-Hb**. The intracellular mechanism of **5-NP-Hb**: promotion of ICD due to oxaliplatin-induced DNA damage and hypoxia reversal by oxygen delivery[233].

the reduced level of HIF-1α protein. Significant antitumor efficacy for **5-NP-Hb** was shown in a triple-negative breast cancer model, exceeding that of OXA and hemoglobin-free **5-NP**. A significant immune response *in vivo* caused by **5-NP-Hb** was confirmed *via* an increase in effector T cells ($CD3^+$, $CD4^+$, $CD8^+$), CRT, and HMGB1, as well as *via* IFN-γ and TNF-α upregulation and IL-10 downregulation.

The importance of the effect on the tumor microenvironment can be assessed by comparing the therapeutic efficacy of **5-NP** and **5-NP-Hb**. Thus, hemoglobin-modified **5-NP-Hb** and unmodified **5-NP** demonstrated the same intratumor accumulation. However, hypoxia-reducing **5-NP-Hb** demonstrated both antitumor efficacy and immunostimulatory properties higher than those of unmodified **5-NP**. This result clearly emphasizes that physical accumulation of the drug in the tumor does not always determine its antitumor efficacy. Thus, NPs capable of reducing the immunosuppressive environment of the tumor are extremely promising for further development of nanomaterials for cancer treatment.

4.2.2. *Nitric oxide delivery*

Nitric oxide (NO) displays a significant function in various physiological functions and has a critical role in modulating the activity of chemotherapeutic drugs[234]. Thus, NO can overcome the multidrug resistance of cancer cells by reducing the expression level of P-gp[235] and increase CDDP efficacy[236,237]. Additionally, NO dilates blood vessels, enhancing delivery of nanoagents[238].

In 2021, Deng et al.[153] designed host−guest Pt(IV) prodrug-based NPs **6-NP** capable of Pt(II) and NO release for targeted therapy of liver cancer (Fig. 17). Combination of Pt and NO in NPs in 1:10 ratio produced strong synergistic antiproliferative effect *in vitro*. In tumor cells **6-NP** released NO with the subsequent formation of peroxynitrite $ONOO^-$, which downregulated GSH level, leading to inhibition of Pt(II) detoxification mechanism. Further *in vitro* studies demonstrated the ability of **6-NP** to prevent the repair of Pt-DNA adducts, which allows **6-NP** to overcome CDDP resistance. Due to the targeting lactose moiety, **6-NP** preferably accumulated in LM3 xenograft tumor model, and inhibited tumor growth more efficiently than CDDP. Importantly, a high intratumoral $ONOO^-$ level and low GSH level was observed in **6-NP**-treated mice and double-strand DNA damage in tumor tissues was also revealed. Comparison of therapeutic efficacy with model **6-NP-m** without NO-donating ability clearly confirmed the significant contribution of the NO-donating ability of **6-NP** to their therapeutic efficacy. **6-NP** also suppressed growth of CDDP resistance orthotopic luc-LM3/CDDP tumor model, with 3-fold lower tumor weight than for CDDP-treated group. Furthermore, **6-NP** exhibited stronger antitumor effect in patient-derived hepatoma model than CDDP, with minimal side effects.

In 2024, Tang et al.[140] reported the use of Pt(IV)-based NPs **7-NP** for non-small cell lung cancer (NSCLC) therapy *via* an inhalation approach (Fig. 18). Pt(IV) prodrug **7** ethacraplatin with GST inhibitor in axial position was encapsulated in NO-releasing azide-affinic micelles, *via* dispersion with pH-sensitive NO-donating PEOz-*b*-PLA-GSNO, with *S*-nitrosoglutathione (GSNO) and dibenzyl cyclooctyne (DBCO)-enriched DSPE-PEG2000-DBCO. Pt(IV) prodrug **7** and NO were actively released from the **7-NP** under pH 5.0 and in the presence of GSH, and **7-NP** showed an ability to overcome resistance by suppressing the expression of P-gp and GST. After i.v. injection, **7-NP** accumulated in liver with almost no accumulation in the lungs. To enhance accumulation of **7-NP** in lungs, mice with orthotopic CDDP-resistant lung adenocarcinoma A549cisR tumors were pretreated *via* inhalation with mannose-azide, capable of labeling the membrane of tumor cells with an azide group, then **7-NP** were administered *via* inhalation. As a result, therapy with **7-NP** significantly decreased the number of lung tumor niches, which was accompanied by the recovery of alveoli completeness. **7-NP** significantly suppressed CDDP-resistant lung cancer without toxicity or weight loss, while CDDP was not therapeutically effective but exhibited significant toxicity. Furthermore, increased platinum levels and decreased GSH were observed in tumor tissues after therapy with **7-NP**, confirming the increased susceptibility of tumor tissues to CDDP therapy due to NO donation.

4.2.3. *Reducing MDSCs*

MDSCs impair the efficacy of chemotherapy by suppressing antitumor immune responses and promoting an immunosuppressive TME[239,240]. MDSCs enhance tumor cell survival by secreting

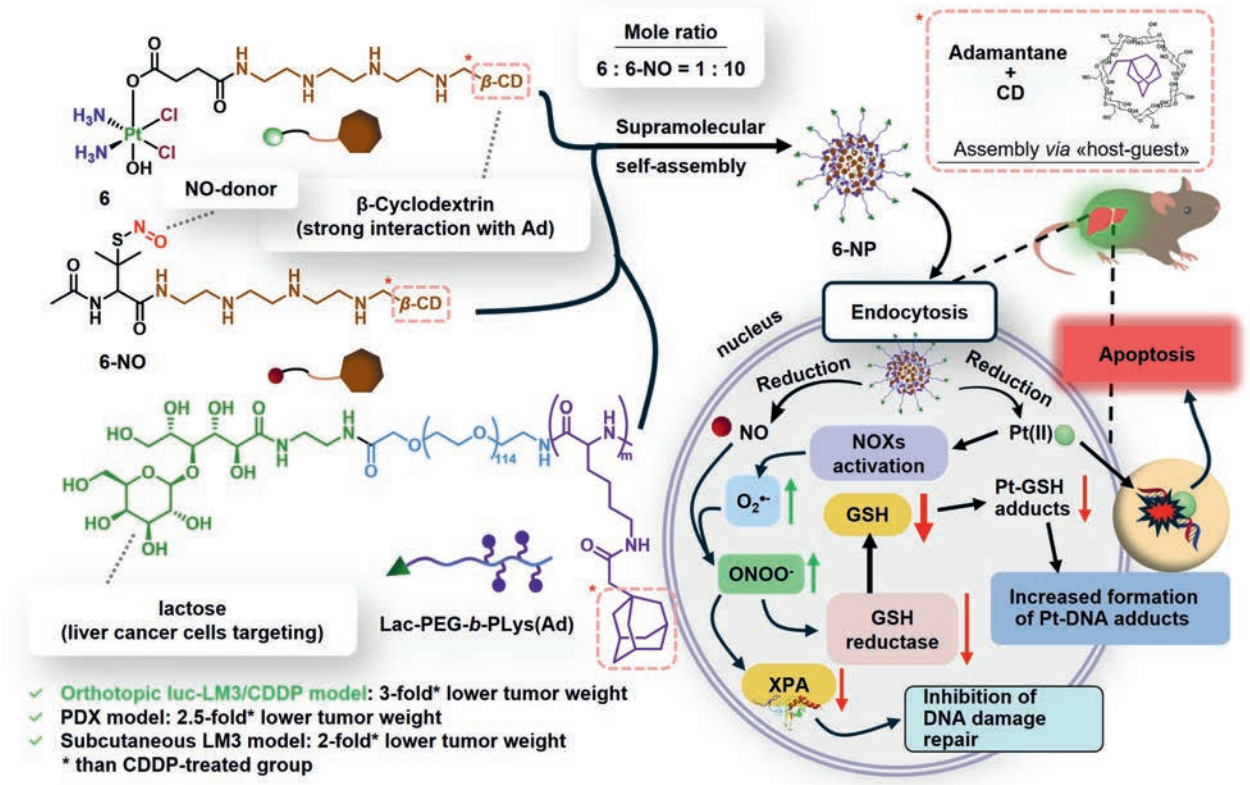

Figure 17 Pt(IV) prodrug **6** and NO-donating **6-NO**, supramolecular self-assembly with lactose containing polymer into **6-NP**. The intracellular mechanism of **6-NP**: apoptosis of cancer cells induced by DNA damage and GSH downregulation *via* NO activity[153].

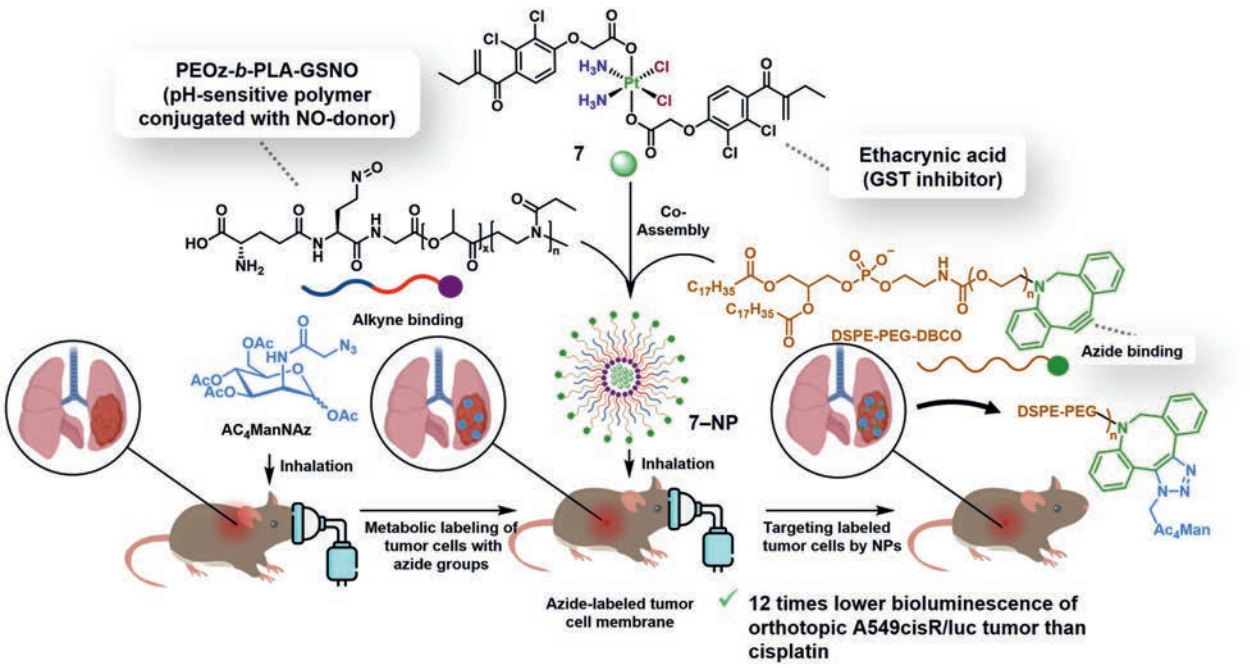

Figure 18 Pt(IV) prodrug ethacraplatin **7** and its encapsulation into micelles obtained through co-assembling polymers PEOz-*b*-PLA-GSNO and DSPE-PEG-DBCO into nanoparticles **7-NP**. The *in vivo* mechanism of **7-NP**: prelabelling of cancer cell membrane with azide groups during inhalation of mannose-azide AC4ManNAz and subsequent binding of **7-NP** to azide-labelled cancer cells *via* click reaction after the second inhalation[140].

pro-tumorigenic factors, such as TGF-β, IL-10 and arginase-1, which reduce oxidative stress, inhibit T-cell activity, and enhance chemoresistance[239]. Targeting MDSCs has been shown to improve therapeutic outcomes, either alone or in combination with other anticancer therapies[241,242].

Retinoic acid (RA) is an anti-hematological tumor agent, which can reduce the population of MDSCs, which in turn improves the populations of M1 macrophages and $CD8^+$ T cells[243]. In 2024, Wang et al.[244] reported PolyRA (**PRA**), which was obtained *via* the polymerization of retinoic acid-based monomer RA, and efficiently reduced the MDSC population in the murine colon adenocarcinoma MC38-bearing mice tumor model. However, despite the reduction in the population of immunosuppressive cells, the antitumor efficacy of RA and **PRA** was low. Then, OXA-based Pt(IV) prodrug **8** was encapsulated in PolyRA carrier yielding **8-NP-RA** NPs (Fig. 19), with **8-NP** (OXA-based NPs without RA) used as a control. OXA-based **8-NP-RA** showed good stability and an ability to release Pt in the presence of GSH, resulting in Pt-induced cytotoxicity. Fluorescent-labeled **Cy5.5−8-NP-RA** accumulated mostly for in the tumor and liver of the MC38 colon cancer model with a maximum on 24 h. p.i. The excellent tumor-suppressive ability of **8-NP-RA** was demonstrated on the same tumor model, which exceeded that of OXA, **RA**, and model **8-NP** with no weight loss. Also, a 60-day survival study showed the undoubted superiority of **8-NP-RA** over unmodified RA-free **8-NP**, which indirectly indicates the immunomodulatory capacity of **8-NP-RA,** which was further confirmed by $CD8^+$ T cell tumor infiltration and macrophage polarization caused by **8-NP-RA**. Thus, the combination of the chemotherapeutic agent OXA with previously ineffective **RA** in one nanoagent, **8-NP-RA** demonstrated an extremely promising antitumor efficacy, thereby emphasizing that the combination of chemotherapy and immunotherapy enhances each other and can hardly be used separately.

Interestingly, co-therapy of **8-NP-RA** with $\alpha CD8^+$ fully reduced its antitumor efficacy, indicating the key role of $CD8^+$ cells in the antitumor effect of **8-NP-RA**. In addition, **8-NP-RA** showed low efficacy in the B16 murine melanoma model, which is characterized by low infiltration with MDSCs. Since the key factors of the antitumor efficacy of **8-NP-RA** are $CD8^+$ T cells, αPD-L1 therapy was proposed to complement its immunostimulatory effect. Thus, therapy with **8-NP-RA** combined with an αPD-L1 antibody on MC38-bearing mice resulted in a significant TGI, which was accompanied by increased of $CD8^+$ T cells infiltration. Using the 4T1-luc lung metastasis model, an anti-metastatic effect, as well as antitumor immunity caused by **8-NP-RA** in combination with αPD-L1 was demonstrated, as well as prevention of tumor metastasis and recurrence.

It should be also noted that the choice of tumor model for immunotherapy is extremely important; thus, **8-NP-RA** was generally ineffective on melanoma B16 due to its low infiltration with MDSCs. The high antitumor efficacy of the combination of **8-NP-RA** and αPD-L1 also demonstrates the importance of combining immunotherapy with checkpoint inhibitors to suppress tumor cell avoidance of T cells and thereby forming favorable conditions for stable T cell immunity.

4.2.4. *Inflammatory reduction*

Chronic inflammation is a hallmark of the TME and is a promotor of metastasis[245]. Inflammatory cells establish a cross-talk with tumor cells that may result in a phenotype switch into tumor-supporting cells and tumor-associated M2 polarization of macrophages[246]. Epithelial-to-mesenchymal transition (EMT) takes center stage as the convergence point between inflammation and tumor progression. EMT is an essential biological process in which epithelial tumor cells lose epithelial polarity, adhesion, motility, and translate to a mesenchymal phenotype, and this is one of the key factors of tumor metastasis[247,248].

In 2024 Zhang et al.[249] reported a Pt(IV) prodrug **9** with carprofen, a COX-2 inhibitor in axial position, capable of EMT suppression *via* Wnt/β-catenin signaling downregulation (Fig. 20). Prodrug **9** was encapsulated onto DSPE-PEG_{2000} yielding **9-NP-m** and further modified with tumor-targeting transferrin (Tf), yielding **9-NP**. Upon cell treatment with **9** and **9-NP**, COX-2, MMP9, and inflammatory cytokines TNF-α and IL-6 down-regulation was shown, thereby confirming anti-inflammatory

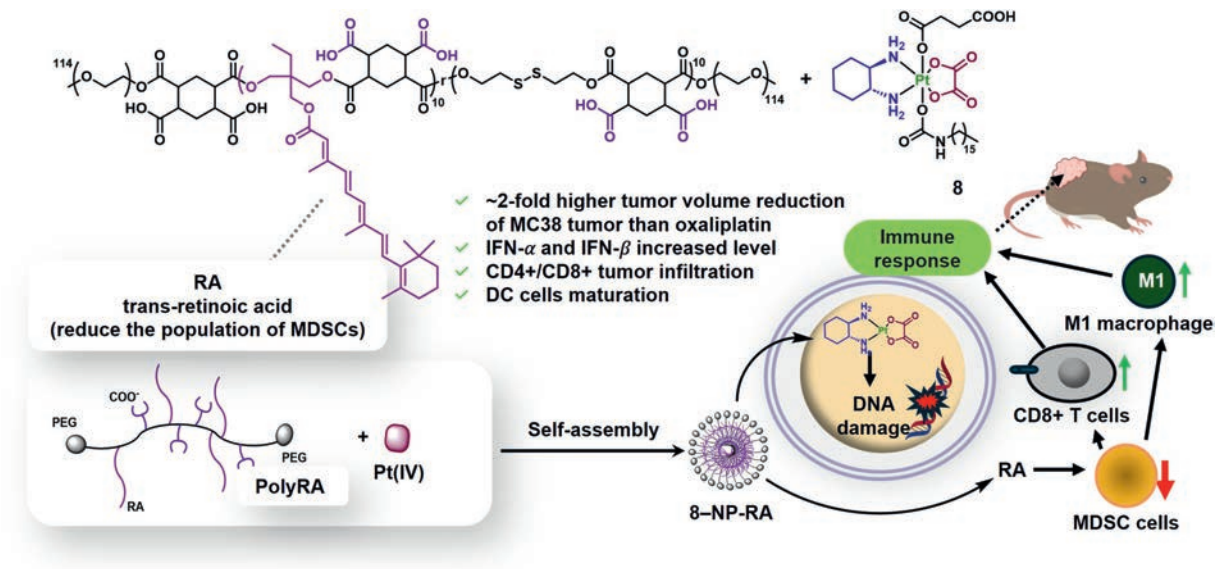

Figure 19 Lipophilic Pt(IV) prodrug **8** and its assembly with poly-RA (retinoic acid) into **8-NP-RA**. The intracellular mechanism of **8-NP-RA**: oxaliplatin-induced DNA damage and TME reversal by RA-induced MDSC suppression[244].

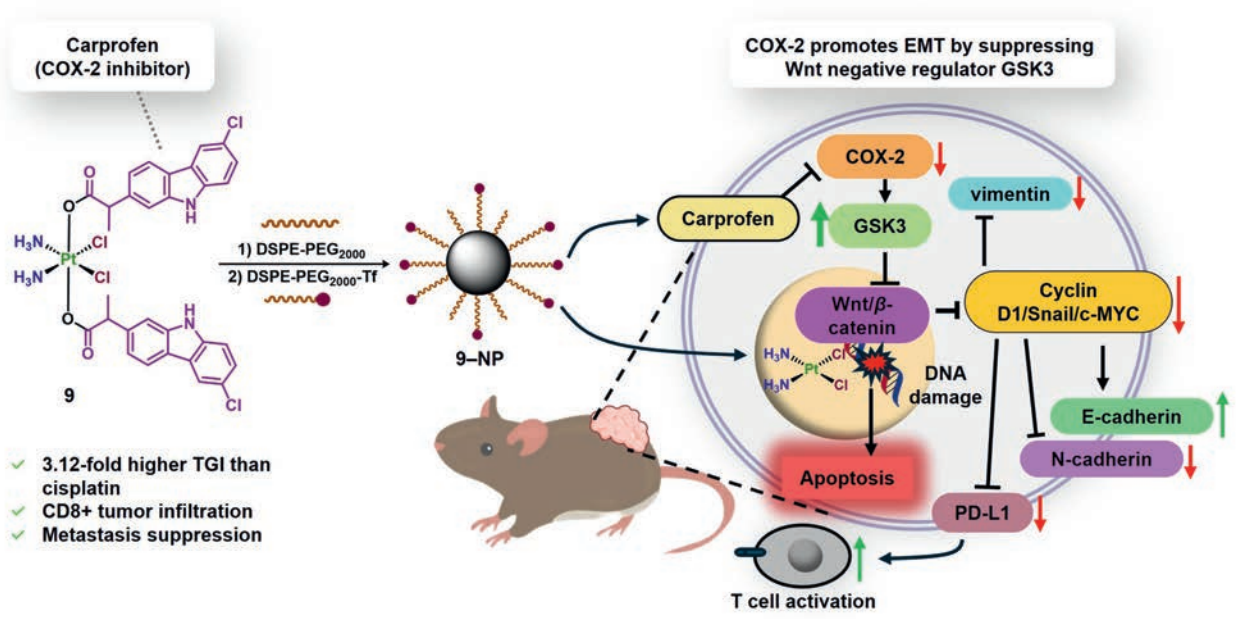

Figure 20 Pt(IV) prodrug **9** with COX-2 inhibitor carprofen as an axial ligand and its assembly with DSPE-PEG2000 modified with tumor targeting transferrin into **9-NP**. The intracellular mechanism of **9-NP**: cisplatin-induced apoptosis and TME reversal by inhibition of COX-2 and EMT suppression[249].

properties of both **9** and **9-NP**. A reversion of the EMT phenotype was verified by the upregulation of E-cadherin and the downregulation of N-cadherin, β-catenin, cyclin D1, and c-Myc both in **9** and **9-NP**-treated tumor cells. An ability of **9-NP** to activate T cell antitumor immunity was also confirmed; immunohistochemical staining showed an improved density of $CD4^+$ and $CD8^+$ cells in tumor-infiltrating lymphocytes (TILs), as well as PD-L1 suppression. Both **9-NP-m** and **9-NP** exhibited a good pharmacokinetic profile with a half-life exceeding that of the prodrug **9** by more than two times, which illustrates the improved bloodstream circulation time of NPs compared to the Pt(IV) complex. A high tumor-targeting ability of **9-NP**, higher than that of non-modified **9-NP-m,** was confirmed *via* fluorescent visualization of DiD-labeled **DiD-9-NP,** with significant accumulation in liver. Evaluation of antitumor efficacy *in vivo* provided on BALB/c mice bearing 4T1 adenocarcinoma showed high antitumor efficacy of **9**, **9-NP-m,** and **9-NP** with a TGI of 71.3%−80.4%, which were significantly more potent than CDDP (TGI = 25.7%). It is worth noting that transferrin-modified **9-NP** showed better antitumor accumulation due to active targeting and, consequently, better antitumor efficacy when compared with **9-NP-m**. **9-NP** also inhibited metastasis *in vivo* with an inhibition rate of 79.2%, higher than Pt(IV) prodrug **9** (65.2%).

It should be noted that the therapeutic efficacy of prodrug **9** alone was more than three times greater than that of CDDP, which undoubtedly confirms the potential of combination therapy and its impact on the tumor microenvironment. However, therapy with prodrug **9** was accompanied by significant weight loss, while its packaging in lipid NPs to produce **9-NP-m** allowed for both a sustained therapeutic effect and a significant reduction in weight loss during therapy. Modification with Tf to produce **9-NP** enhanced the therapeutic effect due to active targeting; these data clearly demonstrate the benefit of reducing inflammation in the tumor environment and using nanoformulations of Pt(IV) prodrugs.

4.2.5. Glycolysis inhibition

The common feature of tumor cells is an increased glucose uptake and fermentation of glucose to lactate, which is known as Warburg effect and considered as one of the most fundamental metabolic alterations during malignant transformation[250,251]. Abnormal lactate metabolism results in production of immunosuppressive metabolism, while glycolytic inhibition is associated with enhanced ICD[252].

In 2025, Yang et al.[143] developed a nanoformulation of OXA Pt(IV) prodrug with two aspirin axial ligands capable of glycolysis inhibition and subsequent immune response stimulation (Fig. 21). The prodrug **10** was encapsulated into redox-responsive polymer to enhance water solubility, resulting in NPs **10-NP**. **10-NP** induced mitochondrial damage, as well suppressed glycolysis of CT-26 cells by reducing glucose uptake and lactate efflux. Since high glycolytic activity is associated with suppressed ICD, **10-NPs** also induced release of damage-assotiated molecular patterns (DAMPs) to a higher extent than OXA or OXA:aspirin mixture 1:2. Nanoformulation **10-NP** delivered Pt in CT-26 tumors more efficiently than OXA, which resulted in much higher tumor inhibition rate *in vivo* 85.2% compared to 57.6% for OXA, while sustaining normal level of general toxicity markers. It is important to note that **10-NP** caused tissue apoptosis, in contrast to OXA, which caused necrosis. Also, down-regulation of glycolytic enzymes Hk2 and Pkm2 in tumor tissues confirmed glycolysis inhibition in *vivo*. Investigation of *in vivo* anticancer immune activation revealed that treatment with **10-NP** enhanced the level of $CD8^+$ T cells, interleukins IL-2 and IL-12 in tumor, while decreasing the proportion of immune-suppressive MDSCs and Tregs.

Targeting tumor microenvironment in addition to platinum-based chemotherapy undoubtedly increases the effectiveness of chemotherapy. Reducing hypoxia and donating NO dilates blood vessels and allows chemotherapeutic agents to penetrate deeper into the tumor, thereby significantly reducing drug resistance.

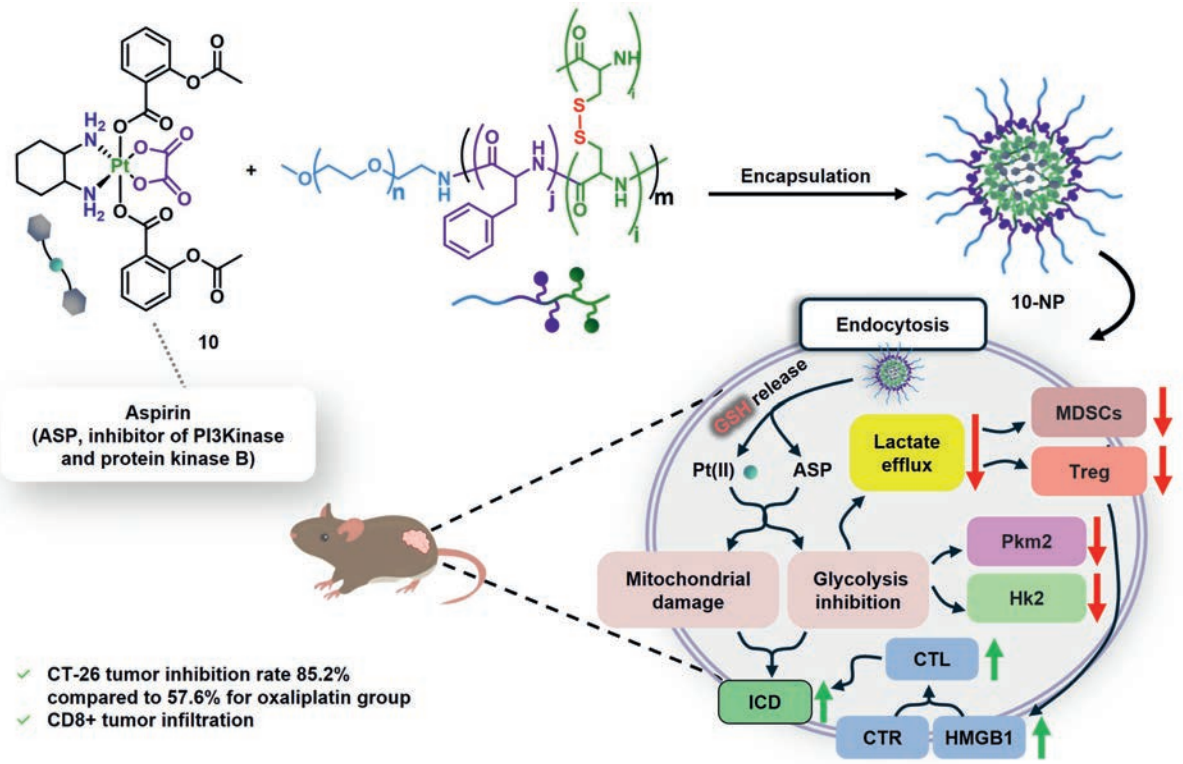

Figure 21 Pt(IV) prodrug **10** with aspirin and its assembly with redox-responsivepolymer into **10-NP**. The intracellular mechanism of **10-NP**: severe mitochondrial damage and ICD induction[143].

Reducing inflammation and inhibiting glycolysis undoubtedly have a powerful synergistic effect, significantly enhancing chemotherapeutic action. Targeting immune-suppressive tumor cells allows for reversal of the tumor's immunosuppressive defenses and the achievement of a powerful therapeutic response unachievable with platinum-based therapy. Thus, coating 5-**NP** NPs with hemoglobin significantly increased therapeutic efficacy compared to unmodified **5-NP-m**. NO delivery *via* **6-NP** and **7-NP** enhances CDDP-induced tissue damage, thereby contributing to overcome resistance, while inhibition of glycolysis *via* **10-NP** stimulates the immune system and significantly mitigates the effects of OXA, leading to apoptosis of tumor tissue rather than necrosis.

4.3. Pt(IV)-based NPs that induce ICD

Several approaches are used to train the immune system to recognize tumor cells as foreign, with ICD being of utmost importance[253]. ICD differs fundamentally from non-immunogenic (*e.g.*, apoptotic) death in that dying or stressed cells release « red flag » molecules that can function as either adjuvants or danger ("eat me") signals for the immune system. Thus, ICD is characterized by the release or cell-surface expression of DAMPs from dying tumor cells, followed by the induction of the innate and adaptive tumor-specific immune responses[254]. As a result, dying cancer cells operate as a vaccine that stimulates a tumor-specific immune response and are capable of inducing immunological memory[255,256].

Additionally, ICD induces macrophage polarization. Tumor-associated macrophages are mononuclear immune cells with phagocytic ability that accumulate at tumor sites and regulate TME by releasing various factors. Tumor-associated macrophages are categorized into two phenotypes, immunostimulatory M1 and pro-inflammatory M2, which can assist tumor escape from immune system surveillance.

Several ICD-stimulating chemotherapeutic agents are currently being developed due to their potential as dual-action drugs[34,257]. Radiotherapy, chemotherapy, and photodynamic therapy can activate ICD in tumor cells[258]. Also, ICD inducers are categorized into two types based on the target they are acting on: type I inducers target DNA replication, cytoplasmic or plasma membrane proteins, and induce ER stress through collateral ER stress effects, while type II inducers utilize the ER as a primary target to induce ICD[259,260]. A generalized mechanism of ICD is presented in Fig. 22.

Immune checkpoints, a series of molecules that are expressed on immune cells, can tune up the degree of immune activation or act as molecular guardians of order, preventing autoimmune reactions[261]. Immune checkpoints inhibitors (ICIs) target specific immune checkpoints, primarily cytotoxic T-lymphocyte-associated antigen-4 (CTLA-4) and programmed cell death protein 1 (PD-1). When the checkpoint and ICI proteins bind together, they send an "off" signal to the T cells, thereby preventing the immune system from destroying the cancer[262,263]. A generalized mechanism of PD1/PD-L1 immune checkpoint is summarized in Fig. 23.

The PD-1/PD-L1 pathway contributes to tumor immune escape, which has been identified as a main mechanism that causes tumors to become resistant to immune response[264,265]. Overexpression of PD-L1 or PD-L2 in cancer cells promotes cell evasion from the immune response; the expression of PD-L1 on tumor cells is correlated with poor prognosis[266]. ICD inducers can

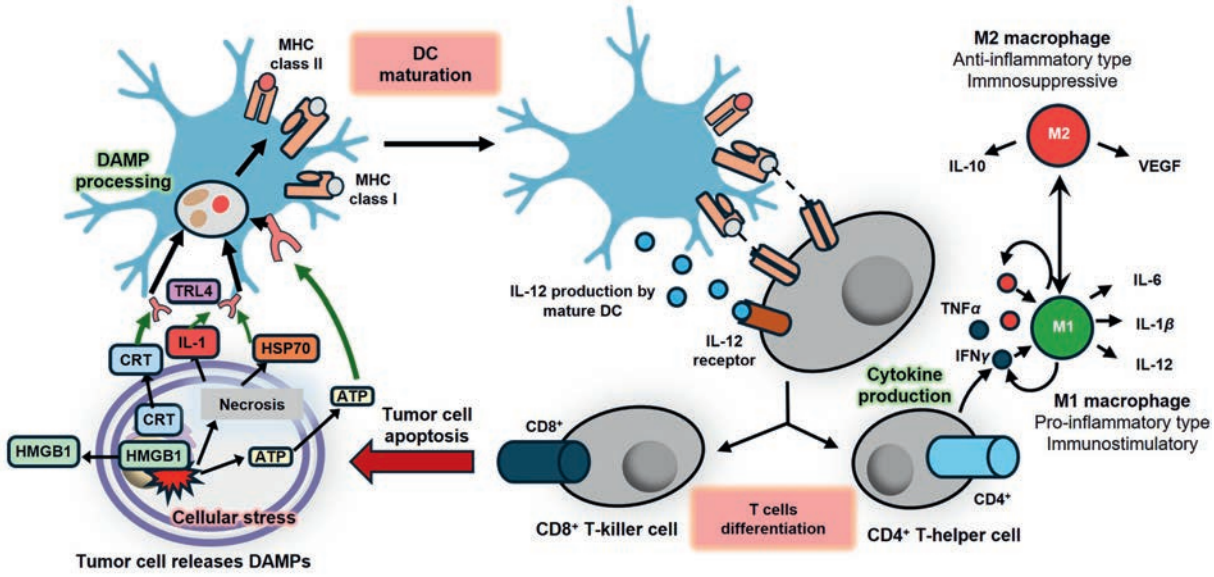

Figure 22 Generalized mechanism of immunogenic cell death (ICD). Cellular stress-promoted DAMP release, DAMPs processing by DCs, maturation of DCs, cytokine production, T-cell differentiation, and activity.

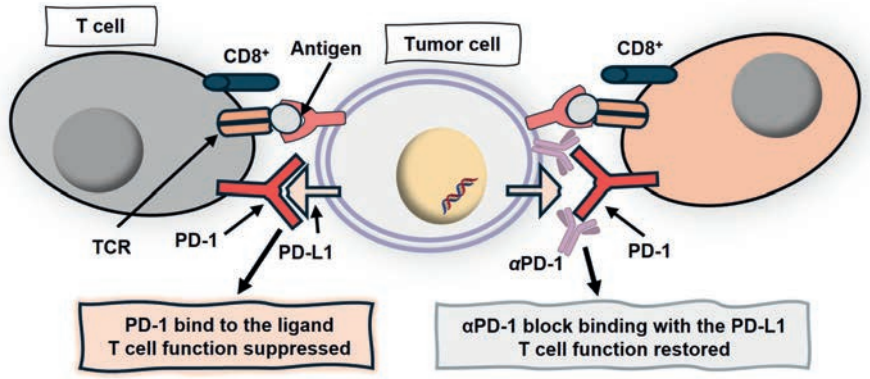

Figure 23 Generalized mechanism of PD1/PDL1 immune checkpoint. Interaction between PD-1 and PD-L1 results in T cell suppression, while PD-1 blockade by αPD-1 antibodies promotes T cell cytotoxic activity.

sensitize tumors to ICIs, and this combination is currently a hot topic in chemoimmunotherapy[267]. In particular, CDDP and OXA chemotherapy induced similar immunogenic changes in preclinical models of head and neck cancer and also demonstrated additive activity when combined with anti-PD-1 therapy[268]. The combination of platinum-based chemotherapy with ICD is an extremely promising approach for the treatment of solid tumors[269]. Also, the combination of ICD-inducing nanomedicines and immunomodulators represents a promising strategy for enhancing chemoimmunotherapy in clinical applications[270]. Overall, ICD-inducing chemotherapeutic agents are attractive candidates for combinational chemo-immunotherapy with anti-PD-1/PD-L1 antibodies to improve the antitumor efficacy[271−273], and this combination is widely used and will definitely be mentioned in this review.

4.3.1. cGAS−STING pathway activation

The cGAS−STING pathway plays a key role in innate immune response. In brief, cGAS−STING pathway results in the production of interferon-1 (IFN-1) in response to the appearance of double-stranded DNA in the cytosol[274]. Since platinum-based antitumor drugs are capable of DNA damage and Pt(IV)-based NPs significantly increase the bioavailability of platinum in tumor cells, significantly enhancing DNA damage, activation of GAS−STING by Pt(IV)-based NPs is a commonly used approach in the design of immunostimulating Pt(IV)-based nanoagents.

In 2022, Cao et al.[275] designed a CDDP-based Pt(IV) prodrug **11** with topoisomerase I inhibitor camptothecin (CPT) in the axial positions (Fig. 24). Since both CDDP and CPT are able to activate the cGAS−STING pathway, their combination could effectively activate innate immunity. Prodrug **11** was co-assembled with ROS-sensitive polymer P1 and $mPEG_{2k}$-DSPE, yielding **11-NP**, capable of H_2O_2-triggered drug release. An ability of **11-NP** to activate the cGAS−STING pathway with subsequent release of IFN-β and IL-6 was confirmed on CT-26 cells. Further co-incubation of bone marrow-derived dendritic cells (BMDCs) with **11-NP**-treated cells induced dendritic cells (DC) maturation which generally followed by active cell migration to draining

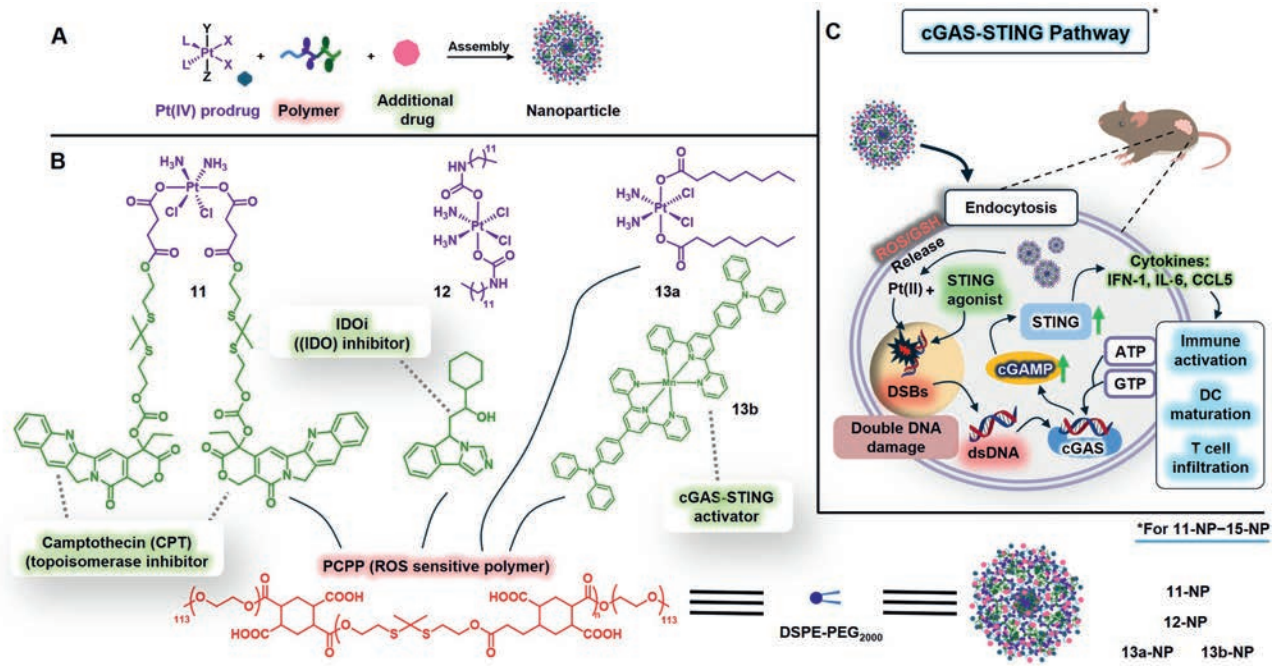

Figure 24 Design and mechanism of multifunctional Pt(IV) prodrug-based nanoparticles. (A) Schematic representation of **11-NP-13NP** assembly from Pt(IV) prodrug, ROS-sensitive polymer, and additional therapeutic agents. (B) Structures of Pt(IV) prodrugs **11**−**13,** additional drugs and ROS sensitive polymer and assembling into **11-NP**−**13-NP.** (C) The intracellular mechanism of **11-NP**−**15-NP**: DNA damage and immune activation *via* cGAS-STING pathway (**14-NP** and **15-NP** are illustrated in Fig. 25)[275,276,280].

lymph nodes and presenting tumor-associated antigens. Also, **11-NP** showed good intratumoral accumulation and better antitumor efficacy on the same tumor model when compared to two separate drugs and a 1:1 CDDP + CPT mixture with low systemic toxicity. A significant DNA damage in tumor tissues of mice treated **11-NP**, higher than that of mice treated with CDDP was demonstrated *via* TUNEL staining. DC maturation in lymph nodes of mice treated with **11-NP**, as well as tumor infiltration with $CD4^+$ and $CD8^+$ T cells revealed a significant activation of innate immunity.

In 2023, Xiang et al.[276] reported NPs **12-NP** based on Pt(IV) prodrug **12** with lipophilic axial ligand and indoleamine 2,3-dioxygenase (IDO) inhibitor NLG919 loaded into thioketal-based ROS-sensitive polymer (Fig. 24). **12-NP** showed the ability to release NLG919 in the presence of H_2O_2, and an ability to enter tumor cells through clathrin-mediated endocytosis. **12-NP** inhibited IDO protein and activated the STING pathway in osteosarcoma cells. An evaluation of an antitumor effect on the orthotopic murine osteosarcoma K7M2-LUC model showed the lowest bioluminescence in the group treated with **12-NP** at day 20 compared with the other groups. **12-NP** also activated an antitumor immune response as evidenced by DC maturation, an increase in infiltration of tumor $CD8^+$ T cells, and a decrease in the M2-like macrophages and Tregs. Thus, **12-NP** could reverse the low immune response of osteosarcoma and reprogram the TME *via* CAS−STING activation.

Mn^{2+} ions are known to activate cGAS, raise cGAS's sensitivity to double-stranded DNA, and activate the cGAS−STING pathway[277−279]. For the synergistic activation of the cGAS−STING pathway and chemotherapy, Zhang et al.[280] suggested the use of a combination of Mn^{2+} with CDDP *via* co-delivery of CDDP Pt(IV) prodrug-based NPs **13a-NP** and Mn^{2+}−based NPs **13b-NP** co-assembled with a ROS-sensitive polymer (Fig. 24). Both Pt(IV)-based **13a-NP** and Mn^{2+}-based **13b-NP** showed H_2O_2-triggered release of platinum and manganese. A combination of **13a-NP** and **13b-NP** upregulated the cGAS−STING pathway, which was confirmed *via* upregulation of cGAS, p-STING, PTBK1, and p-IRF3 protein expression, and downregulation of pro-inflammatory cytokines TNF-α, IL-6, and IL-2. Also, a combination of **13a-NP** and **13b-NP** induced the release of DAMPs from ovarian cancer cells and the maturation of DCs. Fluorescent-labeled **13a-NP** showed significant intratumoral accumulation in the OV-PDX-bearing BALB/c nude mice model, with high accumulation in kidneys. Antitumor and antimetastatic activity was assessed after intraperitoneal administration of labeled murine ovarian surface epithelial ID8-Luc tumor cells; notably, **13a**−**NP** + **13b-NP** inhibited tumor growth but did not completely eliminate the primary tumor, while complete regression of peritoneal metastases was induced in 80% of the mice treated with **13a-NP** + **13b-NP** + α-PD1. Also, a combination of **13a-NP** + **13b-NP** induced tumor tissue necrosis. Additionally, a combination of **13a-NP**+**13b-NP** with α-PD-1 induced the maturation of DCs, promoted $CD8^+$ T cell infiltration, and reduced the proportion of Tregs, which indicates a significant immune response and immunological memory.

WEE1 is a key protein that can inhibit the activity of cyclin-dependent kinase 1 (CDK1), arresting the cell cycle and allowing time for DNA repair[281,282]. In 2024, Wang et al.[283] reported a Pt(IV)-based nanomaterial for muscle-invasive bladder cancer treatment; for prodrug synthesis, MK1775, a WEE1 inhibitor, was covalently conjugated with GSH-sensitive polymer (poly(2-HD-*co*-HPMDA)-mPEG, PHHM) and co-incubated with lipophilic Pt(IV) prodrug **14** yielding **14-NP** (Fig. 25). **14-NP-m**, without MK1775, were also obtained and were used as control. **14-NP** could upregulate p-STING and PD-L1 while downregulating WEE1 and CDK-1 proteins, thereby confirming DNA repair disturbance, activation of the cGAS−STING pathway, and

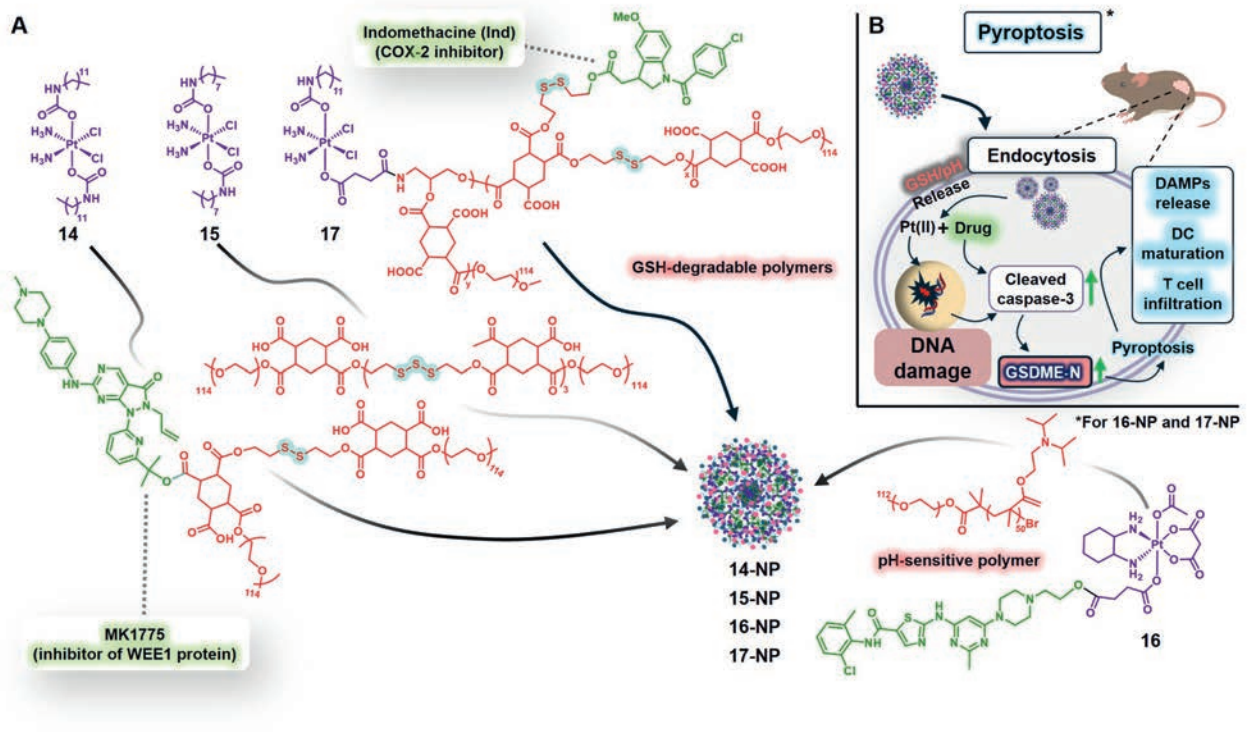

Figure 25 Design and mechanism of multifunctional Pt(IV) prodrug-based nanoparticles (A) Structures of Pt(IV) prodrugs **14**−**17** and ROS/pH-sensitive polymers (with or without additional drugs) used for the assembly of**14-NP**−**17-NP**. (B) The intracellular mechanisms of **16-NP** and **17-NP**: induction of DNA damage and immune activation *via* pyroptosis. (The intracellular mechanism of **14-NP** and **15-NP** is illustrated in Fig. 24)[144,283,288,290].

immune stimulation. Co-incubation of BMDCs extracted from mice with **14-NP**-treated mouse urothelial carcinoma Mb49 cells revealed an increased level of IFN-α and IFN-β and an increase in DC maturation. Fluorescent-labeled **14-NP** demonstrated intratumoral accumulation, along with accumulation in liver and kidneys. The antitumor effect of **14-NP** on the Mb49 tumor model was significantly higher than that of the drug mixture and **14-NP-m** without MK1775 with lower toxicity than that of CDDP and drug mixtures. Immunohistochemistry analysis revealed an increased level of STING protein and $CD8^+$ T cells in the tumor; also, an increase in NK cells and M1/M2 ratio was detected, thereby confirming a significant immune response caused by **14-NP**. Additionally, DS maturation, tumor infiltration with $CD8^+$ cells, reduction of MDSCs, and increased expression of PD-L1 confirmed **14-NP**'s immunogenicity. The combination of **14-NP** and αPD-L1 showed significant antitumor efficacy on the bilateral subcutaneous tumor model of Mb49 with a tumor suppression rate of 95.8% and no distant tumor progression.

In 2024, Li et al.[144] reported a Pt(IV) prodrug **15** loaded into a reduction-responsive trisulfide bond-containing polymer, capable of H_2S release, disrupting the intracellular redox balance, inducing DNA damage, and GAS−STING activation (Fig. 25). **15-NP** showed significant intracellular accumulation *via* endocytosis, as well as the ability to deplete GSH and generate ROS intracellularly to a greater extent than CDDP. Since **15-NP** showed the ability to release H_2S, which is expected to increase cells' sensitivity to CDDP, its high efficacy on CDDP-resistant cells was expected; indeed, **15-NP** showed an IC_{50} value on CDDP-resistant SKOV-3 cells over 300-fold lower than that of CDDP. Considering the increased intracellular accumulation and the ability to enhance the sensitivity of cells to CDDP, **15-NP** apparently damaged DNA to a greater extent than CDDP and caused activation of the GAS−STING pathway, which was confirmed by p-STING and p-IRF3 upregulation. **1-NP** activated *in vivo* antitumor efficacy provided on 4T1 and CT26 xenografts showed enhanced antitumor efficacy when compared with CDDP; also, immunohistochemical analysis revealed that **15-NP** promoted $CD8^+$ T cell infiltration at tumor sites in 4T1 tumor-bearing mice. Importantly, **15-NP** demonstrated a robust hindrance in tumor growth in the 4T1-luc tumor-bearing mouse model after postsurgical tumor cell reinjection compared to CDDP, thereby confirming an antitumor immunity caused by **15-NP**.

4.3.2. Pyroptosis induction

Pyroptosis is gasdermin (GSDM)-mediated programmed ICD, which is characterized by cell swelling and plasma membrane rupture, leading to the release of pro-inflammatory cytokines IL-1β, IL-18, and cellular contents into the extracellular space and activation of inflammatory response[284,285].

Pyroptosis can enhance inflammatory signaling and activate the immune response, as well as overcome the immune de*via*tion caused by apoptosis[286]. Dasatinib is a tyrosine kinase inhibitor with immunoregulatory properties, which also inhibits T-cell activation and proliferation, as well as Treg cell proliferation[287]. In 2022, Zhu et al.[288] reported an OXA-based Pt(IV) prodrug **16** with dasatinib in the axial position to enhance antitumor immunity by inducing pyroptosis of tumor cells (Fig. 25). **16-NP** were constructed by encapsulation of the hydrophobic prodrug **16** to the amphiphilic pH-responsive block-copolymer iPDPA. In the intracellular lysosomes at pH 5.0, iPDPA converted from

hydrophobic to hydrophilic, releasing dasatinib; pH-dependent drug release was confirmed. **16-NP** accumulated in tumor cells and showed cytotoxicity higher than that of OXA. The biodistribution assay provided in the HN-SCC mouse model verified the tumor-specific targeting ability of fluorescent-labeled **DiR-16-NP**. Pyroptosis induction through the caspase-3/GSDME pathway in **16-NP**-treated cells was confirmed, as well as the release of ICD hallmarks. Evaluation of antitumor efficacy *in vivo* on both subcutaneous and orthotopic carcinoma models, with significant TGI after treatment with **16-NP** and no significant damage to normal tissues. Also, reduction of exhausted T cells T_{EX} ($PD1^+TIGIT^+$) and an increase in population of $CD8^+$ in tumor tissues were found, as well as upregulated level of $CD8^+$ and $CD4^+$ memory T cells in lymph nodes, which together confirmed a significant immune response.

Pyroptosis leads to the release of IL-1β, subsequently upregulating COX-2 expression, which may lead to the failure of immunotherapy[289]. In 2024, Yu et al.[290] reported a combination of pyroptosis induction with inhibition of COX-2 expression; Pt(IV) prodrug **17** was conjugated with GSH-sensitive polymer and COX-2 inhibitor indomethacin and could self-assemble into **17-NP** (Fig. 25). **17-NP** showed the ability to release indomethacin and Pt in the presence of GSH, cytotoxicity higher than that of CDDP, as well as the ability to induce pyroptosis, which was confirmed by caspase 3 upregulation and GSDME cleavage. Anti-inflammatory activity of **17-NP** was confirmed by COX-2 as well as PGE expression suppression. Immunostimulatory properties of **17-NP** were confirmed *via* a DC maturation assay after incubation with **17-NP**-treated cells. **17-NP** showed significant antitumor efficiency in Pan02 pancreatic cancer in comparison with model NPs without indomethacin (**17-NP-m**), as well as in comparison with CDDP. In tumor tissues, an increase in the expression of caspase-3 and a decrease in the expression of COX-2 were noted; also, a significant immunostimulatory effect *in vivo* was revealed by an increase in tissue infiltration by $CD8^+$ and NK cells, as well as a decrease in MDSCs.

Stimulation of adaptive immunity by **17-NP** was noted due to an increase in the number of mature DC and memory T cells. Notably, **17-NP-m** did not show the ability to stimulate the immune response, which supports the importance of combining pyroptosis inducers with COX-2 inhibitors. It should also be noted that the combination of **17-NP** and α-PD-L1 effectively suppressed the growth of the primary and distant tumor in a bilateral model, while **17-NP-m** showed sufficient but lower efficacy. These data once again confirm the importance of combining anti-PDL1 therapy with drugs that stimulate the immune response.

It is important to note that pyroptosis itself is ineffective in tumor therapy despite its ability to cause ICD. Also, even though inflammation is one of the cancer's hallmarks, COX-1 and COX-2 inhibitors themselves cannot be considered as effective antitumor agents. At the same time, the competent design of **17-NP** nanoagent was achieved by combining a chemotherapeutic agent, a pyroptosis-initiating agent, and an anti-inflammatory drug with α-PD-L1 therapy, which made it possible to greatly suppress the growth of pancreatic cancer, usually resistant to anti-PD-L1 therapy alone. This result outlines the effectiveness of combined chemo-immunotherapy against pancreatic cancer, where individual components alone are unable to achieve therapeutic effect.

4.3.3. Ferroptosis induction

Ferroptosis is an iron-dependent type of necrotic cell death, characterized by a disruption of the intracellular redox balance and excessive lipid peroxidation. GPX4 is a key enzyme that plays a crucial role in preventing ferroptosis, which catalyzes the reduction of phospholipid hydroperoxides into phospholipid alcohols in the presence of GSH[291−293]. Despite the fact that ferroptosis negatively impacts antigen-presenting cells and hence the adaptive immune response[294], ferroptosis-inducing compounds can enhance the immunogenic effect through the activation of cytotoxic T lymphocytes[295].

In 2023, Wei et al.[156] reported new method for production of ultrasmall Pt(IV)-based NPs within the pores of inorganic NPs that are capable of degrading in the acidic pH of endosomes. Thus, a Pt(IV)-based nanomaterial, **18b-NP,** capable of both ferroptosis and apoptosis induction, as well as Ca^{2+}-mitochondrial overload, which results in ICD, was designed (Fig. 26). Pt(IV) prodrug **18** with thiol in the axial position was linked with $CaCO_3$-based NPs *via* oxidative polymerization and coated with tumor-targeting DSPE-PEG-biotin, yielding a pH-sensitive tumor-targeted **18b-NP**. Also, non-polymerized biotin-coated **18a-NP** were used as a control. **18b-NP** showed the ability to release Ca^{2+} in acidic media, with no Pt release; in contrast, acid-catalyzed degradation of $CaCO_3$-based NPs released ultrasmall **18-NP** with a hydrodynamic size of approximately ∼7.5 nm, which are able to release Pt in the presence of GSH**.** Both **18a-NP** and **18b-NP**-induced Ca^{2+} mitochondrial damage was confirmed *via* loss of mitochondrial membrane potential (MMP), as well as the ability to deplete GSH in CDDP-resistant A549CisR cells, which resulted in ferroptosis, with more pronounced effect for **18b-NP**, which also was able to induce ICD.

An evaluation of the therapeutic efficacy of **18b-NP** provided on the A549CisR tumor-bearing mouse model showed a remarkable TGI in contrast to CDDP. Also, inhibition of GPX4 in tumor tissues after treatment with **18b-NP** confirmed ferroptosis *in vivo*. A prolonged immune response caused by **18b-NP** was also shown in the revaccination experiment. Thus, inoculation of mice with tumor cells dying from **18b-NP** allowed for tumor regrowth after inoculation with live tumor cells 7 days later.

In 2022 Wang et al.[151] reported a CDDP and OXA-based Pt(IV) prodrugs, conjugated with HSA noncovalently or covalently *via* maleimide axial ligand (Fig. 27). Among 4 types of NPs studied, non-covalently bound Abplatin **19-NP** demonstrated the highest activity against ovarian cancer cell lines and was significantly more effective than CDDP on series of patient-derived ovarian cancer cells, including platinum resistant ones. **19-NP** demonstrated excellent biosafety after intraperitoneal administration *in vivo* successfully suppressed growth of orthotopic ES2-luc ovarian tumor model, with tumor volume 65.97% lower than that in CDDP group. In addition, treatment with **19-NP** suppressed formation of malignant ascites, which were formed in 3/6 mice in control group. Antitumor efficiency of **19-NP** *in vivo* was also evaluated on CDDP-resistant cancer stem cell (CSC) subcutaneous tumor model derived from SKOV-3 cells. Treatment with **19-NP** resulted in further reduction in tumor weight and volume than CDDP treatment, indicating that **19-NP** could be used for treatment of recurrent ovarian cancer. Investigation of **19-NP** antitumor activity mechanism *via* RNA-sequencing of CSCs tumors revealed enrichment of ferroptosis markers. Further studies demonstrated that **19-NP** reduced intracellular GSH level while decreasing GPX4 expression and lipid ROS level, which confirmed that **19-NP** induces cell death *via* ferroptosis, allowing it to overcome CDDP resistance in recurrent tumors.

In this section, various combinations of the Pt(IV) prodrug, a stimulus-sensitive polymer, and immune response triggering agent

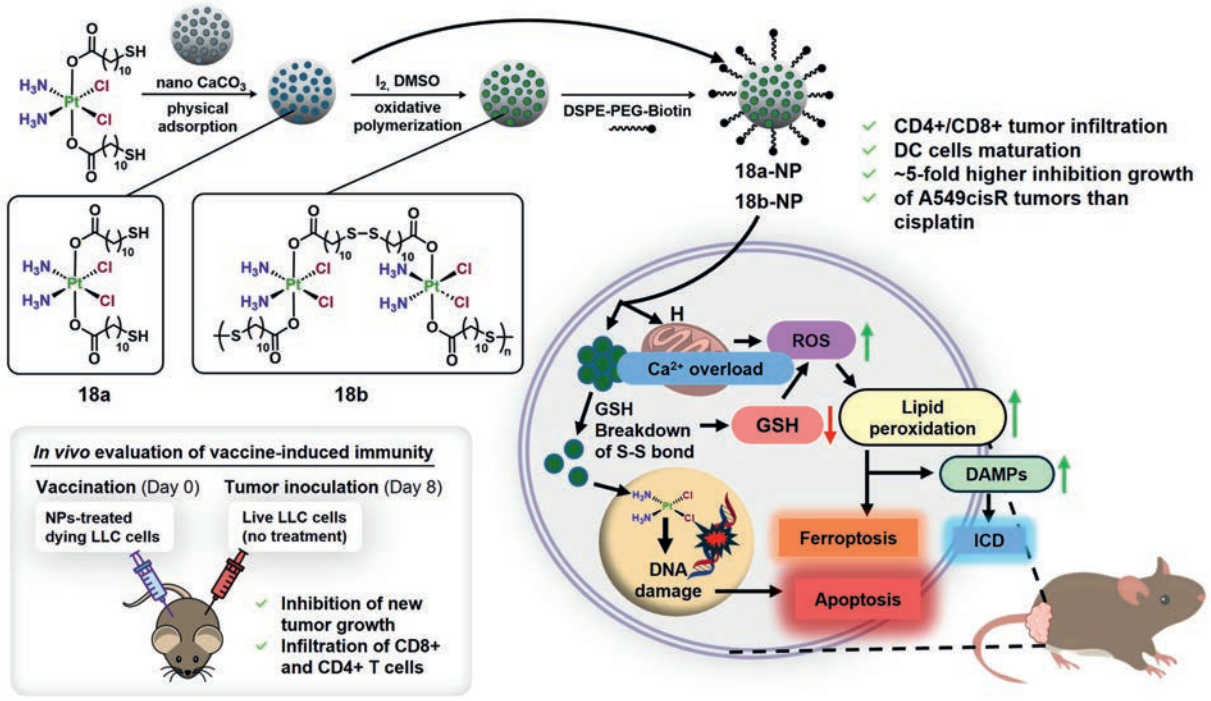

Figure 26 Pt(IV) prodrug **18a** and its polymeric form **18b**, and their loading into $CaCO_3$ nanoparticles with biotin-modified DSPE-PEG_{2000}, resulting in **18a-NP** and **18b-NP**, respectively. The intracellular mechanism of **18b-NP**: Ca^{2+}release-induced ER stress, ER stress-induced ferroptosis and ICD, DNA damaged-induced apoptosis. *In vivo* induction of long-term immune response: preliminary vaccination of mice with **18b-NP**-treated LLC cells on Day 0 inhibited the tumor growth of live LLC cells after inoculation at day 8[156].

were tested. Thus, topoisomerase I inhibitor CPT was conjugated with Pt(IV) prodrug *via* an ROS-sensitive linker, and the prodrug was loaded into an ROS-sensitive polymer yielding ROS-sensitive **11-NP** nanodrug. Otherwise, Pt(IV) prodrug and immune response triggering agent can be loaded into drug carrier separately, as this was implemented for the design of the **12-NP** nanodrug, where

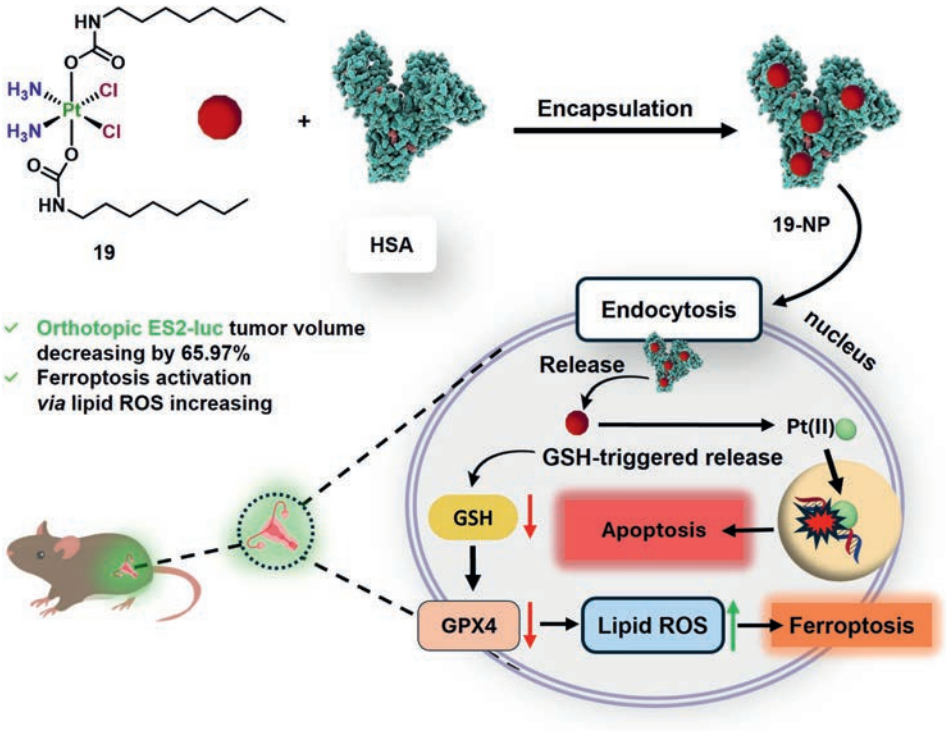

Figure 27 Lipophilic Pt(IV) prodrug **19** and its encapsulation into HSA resulting in **19-NP**. The intracellular mechanism of **19-NP**: cisplatin-induced DNA damage and ferroptosis induction *via* the GSH/GPX4 depletion pathway[151].

model Pt(IV) prodrug and IDO inhibitor NLG91 were separately loaded into an ROS-sensitive polymer. Also, Pt(IV)-based nanodrug can be used in combination with other immune response triggering nanoagent; such therapy design was implemented for **13a-NP** and **13b-NP**, where **13a** is a Pt(IV) prodrug loaded into an ROS-sensitive polymer, which was used in combination with **13b-NP** Mn-based NPs, which are also based on an ROS-sensitive polymer. All three of these nanodrugs **11-NP, 12-NP, 13a + 13b NP** were capable of inducing an immune response by activating cGAS-Sting pathway and demonstrated significant antitumor efficacy. Among these three nanodrugs, the combination of **13a + 13b** demonstrated high toxicity, most likely due to the use of two ROS-sensitive nanodrugs, each of which undoubtedly has its own toxicity. It is interesting to compare the therapeutic efficacy of **12-NP** and **14-NP** nanodrugs, in which the same model Pt(IV) prodrug is loaded into either an ROS-sensitive (**12-NP**) or a GSH -sensitive polymer (**14-NP**); the GSH -sensitive nanosystem **14-NP** exhibited less overall toxicity *in vivo* and weight loss was less pronounced than during therapy with ROS-sensitive **12-NP**. In support of this, loading Pt(IV) prodrug **16** into a pH-sensitive polymer also resulted in significant therapeutic efficacy with minimal weight loss. An interesting approach was demonstrated in the design of **17-NP** nanodrug, where a GSH-sensitive polymer, indomethacin, and the prodrug Pt(IV) were combined into a single amphiphilic prodrug capable of self-assembly. **17-NP** demonstrated significant therapeutic efficacy; unfortunately, weight loss data were not reported in the manuscript. Also noteworthy is the innovative method for producing ultra-small **18-NP** NPs *via* polymerization within the pores of inorganic NPs. Ultra-small **18-NP** obtained after dissolution of the $CaCO_3$ carrier demonstrated extremely high therapeutic efficacy and immune response without significant weight loss.

Overall, the combination of immune response-stimulating agents with platinum-containing chemotherapy undoubtedly enhances efficacy and reduces side effects compared with monotherapy. However, the design of the NPs, their stimuli-sensitivity, and resistance to premature release of therapeutic agents are important factors which are worth taking into account carefully.

4.4. Pt(IV)-based NPs with active targeting

Despite the fact that the use of nanoformulations chemotherapeutic agents possess several advantages over the use of conventional therapeutic agents, such as the ability to overcome low drug solubility and low bioavailability, a poor tumor targeting efficiency still represents a serious challenge to be addressed. Nanocarriers are commonly considered as a promising drug delivery tool capable of spontaneous accumulation in the tumor site through EPR effect[129,296]. However, despite the actual ability of NPs of a certain size (80−120 nm) to accumulate in tumors, this effect is often faint for sufficient tumor accumulation and reduction of side binding, which leads to non-optimal biodistribution of nanoformulations, low therapeutic efficacy and high toxicity. Targeted delivery methods, therefore, make it possible to reduce the dosage of an administered drug and minimize its effect on other cells[297]. Thus, a combination of physical (EPR effect) and specific (active targeting) methods could achieve more accurate drug delivery. Typically, active drug targeting can be classified into three levels: tissue targeting, cells, and organelles[298]. Several examples of the use of combinations of Pt(IV) prodrug nanoformulations in combination with active targeting will be discussed below.

4.4.1. Tissue level targeting

Due to their location within the mineralized bone matrix, bone tumors present a unique drug delivery target. This can be exploited using ligands that bind to hydroxyapatite or bone-specific cellular components for site-specific targeting. This target is of high clinical importance in the treatment of both primary tumors and secondary bone metastases. Alendronate (Ale), a FDA-approved bisphosphonate used in the treatment of osteoporosis, exhibits strong affinity for binding to the bone surface, thus establishing its preferential candidacy as a ligand for targeting bone tissue[299,300]. In 2024, Sun et al.[130] reported an amphiphile CDDP-based Pt(IV) prodrug **20** with Ale in axial position, capable of self-assembling into **20-NP** NPs, for osteosarcoma treatment (Fig. 28). **20-NP** showed good selectivity to Ca-overloading osteosarcoma K7M2 cells due to the presence of phosphate groups on its surface, while being low-toxic to normal cells and other malignant cell lines. A tumor-targeting ability of fluorescent-labeled **20-NP** was confirmed in the K7M2 tumor model, with a fluorescent maximum in 48 h after administration. Also, **20-NP** demonstrated significant antitumor efficacy on the same tumor model, which was significantly superior to that of CDDP, and reduced bone destruction.

In 2024, Yan et al.[131] reported a similar amphiphilic Pt(IV) prodrug **21** based on OXA in order to enhance an immune response of NPs (Fig. 28). **21-NP** were obtained *via* self-assembly of amphiphilic prodrug **21,** demonstrated the ability to release Pt(II) in the presence of ascorbic acid, as well as higher toxicity when compared to the Pt(IV) prodrug **21**, and the ability to induce apoptosis. Also, an active bone-targeting ability was shown *via* Pt uptake in osteosarcoma cells, as well as *in vivo* in K7M2 tumor-bearing mice with a 3.56-fold increase in Pt content in tumor tissues compared to that of OXA. The antitumor effect of **21-NP** was demonstrated on orthotopic osteosarcoma model and was superior to that of OXA and the OXA:ALN (1:1) mixture. Bone-targeted **21-NP** reduced bone destruction by inhibiting osteoclasts. Also, **21-NP** promoted DC maturation, cytokine release, and $CD8^+$ tumor infiltration, thereby confirming a significant immune response.

In 2023, the same scientific group reported a cascade-responsive cationic NPs **22-NP** based on it, which is capable of charge reversal, as well as GAS-STING activation (Fig. 28)[301]. Thus, cationic Pt(IV) prodrug **22** could self-assemble to form cationic NPs **22a-NP** with a ζ of +25.33 mV; Ale was further conjugated onto the NP *via* electrostatic interaction to obtain bone-targeted NPs **22-NP** with a $\zeta^{\sim}-5.09$ mV. Under the acidic conditions, the chelation of Ale with Ca^{2+} was observed, resulting in the shedding of Ale and the subsequent increase in zeta-potential, up to +15.72 mV, thereby confirming a formation of positively charged NP, capable of efficient tumor accumulation (Fig. 28). In addition to both acid media and Ca^{2+}-mediated charge reversal, **22-NP** showed the ability to release Pt in the presence of sodium ascorbate, an ability to accumulate in osteosarcoma K7M2 cells better than CDDP, as well as enhanced cytotoxicity and the ability to activate the GAS-STING pathway. *In vitro* immune activation was investigated; **22-NP** activated DC maturation and activated the expression of IF-1β, IL-6, and IFN-β. Importantly, the negative charge of the **22-NP** contributed to increased circulation in the bloodstream ($t_{1/2}$ = 4.84 h) compared to positively charged **22a-NP** ($t_{1/2}$ = 0.5 h). **22-NP** showed significant accumulation in the K7M2 orthotopic tumor, in contrast to **22a-NP**. The excellent, higher than that of both CDDP and **22a-NP**, antitumor efficacy of **22-NP** was confirmed in the same model. A study of tumors, spleens, and lymphoid tissues of mice

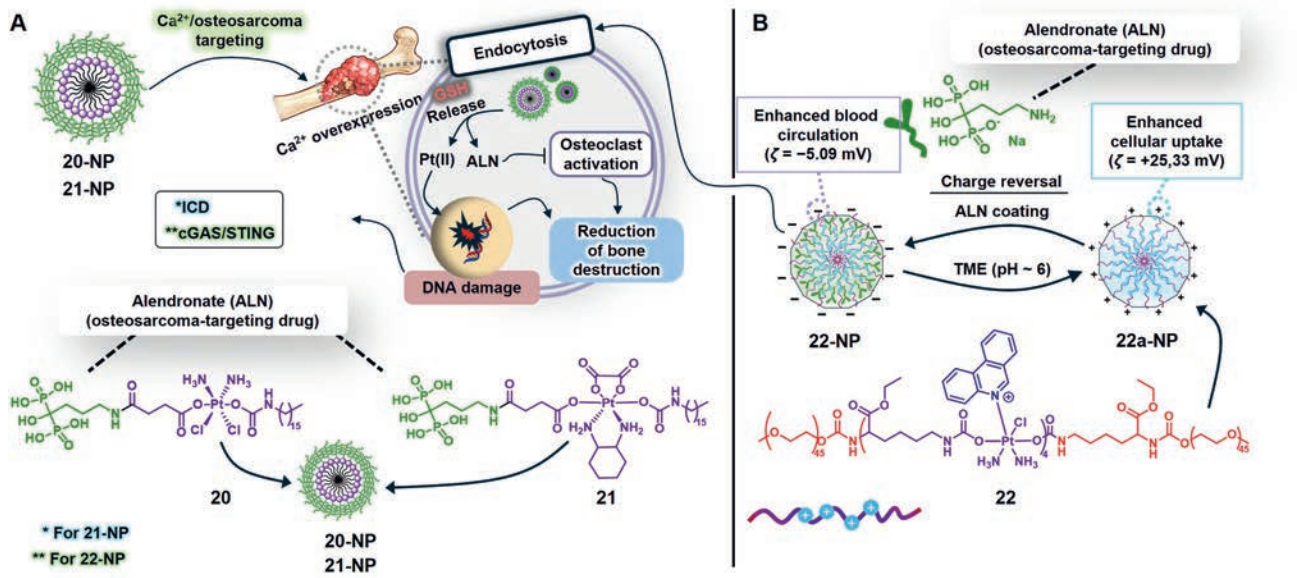

Figure 28 Design and mechanism of multifunctional Pt(IV) prodrug-based nanoparticles. (A) Pt(IV) prodrug **20** and **21** with osteosarcoma-targeting axial ligand alendronate, their self-assembly into **20-NP** and **21-NP**. The intracellular mechanism of **20-NP**−**22-NP**: Pt-induced DNA damage, reduction of bone destruction, induction of ICD (for **21-NP**) and immune activation *via* cGAS−STING pathway (for **22-NP**). (B) Pt(IV) polymer prodrug **22**, its self-assembly into **22a-NP** and alendronate coating with charge reversal into **22-NP**[130,131,301].

after therapy showed a significant immune response *in vivo* induced by **22-NP**, which was expressed in the DC maturation, polarization of macrophages, and T-cell infiltration of the tumor. Thus, charge-reversal **22-NP** are able to enhance on antitumor immunity of osteosarcoma *via* the activation of the STING pathway. To confirm this, a direct comparison of effectiveness α-PD-L1+ **22-NP** combination with **22-NP**-only in treatment of K7M2 orthotopic OS mouse model revealed the undoubted superiority of this combination over monotherapy. Additionally, a high therapeutic efficacy of **22-NP** was confirmed on patient-derived osteosarcoma xenograft model.

4.4.2. *Cell level targeting*

4.4.2.1. Gene therapy. Combination of chemotherapy and gene therapy provides an effective strategy for cancer treatment strategy because gene therapy overcomes multidrug and micro-environmental resistance limitations[302]. The RNA-guided Cas9 nuclease from the microbial clustered regularly interspaced short palindromic repeats (CRISPR) adaptive immune system can be used to facilitate efficient genome engineering in eukaryotic cells[303]. Thus, CRISPR/Cas9 system has become a promising gene editing tool for cancer treatment[304].

EZH2 is frequently overexpressed in several types of cancers (such as prostate, breast, bladder and other cancers); knockdown of EZH2 in cancer cells could results in tumor growth inhibition[305]. In 2020, Zhang et al.[306] reported a Pt(IV)-backboned polymeric nanoplatform for the combined delivery with *EZH2*-targeted CRISPR/Cas9 system (NPCSPt/p*EZH2*) to treat prostate cancer (Fig. 29A). **23-NP** were obtained *via* polymerization of Pt(IV) scaffold with CBTA into prodrug-backbone polymer (PtP), which was covered with oligomethylenimine (OEI1.8k), yielding self-assembling cationic micellar nanoparticle (NPCSPt), which was then covered with plasmid p*EZH2*, yielding **23-NP**. **23-NP-m,** modified with model plasmid, was used as control. **23-NP** could release both CDDP and plasmid in the presence of NaAsc. An ability of **23-NP** to deliver p*EZH2* into PC-3 cells with effective intracellular endo/lysosomal escaping and p*EZH2* unpacking, as well as efficient gene editing *in vitro* was demonstrated; this resulted in increased cytotoxicity of the **23-NP** against PC-3 cells with the lowest IC_{50} value (8.60 μmol/L), which was 11−fold lower than that of **23-NP-m** and CDDP (9.82 μmol/L). **23-NP** demonstrated higher antitumor efficiency *in vivo* compared to CDDP; also, cleavage of *EZH2* gene in the tumor tissue was confirmed. Importantly, **23-NP-m** demonstrated significantly lower antitumor efficacy, which proves the crucial contribution of the genomic editing mechanism to the therapeutic efficacy of **23-NP**.

RNA interference (RNAi) is a powerful high-specific approach for cancer treatment, which acts thought gene silence. However, a delivery of oligonucleotide drug is a great challenge given their easy degradability, while NPs represent a powerful tool for the intact delivery of gene therapy agents (both as monotherapy and as the combination of gene therapy and chemotherapy)[307,308].

In 2020, Zhang et al.[309] reported a photoactivatable Pt(IV) prodrug-backboned polymeric nanoparticle a CNPPtCP/si(c-fos) for synergistic PACT and RNAi, which silence the expression of the DNA-repair-related gene (c-fos), thus effectively enhancing the Pt-based antitumor efficacy (Fig. 29B). **24-NP** was obtained *via* copolymerization of Pt(IV) scaffold and cyclobutane-1,2,3,4-tetracarboxylic dianhydride (CBTA), then covered with oligomethylenimine (OEI1.8K), then with si(c-fos), and finally coated with negatively charged CD44-receptor-targeting PEG-grafted hyaluronic acid. Upon blue light irradiation (450 nm, 20 mW/cm^2, 30 min), **24-NP** underwent photoreduction with the release of Pt(II) and azidyl radical $N_3\cdot$, which allowed for intracellular light-controlled endo/lysosomal escape and rapid si(c-fos) unpacking in CD44$^+$ A2780DDP cells. **24-NP** downregulated c-fos expression which in turn promoted the expression of pro-apoptotic Bax and facilitated DNA platination. As a result, therapy with **24-NP** + blue light successfully inhibited growth of CDDP-

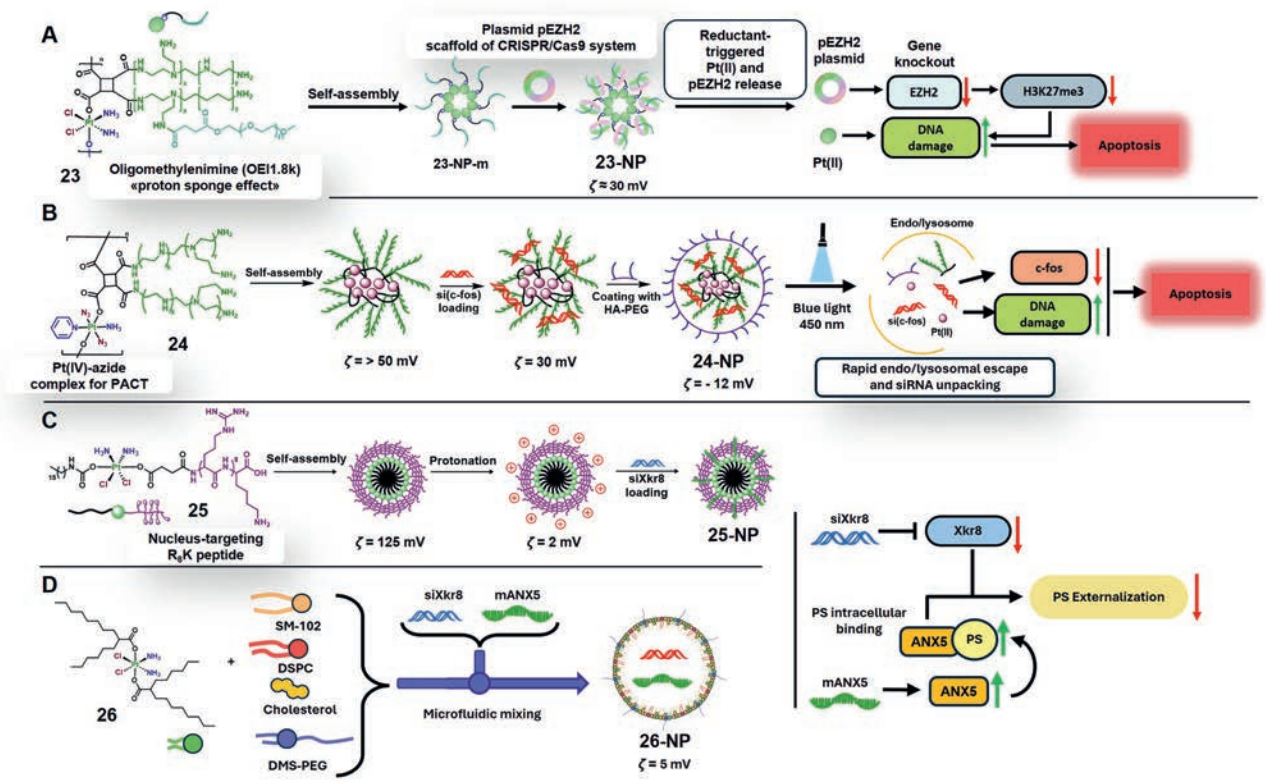

Figure 29 Pt(IV) nanoparticles for combined chemo/gene therapy. (A) **23-NP** loaded with p*EZH2* plasmid for EZH2 knockout. (B) **24-NP** based on Pt(IV)-azide complex loaded with si(c-fos) for light-induced endo/lysosomal escape and suppression of c-fos. (C) **25-NP** with nuclear-targeting peptide, loaded with siXkr8 for suppression of phosphatidylserine (PS) externalization. (D) Lipid-based **26-NP** with encapsulated siXkr8 and mANX5 for synergistic inhibition of PS externalization[139,306,309,311].

resistant A2780/CDDP tumor with no general toxicity. Importantly, **24-NP** demonstrated higher therapeutic efficacy than negative-control **24-NP-m** with ncRNA, thereby confirming the importance of gene-silencing in therapeutic efficacy.

One of the ways cancer cells escape from the immune response is phosphatidylserine (PS) exposure, which is irreversibly translocated to the outer leaflet of cancer cells *via* scramblase such as Xkr8 protein. When outside the cancer cell, PS binds to the receptors of immune cells, which results in immunosuppression. Thus, blocking the expression of Xkr8 to prevent phosphatidylserine from being shunted to the surface may enhance immune response and reduce risk of tumor recurrence[310].

In 2024, Wei et al.[311] reported an amphiphile Pt(IV) prodrug **25** with a hydrophobic lipid chain and a nuclear-targeting hydrophilic peptide R_8K in axial positions (Fig. 29C). Prodrug **25** self-assembled into positively charged **25-NP-m**, which allowed it to be utilized as an ionizable carrier for small interfering RNA of Xkr8 (siXkr8) for silencing the expression of Xkr8 protein, yielding **25-NP**. Nucleus-targeted R_8K peptide facilitated accumulation of **25-NP** in nucleus; also, **25-NP** reduced Xkr8 expression in the 4T1 cells, as well as the exposure of phosphatidylserine on the outer surface. Also, **25-NP** demonstrated significant accumulation in tumor tissue, thereby confirming tumor-targeting ability of R_8K. Expectedly, **25-NP** demonstrated promising antitumor efficacy on 4T1 tumor model, superior to that of CDDP and model NPs without siXkr8. Consequently, therapy with **25-NP** promoted DCs (CD80+, CD86+) maturation both *in vitro* and *in vivo* on 4T1 tumor model, induced macrophage polarization to immune-stimulatory M1 type and induced tumor infiltration with $CD4^+$ and $CD8^+$ effector T cells.

In 2026, Zhang et al.[139] reported a co-loading of both siXkr8 and m*ANX5*, a mRNA for PS-binding protein annexin A5, into Pt(IV)-based lipid NPs, in order to achieve synergistic effect on suppressing PS exposure (Fig. 29D). Due to the presence of Pt(IV) complex, **26-NP** were more rigid than Pt-free ones, which allowed for fast internalization and rapid lysosomal escape, which prevents RNA degradation in acidic media. In 4T1 tumor cells, **26-NP** successfully reduced PS externalization which increased the expression of immune-promoting cytokines in co-cultured bone marrow-derived macrophages. Although **26-NP** could not effectively reach the tumor upon i.v. administration, treatment of 4T1 tumor-bearing mice *via* intratumoral injection resulted in improved immune tumor microenvironment with reduced MDSCs and elevated $CD8^+$ level. As a result, **26-NP** suppressed growth of 4T1 subcutaneous tumor when administered intratumorally and prevented the formation of lung metastases during treatment.

4.4.2.2. Nuclei targeting. In 2024, Wei et al.[312] reported a Pt(IV) prodrug **27** with nucleus-targeting peptide R8K as an axial ligand and nanoprodrug **27-NP** obtained by its self-assembly (Fig. 30). Non-targeted **27-NP-m** were used as control. Both **27** and **27-NP** were able to release OXA under reducing conditions and demonstrated the nucleus-targeting capability, with 74% nucleus-targeting efficiency, 3.6-fold higher than that of OXA and 3.6-fold higher than that of **27-NP-m**. An increased nuclear accumulation resulted in enhanced cell toxicity and blocked DNA

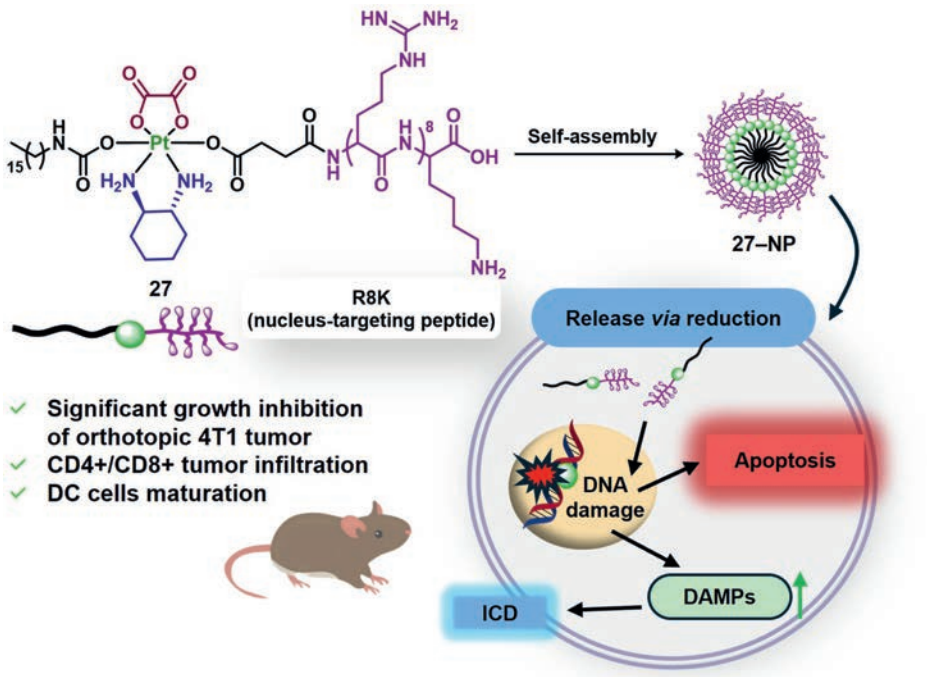

Figure 30 Pt(IV) prodrug **27** with nucleus-targeting peptide R_8K as an axial ligand and its assembly into **27-NP.** The intracellular mechanism of **27-NP**: oxaliplatin-induced DNA damage and subsequent DAMP release[312,313].

replication. **27-NP** also stimulated ICD in drug-treated 4T1 cells, which was confirmed *via* DAMP release detection. Tumor accumulation of fluorescent-labeled **27-NP** was confirmed on the 4T1 tumor model; strong fluorescence was observed 72 h after injection. Also, a significant antitumor response was shown on the same 4T1 tumor model, with superior therapeutic efficacy of **27-NP** compared to prodrug **27-NP-m** and OXA. Notably, non-tumor-targeted **27-NP-m** caused strong weight loss, which may indicate strong side to proteins, while nuclear-targeted **27-NP** showed stable weight during therapy of ∼16g. A significant immune response *in vivo* was also demonstrated, with an increase in the level of mature DCs, $CD4^+$, and $CD8^+$ T cells tumor infiltration, a decrease in regulatory T cells; additionally, an increased level of IFN-γ and TNF-α in the serum, as well as downregulation in IL-10 level, was confirmed.

4.4.2.3. Mitochondria targeting. A mitochondria-targeting strategy for platinum-based drug delivery is a promising approach since it increases drug accumulation by avoiding nuclear export pumps, amplifies oxidative stress-induced DNA damage, disrupts mitochondrial DNA (mtDNA) repair mechanisms, and triggers synergistic apoptosis *via* dual nuclear and mitochondrial genomic instability.

In 2023, Yang et al.[313] designed Pt(IV)-based dual-targeting **28-NP** to enhance both tumor accumulation and mtDNA damage (Fig. 31A). For this, Pt(IV) prodrug **28** with a mitochondria-targeted triphenylphosphine (TPP) moiety was loaded into a hepatocellular carcinoma-targeted amphiphile polymer with a GSH-depleting disulfide bond; a polymer without galactose moiety P2 and without disulfide bond P3 were used as controls. The resulting **28-NP** rapidly disassembled with Pt release in the presence of GSH, thereby decreasing intracellular GSH level. The ability of **28-NP** to accumulate in mitochondria of CDDP-resistant hepatocellular carcinoma cells was confirmed by increased ROS levels accompanied by the decreased ATP and MMP levels. RNAseq analysis further demonstrated the increased expression of apoptosis- and autophagy-related genes, together with down-regulated expression of autophagy-suppressing mTOR-related genes in **28-NP**-treated 7404DDP cells. **28-NP** did not show significant tumor accumulation, however, tumor accumulation of AGPR-affine **28-NP** was higher than that of Gal-free model particles. Evaluation of **28-NP** antitumor performance *in vivo* on patient-derived tumor xenograft model of hepatocellular carcinoma demonstrated almost 3-fold lower tumor volume and weight compared to CDDP after therapy with **28-NP**, with no damage observed in healthy tissues. It is worth noting that NPs based on the model polymer without galactose or without disulfide showed lower therapeutic efficacy, thereby demonstrating the contribution of both the galactose fragment and the disulfide bond in the resulting therapeutic efficacy.

In 2023, Liu et al.[314] reported amphiphile CDDP-based prodrug **29,** with a mitochondria-targeted TPP and ROS-generating cinnamon aldehyde (CA) acetal as axial ligands with a pH-cleavable acetal link (Fig. 31B). Cationic **29-NP** were obtained *via* self-assembly of prodrug **29**, demonstrated accumulation in mitochondria followed by pH- and GSH-sensitive release of CDDP, as well as elevated intracellular ROS levels due to the CA release from the prodrug[315], resulting in a notable MMP decrease and an increase in lipid peroxidation of CDDP-resistant lung adenocarcinoma A549cisR cells. Biodistribution studies demonstrated a significant accumulation of **29-NP** in liver; however, an elevated level of Pt in the A549/DDP tumor when compared to CDDP and Pt(IV) prodrugs allows to suggest an EPR effect.

29-NP inhibited the growth of the A549cisR xenograft tumor more efficiently than CDDP and Pt(IV) prodrugs, with 3.6-fold lower tumor weight by the end of the therapy. A comparison of

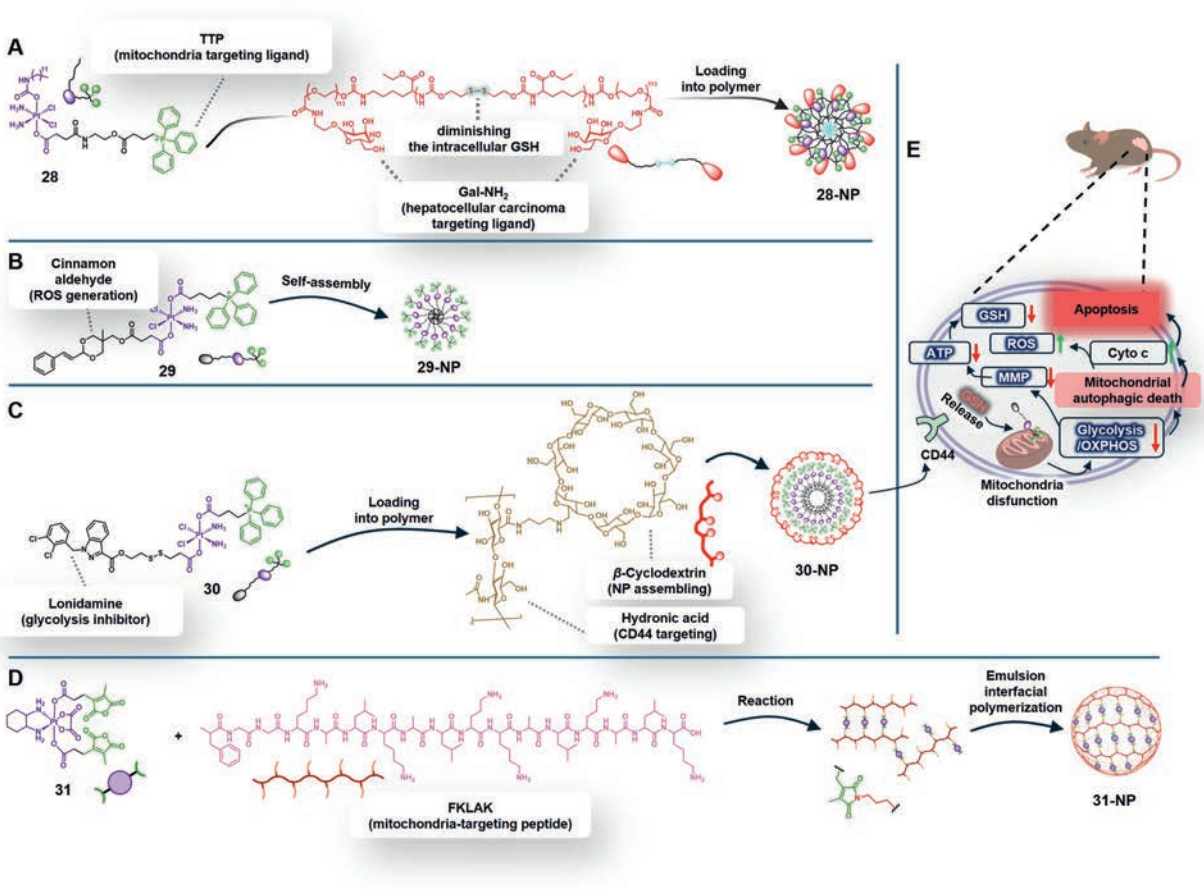

Figure 31 Design and mechanism of mitochondria-targeted Pt(IV) prodrug-based nanoparticles. (A) Pt(IV) prodrug **28** with mitochondria targeting ligand TTP and its loading into GSH-sensitive polymer resulting in **28-NP**. (B) Pt(IV) prodrug **29** with TTP and its self-assembly into **29-NP**. (C) Pt(IV) prodrug **30** with glycolysis inhibitor lonidamine and its loading into polymer *via* host−guest interaction resulting in **30-NP**. (D) Pt(IV) prodrug **31** and its emulsion interfacial polymerization with FKLAK into **31-NP**[313,314,318,319]. (E)The intracellular mechanism of **30-NP** (as general example of mitochondria targeting nanoparticles): glycolysis inhibition, mitochondrial autophagic death and apoptosis[318].

weight loss during therapy in the **29-NP**, Pt(IV) prodrugs with TPP or CA axial ligands**,** and CDDP groups clearly demonstrate the reduced toxicity of NPs compared to Pt(IV) prodrugs, whose toxicity may be indistinguishable from that of CDDP due to low stability of the prodrug in the bloodstream. Even though mitochondria-targeted Pt(IV) prodrug with TPP moiety effectively suppresses tumor growth, significant weight loss during therapy can seriously hinder its application; the use of self-assembling NPs based on it **29-NP** succeeded in significantly reducing drug toxicity.

It is known that tumor cells demonstrate an increase in aerobic glycolysis, known as the "Warburg effect," which contributes to tumor progression and metastasis[250]. Tumors could also adapt to the external changes in the environment by switching between aerobic glycolysis and oxidative phosphorylation (OXPHOS)[316]. Lonidamine is a glycolysis inhibitor that suppresses cancer cells' energy metabolism through hexokinase II (HK II) inhibition and disrupts mitochondrial respiration[317]. In 2024, Lu et al.[318] reported a dual-targeting self-assembled drug delivery system, **30-NP** (Fig. 31C), based on CDDP-based prodrug **30** with TPP moiety and lonidamine in axial positions conjugated *via* a GSH-sensitive disulfide bond. Nanoprodrug **30-NP** was obtained *via* encapsulation of prodrug **30** in CD44-targeting *β*-cyclodextrin-grafted hydronic acid (HA-CD) NPs. **30-NP** were able to intercept glycolysis by reducing the HK II level in tumor cells, hindering OXPHOS, induce apoptosis and mitochondrial autophagic death in CDDP-resistant A549CisR tumor cells. Cy5.5-labeled **30-NP** showed high intratumoral accumulation in A549/CDDP tumor with maximum fluorescence at 24 h that persisted at 48 h. The Pt content in the tumor tissue after treatment with **30-NP** exceeded that of in the liver and kidneys by ∼ 4-fold, thereby justifying the feasibility of CD-44 targeting. Evaluation of antitumor efficacy *in vivo* provided on A549, and orthotopic lung tumor models showed complete TGI in mice treated by both **30-NP**, with the therapeutic efficacy significantly superior to that of CDDP and Pt(IV) prodrug **30**. Along with high antitumor efficacy for both **30** and **30-NP**, the 30-day survival rate in the group treated with **30-NP** was 100%, while in the group treated with Pt(IV) prodrug **30** 30-day survival rate was only 50%, which clearly supports the use of nanoformulations of Pt(IV) prodrugs, as well as the importance of active tumor targeting.

In 2024, Yang et al.[319] reported a fundamentally different approach to obtaining mitochondrial-terminated NPs is the use of mitochondrial-terminated peptide and prodrug Pt(IV) as monomers to obtain NPs by a polymerization reaction at the phase boundary (Fig. 31D). In order to avoid the use of drug carriers,

polymeric NPs **31-NP** were obtained *via* emulsion interfacial polymerization of mitochondria-targeted cytotoxic peptide FKLAK and anhydride-bearing oxoplatin prodrug in molar ratio of 1:2. **31-NP** were pH-responsive; at pH 6.5 depolymerization and release of both cytotoxic FLAC peptide and Pt was observed, thereby highlighting **31-NP** as an ideal prodrug for endosomal drug release. **31-NP** reduced intracellular GSH levels and induced mitochondrial disruption as evidenced by a decrease in MMP and ATP; lactate dehydrogenase (LDH) leakage indicated cell membrane disruption. The ability of **31-NP** to accumulate in tumor tissues more efficiently than OXA was confirmed by computer tomography of organs and the A549 tumor *ex vivo*. **31-NP** significantly inhibited the growth of xenograft A549 tumors with a TGI rate almost 6 times higher than that of OXA and was also effective in suppressing the growth of patient-derived xenograft models, with tumor volume almost 2-fold lower than for OXA.

4.4.2.4. Endoplasmic reticulum targeting. CDDP is a well-known non-immunogenic chemotherapeutic agent. However, chemical modification of CDDP with electron-acceptor axial ligands turns it into a source of endoplasmic reticulum stress and, therefore, an ICD-inducer. In 2024, Xie et al.[150] reported a perfluorocarbon-functionalized Pt(IV) prodrug **32** capable of ER accumulation and Type II ICD induction (Fig. 32). The high electron-acceptor property of the axial ligand determined the short lifetime of the prodrug **32** in the presence of sodium ascorbate (∼0.78 h) due to its high reactivity with nucleophiles. Cell treatment with the complex resulted in increased expression of ER stress markers BiP, eIF2α, and CHOP proteins. The release of ICD hallmarks ATP and HMGB1 upon cell treatment with **32** revealed its ability to stimulate an immune response. To improve the bioavailability of the prodrug **32**, HSA-coated NPs **32-NP** were obtained. Cell treatment with **32-NP** resulted in increased ER stress, ATP, and CRT secretion, indicating a strong ICD effect. Also, both **32** and **32-NP** were demonstrated to efficiently induce the maturation of DCs. Importantly, fluorescent-labeled **32-NP** demonstrated significant intratumoral accumulation on BALB/c mice bearing the orthotopic K7M2 osteosarcoma model, ∼3-fold higher than that of in liver and kidney, thereby confirming a tumor-targeting ability of HSA. Evaluation of antitumor efficacy *in vivo* on the same tumor model showed significant antitumor efficacy of both **32** and **32-NP**, with both being more effective than CDDP. An enhanced level of mature DC and $CD8^+$ T cells in the tumor was detected after treatment, thereby confirming an immune response *in vivo*. Importantly, after vaccination with K7M2 cells treated with **32** and substituent injection with living K7M2 cells, strongly reduced tumor growth in the immunized animal models was detected. The immunostimulatory properties of prodrug **32** are clearly and indisputably evident in the bilateral tumor model: while the non-ICD-inducer CDDP was expectedly ineffective in the bilateral model, prodrug **32** was able to irradiate the secondary tumor, thereby supporting the undoubted advantages of ICD-stimulating drugs over chemotherapy alone and highlighting the possibilities of fine-tuning the pharmacological profile of Pt(IV) prodrugs.

In summary, direct tissue targeting of Pt(IV) prodrug-based NPs provides superior selectivity, therapeutic effect, and reduced toxicity compared to Pt-based monotherapy, as demonstrated for the **20-22-NP**. Thus **21-NP, 22-NP** demonstrated excellent accumulation in tumor tissues in combination with toxicity reduction and effective stimulation of the immune response, leaving no doubt about the prospects of using nanomedicines for the treatment of osteosarcoma. An ability of charge-reversal **22-NP** to stimulate GAS−Sting pathway activation, which means extremely strong DNA damage due to the excellent penetrating properties of **22-NP**, which is due to its charge-inversion property. These results highlight the potential of designing charge-inverted NPs, which can circulate in the bloodstream as anionic NPs and then, at the tumor site, reverse their charge, resulting in high accumulation in tumor tissue.

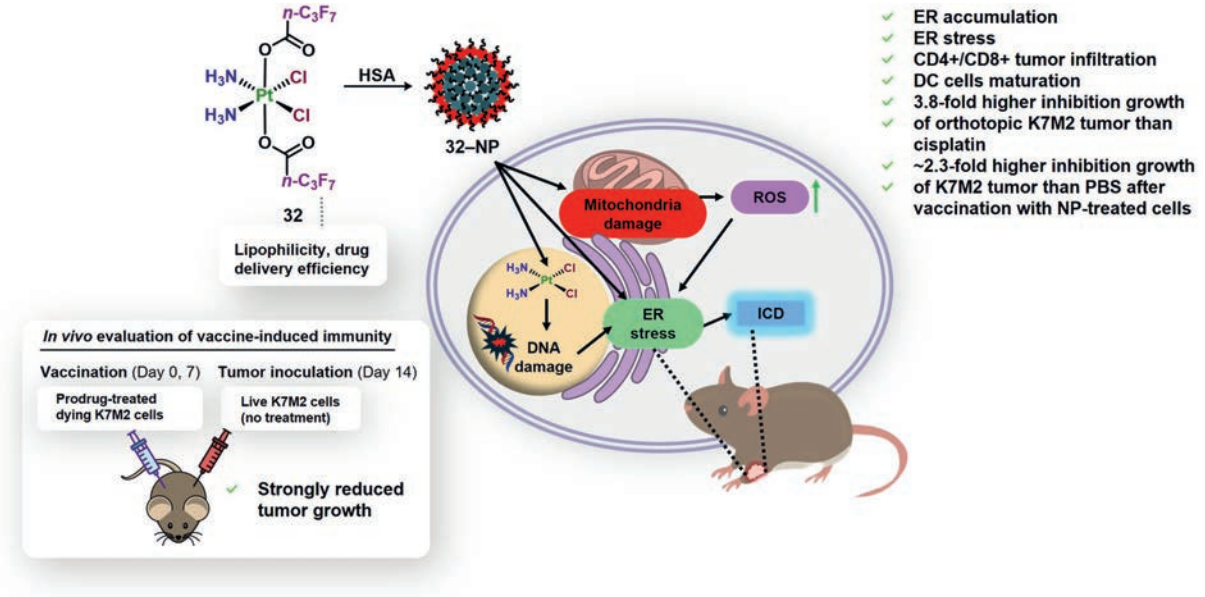

Figure 32 Pt(IV) prodrug **32** with perfluorocarbon chain as axial ligands and their assembly with HSA into **32-NP**. The intracellular mechanism of **32-NP**: ER stress and mitochondria damage-induced ICD. *In vivo* induction of long-term immune response: preliminary vaccination of mice with **32-NP**-treated K7M2 cells on Days 0, 7 inhibited the tumor growth of live K7M2 cells after inoculation on Day 14[150].

The combination of gene therapy and chemotherapy with Pt(IV) prodrugs in a single nanodrug represents a powerful therapeutic approach, allowing for the simultaneous reduction of the toxicity of Pt-based chemotherapy and the intact delivery of nucleic acids to the tumor. However, careful design of such NPs is essential, specifically ensuring sufficient stability, a negative charge, and control over the safe release of RNA from the endosome. Thus, positively charged **23-NP** NPs demonstrated therapeutic improvement over CDDP; the same research group demonstrated that PEG coating of the NPs and CD44 targeting, combined with light-induced drug release in design of **24-NP** is able to significantly enhance therapeutic efficacy. Despite the extremely powerful potential of **26-NP**, they were not able to deliver NPs to the tumor, which means the need for further improvement of the design and protection of the nanodrug from MPS.

Cell-level targeting is a mechanism of drug efficiency enhancement that should work once the nanodrug has already reached the tumor and penetrated the cell. Once nanodrug enters the cell, targeted action on specific cellular compartments can significantly enhance the therapeutic effect compared to conventional Pt-based therapy. Thus, an increase in drug accumulation in nuclei or mitochondria may increase cell sensitivity to CDDP and reduce drug resistance. However, before entering the tumor cell, nanodrug should successfully reach the tumor tissue; and the ability of the nanodrug to reach the tumor is in turn determined by its physico-chemical properties and depends on its production method. Thus, comparing four methods for mitochondria-targeted NPs **28-31-NP** production, namely, loading of the Pt(IV) prodrug **28** into an AGPR-targeted self-assembling polymer yielding **28-NP**, self-assembly of an amphiphilic Pt(IV) prodrug **29** into cationic NPs **29-NP**, loading the Pt(IV) prodrug into CD-44-targeted anionic cyclodextrins yielding **30-NP**, and interfacial polymerization to produce anionic pH-sensitive polymeric NPs **31-NP**, it can be noted that significant tumor accumulation and a significant therapeutic effect were achieved with the use of anionic CD-44-targeted NPs. In other cases, significant Pt accumulation in vital organs was observed despite a decrease in toxicity during therapy compared to Pt(II)-based therapy. It is worth noting the excellent ability of the nucleus-targeting peptide R8K to increase tumor accumulation: being a vector capable of acting intracellularly, it demonstrates a high selectivity to the tumor tissue. Also, hemoglobin-coated **32-NP** demonstrated significant accumulation in osteosarcoma tissue, thereby providing both significant therapeutic efficacy and a significant immune response. Otherwise, the ability of NPs to reach the tumor is the most important factor ultimately determining the therapeutic effect.

4.5. Theranostic and stimuli-sensitive NPs based on Pt(IV) prodrugs

NP-based theranostics represents a promising approach for simultaneous tumor diagnosis and therapy. This could be realized by co-loading of therapeutic cargos (*e.g.*, Pt-based chemotherapy) and imaging agents (fluorescent dyes, CT or MRI agents) for real-time tracking and targeted treatment. For fluorescent dyes, transparency window of biological tissues (650−1350 nm) is the desirable range for bioimaging since light has its maximum depth of penetration in tissue there[320,321]. Endogenous activation occurs *via* tumor-specific conditions, such as an acidic microenvironment, while exogenous activation is realized on demand *via* localized physical factors, such as light, ultrasound, or a magnetic field.

4.5.1. Endogenous activation

In 2019, Yan et al.[322] proposed an elegant approach to *in situ* self-assembly of membrane-localized NPs in the presence of endogenous alkaline phosphatase (ALP) overexpressed on cell membranes. In 2023, Wen et al.[323] presented ALP-triggered self-assembly of NPs based on Pt(IV) prodrug **33** with phosphorylated merocyanine as an axial ligand with subsequent intracellular reassembly of NPs under the action of glycoproteins with substituent release of CDDP (Fig. 33). The ALP-sensitive assembly of fluorescent **33-NP** was simulated in solution and could be monitored by the increase in the fluorescence signal (λ_{em} = 710 nm) and photoacoustic signals (λ = 700 nm, 750 nm). The release of CDDP from **33-NP** was confirmed by X-ray photoelectron spectroscopy (XPS) analysis and NMR. In ALP-positive tumor tissues, prodrug **33** was dephosphorylated with the formation of fluorescent NPs switching on NIR fluorescence (λ_{em} = 710 nm) and photoacoustic signals (λ = 700 nm), which in turn released Pt(II) in the presence of GSH. **33-NP** preferentially accumulates in HeLa tumors with strong fluorescent and photoacoustic signals. In contrast, fluorescent imaging performed with pre-assembled **33-NP-p** showed ∼2.7-fold lower fluorescence of the tumor, thereby confirming the importance of the design of self-assembled **33-NP**. Consequently, therapy with **33-NP** resulted in complete TGI of HeLa xenografts. Moreover, orthotopic hepatocellular carcinoma HepG2/Luc therapy with **33-NP** resulted in 13- and 10.7-fold lower bioluminescence levels than for control and CDDP, respectively, with no metastasis observed in the **33-NP** group. This new paradigm for *in situ* production of NPs directly at the tumor site allows for a significant increase in intratumor accumulation and a reduction in the side effects of therapy.

In 2024, Yu et al.[324] reported theranostic NPs **34-NP** based on Pt(IV) prodrug **34** with hand-holding fluorophore polymer chains, conjugated with a caspase-3 cleavable short peptide probe (5′-FAM-DEVD-dabcyl), an apoptosis reporter, and a tumor-targeting cyclic arginine-glycine-aspartic acid (RGD) tripeptide (Fig. 34). **34-NP** was obtained *via* self-assembly of 16.7 kDa polymer Polyplatin yielding **34-NP** (≈110 nm), which showed the ability to release Pt(II) in the presence of GSH, which was confirmed by XPS. After coating with 5′-FAM-DEVD-dabcyl, **34-NP** were able to serve as a theranostic probe, which was shown by an increase in green fluorescence (522 nm) in cells due to its cleavage by caspase-3 and disruption of FRET quenching of fluorescence. **34-NP** showed the ability to inhibit tumor cells proliferation and induce apoptosis to a greater extent than CDDP. After coating with RGD tripeptide, greater tolerability *in vivo* for **34-NP** compared to CDDP was proved, and **34-NP** also demonstrated an ability for NIR-II bioimaging (997 nm) of tumor tissues in a luciferase-labeled model of advanced-stage III/IV high-grade serous ovarian cancer. A high therapeutic efficacy for **34-NP**, superior to that of CDDP, was demonstrated on the same tumor model, along with less body weight loss.

In 2023, Wang et al.[121] reported polymeric Pt(IV) prodrug **35** obtained *via* copper-free click approach with PP2A inhibitor demethylcantharidin and folate-targeting group, which could self-assemble into micelles (Fig. 35). Due to the presence of acid-labile β-carboxylic amid, at tumor pH 6.5 **35-NP** could induce conversion of the potential charge of micelles from negative to positive. Indeed, a conversion of surface charge of **35-NPs** from −10.4 to +6.0 mV under 6.5 pH was observed. Also, **35-NP** released Pt(II) complex in the presence of sodium ascorbate under pH 5.5. Supporting that the positive charge of NPs promotes intracellular internalization, the FITC-labeled **35-NPs** could

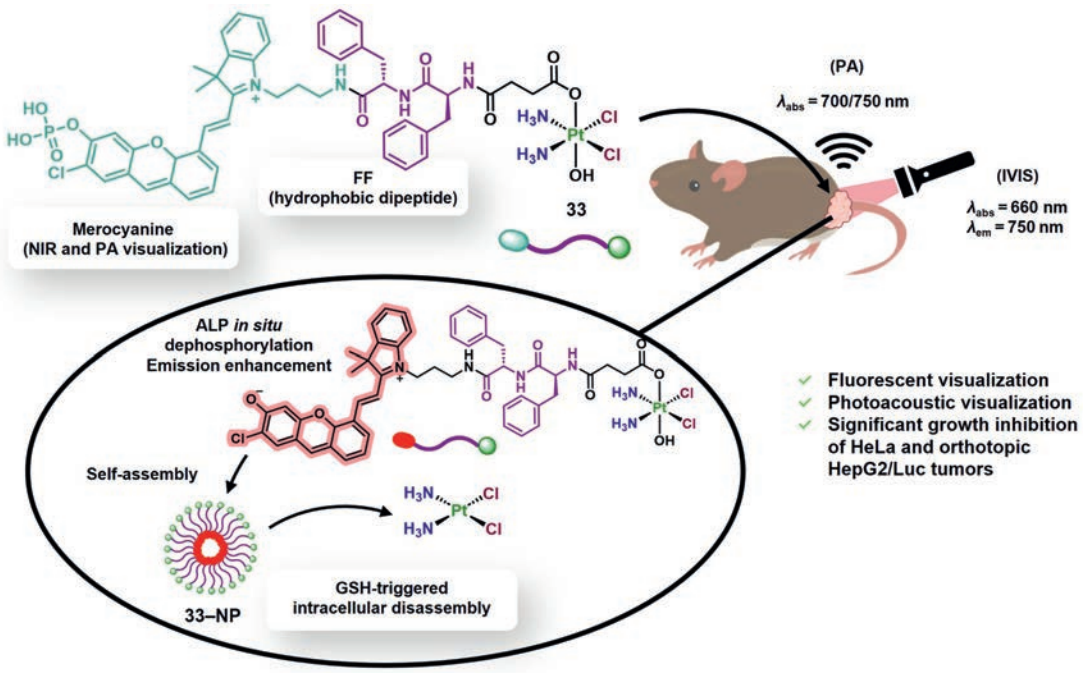

Figure 33 Pt(IV) prodrug **33** functionalized with hydrophobic dipeptide FF and NIR-absorbing PA-sensitive merocyanine and its self-assembly *via* dephosphorylation into nanoparticles **33-NP**[323,324].

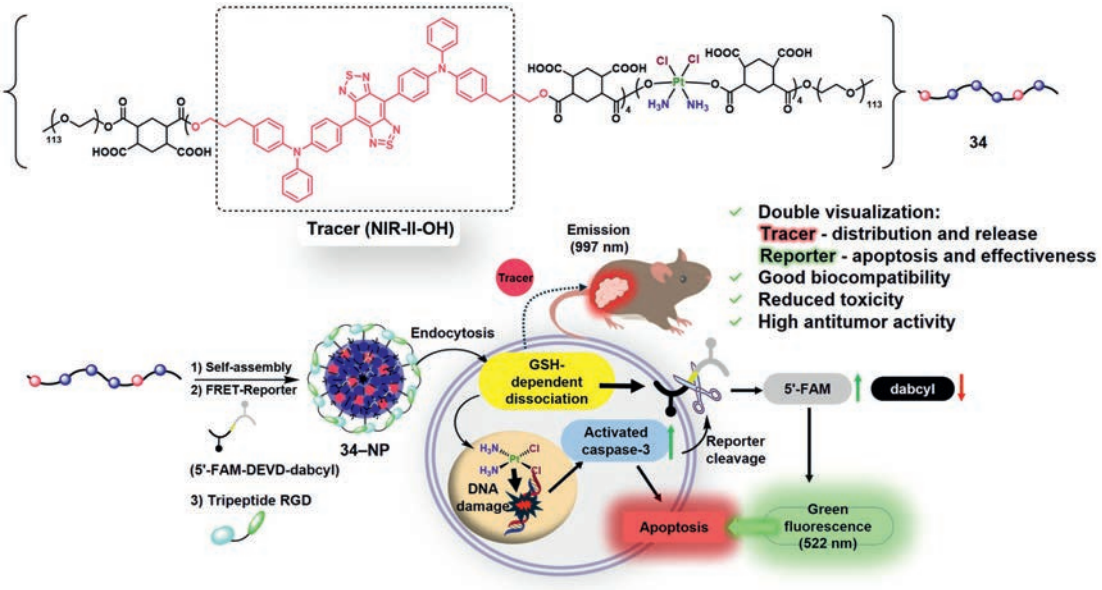

Figure 34 Pt(IV) prodrug polymer **34** functionalized with tracer NIR-II-OH and its self-assembly with FRET-reporter (5'-FAM-DEVD-dabcyl) and tumor targeting tripeptide (RGD) into nanoparticles **34-NP**. The *in vivo* therapeutic and imaging performance of **34-NP**: real-time tracing and visualization of apoptosis through cleavage of the reporter chain by caspase-3[324].

accumulate in the center of SKOV-3 tumor spheroids. **35-NPs** demonstrated high SKOV-3 tumor accumulation at 24 h post-injection which was attributed to active folate targeting. *In vivo* acute toxicity test revealed that LD_{50} of **35-NPs** were 6 times that of CDDP, indicating higher biocompatibility of the former. Anti-tumor efficiency of **35-NPs** on subcutaneous SKOV-3 tumor model was found to be similar to that of CDDP with comparable tumor growth inhibition and Pt content after 28 days of therapy. However, **35-NPs** demonstrated higher survival rate of mice during the experiment and demonstrated little to no general toxicity.

4.5.2. Exogenous activation

4.5.2.1. Ultrasound-activated NPs. An ultrasound drug activation combines the advantages of non-invasive, non-ionizing radiation with high temporal and spatial precision and potential imaging utility. The primary mechanisms through which

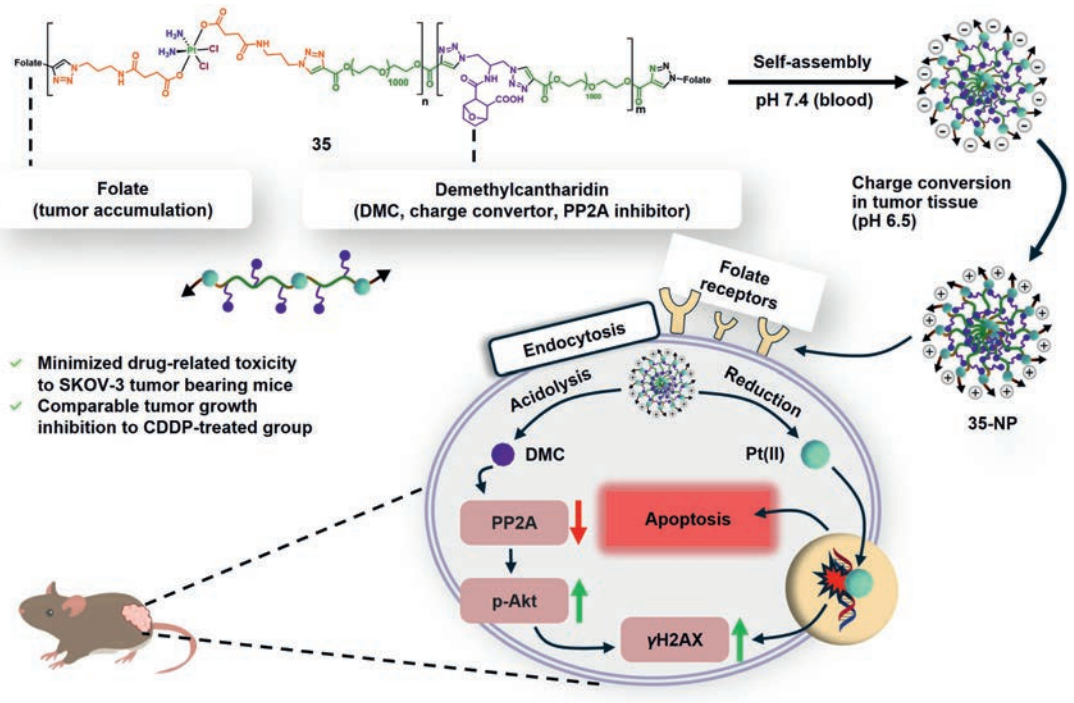

Figure 35 Polymeric Pt(IV) prodrug **35** with folate group, its self-assembly into micellesand charge conversion *via* acid-labile amide group into **35-NP**. The intracellular mechanism of **35-NP**: DNA damage and cell apoptosis[121].

ultrasound enhances targeted drug delivery and drug release are the physical effects generated by the oscillation and implosion of these cavitation bubbles[325]. The implosion of cavities can lead to extreme rises in temperature and pressure, which causes numerous chemical reactions, including the concentration of energy sufficient to generate light, known as sonoluminescence[326]. Since ultrasound is actively used in clinics as a simple and informative diagnostic tool, the use of ultrasound-based nanoagents could be convenient.

In 2023, Liang et al.[32] used hemoglobin as a sonosensitizer for an ultrasound activation of Pt(IV) prodrug **36** with lipophilic tails as axial ligands (Fig. 36A). Pt(IV) prodrug **36** was encapsulated into hemoglobin-based NPs **36-NP**, capable of reduction to Pt(II) upon exposure to ultrasound radiation (1.5 W/cm^2) for 10 min, which was monitored by XPS. **36-NP** showed the ability to generate singlet oxygen when exposed to ultrasound, and caused γ-H2AX expression, resulting in stimulus-sensitive cell death. Cy5.5—labeled **36-NP** showed high tumor accumulation after 36 h in the murine colorectal carcinoma CT-26 tumor mice model, significantly exceeding that in the liver and kidneys, thereby confirming the tumor-specific properties of hemoglobin. Also, **36-NP** exhibited a strong antitumor effect when combined with focused ultrasound on the CT-26 tumor model, which was proven to be more effective than CDDP. Importantly, tumors that were covered with a tissue fantom (chicken breast) were nearly fully eradicated, which demonstrates the unique ability of the ultrasound to prompt Pt(IV) nanoparticle activation in deep tumors.

In 2025, Shen et al.[327] reported OXA-based polymer prodrug **37**, co-assembled with sonosensitizer Ce6 into OXA-Ce6 **37-NP** for combined sonosentizing therapy and ultrasound-controlled release of OXA (Fig. 36B). XPS- and ICP-MS-monitored studies of **37-NP** degradation under US demonstrated reduction of Pt(IV) prodrug **37** and subsequent release of 85% of OXA from **37-NP** over 48 h. Ultrasound promoted cellular uptake of **37-NP** in CT-26 cells and induced ROS formation in **37-NP**-treated cells. Also, **37-NP** were found to induce ICD in CT-26 cells as evidenced by CRT translocation, HMGB1 externalization, and ATP secretion. Consequently, DC maturation *in vitro* was also demonstrated for BMDCs, incubated in the presence of **37-NP**-treated CT-26 cells. **37-NP** exhibited strong antitumor effect *in vivo* in combination with ultrasound treatment, with tumor suppression rate up to 90%. Therapy with **37-NP** induced infiltration of CT-26 tumor with CD8$^+$ T cells and polarization of macrophages into M1 type. As a result, **37-NP** enhanced the effect of αPD-1 treatment in combination therapy, which resulted in significant tumor suppression and formation of long-term immunological "memory reservoir", as evidenced by an increase in central memory T cells in spleen.

4.5.2.2. Light-activated NPs. Photoactive NPs possess significant advantages due to the ability of activation on demand by applying light directly to tumor tissues, where light-driven chemotherapeutic agent release may occur[328,329]. Various nanomaterials based on boron-dipyrromethenes (BODIPYs)[328,330], cyanine dyes[331] and UCNPs[332] have been proposed; however, only a few NPs capable of light-induced drug release based on Pt(IV) prodrugs were reported. Varying the nature of the fluorophore opens up possibilities for the design of agents for photoactivated chemotherapy, photodynamic (PDT) and photothermal therapy (PTT) as part of a single molecule or nanodrug. PDT and PTT offer a greater degree of spatiotemporal control compared to systemic therapies, reducing off-target toxicities[333].

4.5.2.2.1. Pt(IV) prodrug loaded in UCNPs. UCNPs are capable of generating ultraviolet or visible light luminescence by absorbing long-wavelength NIR light *via* two-photon or multiphoton emission mechanisms[334]. Upconversion luminescence

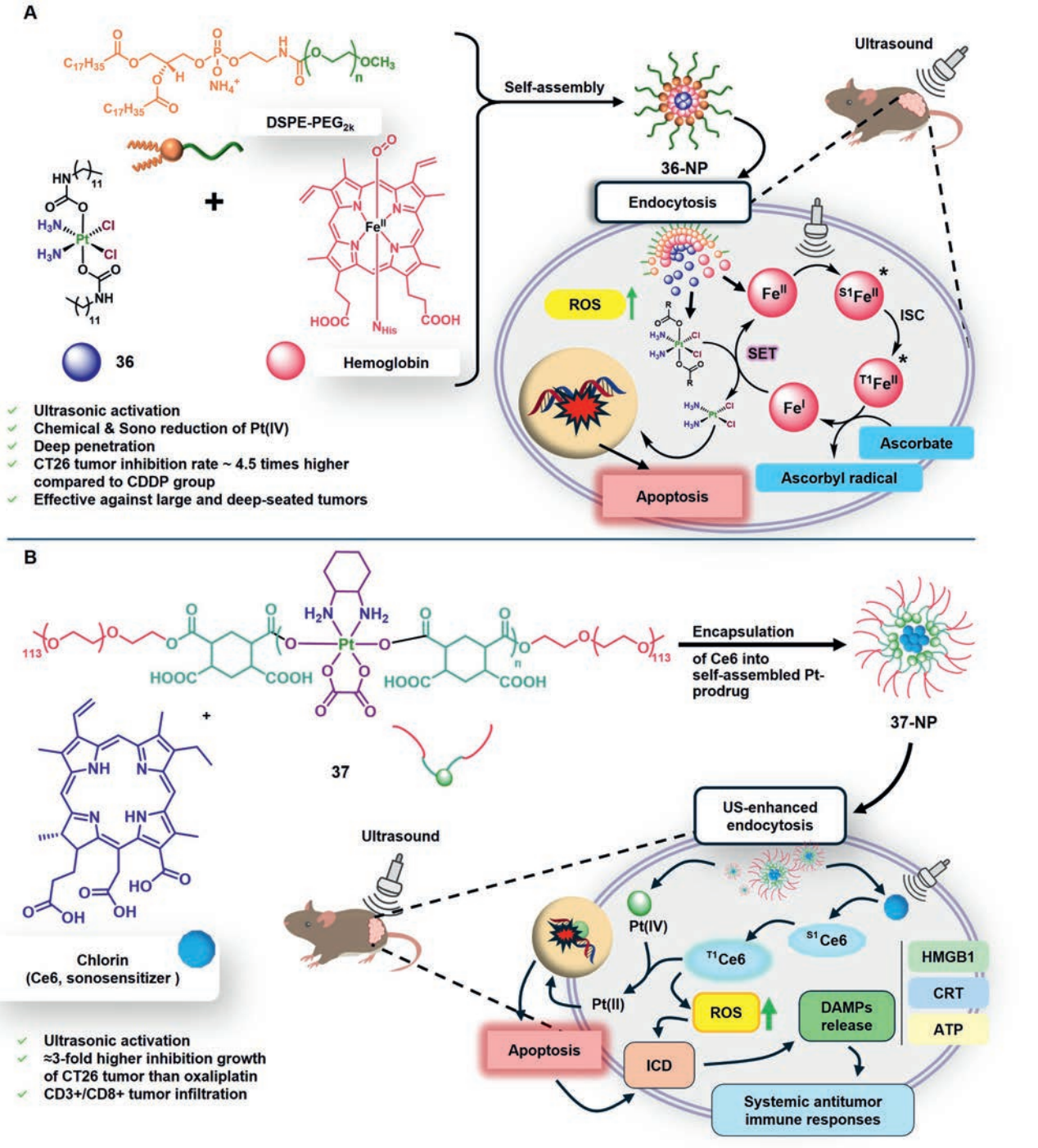

Figure 36 (A) Pt(IV) prodrug **36** and its self-assembly with DSPE-PEG$_{2k}$ and hemoglobin into nanoparticles **36-NP**. The intracellular mechanism of **36-NP**: ultrasound-mediated SET from hemoglobin to Pt(IV) with subsequent apoptosis induction *via* Pt(II) activity. (B) Pt(IV) prodrug **37**, its self-assembly and encapsulation with Ce6 into nanoparticles **37-NP**. The intracellular mechanism of **37-NP**: ultrasound-mediated electron transfer from chlorin to Pt(IV) with subsequent apoptosis and ICD[32,327].

could be utilized for UV light-triggered axial bond cleavage of Pt(IV) prodrugs with the release of cytotoxic Pt(II)[157].

In 2024, Liu et al.[157] reported dual-stimuli responsive NPs **38-NP** based on Pt(IV) prodrug **38** with phenylbutyrate as an axial ligand loaded into UCNPs with RGD peptide (**38b-NP**) for tumor cell targeting, RGD-free **38a-NP** were used as control (Fig. 37). **38b-NP** rapidly released CDDP specifically in the presence of GSH alone and under 980 nm light (0.48 W/cm^2). Both **38a-NP** and **38b-NP** demonstrated ~1.51-fold increase in toxicity under NIR light irradiation, demonstrating sufficient toxicity and in the absence of irradiation, probably due to the accumulation of particles in cells and GSH-induced release of Pt. Upconversion luminescence allowed for real-time visualization of **38b-NP** tumor accumulation which reached a maximum at 2 h post-injection.

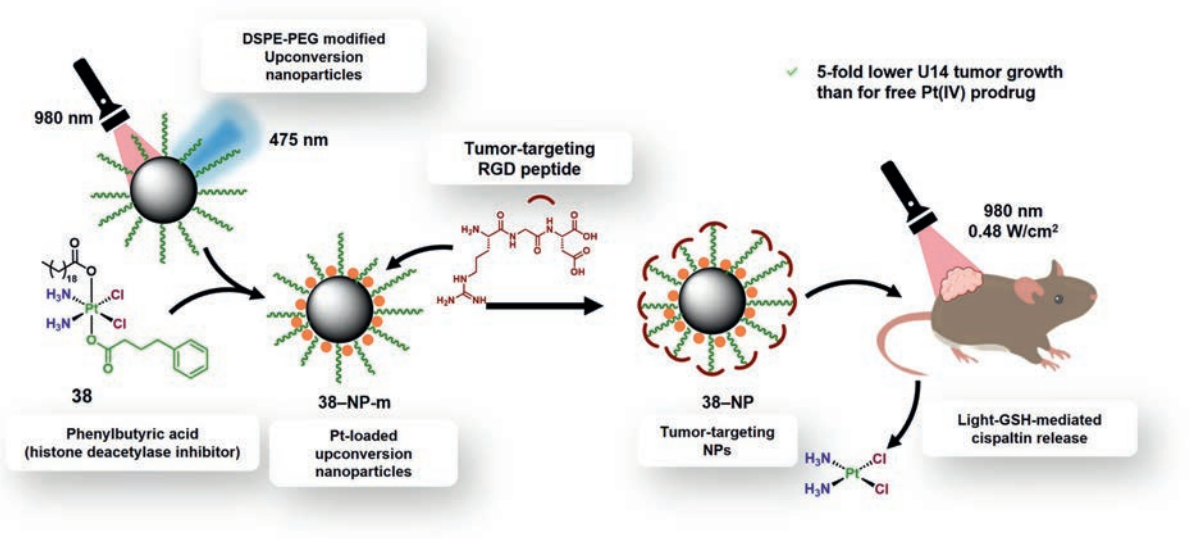

Figure 37 Pt(IV) prodrug **38** modified with histone deacetylase inhibitor phenylbutyric acid, its loading into DSPE-PEG modified UCNP (**38-NP-m**) and subsequent conjugation with tumor-targeting RGD peptide to yield nanoparticles **38-NP**[157].

RGD moiety allowed for enhanced tumor accumulation, compared to RGD-free **38a-NP**, as evidenced by Pt biodistribution. Consequently, **38b-NP** demonstrated almost complete tumor inhibition growth under 980 nm light (5 min, 0.48 W/cm^2), with tumor volume almost 5-fold lower than for free Pt(IV) prodrug **38**. Although the RGD peptide increased **38b-NP**'s accumulation in the tumor, biodistribution data demonstrated significant accumulation of Pt in major organs, primarily the liver and lungs. However, despite the lack of selectivity for accumulation in tumor tissue, **38b-NP** treatment of mice did not cause significant weight loss. It is also worth noting that **38b-NP** demonstrated significant therapeutic efficacy even in the absence of irradiation, indicating strong release of drugs from NPs in the dark.

4.5.2.2.2. Pt(IV) prodrug conjugated with photo-responsive polymer. In 2022, Wei et al.[148] reported self-assembled prodrug **39** with OXA core conjugated with a aggregation-induced emission photosensitizer that could be excited within the NIR region at 808 nm and cancerous tissue/nucleus targeting peptide R8K (Fig. 38A). Pt(IV)-based NPs **39-NP** were obtained *via* self-assembly of Pt(IV) prodrug **39** and demonstrated strong

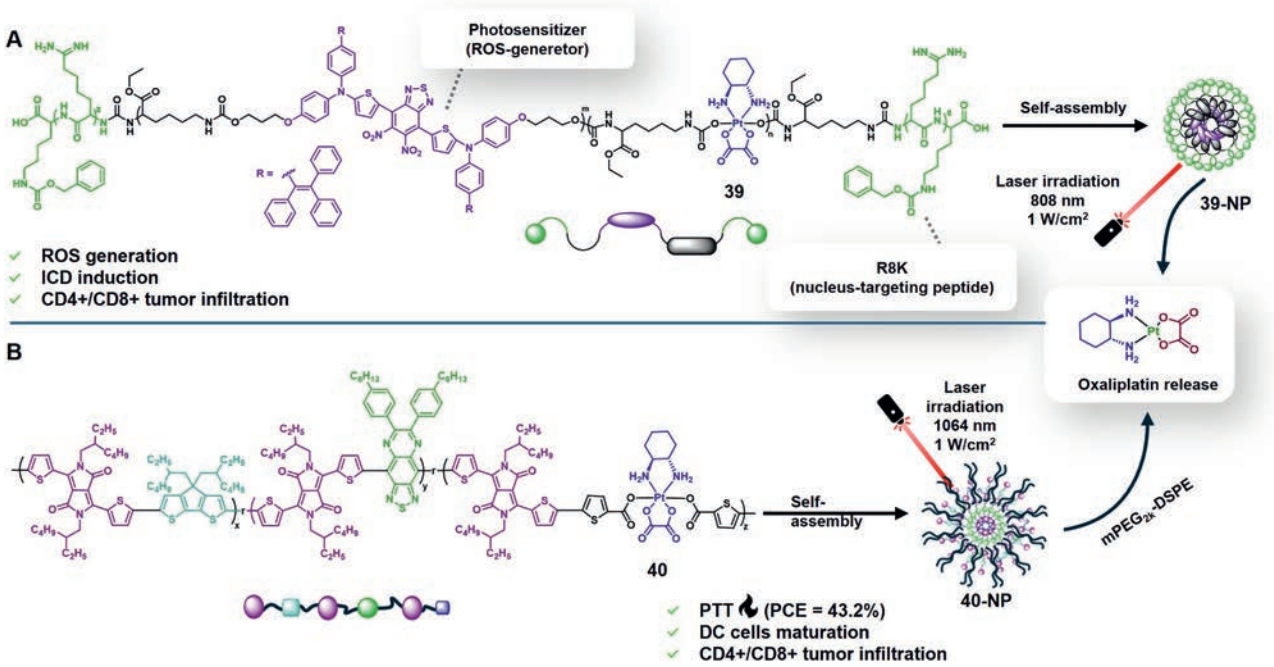

Figure 38 Polymeric Pt(IV) prodrugs **39** (A)and **40** (B) and their self-assembly into **39-NP** and **40-NP** capable of light induced Pt release[148,335].

fluorescence at 1000 nm upon excitation with 808 nm. **39-NP** remained intact in the dark, while upon irradiation Pt release was observed, which was confirmed *via* XPS. Also, **39-NP** demonstrated the ability to cause light-induced DNA platination and a significant accumulation in cell nuclei, with ∼5-fold compared to OXA and non-targeted **39m-NP**. Light-induced release of ICD hallmarks ATP and HMGB1 was confirmed on 4T1 cells after treatment with **39-NP** and 808 nm light irradiation. A high intratumoral accumulation of **39-NP** on the 4T1 orthotopic breast cancer BALB/c mouse model was observed with fluorescence maximum at 24 h; moreover, the accumulation in the tumor was ∼1.1 times greater than that in the liver. Also, a significant tumor inhibition after treatment with **39-NP** and irradiation (808 nm, 1 W/cm^2) was demonstrated, and an increased number of mature DC was found in tumor tissues when compared to the OXA group. Importantly, non-targeted **39m-NP** NPs were not superior to OXA in the absence of irradiation, while in the presence of irradiation demonstrated therapeutic efficacy similar to that of nuclei-targeted **39m-NP**, thus confirming the need for active targeting of NPs.

In 2023, Tang et al.[335] reported a NIR-II light-activated pseudo semiconducting polymer **40** based on OXA, which was synthesized *via* Stille polycondensation of monomers and Oxa-Br, for PTT, chemotherapy, and immunotherapy (Fig. 38B). Upon irradiation of polymer **40** with 1064 nm NIR-II light acceleration of the Pt(IV) reduction and degradation of the polymer was observed. **40-NP** showed a photothermal conversion efficiency (PCE) of 43.2%, with good photostability. Also, the ascorbate-induced release of OXA was detected, which was accelerated under NIR-II light irradiation (1064 nm, 1.0 W/cm^2, 10 min). **40-NP** demonstrated the ability to induce ICD in CT-26 cells after irradiation. Fluorescent-labeled **Cy5.5-40-NP** showed significant intratumoral accumulation after 8 h post i.v. administration in the CT26-tumor-bearing mouse model, which, however, did not exceed the accumulation in the liver. Also, a significant photothermal effect *in vivo* was demonstrated after tumor irradiation: the temperature rose by 32 °C within 8 min of irradiation after i.v. injection of **40-NP**. As a result, **40-NP** and light completely inhibited CT26 tumor growth, triggered ICD with HMGB1, ATP, and CRT DAMPs release, which resulted in tumor infiltration with CD4$^+$ and CD8$^+$ T cells as well as DC maturation. It is also worth noting that **40-NP** demonstrated significant therapeutic efficacy even in the absence of irradiation.

4.5.2.2.3. Pt(IV) prodrug co-assembled with dye into drug carrier. In 2022, Ding et al.[336] reported a BSA-conjugated Pt(IV) prodrug and luminogen capable of aggregation-induced emission co-loaded into BSA (bovine serum albumin) for dual bladder cancer treatment (Fig. 39A). Pt(IV prodrug **41** was covalently conjugated with BSA, then NPS with 15% BIIT were obtained. Since BIIT was subject to conformational constraints in BSA, **41-NP** demonstrated fluorescence at ∼900 nm with ϕ 4.64% and photothermal efficiency 26.35%. Furthermore, **41-NP** were degraded at temperatures above 60 °C and exhibited GSH-stimulated release of Pt, which was significantly accelerated by laser irradiation; also, a reduction of Pt(IV) to Pt(II) was confirmed *via* XPS. **41-NP** demonstrated significant phototoxicity after laser irradiation, with reduction of Pt IC_{50} by 235-fold in the **41-NP** compared with Pt(IV) prodrug **41**-BSA conjugate and BITT@BSA. Biodistribution studies provided on subcutaneous MB49 tumors revealed an accumulation of **41-NP** in liver, tumor and intestine. After 6 h p.i. tumors were irradiated (0.3 W/cm^2, 10 min), with heating up of tumor tissue up to 43 °C. *In vivo* antitumor efficacy of **41-NP** was evaluated on MB49 tumor-bearing mice, while **41-NP** didn't demonstrate therapeutic efficacy, a combination of **41-NP** + lased lead to tumor growth inhibition; hematoxylin and eosin staining demonstrated tumor cell necrosis with no damage to main organs. It is important to note that weight loss in the **41-NP** + laser group was identical to that in the BIIT + laser group, while the therapeutic efficacy of **41-NP** was significantly higher, approximately four times greater than that of BIIT. These further underscores the potential of incorporating Pt(IV) prodrugs into nanoagents, thereby combining chemotherapy with photothermal and photodynamic therapy.

In 2023, Wan et al.[337] reported a paclitaxel-OXA (PTX-OXA) Pt(IV) prodrug **42** with the chlorin e6 (Ce6) photosensitizer that covalently self-assembled with a double-selenium cross-linker, yielding diselenide nanoprodrug **42-NP** for combined chemotherapy, PDT, and immunotherapy through pyroptosis induction (Fig. 39B). Diselenide bond was used instead of commonly used S−S since its ability to respond to two stimuli, GSH and ROS, with reduction and oxidation of diselenide, respectively. **42-NP** showed light-induced cellular toxicity 660 nm (0.5 W/cm^2, 5 min), superior to that of the prodrug **42**, paclitaxel, and chlorin, thereby confirming the combined action of the components of **42-NP**. Also, **42-NP** demonstrated an excellent pyroptosis induction ability after red light irradiation, which was confirmed *via* release of LDH as well as ICD hallmarks HMGB1 and ATP in 4T1 cells. *In vivo* biodistribution in 4T1 tumor-bearing mice showed a high fluorescence level at tumor, higher than that in liver, at 24 h after injection which remained even after 72 h. *In vivo* antitumor efficacy of **42-NP** combined with tumor irradiation on 4T1 and 4MOSC2 oral tongue carcinoma tumor models showed a prominent inhibitory effect with complete tumor disappearance; also, pyroptosis induction in tumor tissues was confirmed. **42-NP** stimulated immune response *in vivo via* DC maturation, down-regulation of MDSCs and Treg, and increased amount of CD8$^+$ T cells in the spleen. Synergetic effect of **42-NP,** light and αPD-1 was shown on 4T1 bilateral tumor mouse model, the combination not only restrained the primary tumor but also inhibited the growth of distant tumors. The ability of antitumor immunity post-treatment to suppress recurrent tumors was also shown, which could be blocked *via* CD4$^+$ and CD8$^+$ antibodies, thereby confirming memory T cells involvement.

In 2025, Zhang et al.[338] reported a Pt(IV) prodrug **43** with fenofibrate and TPP as axial ligands, which was co-assembled onto Pt(IV)-based NPs **43-NP** with IR780 coupling DSPE-PEG2K in order to combine mitochondria-targeted delivery, disrupting mitochondrial structure and respiratory function, and phototherapy (Fig. 39C). **43-NP** demonstrated light-induced release of CDDP and photothermal efficiency exceeding that of IR780. Light-induced toxicity, an intracellular mitochondria accumulation, and mitochondrial depolarization were proved for **43-NP** *in vitro*. Also, **43-NP** demonstrated an increased circulation time in the bloodstream compared to Pt(IV) prodrug **43** (42.65 h *vs*. 0.97 h), and the ability to accumulate in 4T1 tumor; however, accumulation of **43-NP** in the liver exceeded that in the tumor. Significant antitumor efficacy of **43-NP** on the 4T1 model was observed; **43-NP** in combination with radiation (808 nm, 1.5 W/cm^2, 3 min) showed the greatest efficiency and almost complete ablation of tumors, with a TGI up to 90%, as well as lung metastasis inhibition.

4.5.2.2.4. Self-assembly of photoactive Pt(IV) prodrug. In 2024 we reported NIR-light absorbing Pt(IV)-prodrug-based NPs **44-NP** for both tumor bioimaging and chemo-PTT therapy

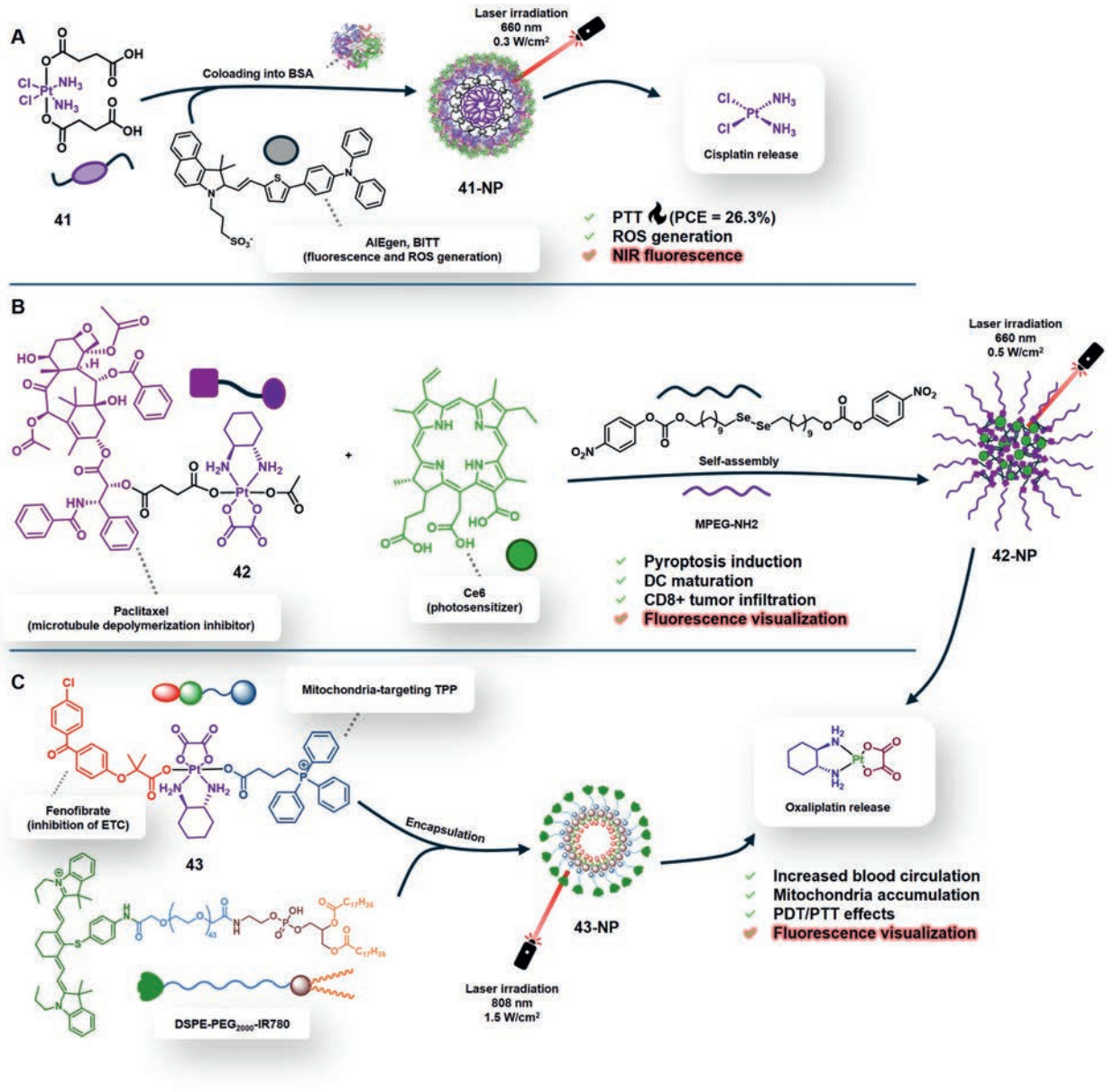

Figure 39 Photoresponsive Pt(IV)-based nanoparticles capable of light induced Pt release. (A) Pt(IV) prodrug **41** and its coloading with BITT into BSA resulting in **41-NP**. (B) Pt(IV) prodrug **42** and its self-assemble with Ce6, MPEG and diselenide cross-linker into **42-NP**. (C) Pt(IV) prodrug **43** and its encapsulation into DSPE-PEG_{2000}-IR780 into **43-NP**[336,337,338].

(Fig. 40A)[339]. In aqueous solutions, Pt(IV) prodrug **44** formed J-aggregates *via* self-assembly with batochromically shifted absorption, resulting in the formation of **44-NP** that demonstrated rapid CDDP release under 400 mW/cm^2 660 nm light irradiation and exhibited substantial photothermal effects *in vitro* with a PCE of 42.1%. **44-NP** proved to be potent as a theranostic agent, combining the capabilities of a photothermal agent, photothermal and fluorescence imaging agent with photo-activated chemotherapy. Thus, **44-NP** showed high intratumoral accumulation 24 h after i.v. injection in CT-26 tumor-bearing BALB/c mice, while *in situ* injection of **44-NP** with subsequent irradiation with mild NIR light (660 nm, 0.2 W/cm^2) heated up the tumor up to 49 °C, which is sufficient for tumor ablation[340].

In 2026, we reported a NIR-light-activatable theranostic nanoplatform **45-NP** with dual antitumor action, PTT/PACT, based on Pt(IV) prodrug **45**, capable of fluorescent and photothermal imaging of tumor tissues (Fig. 40B)[341]. A barrier-free CF_3 rotor moiety in the BODIPY core provides excellent photothermal efficacy for the nanoplatform, while both the Pt(IV) prodrug **45** and **45-NP** were able to release CDDP under 740 nm light irradiation. Metabolomic profiles of **45-NP**-treated MCF-7 cells confirmed strong thermal- and CDDP-induced responses of cells. Also, **45-NP** demonstrated the ability to accumulate *in vivo* in CT-26 tumors, which was confirmed *via* fluorescent visualization and ICP-MS. A strong photothermal effect *in vivo* was confirmed after both intratumoral and i.v. administration of **45-NP** with 808 nm laser irradiation.

4.5.2.3. Radiotherapy-activated NPs. In 2022, Xiao et al.[342] reported ASGPR-targeting NPs **46-NP** based on Pt(IV) prodrug **46**

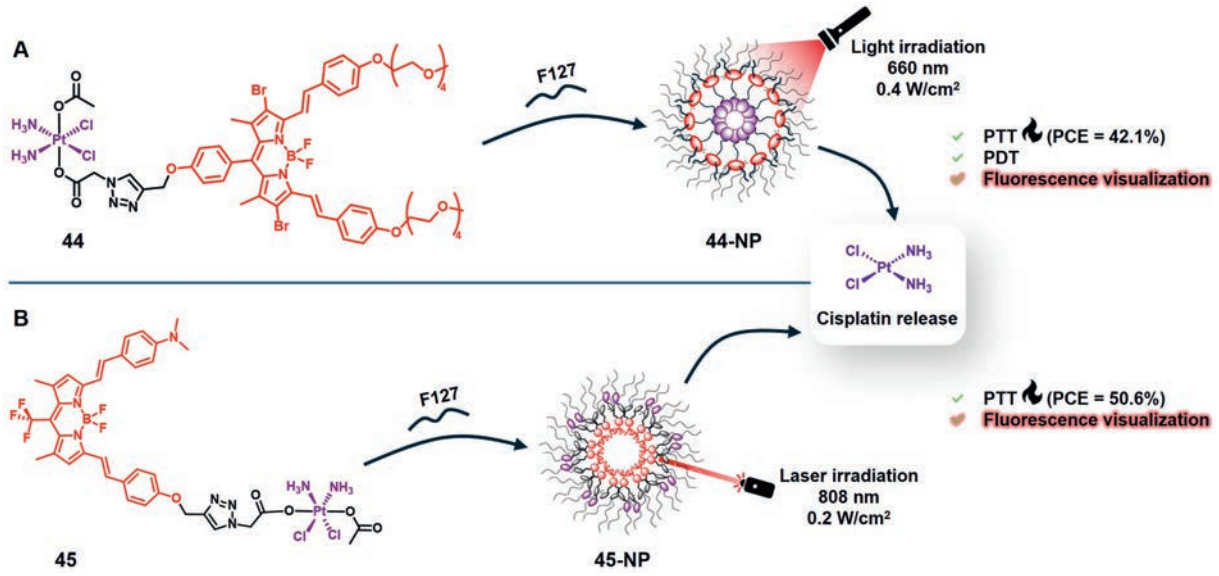

Figure 40 Photoresponsive Pt(IV) prodrugs with BODIPY **44** and **45** and their self-assembly with F127 into **44-NP** and **45-NP**[339,341].

conjugated with ASGPR-affine lactose scaffolds as a radiosensitizing agent for combined radio/chemotherapy (Fig. 41). Amphiphilic prodrug **46** self-assembled into anionic spherical **46-NP,** which demonstrated the ability to accumulate specifically in ASGPR(+) Hepa1-6 and HepG2 cells lines, as well as enhancement antiproliferative activity of **46-NP** in combination with X-rays (4 Gy) compared to **46-NP** alone. Western blot assay revealed that **46-NP** arrest the cell cycle in radiation-sensitive G2/M phase by upregulating p-Chk1 protein. **46-NP** showed more than 5-fold higher Hepa1-6 tumor accumulation level compared to CDDP; owning to the ASGPR-targeting, **46-NP** also accumulated in liver. **46-NPs** were also utilized for Pt-based CT imaging, which confirmed high Pt content in Hepa1-6 tumor and liver. Acute toxicity studies demonstrated high biosafety of **46-NPs**, with LD_{50}

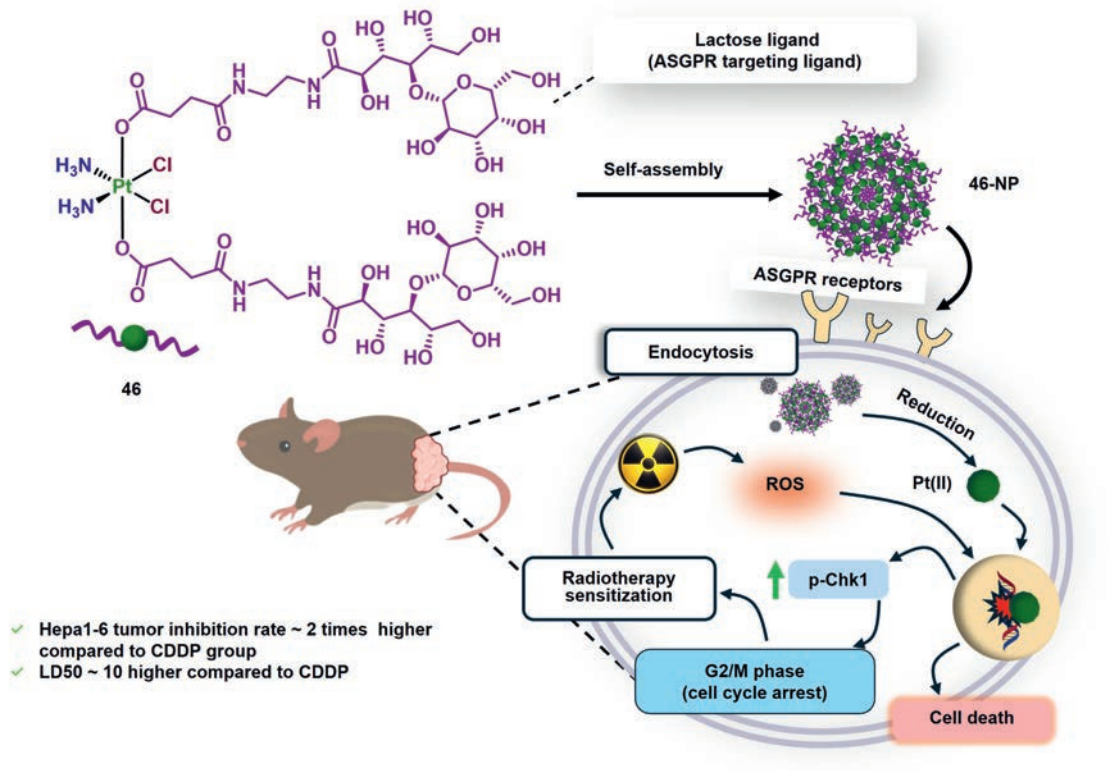

Figure 41 ASGPR-targeting Pt(IV) prodrug **46** with lactose and its self-assembly into **46-NP**. The intracellular mechanism of **46-NP**: DNA damage and cell apoptosis *via* both Pt and X-ray activity[342].

almost 10-fold higher than for CDDP, 32.5 and 3.5 mg Pt/kg, respectively. Antitumor efficiency of **46-NPs** in combination with X-rays (6 Gy) were evaluated on Hepa1-6 tumor model; after 10 days of therapy, **46-NPs** (13.5 mg Pt/kg) + X-rays suppressed tumor growth more efficiently than CDDP (2 mg Pt/kg) + X-rays, while exhibiting no general toxicity.

In 2024, Wang et al.[343] reported bimetallic Pt(IV)-Fe NPs **47-NP** for chemo/radio/immunotherapy, capable of sensitizing tumor cells to X-ray irradiation due to hypoxia reduction and activate immune response (Fig. 42). **47-NP** were obtained *via* self-assembly oxa-dextrane conjugate, conjugated with dopamine coordinated with Fe^{2+}, thereby obtaining spherical anionic NPs with a Pt and Fe content of approximately 1:1, the presence of Fe^{2+} cations which are prone to Fenton-type Haber−Weiss reaction was demonstrated by ЧPS. **47-NPs** demonstrated great accumulation in CT26 cells and when combined with X-ray irradiation (6 Gy) induced 8.3-fold increase in OH· radicals compared to radiotherapy alone due to the OXA-induced H_2O_2 production and subsequent catalytic reduction of peroxide to OH· and O_2. Thus, combination of **47-NPs** and X-rays (6 Gy) alle*via*ted hypoxia of CT-26 cells and demonstrated radiosensitizing effect. Subsequently, **47-NPs** + X-rays induced DAMP release of CT-26 tumor cells which promoted DC maturation *in vitro*. The ability of **47-NPs** to induce significant immune response *in vivo* was also demonstrated on bilateral CT-26 tumor model; growth of both primary and abscopal tumors of mice treated with **47-NPs** + X-rays were significantly inhibited after 20 days, with level of CD4, CD8, IFN-γ^+ T lymphocytes notably increased in both tumors. Combination of **47-NPs** + X-rays was also shown to suppress the growth of lung metastases which also illustrate great immunostimulatory properties of **47-NP**. **47-NP** in combination with X-rays were found to induce long-term immunological memory on 4T1 tumor model. Mice treated with **47-NP** + X-rays demonstrated the highest inhibition of re-challenged tumor growth compared to treatment *via* surgery of OXA + X-rays. In general, significant potential was shown for the use of platinum chemotherapy with radiation in the presence of the hypoxia-overcoming agent Fe^{2+}.

Stimulus-sensitive NPs are capable of significantly altering their properties under the influence of either the tumor microenvironment (endogenous stimuli) or external stimuli (exogenous stimuli), thereby enhancing their therapeutic effect. In this section, the innovative approach to stimulus-sensitive nanoparticle assembly on a cell membrane, presented by Xiao, deserves special mention. Thus, *in situ* formation of theranostic **33-NPs** directly at the tumor site resulted in significant therapeutic effect, not observed for the pre-synthesized **33-NPs.** Nanomedicines can also be activated by external stimuli, such as ultrasound, light, or radiation. Stimulus-sensitive NPs ideally exert their therapeutic effect only under the influence of an external stimulus, remaining "muted" until an external pulse is applied. Thus, polymer **37-NP** co-loaded with Ce6 demonstrated therapeutic effect similar to that of OXA without ultrasound, while completely suppressing tumor growth after US was applied. For UCNP **44-NP**, the therapeutic effect is high in the absence of radiation, which indicates premature release of the drug and the lack of light control over its action. For polymeric NPs **38-NP** and **39-NP**, the therapeutic effect is significantly enhanced by irradiation. In section 4.5.2.3., controllable release of Pt(II) from Pt(IV) prodrugs under ionizing radiation was discussed; that said, Pt(IV) prodrugs could also act as radiosensitizers. **46-NP** exhibited increased radiosensitizing activity compared to cisplatin, while bimetallic Pt-Fe **47-NP** have been found to effectively form ROS and reduce hypoxia in tumor

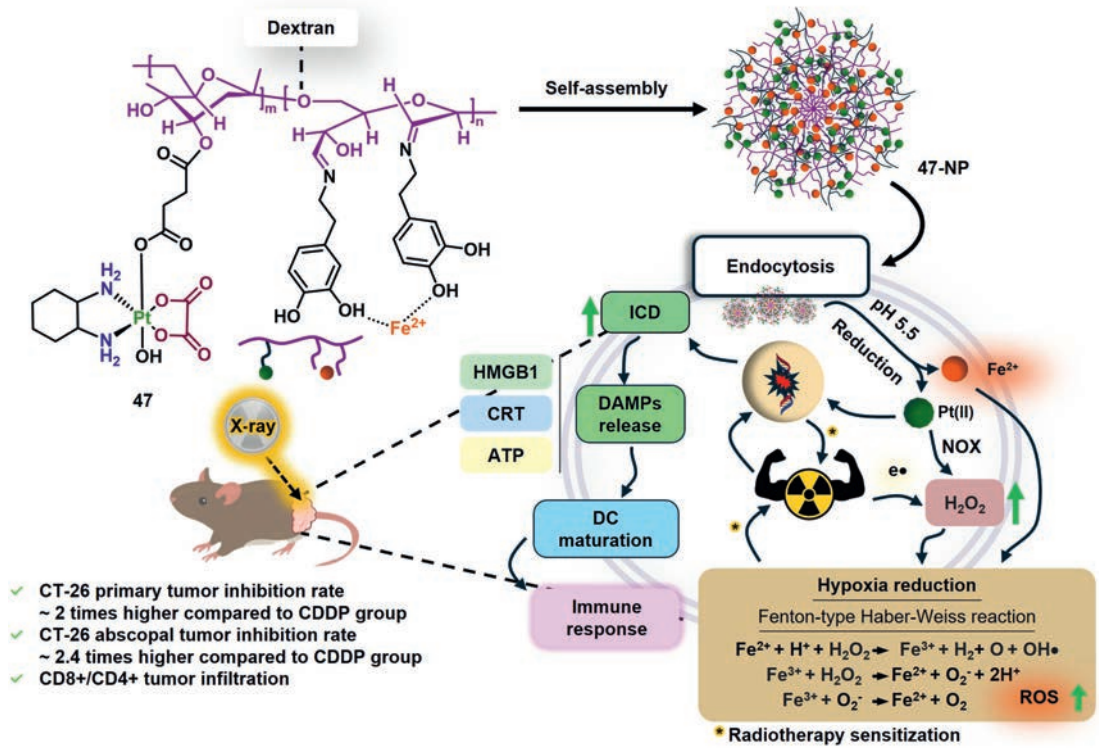

Figure 42 Polymeric bimetallic Pt(IV)-Fe prodrug **47** with and its self-assembly into **47-NP**. The intracellular mechanism of **47-NP**: DNA damage *via* Pt activity and X-ray radiation, hypoxia alleviating and ICD induction[343].

cells under low-dose radiation, while also promoting a remarkable anti-tumor immune response.

5. Discussion

CDDP is the first-line drug for a broad range of tumors, including bladder, ovarian, testicular, lung, gastric, colorectal, and head and neck cancers, and one of the most widely used and clinically important therapeutic agents worldwide. However, CDDP, as well as carboplatin and OXA are commonly associated with high toxicity and resistance, which forces increases in chemotherapy doses and significantly worsens the quality of life of patients. Current advances in the field of nanotechnology, immunology, and molecular biology open up several ways to overcome the limitations of Pt-based therapy and enhance its practical value in clinics.

The design of nanodelivery platforms of Pt(IV) prodrugs is a rapidly emerging trend that possesses undeniable advantages, such as long bloodstream circulation time, passive tumor targeting *via* the EPR effect, thus preventing unwanted adverse reactions before reaching the tumor tissue, active targeting, and the ability to encapsulate several drugs into one nanovehicle. Moreover, nanocarriers of Pt(IV) prodrugs can release their low-molecular components in the tumor-specific environment, such as acidic pH or high GSH level, thus increasing the selectivity of the nanoprodrugs towards malignant neoplasms. Up to date, a number of high-effective CDDP- and OXA-based NPs are reported. Several approaches could be proposed as the most perspective to obtain the Pt(IV)-based nanotherapeutics with high potential for further research.

First approach is the design of NPs capable of overcoming CDDP resistance. The design of such NPs may involve conjugating a bioactive "antiresistant" moiety to the axial position of Pt(IV), which can overcome one of the possible mechanisms of CDDP inactivation or repair the CDDP-induced cell damage. This design was used for **1-NP** and **4-NP** with HO inhibitor and fenofibrate acid in the axial position. Also, an "anti-resistance" additive can be co-loaded into Pt(IV) prodrug-based NPs, as was realized for **2-NP** and **3-NP**. In all cases, the addition of an "anti-resistance" component improved therapeutic efficacy and reduced the side effects of platinum-based therapy.

Second, it is the combination of CDDP-based NPs with the immunology response inducers. Stimulation of the immune response in addition to effective Pt(IV)-based chemotherapy is extremely promising, due to the possibility of not only effectively overcoming general disadvantages of platinum-based therapy, but also forming long-term immune memory, preventing the emergence of new tumors. It could be realized *via* the direct co-delivery of CDDP and immunological compounds (**10-NP, 20-NP,** etc.) and indirect influence (*e.g.*, the ER stress induction that in turn activate complex immunological cascade). This approach also allows involving the immunogenic death pathways, non-typical for CDDP. OXA is capable of causing ICD, and OXA-based NPs are also ICD inducers; however, the involvement of additional mechanisms for enhancing immune response is necessary for a long immunological memory capable of tumor recurrence preventing. Immunotherapy alone is often ineffective, but its combination with platinum drugs in one nanoagent allows achieving impressive results. Thus, after therapy with CDDP, repeated injection of tumor cells leads to tumor relapse, while after therapy with immunostimulatory NPs **8-NP-RA, 18b-NP, 37-NP** + irradiation+αPD-1, a significant decrease or complete absence of recurrent tumor was observed, which undoubtedly indicates the prospects for the development of immunostimulating nanomaterials, significantly superior in their effectiveness to clinically used CDDP and OXA.

Third approach is the target delivery of Pt(IV)-based NPs to the desirable area, which could be the whole tumor (*e.g.*, osteosarcoma), the part of the tumor microenvironment (*e.g.*, MDSCs), or the organelles within tumor cells (*e.g.*, mitochondria). Even though NPs are commonly considered to be able to accumulate in the tumor due to the EPR effect, a high tumor accumulation rarely realized adequately, and the accumulation of NPs in the liver is usually sufficient. Active targeting of NPs allows to accurately localize the site of their therapeutic action and significantly reduce side effects. Thus, **7-NP** showed significant accumulation in the liver with no accumulation in the lungs, while active targeting *via* inhalation approach has made it possible to achieve significant success in the treatment of lung cancer. Also, a high effectiveness of active targeting is obvious when comparing the therapeutic efficacy of **9-NP-m** and transferrin-modified **9-NP**, in which active targeting contributed to a significant accumulation of NPs in the tumor and an increase in their therapeutic efficacy. Despite the fact that both Pt(IV) prodrug **30** and CD-44-targeted **30-NP** demonstrated high antitumor efficacy, the comparison of the 30-day survival rate between the treated groups clearly supports the importance of active tumor targeting in order to reduce toxicity of chemotherapy.

Fourth approach is the remodeling of tumor microenvironment (TME) (*e.g.* with increasing oxygen concentration or with the regulation of inflammation). Thus, physical accumulation of the drug in the tumor does not always determine its antitumor efficacy, since tumor cells use various molecular mechanisms to reduce the effectiveness of chemotherapeutic and immunostimulatory agents. A comparison of the therapeutic efficacy of **5-NP** and hemoglobin-modified **5-NP-Hb** clearly emphasizes the importance of the effect on the TME. Hypoxia-reducing **5-NP-Hb** demonstrated both antitumor efficacy and immunostimulatory properties higher than those of unmodified **5-NP**, despite the similar intratumor accumulation for both NPs, thus emphasizing that reducing tumor tissue hypoxia is an extremely attractive strategy. Reduction of inflammation is a well-established strategy in the design of antitumor agents, since regulation of COX-2 expression can increase the regulation of prostaglandins and PD-L1, thereby stimulating the immune response. Thus, CDDP-based prodrug **9** with carprofen in the axial position and NPs based on it **9-NP** have shown the ability to stimulate the immune response, as well as **10-NP** with glycolysis inhibitor aspirin. The importance of COX-2 regulation for enhancing antitumor efficacy and immune response is also clearly demonstrated when comparing therapeutic efficacy of indomethacin-based **17-NP**, which demonstrated high antitumor efficacy in both primary and bilateral tumor models. Thus, NPs capable of reducing the immunosuppressive environment of the tumor are extremely promising for further development of nanomaterials for cancer treatment.

Fifth approach is the development of stimuli-response NPs, that could be activated both with intratumoral conditions (*e.g.*, GSH excess) or extra-tumoral factors (light, ultrasound, X-Ray, etc.). However, endogenous stimuli such as an excess of reducing agent are unlikely to provide controlled release of pharmacological agents in a given area. Thus, NPs that respond to endogenous stimuli such as GSH excess, ROS, and decreased pH is complex because, after entering the bloodstream, NPs are

subject to multiple volatile factors, and endogenous stimuli can easily reach them "on the way" toward their therapeutic target. For example, several NPs produced by loading of drugs into an ROS-responsive polymer demonstrated weight loss during therapy, which may indicate preliminary drug release before reaching the therapeutic target. Also, charge-reversing NPs, which are able to reverse their charge in the tumor microenvironment, can be classified as stimulus-sensitive. Thus, **22-NP**, which reverses its charge due to the chelation of alendronate with calcium cations, demonstrated a remarkable therapeutic effect significantly superior to that of CDDP, while pH-sensitive charge-reversing **35-NP** demonstrated a therapeutic effect similar to that of CDDP, from which it can be concluded that charge reversal of NPs under the influence of tumor-specific factors is a more effective approach.

In contrast, the use of exogenous stimuli allows one to control and localize the site of action of the drug. In addition to stimuli-controlled drug release, a combination of Pt(IV) prodrugs with photoabsorbers results in theranostic nanoplatforms, capable of fluorescent and photoacoustic tumor imaging. However, the theranostic nanoplatform should contain a minimum number of additional substrates to minimize the interaction of the drug and exogenous stimulus (*e.g.*, light) with the external carrier. Also, all therapeutic actions should be easily controlled, and pharmacokinetics of theranostic nanoplatform should be easily tunable and well-controlled. Thus, **40-NP** based on pseudo semiconducting polymer, capable of chemo, PTT and immunotherapy, are able to exert thermal effect upon irradiation with light, while the release of OXA occurs in the presence of a reducing agent. As a result, the "chemotherapeutic" part of **40-NP** is not light-controlled. Thus, despite the impressive results in the design of the theranostic multi-action NPs described in this review, much effort still required to design a suitable theranostic agent of sufficient stability and antitumor efficacy.

It is well-known that Pt(IV) prodrugs suffer from rapid (instantaneous) reduction in the bloodstream, what determines their therapeutic efficacy is hardly distinguishable from parent CDDP/OXA. The use of nanoformulations should resolve this issue, but the stability of the prodrug that forms the basis of NPs should be also carefully studied. Thus, **1a-NP** were obtained from low-stable Pt(IV) prodrug **1a**, and, as a consequence, **1a-NP** demonstrated rapid release of CDDP in a reducing environment and, as a result, their use as therapeutic agents was accompanied by a significant loss in body weight and high toxicity. Thus, the nanoformulation of Pt(IV) prodrug should be able to deliver its constituent parts to the site of therapeutic action, without losing them along the way in the bloodstream. To achieve this, the parent Pt(IV) prodrug must be able to gradually release the therapeutic agent and possess sufficient stability in the biological environment. Also, special attention should be paid to the issue of prodrug's stability, on the basis of which NPs are obtained.

NPs exhibit greater stability than Pt(IV) prodrugs under physiological conditions, which determines their success in tumor therapy. Pt(IV) prodrugs generally show an improvement in therapeutic efficacy by 10%−20% when compared to CDDP and OXA, while Pt(IV)-based NPs usually provide significant tumor inhibition. A comparison of toxicity *in vivo* of **23-NP**, Pt(IV) prodrug **23,** and CDDP clearly demonstrates the reduced toxicity of NPs compared to Pt(IV) prodrugs and CDDP. Even though mitochondria-targeted Pt(IV) prodrug **23** effectively suppresses tumor growth, its overall toxicity and substituent weight loss is indistinguishable from that of CDDP due to low stability of the prodrug **23** in the bloodstream.

The design of multi-action nanomaterials is an extremely attractive strategy. By combining several bioactive components in one nanovehicle, a single nanoprodrug with synergistic therapeutic effects could be successfully obtained. Thus, encapsulation of Pt(IV) prodrugs into NPs allows one to focus on the design of antitumor drugs with a favorable bioactivity profile without structure optimization for the suitable physico-chemical properties and kinetical inertness of the prodrugs. It is important to note that the design of nanoformulations also allows for a significant synergistic effect. Thus, PRA immunotherapy did not show any antitumor efficacy, while the combination of the chemotherapeutic agent OXA with PRA in one nanoagent, **8-NP-RA** demonstrated extremely promising antitumor efficacy. The competent design of **16-NP** nanoagent that combines CDDP prodrug, a pyroptosis-initiating agent, and an anti-inflammatory drug Indometacin in combination with anti-PD-L1 resulted in successful therapy of pancreatic cancer, usually resistant to anti-PD-L1 therapy alone. This is an excellent result of synergetic action of several drugs within one nanoagent.

In this review, we also focused on the method of nanoparticle production. In Table 2, we categorized the **1-47 NP** discussed in this review according to their production method, and also provided data on their stability, drug release conditions, and accumulation in key organs to assess the impact of the production method on stability and biodistribution. Several key points regarding this should be discussed.

Carrier-free self-assembly approach allows us to reach high drug loading level, unlike polymer-based methods that typically yield $<10\%$ drug loading. However, without a protective PEG layer, these self-assembly NPs are susceptible to aggregation and premature drug release, as was observed for carrier-free **4-NP** which caused notable body weight loss. An efficient and elegant approach to overcome those drawbacks demonstrated in several reports is to generate NPs from lipid-mimicking Pt(IV) prodrugs. Such NPs, including biotin receptor-targeting **3-NP,** osteosarcoma-targeting **20-NP** and **21-NP**, and nucleus-targeting **27-NP** were assembled from Pt(IV) prodrugs with one tumor-targeting hydrophobic and one hydrophilic axial ligand. This design creates micelle-like structure that facilitate active drug delivery into tumor, resulting in enhanced intratumoral accumulation and superior tumor suppression *in vivo*. Furthermore, control over the surface charge of micelle-like **25-NP** allowed subsequent coating with gene-silencing siXkr8 RNA, which enhanced immunostimulatory activity of the nanoformulation.

Recently reported lipid NPs that carry Pt(IV) prodrugs, including **7-NP, 9-NP, 26-NP** and **43-NP** all demonstrated common issues, including high level of Pt release under pH 7.4 and accumulation mainly in liver instead of tumor tissues. In case of **26-NP**, assembled from 4 different lipids to deliver Pt(IV) prodrug and 2 RNA sequences, low level of Pt in tumor necessitated intratumoral administration of nanoformulation. That said, an elegant approach towards targeted delivery of LNPs into orthotopic lung tumor and, consequently, high tumor inhibition rate was demonstrated for inhalation-administered **7-NP**, which drastically reduced accumulation in other organs.

Pt(IV) prodrugs could also be loaded into PEGylated stimuli-sensitive polymers, which contain cleavage motifs that break down in tumor-specific conditions, such as low pH (**16-NP)**, high GSH content (**8-NP, 10-NP, 14-15-NP** and **28-NP**), or ROS (**11-13-NP**), which ensures endogenously controlled release of the active Pt(IV) prodrug. The versatility of this approach allows co-loading of several drugs into one nanocarrier, as was the case for

Table 2 Structural type, drug release data, tumor targeting data, and *in vivo* antitumor activity for 1−47 NP.

Ref		NP structural type, assembly method	Self-assembly		
			Drug release rate	Tumor targeting, relative accumulation level	*In vivo* tumor model (treatment regimen), antitumor effect
	Carrier-free self-assembly				
202	1a-NP	Type 1 Carrier-free self-assembly	Drug release (24 h): pH 7.4: 5% pH 5.5: 15% pH 5.5 + 1 mmol/L GSH: 35% pH 7.4 + 1 mmol/L GSH + 1 mmol/L ascorbic acid: 40% pH 5.5 + 1 mmol/L GSH + 1 mmol/L ascorbic acid: 60%	Passive targeting Pt in tumor, fold increase (after treatment, 5 times over 20 days) Liver: 0.77 Kidney: 1.2	Subcutaneous A2780 ovarian tumor (3.5 mg Pt/kg): TIR: 1a-NP ∼78.92%, Cisplatin ∼9.24%
211	2-NP 2-NP-m − ISL-free NP	Type 1 (CFSA) Pt(IV) prodrug 2 is conjugated with PEG polymer axial position	Pt release (72 h): PBS: 15% 10 mmol/L GSH: 75% ISL release (72 h): PBS: 15% 0.1 mmol/L H_2O_2: 35	Passive targeting Fluorescence in tumor (Cy5-labeled 2-NP)/Pt in tumor, fold increase (36 h) Liver: 3.7/5.0 Kidney: 11.0/5.0	Subcutaneous patient-derived xenograft ovarian tumor (2.5 mg Pt/kg): Tumor volume, mm^3: PBS ∼1450, Cisplatin ∼550 2-NP-m ∼550 2-NP ∼200
216	3-NP	Type 1 (CFSA) Pt(IV) prodrug 3 has hydrophobic lipid chain and hydrophilic biotin as axial ligands	Pt & Rib release (72 h): PBS: 5% 10 mmol/L NaAsc: 75%	Active targeting (biotin) Fluorescence in tumor (Cy7-labeled 3-NP)/Pt in tumor, fold increase (24 h) Liver: 4.6/2.6 Kidney: nd/7.2	Subcutaneous MB49 bladder tumor (3.5 mg Pt/kg): Relative tumor volume, V/V_0: Saline ∼10 Cisplatin ∼10 3 ∼14 3-NP ∼5
220	4-NP	Type 1 (CFSA)	Pt release (72 h): pH 7.4, pH 5.0: 0% pH 7.4 + 2 mmol/L GSH: 16.3% pH 5.0 + 10 mmol/L GSH: 93.78%	Passive targeting Pt in tumor (4-NP), fold increase (after treatment, 6 times over 15 days) Liver: 0.48 Kidney: 3.6	Subcutaneous Hepa1−6 syngeneic hepatoma tumor (2.5 mg Pt/kg): TIR: Cisplatin: 43.21%, 4: 58.23%, 4-NP: 65.88%, 4-NP-high-dose (5 mg-Pt/kg): 80.35%
130	20-NP lipid mimic	Type 1 Carrier-free self-assembly of Pt(IV) prodrug 20 with hydrophobic lipid and hydrophilic alendronate axial ligands	No data	Active targeting (enhanced accumulation in osteosarcoma K7M2 cells) Fluorescence in tumor (fluorescent dye-labeled 20-NP)/μg Pt/g tumor tissue, fold increase (72 h) Liver: 4.2/3.4 Kidney: 6.4/6.6	Orthotopic osteosarcoma K7M2 tumor (3.5 mg Pt/kg): Tumor volume, mm^3: PBS ∼ 1500, Cisplatin ∼600, 20-NP ∼200
131	21-NP lipid mimic	Type 1 Carrier-free self-assembly of Pt(IV) prodrug 21 with hydrophobic lipid and hydrophilic alendronate axial	Pt release (48 h) pH 7.4 ∼ 5% pH 5.0 ∼ 5% 10 mmol/L NaAsc, pH 5.0 ∼ 70%	Active targeting (enhanced accumulation in osteosarcoma K7M2 cells) Fluorescence in tumor (fluorescent	Orthotopic osteosarcoma K7M2 tumor (3 mg Pt/kg): Relative tumor volume, V/V_0: Saline ∼8,

(*continued on next page*)

Table 2 (*continued*)

Ref		NP structural type, assembly method	Self-assembly		
			Drug release rate	Tumor targeting, relative accumulation level	*In vivo* tumor model (treatment regimen), antitumor effect
		ligands		dye-labeled 21-NP)/μg Pt/g tumor tissue, fold increase (72 h) Liver: 2.8/2.6 Kidney: 8.2/6.1	OXA ~4, 21-NP ~2
311	25-NP 25a-NP − Nanoparticles before siRNA loading Lipid mimic	Type 1 Carrier-free self-assembly of Pt(IV) prodrug 25 with hydrophobic lipid and hydrophilic R_8K nucleus-targeting peptide. Subsequent coating of NP with siXkr8 RNA	Pt release (48 h): pH 7.4 ~5% pH 5.0 ~5% 10 mmol/L NaAsc ~75%	Passive tumor targeting, active nuclear-targeting Fluorescence in tumor (Cy7-labeled 25-NP), fold increase (96 h) Kidney: 5.5 Liver: 2.5	Subcutaneous 4T1 triple-negative breast tumor (3.5 mg Pt/kg): Relative tumor volume, V/V_0 PBS ~13, Cisplatin ~11, Complex 8 ~7, 25-NP ~2.5 Recurrent subcutaneous 4T1 tumor Relative volume of recurrent tumor V/V_0: PBS ~10, Cisplatin ~8, 25 ~6, 25-NP ~0
312	27-NP lipid mimic	Type 1 Carrier-free self-assembly of Pt(IV) prodrug 25 with hydrophobic lipid and hydrophilic R_8K nucleus-targeting peptide.	Pt release (72 h): pH 7.4 ~5% pH 5.0 ~5% 10 mmol/L NaAsc: 75%	Passive tumor targeting, active nuclear-targeting Fluorescence in tumor (Cy7.5-labeled 27-NP)/μg Pt/g tumor tissue, fold increase (72 h) Liver: 2/3.1 Kidney: 5/3.0	Subcutaneous triple-negative 4T1 tumor, (3.5 mg Pt/kg): Relative tumor volume V/V_0 PBS ~15 (Day 12) OXA ~9 (Day 12) 27-NP ~2 (Day 18)
314	29-NP	Type 1 Carrier-free self-assembly of Pt(IV) prodrug 1	Pt release (72 h) pH 7.4: 35% pH 6.5: 40% pH 7.4 + 10 mmol/L GSH: 75% pH 6.5 + 10 mmol/L GSH: 80%	Passive tumor targeting, active mitochondria targeting μg Pt/g tumor tissue, fold increase (24 h) Liver: 0.63 Kidney: 1.75	Subcutaneous cisplatin-resistant A549/DDP tumor (3 mg Pt/kg) Tumor volume, mm^3: PBS ~880, Cisplatin ~720, 29-NP ~200
342	46-NP	Type 1 (CFSA) Pt(IV) prodrug 46 with lactose as axial targeting ligands	Pt release (24 h): 0.1 mmol/L NaAsc: 24% 5 mmol/L NaAsc: 61%	Active targeting (ASGPR-targeting ligand) No quantitative data on tumor accumulation	Subcutaneous hepatoma Hepa1-6 tumor (15 mg Pt/kg 46-NP, 2 mg Pt/kg cisplatin, 4 Gy) Tumor volume, mm^3 46-NP + X-ray ~130 Cisplatin + X-ray ~210
	Lipid nanoparticles				
140	7-NP	Type 2 Pt(IV) prodrug 1 was loaded into DSPE-PEG2000-DBCO and PEOz-b-PLA-GSNO	Pt release (48 h): pH 7.4: 50% pH 5.0: 85% NO release (48 h): pH 7.4: 35% pH 7.4 + 10 mmol/L GSH: 55% pH 5.0 + 10 mmol/L GSH: 85%	Active targeting (mannose-azide labeling of tumor cells, bioorthogonal click-reaction with DABCO-labeled NP) Fluorescence in lungs (Cy5-labeled 7-NP) after inhalation, fold increase (24 h) Liver: 4.3	Orthotopic cisplatin-resistant A549/DDP-luc lung tumor (inhalation of1.5 mg Pt/kg, 7 times for 3 days) Relative tumor radiance: Control ~14, Cisplatin ~12.5, 7-NP ~5, Ac4ManNAz+7-NP ~1.25

				Kidney: 5.2	
249	9-NP	Type 2 Loading of Pt(IV) prodrug 9 into DSPE-PEG_{2000}	Pt release (4 h): PBS + 5% DMF ~80%	Active targeting (transferrin receptor) Fluorescence in tumor (DiD-labeled 9-NP), fold increase (24 h) Liver: 0.58 Kidney: nd	Subcutaneous triple-negative 4T1 breast tumor (2 mg Pt/kg): TGI: Cisplatin: 25.7%, 9-NP: 80.4% Tumor volume, mm^3 Cisplatin ~600, 9-NP ~300 4T1 metastasis model, (2 mg Pt/kg): TGI Cisplatin: 25.5%, 9-NP: 79.2%
139	26-NP	Type 2 Loading of Pt(IV) prodrug with lipid axial ligands, siXkr8, and mANX5 RNA into LNP consisted of 4 lipids (SM-102:DSPC:Cholesterol:DMG-PEG)	Pt release (72 h): PBS ~20% Murine serum with 10 mmol/L; GSH: 60.8% Endo/lysosomal escape (2 h): full release	No tumor targeting Fluorescence in tumor (DiR-labeled 26-NP), fold increase (24 h) (i.v.) Kidney: 1 Liver: 0.05	Subcutaneous 4T1 tumor (1.35 mg Pt (IV)/kg): Tumor volume, mm^3 26-NP ~78 Cisplatin ~780 Bilateral subcutaneous 4T1 tumors (1.35 mg Pt(IV)/kg) Secondary tumor volume, mm^3, mm^3 26-NP ~100 Cisplatin ~400
338	43-NP Loading into polymers GSH-responsive polymers	Type 2 DSPE-PEG-based lipid nanoparticles encapsulating Pt(IV) prodrug 43.	Pt release (48 h): pH 7.4: 10% pH 5.5: 12% pH 7.4 + NIR light: 25% pH 5.5 + NIR light: 25% 10 mmol/L GSH: 35% 10 mmol/L GSH + NIR light: 65%	Passive tumor targeting, active mitochondria targeting Fluorescence in tumor/μPt per g tissue in tumor, fold increase (24 h) Liver: 0.47/0.8 Kidney: 6.2/1.9	Subcutaneous 4T1 tumor (2 mg/kg) TIR 43 ~44% 43-NP ~77% 43-NP + light ~90%
244	8-NP	Type 3 Polymer cleavage − GSH Pt(IV) prodrug 8 axial lipid chain was loaded into GSH-responsive polymer with retinoid acid side chain	Stable for 20 days by size and PDI Pt release (72 h): PBS ~5% 10 mmol/L GSH ~70%	Passive targeting Fluorescence in tumor (Cy5.5-labeled 8-NP)/Pt in tumor, fold increase (24 h) Liver: 0.7/0.7 Kidney: 2.1/1.3	Subcutaneous MC38 colon cancer tumor (dose not stated): TGI: 8-NP-RA: 70.1% 8-NP (without retinoic acid): 58.7% PRA: 19.5% Survival rate after 60 days: 8-NP (without retinoic acid): 20% 8-NP-RA: 60% PBS: 0% Subcutaneous MC38 colon cancer tumor (8-NP dose not stated, 150 μg aCD8 per dose): Ratio of tumor volume V/V_{PBS}: 8-NP-RA + αCD8 ~100%, 8-NP ~27% Subcutaneous MC38 colon cancer

(*continued on next page*)

Table 2 (*continued*)

Ref		NP structural type, assembly method	Self-assembly		
			Drug release rate	Tumor targeting, relative accumulation level	*In vivo* tumor model (treatment regimen), antitumor effect
					tumor (8-NP dose not stated, 150 μg αPD-L1 per dose): Ratio of tumor volume V/V_{PBS}: 8-NP-RA+ αPD-L1: 5.5% (2/5 tumors eradicated) 8-NP-RA: 36% αPD-L1 ~81% Subcutaneous 4T1-luc recurrent model (8-NP dose not stated, 150 μg αPD-L1 per dose): Tumor recurrence: PBS: significant tumor recurrence 8-NP: tumor recurrence, 8-NP-RA+ αPD-L1: negligible tumor recurrence
143	10-NP	Type 3 Polymer cleavage: GSH Loading of Pt(IV) prodrug 10 into (mPEG−P(Phe-*co*-Cys2))	Pt release (24 h): PBS solution: 24 h ~23% 10 mmol/L GSH: 24 h ~87%	Passive targeting Pt in tumor (10-NP), fold increase (48 h) Liver: 0.42 Kidney: 0.65	Subcutaneous CT-26 colon tumor (5 mg oxaliplatin/kg): TIR 10-NP ~85.2% oxaliplatin ~57.6%
283	14-NP	Type 3 Polymer cleavage: GSH Loading of Pt(IV) prodrug 14 into (poly(2-HD-*co*-HPMDA)-mPEG-MK1775	Pt release (24 h): PBS solution: ~13% 10 mmol/L GSH: ~68%	Passive targeting Fluorescence in tumor (Cy7.5-labeled 14-NP, fold increase (48 h) Liver: 0.88 Kidney: 1.05	Subcutaneous Mb49 bladder tumor (3 mg Pt/kg): TSR: Cisplatin: 63.6%, 14-NP: 86.4% Bilateral subcutaneous Mb49 tumor (3 mg Pt/kg): TSR, Primary tumor: αPD-L1: 45.3% 14-NP: 75.7% 14-NP+αPD-L1: 95.8% Tumor volume, mm^3, Distant tumor: PBS: 335 14-NP: 180 αPD-L1: 28 14-NP + αPD-L1: 0
144	15-NP	Type 3 Polymer cleavage: GSH Loading of Pt(IV) prodrug 15 into GSH-responsive polymer Poly3S	Pt release (48 h): pH 7.0 & 5.5 ~5% 10 mmol/L GSH ~ 25%	Passive targeting Fluorescence in tumor (Cy-labeled 15-NP)/Pt in tumor, fold increase (48 h) Liver: 1.5/1.3 Kidney: 3.5/2.15	Subcutaneous 4T1 triple-negative breast tumor (1.5 mg Pt/kg): Relative tumor volume (V/V_0) PBS ~15, Cisplatin ~10, 15-NP ~1 Tumor weight, mg PBS: 564, Cisplatin: 340,

					15-NP: 114
313	28-NP	Type 3 Cleavage type: GSH Loading of Pt(IV) prodrug into GSH-responsive polymer P1	Pt release (24 h): PBS: 13% 10 mmol/L GSH: 75%	Active targeting (ASGPR-targeting motif) μg Pt/g tumor tissue, fold increase (72 h) Liver: 1.05 Kidney: 1.2	Subcutaneous patient-derived hepatocellular carcinoma tumor (2 mg Pt/kg) Tumor volume, mm^3: PBS: 2200 Cisplatin: 1800 28-NP: 600 Tumor weight, g: 28-NP: 0.41, PBS: 1.81, Cisplatin: 1.32
	ROS-responsive polymers				
275	11-NP	Type 3 Polymer cleavage: ROS Loading of Pt(IV) prodrug into ROS-sensitive polymer P1 and mPEG2k-DSPE	Pt release (48 h): PBS solution: ~15% 0.5 mmol/L H_2O_2 ~50% 5 mmol/L H_2O_2 ~70% 10 mmol/L H_2O_2 ~85%	Passive targeting Fluorescence in tumor (Cy7.5-labeled 11-NP, fold increase (48 h) Liver: 0.95 Kidney: 1.12	Subcutaneous murine colon CT-26 tumor (3 mg Pt/kg) Tumor weight, g: CDDP: 0.842, 11-NP: 0.271
276	12-NP	Type 3 Polymer cleavage − ROS Loading of Pt(IV) prodrug 12 and IDO inhibitor NLG919 into ROS-responsive polymer	Release of IDOi (24 h): PBS solution: ~25% 1 mmol/L H_2O_2: ~78%	Passive targeting Fluorescence in tumor (Cy7.5-labeled 12-NP, fold increase (48 h) Liver: 1.46 Kidney: 1.78	Orthotopic K7M2-LUC osteosarcoma tumor (3.5 mg Pt/kg) Average bioluminescence, $p/s/cm^2/sr$: 12-NP: 3.50×10^9 CDDP: 11×10^9
280	13-NP	Type 3 Polymer cleavage: ROS Loading of Pt(IV) prodrug 13a or Mn complex 13 into ROS-responsive PCPP and DSPE-PEG_{2000}	Pt release (108 h) PBS: 11.3% 10 mmol/L H_2O_2: 67.3% Mn release (108 h) PBS: 10.9% 10 mmol/L H_2O_2: 48.5%	Passive targeting Fluorescence in tumor (Cy5.5-labeled 13a-NP), fold increase (60 h) Liver Kidney: 0.48 Liver: 1.7	Subcutaneous patient-derived ovarian tumor (1 mg Pt/kg, 3.5 mg Mn/kg): TIR Cisplatin - 35.2%, 13a-NP + 13b-NP: 92.9% ID8-Luc ovarian cancer peritoneal metastatic model (3.5 mg Pt/kg): Average bioluminescence, $p/s/cm^2/sr$: PBS: 2.3×10^6, 13a-NP+13b-NP: 6.1×10^5, 13a-NP + 13b-NP + α-PD-1: 2.2×10^5
	Polymers with other response modes				
288	16-NP	Type 3 Polymer cleavage: pH 5.0 Loading of Pt(IV) prodrug 16 into pH-sensitive poly(ethyleneglycol)-*b*-poly(2-(diisopropylamino) ethyl methacrylate) (iPDPA)	Dasatinib release (12 h) pH 7.4 ~20% pH 5.0 ~80%	Passive targeting Fluorescence in tumor (DiR-labeled 16-NP), fold increase (96 h) Kidney ~5 Liver: 1.8	Subcutaneous head and neck squamous cell carcinoma tumor (5 mg OXA/kg): Tumor volume, mm^3 OXA ~380, 16-NP ~220 Orthotopic HNSCC tumor (5 mg OXA/kg): (*continued on next page*)

Table 2 (*continued*)

Ref		NP structural type, assembly method	Self-assembly		
			Drug release rate	Tumor targeting, relative accumulation level	*In vivo* tumor model (treatment regimen), antitumor effect
					Tumor volume, mm^3 OXA ~34, 16-NP ~10
337	42-NP	Type 3 Cleavage type: GSH & ROS Covalent self-assembly using a diselenide cross-linker with dual GSH/ROS-responsive release	Ce6 release (36 h): PBS: 15% 10 mmol/L DTT: 70% 10 mmol/L H_2O_2: 75%	Passive targeting Fluorescence in tumor, fold increase (72 h) Liver: 1.2 Kidney: 1.9	Subcutaneous 4T1 tumor (5 mg OXA/kg) Tumor volume, mm^3 PBS ~360, OXA ~180, Complex 60 ~150, 42-NP ~120, 42-NP + irradiation 660 nm, 0.5 W/cm^2, 5 min ~40 Orthotopic MOSC2 oral tongue carcinoma (5 mg OXA/kg): Tumor volume, mm^3: PBS ~28, OXA ~20, 42 ~17, 42-NP ~14, 42-NP + irradiation 660 nm, 0.5 W/cm^2, 5 min ~10 Bilateral 4T1 model: 42-NP + irradiation + αPD-1: distant tumor growth suppression 4T1 tumor recurrence model: 42-NP + irradiation + αPD-1: recurrent tumor growth suppression
339	44-NP	Type 3 Pt(IV) prodrug 44 + F127 polymer	Pt release: Dark: 4.2% (24 h) 660 nm (0.4 W/cm^2): 48.7% (5 h)	Passive targeting Fluorescence in tumor, fold increase (26 h) Liver: 1.3 Kidney: 1.1	No antitumor efficiency data
341	45-NP	Type 3 Pt(IV) prodrug 45 + F127 polymer	Pt release (6 h): Dark: 1.5% 0.21 mmol/L NaAsc: 23% 740 nm (0.055 W/cm^2): 15.5% 740 nm (0.2 W/cm^2): 55.2% NaAsc + 740 nm (0.2 W/cm^2): 63%	Passive targeting Fluorescence in tumor/Pt content in tumor tissue, fold increase (24 h) Liver: 0.65/0.18 Kidney: 0.74/5.0	No antitumor efficiency data
	Pt(IV) prodrugs as part of the polymer chain				
290	17-NP	Type 4 Polymer cleavage: GSH Pt(IV) complex is conjugated with the side chain of the GSH-responsive polymer PHDT-Pt-In	Pt release (24 h) PBS: 18% 10 mmol/L NaAsc: 88%	Passive targeting No biodistribution	Subcutaneous Pan02 pancreatic tumor (3 mg Pt/kg): TGI: 17-NP: 81%, 17-NP (without indomethacin): 59%,

					Cisplatin: 30% Tumor weight, g:17-NP: 0.27, 17-NP (without indomethacin): 0.65, Cisplatin: 0.99, PBS: 1.4 Bilateral subcutaneous Pan02 pancreatic tumor, number of mice with distant tumor, mm^3 (3 mg Pt/kg): PBS: 5/5, ~300, αPD-L1 (50 mg/kg): 5/5, ~206, 17-NP: 4/5, ~30, 17-NP + αPD-L1 (50 mg/kg): 0/5
301	22-NP	Type 4 Polymer cleavage: NaAsc Pt(IV) prodrug was part of polymer chain. Polymer self-assembled into NP with subsequent coating with alendronate	Pt release (48 h) PBS ~12% 10 mmol/L NaAsc ~80%	Active targeting (ALE-induced accumulation in osteosarcoma K7M2 cells) Fluorescence in tumor (Cy7.5-labeled 22-NP)/μg Pt/g tumor tissue, fold increase (72 h) Liver: 1.8/2.3 Kidney: 2.9/3.5	Orthotopic osteosarcoma K7M2 tumor, (3 mg Pt/kg): TIR Cisplatin: 36.5%, 22a-NP: 54.1%, 22-NP: 76.3%, Orthotopic osteosarcoma K7M2 tumor (combination therapy with 230 mg/kg αPD-L1, 3.5 mg Pt/kg) Tumor volume, mm^3: PBS ~1300 (Day 16) αPD-L1 ~1300 (Day 22) 22-NP ~700 (Day 30) 22-NP + αPD-L1 ~200 (Day 30) Patient-derived osteosarcoma tumor: Tumor volume, mm^3 (3.5 mg OXA/kg): Cisplatin: 527, 22a-NP: 381 22-NP: 197
306	23-NP 23a-NP: NP without pEZH2	Type 4 Polymer cleavage: NaAsc Polymer Pt(IV) prodrug self-assembled into NP with subsequent coating with pEZH2 plasmid	Pt release (48 h) PBS: 10% 5 mmol/L NaAsc: 67.8% Non-coding plasmid (pNC) release (48 h) PBS: 8.5% 5 mmol/L NaAsc: 62.8% Endo/lysosomal escape 6 − 12 h: full escape	Passive targeting No biodistribution data	Subcutaneous PC-3 prostate tumor (2.56 mg Pt/kg) Tumor volume, mm^3 Control: 2050 23a-NP: 1200 Cisplatin: 570 23-NP: 310
309	24-NP	Type 4 Polymer cleavage: 450 nm light Polymer Pt(IV) prodrug self-assembled into NP with subsequent coating with si(c-fos) RNA	Pt release (48 h): Dark: 12% 30 min pre-irradiation (450 nm, 20 mW/cm^2): 58% si(c-fos) release (48 h):	Active targeting: CD44-specific HA coating No biodistribution data	Subcutaneous cisplatin-resistant A2780/CDDP ovarian tumor (2.77 mg Pt/kg): Tumor volume, mm^3: 24-NP: 185

(*continued on next page*)

Table 2 (*continued*)

Ref		NP structural type, assembly method	Self-assembly		
			Drug release rate	Tumor targeting, relative accumulation level	*In vivo* tumor model (treatment regimen), antitumor effect
			Dark: 11% 30 min preirradiation (450 nm, 20 mW/cm^2): 55% Endo/lysosomal escape, colocalization ratio (FAM-si(c-fos)), endo/lysosome): Dark, 12 h: 64% 20 min irradiation, 4 h: 40%		Cisplatin: 1060
324	34-NP	Type 4 Polymer cleavage: NaAsc	Pt release (24 h): PBS: 20% 10 mmol/L NaAsc: 80%	Active targeting (RGD peptide) NIR-II Fluorescence in tumor/ relative Pt content in tumor, fold increase (72 h) Liver: 2.2/2.0 Kidney: 2.9/3.3.	Murine model of advanced-stageIII/ IV HGSOC (4 mg Pt/kg): Impressive tumor inhibition: no quantitative analysis
121	35-NP	Type 4 Polymer cleavage: pH = 6.5 Pt(IV) prodrug is part of the polymer chain.	Pt release (48 h): pH 7.4: 30% pH 6.5: 40% pH 5.0 + 5 mmol/L NaAsc: 54.5%	Active targeting (folate) μg Pt/g tumor tissue, fold increase (4 h) Liver: 0.7 Kidney: 1.9	Subcutaneous SKOV-3 ovarian tumor (2 mg Pt/kg): Tumor volume, mm^3 35-NP: 395 Cisplatin: 375
327	37-NP	Type 4 Polymer cleavage: Ultrasound Pt(IV) prodrug is part of the polymer chain.	Pt release (48 h): PBS: 11% 5 mmol/L NaAsc: 50% 5 mmol/L NaAsc + US (1.5 W/cm^2): 85%	Passive targeting Fluorescence in tumor, fold increase (48 h) Liver: 0.5 Kidney: 0.9	Subcutaneous CT-26 tumor (3.5 mg Pt/kg): Tumor volume, mm^3: PBS ∼1500, Oxaliplatin ∼1000, 37-NP + US (1 MHz, 1.5 W/cm^2, 5 min) ∼150
148	39-NP	Type 4 Polymer cleavage: NIR irradiation (808 nm) Pt(IV) prodrug is part of the polymer chain.	Pt release (16 h): Dark: 5% 808 nm light (1 W/cm^2): 80%	Passive tumor targeting, active nuclear-targeting Fluorescence in tumor, fold increase (72 h) Liver: 1.2 Kidney: 5.3	Orthotopic triple-negative 4T1 breast tumor (3.5 mg Pt/kg): Ratio of tumor volume, V/V_0: PBS ∼14 (day 12) OXA ∼11 (day 12) 39−NP ∼3 (day 18) 39−NP + irradiation (808 nm, 1 W/cm^2, 10 min) ∼ 1 (Day 18)
335	40-NP	Type 4 Polymer cleavage - NIR-II irradiation (1064 nm) Pt(IV) prodrug is part of the polymer chain.	Released Pt concentration (32 h): Dark: 0.3 μmol/L Light 1064 nm (1 W/cm^2, 10 min): 0.5 μmol/L	Passive targeting Fluorescence of main organs (Cy5.5-labeled 40-NP) (50 h): High fluorescence in liver, low fluorescence in kidneys and tumor	Subcutaneous CT26 colon tumor (1 mg Pt/kg) Tumor volume, mm^3: PBS ∼1000, OXA ∼750, 40-NP ∼480, 40-NP + 1064 nm, 1 W/cm^2, 10 min irradiation ∼0 Subcutaneous 4T1 triple-negative

					breast tumor (1 mg Pt/kg): Tumor volume, mm^3 PBS ~600, OXA ~350, 40-NP ~220, 40-NP + irradiation 1064 nm, 1 W/cm^2, 10 min ~0
343	47-NP	Type 4 Polymer cleavage: GSH Pt(IV) prodrug 47 is part of the polymer chain.	Pt release (48 h): pH 7.4: 17.6% pH 5.5 + 5 mmol/L GSH: 71.6% Fe release (48 h): pH 7.4: 12.6% pH 5.5 + 5 mmol/L GSH: 59.1%	Passive targeting μPt/g tissue in tumor, fold increase (24 h): Liver: 0.6 Kidney: 1.6	Bilateral subcutaneous CT-26 tumor (2.5 mg Pt/kg, 6 Gy) Tumor volume, mm^3 Primary tumor: Oxaliplatin + X-ray ~380 47-NP + X-ray ~200 Abscopal tumor: Oxaliplatin + X-ray ~240 47-NP + X-ray ~100 B16-luc lung metastasis model (2.5 mg Pt/kg, 6 Gy) oxaliplatin: high luc signal 2/4 survival (Day 15) 47-NP + X-ray low luc signal, 4/4 survival (Day 15) Subcutaneous 4T1 recurrent model, rechallenge study (Treatment (2.5 mg Pt/kg, 6 Gy), then rechallenge of a second tumor) Secondary tumor volume, mm^3: Surgery ~720 Oxaliplatin + X-ray ~350 47-NPs + X-ray ~140
	Host−guest interactions				
153	6-NP	Type 5 Host−guest interaction between CD-conjugated Pt(IV) prodrug 6 and Lac-PEG-*b*-PLys(Ad)	Stable for 7 days by size and PDI Pt release (24 h): PBS: 20% 10 mmol/L ascorbic acid: 90% NO release (24 h): PBS: 25% 10 mmol/L ascorbic acid: 90%	Active targeting (lactose) Fluorescence in tumor (IR820-labeled 6-NP), fold increase (24 h) Liver: 2.7 Kidney: 3.2	Subcutaneous LM3 hepatoma tumor, (3 mg Pt/kg): Relative tumor volume, V/V_0 6-NP: 2.9 Cisplatin: 4.6 Orthotopic cisplatin-resistant luc-LM3/CDDP (3 mg Pt/kg): Luminescence, p/s/cm^2/sr 6-NP ~4 Cisplatin ~20 Subcutaneous patient-derived hepatoma (3 mg Pt/kg): Relative tumor volume, V/V_0 6-NP: 2.2 Cisplatin: 3.8
318	30-NP	Type 5 Loading of Pt(IV) 30 into CD-grafted HA	30 release (24 h): pH 7.4: 90% (24 h) LND release (24 h): pH 7.4: 5% 5 mmol/L GSH: 45% 10 mmol/L GSH: 72%	Active targeting (CD44-targeting) Tumor radiance (Cy5.5-labeled 30-NP)/μg Pt/g tumor tissue, fold increase (72 h) Liver: 4.8/6.8	Subcutaneous cisplatin-resistant A549/DDP tumor (2 mg Pt/kg) Tumor volume, mm^3: PBS ~660, Cisplatin ~400, (*continued on next page*)

Table 2 (*continued*)

Ref		NP structural type, assembly method	Self-assembly		
			Drug release rate	Tumor targeting, relative accumulation level	*In vivo* tumor model (treatment regimen), antitumor effect
				Kidney: 7.5/5.2	LND 30 ~250, 30-NP ~90 Orthotopic cisplatin-resistant A549/DDP tumor Tumor volume, mm^3 PBS ~25, Cisplatin ~10, 30 ~5, 30-NP ~2
	Loading into proteins				
233	5-NP-Hb	Type 6 Loading of Pt(V) prodrug 5 into hemoglobin (Hb)	Pt release (72 h): pH 7.4: 5% 10 mmol/L NaAsc: 80%	Active targeting (biotin) Fluorescence in tumor (DiD-labeled 5-NP-Hb)/Pt in tumor, fold increase (24 h) Liver: 2.6/2.4 Kidney: 2.6/2.4	Subcutaneous 4T1 triple-negative breast tumor (3.5 mg Pt/kg) Tumor inhibition rate: 5-NP-Hb: 78%, 5−NP (Without hemobgobin): 51%, OXA: 16%, OXA + Biotin: 15%
152	19-NP	Type 6 Loading of Pt(IV) prodrugs into HSA	Pt release (48 h) pH 7.4 ~10 nmol pH 5.0 ~10 nmol 10 mmol/L GSH ~30 nmol	Passive targeting Fluorescence in tumor (Cy7.5-labeled 19-NP), fold increase (96 h) Kidney: 4.2 Liver: 0.9	Orthotopic ES2-luc-derived tumor (1.5 mg Pt/kg): Tumor reduction, compared to cisplatin 19-NP: 65.97% Subcutaneous SKOV-3-derived cancer stem cell tumor, (1.5 mg Pt/kg): Tumor volume, mm^3 19-NP: 83.4 Cisplatin: 179.8
150	32-NP	Type 6 Loading of Pt(IV) prodrug 32 with perfluorocarbon axial ligands into HSA	No data on Pt release from NP	Passive targeting Fluorescence in tumor (Cy7.5-labeled 32-NP) (72 h) Liver: 3.2 Kidney: 2.6	Orthotopic K7M2 osteosarcoma tumor (3 mg Pt/kg): Tumor volume reduction compared to control: Cisplatin - 43%, 32: 69%, 32-NP: 85% Subcutaneous K7M2, after vaccination Tumor volume, mm^3 PBS: 1200, 32-NP: 500

32	36-NP	Type 6 Loading of Pt(IV) prodrug 36 into hemoglobin	Pt reduction: 5 mmol/L NaAsc: 32% (24 h) 5 mmol/L NaAsc + US (1.5 W/cm^2: 100% (3 min)	Passive targeting Fluorescence in tumor (Cy5.5-labeled 36-NP), fold increase (72 h) Liver: 3.2 Kidney: 3.8	Subcutaneous CT26 murine colon tumor, (1.5 mg Pt/kg) Tumor volume, mm^3: PBS ~1800, Cisplatin ~450, 36-NP + US ~100
336	41-NP	Type 6 Loading of Pt(IV) prodrug 41 into HSA	Pt release (72 h): PBS: 5% 660 nm light (0.3 W/cm^2, 10 min): 48% 10 mmol/L GSH: 55% 10 mmol/L GSH + 660 nm light: 88%	Passive targeting Fluorescence in tumor, fold increase (6 h) Liver: 0.47 Kidney: 2.8	Subcutaneous MB49 bladder tumor Relative tumor volume, V/V_0 PBS ~22 41-NP ~21 41-NP + 660 nm (0.3 mW/cm^2, 10 min) ~7
	Other types				
156	18a-NP 18b-NP	Type 7 Loading of Pt(IV) prodrug 18a into $CaCO_3$ nanoparticles with subsequent oxidative polymerization of axial SH groups	NP stability (12 h) Stable NP at pH 7.4 and 6.0, 85.5% Ca^{2+} release at pH 5.0. Pt release (12 h) pH 5.0: no release pH 5.0 + 0.1 mmol/L GSH: 75%	Active targeting (biotin-coated) Pt in tumor, fold increase (24 h) Kidney: 1.6 Liver: 0.29	Subcutaneous A549 lung tumor (5 mg/kg): Tumor volume, mm^3 Cisplatin ~1400, 18a−NP ~ 300, 18b−NP ~ 25 Tumor weight, g Cisplatin ~0.62, 18a-NP ~0.27, 18b-NP ~0.12 Lewis lung carcinoma, vaccination (1.95 mg/kg Pt^{4+} 18a-NP & 18b-NP, 5.95 mg/kg cisplatin) Tumor volume, mm^3 after vaccination): Cisplatin ~1300, 18a-NP ~500, 18b-NP ~40
319	31-NP	Type 7 Fabrication of 31-NP by emulsion interfacial polymerization of FKLAK peptide and Pt(IV) prodrug 31	Pt release (8 h): pH 7.4: 23% pH 6.5: 85% FKLAK release (8 h) pH 7.4: 11% pH 6.5: 80%	Passive tumor targeting, active mitochondria targeting CT signal in tumor, fold increase (12 h): Liver: 0.6 Kidney: 2.1	Subcutaneous A549 tumor (3.5 mg Pt/kg) TIR 31-NP: 74.5% FKLAK: 19.0%, Oxaliplatin: 12.6% Lung cancer PDX mode TIR (3.5 mg Pt/kg) 31-NP: 78.8% FKLAK: 14%, Oxaliplatin: 58.9%
323	33-NP	Type 7 *In situ* dephosphorylation of axial merocyanine ligand of Pt(IV) prodrug 33 and self-assembly into nanoparticles	Pt release (1 h): 10 mmol/L GSH: 100%	Passive targeting μg Pt/g tumor tissue, fold increase (4 h) Liver: 2.5 Kidney: 4.3	Subcutaneous HeLa tumor (2.25 mg Pt/kg): Relative tumor volume (V/V_0): PBS ~21, Cisplatin ~16, (*continued on next page*)

Table 2 (*continued*)

Ref	NP structural type, assembly method	Self-assembly		
		Drug release rate	Tumor targeting, relative accumulation level	*In vivo* tumor model (treatment regimen), antitumor effect
				33-NP ~ 13
				33 (self-assembly of NPs *in vivo*) ~ 1
				Orthotropic hepatocellular carcinoma HEPG2 tumors
				Luminescence intensity (10^5 photons)
				PBS ~ 13.0
				Cisplatin ~ 10.7
				33-NP ~ 5.7
				33 (self-assembly of NPs *in vivo*) ~ 1
157	38-NP Type 7 Loading of Pt(IV) prodrug 38 into stable core−shell UCNP	Pt release (72 h): pH 7.4 − 5.0: 15% 1 μmol/L GSH: 30% 5 μmol/L GSH: 40% 10 μmol/L GSH: 60% 10 μmol/L GSH + pH 5.0 + 980 nm (0.48 W/cm^2): 90% (30 min)	Active targeting (RGD peptide) μPt/g tissue in tumor, fold increase (24 h): Liver: 1.0 Kidney: 1.3	Subcutaneous U14 squamous cell carcinoma tumor (2.0 mg Pt/kg): Tumor volume, mm^3: Control ~ 1500 38-NP ~ 560 38-NP + 980 nm (0.48 W/cm^2) ~ 180 Fluorescence tumor visualization

12-NP, or graft the drug into the side of the polymer chain, which was implemented for **14-NP**. This yields multi-action nanoformulations, capable of strong immunostimulatory activity.

Instead of loading the small-molecule Pt(IV) prodrug into the polymer, the Pt(IV) complex can be incorporated into the polymer chain *via* axial positions, yielding polymeric Pt(IV) prodrug. In several reports, *i.e.,* **22-NP**, **23-NP** or **34-NP** Pt(IV) link was utilized as a reduction-sensitive cleavage point, releasing active Pt(II) drug under high GSH or NaAsc concentration. However, release of Pt(II) drug could be achieved controllably *via* external factors like light or ultrasound, as was the case for **24-NP**, **37-NP**, **39-NP, 40-NP**. Controllable release of Pt from NPs could be achieved either by incorporating light-sensitive motifs into the polymer chain (**39-NP, 40-NP**) or by co-assembly of Pt(IV) polyprodrug with the photosensitizer (**37-NP**). Aside from controlling Pt release from NPs, photo- and sonosensitizers induce additional antitumor effects *via* PDT, focused ultrasound, and PTT, markedly enhancing tumor inhibition relative to treatment with Pt-based therapy. It can also be noted that Pt(IV) polyprodrugs with active tumor-targeting moieties like alendronate or RGD peptide in **22-NP** and **34-NP** demonstrated improved tumor-accumulation properties as compared to NPs with passive accumulation only.

Nanodelivery platforms for Pt(IV) prodrugs could also be designed based on host−guest interactions of β-cyclodextrin and its derivatives. For **6-NP**, Pt(IV) prodrug was covalently conjugated with CD and loaded into adamantane-bearing polymer. Alternatively, **30-NP** were obtained by loading small-molecule Pt(IV) prodrug into CD. Both **6-NP** and **30-NP** contain active targeting moieties, which ensured efficient delivery of Pt into tumors and superior antitumor activity. That said, for both NPs a significant amount of the drug was released from NPs in neutral conditions, with 90% of prodrug **30** released from **30-NP** over 24 h.

Biogenic proteins, like HSA and hemoglobin could also serve as a nanocarriers for Pt(IV) prodrugs. HSA loading can ensure long bloodstream circulation time, which was employed for **19-NP**, **32-NP, 41-NP** while hemoglobin could also act as oxygen carrier into hypoxic tumors and as a photo/sonosensitizer, as demonstrated for **5-NP** and **36-NP**. Notably, both hemoglobin-based NPs showed high tumor accumulation with minimal liver uptake, while HSA-loaded **19-NP** and **41-NP** exhibited liver accumulation equal to or less than in tumors.

To outline the advancements in the design of effective NPs based on Pt(IV) prodrugs, the following positive trends could be highlighted:

1. Multi-action NPs can be designed *via* several ways, such as co-loading of several small molecule drugs into a single nanocarrier, or covalent conjugation of one drug to nanocarrier, or loading of the chemotherapuitic drug, a co-drug, and a theranostic agent on an external carrier, resulting in a single theranostic nanoplatform. These components in multi-action nanoformulation act in additive or synergistic way to overcome platinum resistance, stimulate antitumor immune response, etc. In general, active components loaded into NPs exert their antitumor properties upon delivery to tumor tissues. Regardless of the production route, the drugs loaded in the nanocarrier will act synergistically at the tumor site. However, careful control of the physicochemical properties of the nanocarriers, such as surface charge and chemical stability in the physiological environment, is urgently needed.

2. NPs with tumor-targeting groups generally demonstrate superior tumor drug delivery capabilities and, consequently, therapeutic efficacy compared to passively delivered nanocarriers; therefore, active targeting of NPs is highly recommended. However, it should be noted that widely used PEGylation of NPs can “hide" the vector from the receptor on tumor surface. It should be especially noted that micelles obtained by self-assembly of the Pt(IV) prodrugs with the vector fragment in an axial position, demonstrate high tumor-targeting capacity, presumably due to the high concentration of the tumor-specific molecule on the micelle surface.
3. Proteins serve as an efficient vehicle for Pt(IV) prodrugs, which therewith are able to enhance an accumulation of nanodrugs in tumor tissue. Hemoglobin is an especially versatile platform for NP design as it is also capable of alle*via*ting hypoxia by oxygen delivery, thereby increasing the effectiveness of chemotherapy and reducing resistance, and is also capable of serving as a photo/sonosensitizer due to the photophysical properties of the heme;
4. Lipid NPs basically demonstrate strong liver accumulation, which hinders delivery of active drugs into subcutaneous tumors or orthotopic tumors located in other organs. However, this property could be utilized to design NPs to specifically target hepatomas.
5. Controllable release of drugs from nanocarrier under external or internal stimuli allows localization of the site of therapeutic action and minimization of the impact of drugs on healthy tissues, while ensuring drug release in tumor tissues. Both endogenous (GSH, pH, ROS-sensitive) and exogenous (light, ultrasound) activation modes could be implemented, they could also be combined within single nanoplatform to achieve burst-like activation in tumor-specific conditions.

To summarize, an ideal nanoprodrug should possess active tumor-targeting groups to localize the drug in tumor tissues, implement stimuli-responsive release to activate the drug specifically in tumors, and ensure synergy between active components for maximum tumor-eradicating effect. Optimal platforms for such NPs may include proteins like hemoglobin or HSA, polymer-loaded systems, and self-assembled nanostructures, each enabling enhanced tumor targeting and strong antitumor effects.

6. Conclusions

The use of Pt(IV)-based nanoplatforms with prolonged bloodstream circulation time and tumor-targeting capabilities results in the delivery of therapeutic agents in tumor tissues without unwanted side-reactions, which greatly boosts the antitumor efficiency. The overwhelming majority of NPs discussed in this review surpasses CDDP and its analogues in their therapeutic efficacy and are capable of significantly improving antitumor therapeutic efficacy by acting on multiple targets, suppressing various resistance mechanisms, stimulating native and adaptive antitumor immunity, and significantly increasing drug accumulation in tumor tissue. The possibility of co-loading an additional drug, modifying NPs with tumor-targeted moieties opens the way to the design of targeted nanoplatforms with multiple effects. Also, the possibility of varying the axial ligands of Pt(IV) prodrugs allows us to impart the resulting nanoplatform with a wide variety of physico-chemical properties and biological activity. Overall, the use of nanoformulations of Pt(IV) prodrugs allows for a significant enhancement of the therapeutic efficacy of platinum-based chemotherapy and may open a new paradigm in the use of platinum drugs in medicinal chemistry.

Despite the impressive potential of NPs in laboratory studies, the translation from laboratory research to clinical practice faces challenges, and significant gaps remain to be overcome to achieve clinical application of NPs. First, the efficacy and mechanism of action of nanomedicines must be thoroughly studied in clinically representative organoid models, as significant discrepancies can exist between laboratory experiments and clinical trials. Second, the technology of nanomedicines production and maintaining homogeneity between different batches of NPs are also crucial. The difficulty of precise control over the composition of NPs, especially complex and multicomponent ones, from batch to batch is a serious challenge. Even slight alterations in the structure, surface properties, and composition of the nanomedicines can easily lead to altered drug metabolism and uncontrollable side effects. Third, significant difficulties arise in obtaining regulatory approval for the use of NPs in clinical practice.

We believe that the individual achievements and general trends highlighted in this review would contribute to further advancement in the field of anticancer nanotherapeutics and that this review would serve as a helpful guide for researchers.

Acknowledgements

The work was carried out with financial support from the Russian Science Foundation 22-15-00182-II.

Author contributions

Olga Krasnovskaya conceptualized the review. Olga Krasnovskaya, Daniil Spector and Roman Akasov wrote the original draft of the manuscript with the input from all coauthors. Vladislav Bykusov, Georgy Karetnikov, Anastasia Zharova and Daniil Spektor designed and created the illustrations. Olga Krasnovskaya, Daniil Spector, Georgy Karetnikov, Roman Akasov and Elena Beloglazkina revised and edited the manuscript. Elena Beloglazkina and Roman Akasov provided guidance and supervision during the preparation of the manuscript.

Conflicts of interest

The authors declare no conflicts of interest.

References

1. Mariconda A, Ceramella J, Catalano A, Saturnino C, Sinicropi MS, Longo P. Cisplatin, the timeless molecule. *Inorganics* 2025;**13**:246.
2. Ghosh S. Cisplatin: the first metal based anticancer drug. *Bioorg Chem* 2019;**88**:102925.
3. Galluzzi L, Vitale I, Michels J, Brenner C, Szabadkai G, Harel-Bellan A, et al. Systems biology of cisplatin resistance: past, present and future. *Cell Death Dis* 2014;**5**:e1257.
4. Dasari S, Bernard Tchounwou P. Cisplatin in cancer therapy: molecular mechanisms of action. *Eur J Pharmacol* 2014;**740**:364−78.
5. de Vries EGE, Willemse PHB, Chabner BA, Longo DL. Cancer chemotherapy and biotherapy: principles and practice. *Ann Oncol* 2002;**13**:1325.
6. Lokich J, Anderson N. Carboplatin *versus* cisplatin in solid tumors: an analysis of the literature. *Ann Oncol Off J Eur Soc Med Oncol* 1998;**9**:13−21.

7. Stojanovska V, Prakash M, McQuade R, Fraser S, Apostolopoulos V, Sakkal S, et al. Oxaliplatin treatment alters systemic immune responses. *Biomed Res Int* 2019;**2019**:4650695.
8. Montagnani F, Turrisi G, Marinozzi C, Aliberti C, Fiorentini G. Effectiveness and safety of oxaliplatin compared to cisplatin for advanced, unresectable gastric cancer: a systematic review and meta-analysis. *Gastric Cancer* 2011;**14**:50−5.
9. Kee JX, Yau JNN, Kumar Muthuramalingam RP, Wang X, Chng WH, Lopez-Sanchez A, et al. Colorectal cancer at the crossroads: the good, the bad, and the future of platinum-based drugs. *Chem Rev* 2025;**125**:10248−341.
10. Johnstone TC, Suntharalingam K, Lippard SJ. The next generation of platinum drugs: targeted Pt(II) agents, nanoparticle delivery, and Pt(IV) prodrugs. *Chem Rev* 2016;**116**:3436−86.
11. Hartmann JT, Lipp HP. Toxicity of platinum compounds. *Expert Opin Pharmacother* 2003;**4**:889−901.
12. Dilruba S, Kalayda GV. Platinum-based drugs: past, present and future. *Cancer Chemother Pharmacol* 2016;**77**:1103−24.
13. Ravera M, Gabano E, McGlinchey MJ, Osella D. Pt(IV) antitumor prodrugs: dogmas, paradigms, and realities. *Dalt Trans* 2022;**51**: 2121−34.
14. Spector D, Pavlov K, Beloglazkina E, Krasnovskaya O. Recent advances in light-controlled activation of Pt(IV) prodrugs. *Int J Mol Sci* 2022;**23**:14511.
15. Xu Z, Wang Z, Deng Z, Zhu G. Recent advances in the synthesis, stability, and activation of platinum(IV) anticancer prodrugs. *Coord Chem Rev* 2021;**442**:213991.
16. Spector DV, Bubley AA, Beloglazkina EK, Krasnovskaya OO. Platinum(IV)-based prodrugs as an alternative to Pt(II)-based drugs: synthesis and biological action. *Russ Chem Rev* 2023;**92**: RCR5096.
17. Cai L, Chen H, Wang Y, Zhang J, Song D, Tan Y, et al. Platinum(IV) complexes trigger death receptors and natural killer cells to suppress breast cancer. *J Med Chem* 2025;**68**:9162−75.
18. Wei F, Liang J, Shen XC, Pan Y, He Y, Chao H. Recent advances in the development of metallodrugs for cancer chemoimmunotherapy. *Coord Chem Rev* 2025;**526**:216319.
19. Jin S, Guo Y, Wang X. Development of platinum complexes for tumor chemoimmunotherapy. *Chemistry* 2024;**30**:e202302948.
20. Spector D, Zharova A, Bykusov V, Karetnikov G, Beloglazkina E, Krasnovskaya O. Recent advances in antitumor Pt(IV) complexes: dual targeting and chemoimmunotherapy. *Coord Chem Rev* 2025; **541**:216808.
21. Tu Y, Gong J, Mou J, Jiang H, Zhao H, Gao J. Strategies for the development of stimuli-responsive small molecule prodrugs for cancer treatment. *Front Pharmacol* 2024;**15**:1434137.
22. Xie A, Hanif S, Ouyang J, Tang Z, Kong N, Kim NY, et al. Stimuli-responsive prodrug-based cancer nanomedicine. *EBioMedicine* 2020; **56**:102821.
23. Huang J, Ding W, Zhu X, Li B, Zeng F, Wu K, et al. Ligand evolution in the photoactivatable platinum(IV) anticancer prodrugs. *Front Chem* 2022;**10**:876410.
24. Steblevskaya N, Belobeletskaya M, Medkov M, Shevchenko O. Platinum coordination compounds: synthesis and application in the treatment of oncological diseases. *Probl Biol Med Pharm Chem* 2025; **28**:50−8.
25. Maji M, De Franco M, Acharya S, Gibson D, Gandin V. A new class of multitargeting Pt^{IV} anticancer agents: prodrugs that release Pt^{II} drugs and bioactive moieties tethered to Pt^{IV} *via* a tertiary amine. *J Med Chem* 2026;**69**:2539−53.
26. Spector D, Krasnovskaya O, Pavlov K, Erofeev A, Gorelkin P, Beloglazkina E, et al. Pt(IV) prodrugs with NSAIDs as axial ligands. *Int J Mol Sci* 2021;**22**:3817.
27. Štarha P, Křikavová R. Platinum(IV) and platinum(II) anticancer complexes with biologically active releasable ligands. *Coord Chem Rev* 2024;**501**:215578.
28. Chen CKJJ, Zhang JZ, Aitken JB, Hambley TW. Influence of equatorial and axial carboxylato ligands on the kinetic inertness of platinum(IV) complexes in the presence of ascorbate and cysteine and within dld-1 cancer cells. *J Med Chem* 2013;**56**:8757−64.
29. Kastner A, Poetsch I, Mayr J, Burda JV, Roller A, Heffeter P, et al. A dogma in doubt: hydrolysis of equatorial ligands of Pt^{IV} complexes under physiological conditions. *Angew Chem Int Ed Engl* 2019;**58**: 7464−9.
30. Chen QB, Zhou LY, Shi LX, Cheng Y, Wu K, Yuan Q, et al. Platinum(IV) complex-loaded nanoparticles with photosensitive activity for cancer therapy. *Coord Chem Rev* 2022;**472**:214789.
31. Ferrari G, Lopez-Martinez I, Wanek T, Kuntner C, Montagner D. Recent advances on Pt-based compounds for theranostic applications. *Molecules* 2024;**29**:3453.
32. Liang G, Sadhukhan T, Banerjee S, Tang D, Zhang H, Cui M, et al. Reduction of platinum(IV) prodrug hemoglobin nanoparticles with deeply penetrating ultrasound radiation for tumor-targeted therapeutically enhanced anticancer therapy. *Angew Chem Int Ed Engl* 2023;**62**:e202301074.
33. Chang X, Bian M, Liu L, Yang J, Yang Z, Wang Z, et al. Induction of immunogenic cell death by novel platinum-based anticancer agents. *Pharmacol Res* 2023;**187**:106556.
34. Zhai J, Gu X, Liu Y, Hu Y, Jiang Y, Zhang Z. Chemotherapeutic and targeted drugs-induced immunogenic cell death in cancer models and antitumor therapy: an update review. *Front Pharmacol* 2023;**14**: 1152934.
35. Wang M, Yi H, Zhan Z, Feng Z, Yang G, Zheng Y, et al. A self-assembled nanomedicine for glucose supply interruption-amplified low-temperature photothermal therapy and anti-prometastatic inflammatory processes of triple-negative breast cancer. *Aggregate* 2024;**5**:e622.
36. Zhou Z, Shi P, Wang C, Sun Y, Gao C. Recent updates in nanoscale delivery systems of platinum(IV) antitumor prodrugs. *Coord Chem Rev* 2024;**508**:215774.
37. Wang T, Wu C, Hu Y, Zhang Y, Ma J. Stimuli-responsive nanocarrier delivery systems for Pt-based antitumor complexes: a review. *RSC Adv* 2023;**13**:16488−511.
38. Luo FR, Wyrick SD, Chaney SG. Comparative neurotoxicity of oxaliplatin, ormaplatin, and their biotransformation products utilizing a rat dorsal root ganglia *in vitro* explant culture model. *Cancer Chemother Pharmacol* 1999;**44**:29−38.
39. Deng Z, Yao H, Wang Z, Zhu G. Platinum anticancer drugs: targeting and delivery. In: Reedijk J, Poeppelmeier KR, editors. *Comprehensive Inorganic Chemistry III*. Amsterdam: Elsevier; 2023. p. 808−46.
40. McKeage MJ. Satraplatin in hormone-refractory prostate cancer and other tumour types. *Drugs* 2007;**67**:859−69.
41. Choy H, Park C, Yao M. Current status and future prospects for satraplatin, an oral platinum analogue. *Clin Cancer Res* 2008;**14**: 1633−8.
42. Liang W, Huang Y, Wang Y, Lu D, Sun Q. Research progress of platinum-based complexes in lung cancer treatment: mechanisms, applications, and challenges. *Int J Mol Sci* 2025;**26**:7958.
43. Zheng S, Li G, Shi J, Liu X, Li M, He Z, et al. Emerging platinum(IV) prodrug nanotherapeutics: a new epoch for platinum-based cancer therapy. *J Control Release* 2023;**361**:819−46.
44. Apps MG, Choi EHY, Wheate NJ. The state-of-play and future of platinum drugs. *Endocr Relat Cancer* 2015;**22**:R219−33.
45. Nabavizadeh SM, Shahsavari HR, Namdar M, Rashidi M. Substitution reactions involving cyclometalated platinum(II) complexes: kinetic investigations. *J Organomet Chem* 2011;**696**:3564−71.
46. Lee YA, Ho Yoo K, Jung OS. Oxidation of Pt(II) to Pt(IV) complex with hydrogen peroxide in glycols. *Inorg Chem Commun* 2003;**6**: 249−51.
47. Xu Z, Li C, Tong Z, Ma L, Tse M, Zhu G. Halogenated Pt^{IV} Complexes from *N* -halosuccinimide oxidation of Pt^{II} antitumor drugs: synthesis, mechanistic investigation, and cytotoxicity. *Eur J Inorg Chem* 2017;**2017**:1706−12.
48. Chung TS, Na YM, Kang SW, Jung OS, Lee YA. Facile generation of platinum(IV) compounds with mixed labile moieties. Hydrogen peroxide oxidation of platinum(II) to platinum(IV) compounds. *Transit Met Chem* 2005;**30**:541−5.

49. Wilson JJ, Lippard SJ. Synthetic methods for the preparation of platinum anticancer complexes. *Chem Rev* 2014;**114**:4470−95.
50. Yempala T, Babu T, Karmakar S, Nemirovski A, Ishan M, Gandin V, et al. Expanding the arsenal of Pt^{IV} anticancer agents: multi-action Pt^{IV} anticancer agents with bioactive ligands possessing a hydroxy functional group. *Angew Chem Int Ed Engl* 2019;**58**:18218−23.
51. Xu Z, Tang WK, Zhou Q, Chen S, Siu CK, Zhu G. On the hydrolytic stability of unsymmetric platinum(IV) anticancer prodrugs containing axial halogens. *Inorg Chem Front* 2021;**8**:3794−802.
52. Zhou Q, Chen S, Xu Z, Liu G, Zhang S, Wang Z, et al. Multitargeted platinum(IV) anticancer complexes bearing pyridinyl ligands as axial leaving groups. *Angew Chem Int Ed Engl* 2023;**62**:e202302156.
53. Wexselblatt E, Yavin E, Gibson D. Platinum(IV) prodrugs with haloacetato ligands in the axial positions can undergo hydrolysis under biologically relevant conditions. *Angew Chem Int Ed Engl* 2013;**52**:6059−62.
54. Ritacco I, Mazzone G, Russo N, Sicilia E. Investigation of the inertness to hydrolysis of platinum(IV) prodrugs. *Inorg Chem* 2016; **55**:1580−6.
55. Zhao J, Xu Z, Lin J, Gou S. Exploring the hydrolytic behavior of the platinum(IV) complexes with axial acetato ligands. *Inorg Chem* 2017;**56**:9851−9.
56. Chen S, Yao H, Zhou Q, Tse MK, Gunawan YF, Zhu G. Stability, reduction, and cytotoxicity of platinum(IV) anticancer prodrugs bearing carbamate axial ligands: comparison with their carboxylate analogues. *Inorg Chem* 2020;**59**:11676−87.
57. Chen S, Ng K-Y, Zhou Q, Yao H, Deng Z, Tse MK, et al. The influence of different carbonate ligands on the hydrolytic stability and reduction of platinum(IV) prodrugs. *Dalt Trans* 2022;**51**:885−97.
58. Nemirovski A, Vinograd I, Takrouri K, Mijovilovich A, Rompel A, Gibson D. New reduction pathways for *ctc*-$[PtCl_2(CH_3CO_2)_2(NH_3)(Am)]$ anticancer prodrugs. *Chem Commun* 2010;**46**:1842−4.
59. Karges J. Chemical and photophysical triggers for the reduction of Pt(IV) prodrugs for anticancer therapy. *ChemNanoMat* 2023;**9**: e202300295.
60. Ponte F, Scoditti S, Mazzone G, Sicilia E. The current status in computational exploration of Pt(IV) prodrug activation by reduction. *Phys Chem Chem Phys* 2023;**25**:15586−99.
61. Xu L, Kong X, Li X, Zhang B, Deng Y, Wang J, et al. Current status of novel multifunctional targeted Pt(IV) compounds and their reductive release properties. *Molecules* 2024;**29**:746.
62. Chen S, Zhou Q, Ng KY, Xu Z, Xu W, Zhu G. Advances in technical strategies for monitoring the reduction of platinum(IV) complexes. *Inorg Chem Front* 2024;**11**:3085−118.
63. Wexselblatt E, Gibson D. What do we know about the reduction of Pt(IV) pro-drugs?. *J Inorg Biochem* 2012;**117**:220−9.
64. Zhang JZ, Wexselblatt E, Hambley TW, Gibson D. Pt(IV) analogs of oxaliplatin that do not follow the expected correlation between electrochemical reduction potential and rate of reduction by ascorbate. *Chem Commun* 2012;**48**:847−9.
65. Gibson D. Platinum(IV) anticancer prodrugs—hypotheses and facts. *Dalt Trans* 2016;**45**:12983−91.
66. Lemma K, Sargeson AM, Elding LI. Kinetics and mechanism for reduction of oral anticancer platinum(IV) dicarboxylate compounds by L-ascorbate ions. *J Chem Soc Dalt Trans* 2000;**29**:1167−72.
67. McCormick MC, Keijzer K, Polavarapu A, Schultz FA, Baik MH. Understanding intrinsically irreversible, non-nernstian, two-electron redox processes: a combined experimental and computational study of the electrochemical activation of platinum(IV) antitumor prodrugs. *J Am Chem Soc* 2014;**136**:8992−9000.
68. Ponte F, Russo N, Sicilia E. Insights from computations on the mechanism of reduction by ascorbic acid of Pt(IV) prodrugs with asplatin and its chlorido and bromido analogues as model systems. *Chemistry* 2018;**24**:9572−80.
69. Tolbatov I, Coletti C, Marrone A, Re N. Insight into the electrochemical reduction mechanism of Pt(IV) anticancer complexes. *Inorg Chem* 2018;**57**:3411−9.
70. Basolo F, Messing AF, Wilks PH, Wilkins RG, Pearson RG. Mechanisms of exchange and substitution reactions in platinum(IV) complexes. *J Inorg Nucl Chem* 1958;**8**:203−8.
71. Imberti C, Zhang P, Huang H, Sadler PJ. New designs for phototherapeutic transition metal complexes. *Angew Chem Int Ed Engl* 2020;**59**:61−73.
72. Bednarski PJ, Mackay FS, Sadler PJ. Photoactivatable platinum complexes. *Anti Cancer Agents Med Chem* 2007;**7**:75−93.
73. Shi H, Clarkson GJ, Sadler PJ. Tuning the phototherapeutic activity of Pt(IV) complexes for bladder cancer *via* modification of *trans N*-heterocyclic ligands. *Inorg Chem Front* 2024;**11**:7898−909.
74. Wang Z, Wang N, Cheng SC, Xu K, Deng Z, Chen S, et al. Phorbiplatin, a highly potent Pt(IV) antitumor prodrug that can be controllably activated by red light. *Chem* 2019;**5**:3151−65.
75. Spector D, Bykusov V, Isaeva Y, Akasov R, Zharova A, Rodin I, et al. Green light activated dual-action Pt(IV) prodrug with enhanced PDT activity. *ChemMedChem* 2025;**20**:e202400786.
76. Tang L, Luo Y, Luo W, Sun G, Jiang Y, Zhang Z, et al. Pt(IV) prodrug photoactivation: a promising strategy for cancer therapy. *Curr Protein Pept Sci* 2024;**25**:797−813.
77. La Monica G, Bono A, Alamia F, Lauria A, Martorana A. Spatiotemporal control of prodrug activation through external stimuli for effective and safe on-site release in solid tumors: from current advances to future perspectives. *Drug Discov Today* 2026;**31**: 104595.
78. Deng Z, Li H, Chen S, Wang N, Liu G, Liu D, et al. Near-infrared-activated anticancer platinum(IV) complexes directly photooxidize biomolecules in an oxygen-independent manner. *Nat Chem* 2023;**15**: 930−9.
79. Alonso-De Castro S, Ruggiero E, Ruiz-De-Angulo A, Rezabal E, Mareque-Rivas JC, Lopez X, et al. Riboflavin as a bioorthogonal photocatalyst for the activation of a Pt^{IV} prodrug. *Chem Sci* 2017;**8**: 4619−25.
80. Alonso-de Castro S, Cortajarena AL, López-Gallego F, Salassa L. Bioorthogonal catalytic activation of platinum and ruthenium anticancer complexes by FAD and flavoproteins. *Angew Chem Int Ed Engl* 2018;**57**:3143−7.
81. Sánchez-Camacho J, Carrasco AC, Pieslinger GE, Martínez Á, Lobinski R, Ronga L, et al. Catalytic glutathione oxidation and platinum(IV) prodrug activation *via* a ruthenium-flavin catalyst. *Organometallics* 2025;**44**:944−51.
82. Kaub L, Schmitz C. Comparison of the penetration depth of 905 nm and 1064 nm laser light in surface layers of biological tissue *ex vivo*. *Biomedicines* 2023;**11**:1355.
83. Hu JJ, Lei Q, Zhang XZ. Recent advances in photonanomedicines for enhanced cancer photodynamic therapy. *Prog Mater Sci* 2020;**114**: 100685.
84. Pham TC, Nguyen VN, Choi Y, Lee S, Yoon J. Recent strategies to develop innovative photosensitizers for enhanced photodynamic therapy. *Chem Rev* 2021;**121**:13454−619.
85. Poggi C, Palavecino M. Ultrasound principles and instrumentation. *Surg Open Sci* 2024;**18**:123−8.
86. Wang X, Kim G, Chu JL, Song T, Yang Z, Guo W, et al. Noninvasive and spatiotemporal control of DNAzyme-based imaging of metal ions *in vivo* using high-intensity focused ultrasound. *J Am Chem Soc* 2022;**144**:5812−9.
87. Lee LC, Lo KK. Ultrasound-activatable transition metal complexes to potentiate sonodynamic therapy. *Chem Sci* 2025;**16**:22266−90.
88. Lafond M, Yoshizawa S, Umemura S. Sonodynamic therapy: advances and challenges in clinical translation. *J Ultrasound Med* 2019; **38**:567−80.
89. Ding Y, Yang Y, Aras O, An F, Zhou M, Chai Y. Development and application of organic sonosensitizers in cancer therapy. *Aggregate* 2025;**6**:e70032.
90. Xing X, Zhao S, Xu T, Huang L, Zhang Y, Lan M, et al. Advances and perspectives in organic sonosensitizers for sonodynamic therapy. *Coord Chem Rev* 2021;**445**:214087.

91. Liu G, Zhang Y, Yao H, Deng Z, Chen S, Wang Y, et al. An ultrasound-activatable platinum prodrug for sono-sensitized chemotherapy. *Sci Adv* 2023;**9**:eadg5964.
92. Wang C, Zhang Z, Liu Z. Radiotherapy-activated prodrug: past, present and beyond. *ACS Cent Sci* 2025;**11**:1306−20.
93. Wei Q, Qiao S, Fu Q, Liu Z. Perspective to clinical translation of radiotherapy-activated prodrugs: challenges and advances. *Med Plus* 2025;**2**:100076.
94. Han HH, Wang HM, Jangili P, Li M, Wu L, Zang Y, et al. The design of small-molecule prodrugs and activatable phototherapeutics for cancer therapy. *Chem Soc Rev* 2023;**52**:879−920.
95. Ding Z, Guo Z, Zheng Y, Wang Z, Fu Q, Liu Z. Radiotherapy reduces *N*-oxides for prodrug activation in tumors. *J Am Chem Soc* 2022;**144**: 9458−64.
96. Fu Q, Zhang S, Shen S, Gu Z, Chen J, Song D, et al. Radiotherapy-triggered reduction of platinum-based chemotherapeutic prodrugs in tumours. *Nat Biomed Eng* 2024;**8**:1425−35.
97. Guo Z, Wang X, Han Y, Shen S, Tian P, Hu Y, et al. Targeted radionuclide therapy activates prodrugs for treating metastasis. *ACS Cent Sci* 2024;**10**:2321−30.
98. Wang C, Xu M, Zhang Z, Zeng S, Shen S, Ding Z, et al. Locally unlocks prodrugs by radiopharmaceutical in tumor for cancer therapy. *Sci Bull* 2024;**69**:2745−55.
99. Greish K. Enhanced permeability and retention (EPR) effect for anticancer nanomedicine drug targeting. In: Grobmyer S, Moudgil B, editors. *Cancer Nanotechnology. Methods in Molecular Biology.* vol 624. Humana Press; 2010. p. 25−37.
100. Mi K, Chou WC, Chen Q, Yuan L, Kamineni VN, Kuchimanchi Y, et al. Predicting tissue distribution and tumor delivery of nanoparticles in mice using machine learning models. *J Control Release* 2024;**374**:219−29.
101. Austria E, Bilek M, Varamini P, Akhavan B. Breaking biological barriers: engineering polymeric nanoparticles for cancer therapy. *Nano Today* 2025;**60**:102552.
102. Pan J, Wang Y, Chen Y, Zhang C, Deng H, Lu J, et al. Emerging strategies against accelerated blood clearance phenomenon of nanocarrier drug delivery systems. *J Nanobiotechnol* 2025;**23**:138.
103. Zelepukin IV, Shevchenko KG, Deyev SM. Rediscovery of mononuclear phagocyte system blockade for nanoparticle drug delivery. *Nat Commun* 2024;**15**:4366.
104. Zein R, Sharrouf W, Selting K. Physical properties of nanoparticles that result in improved cancer targeting. *J Oncol* 2020;**2020**:194780.
105. Blanco E, Shen H, Ferrari M. Principles of nanoparticle design for overcoming biological barriers to drug delivery. *Nat Biotechnol* 2015;**33**:941−51.
106. Joudeh N, Linke D. Nanoparticle classification, physicochemical properties, characterization, and applications: a comprehensive review for biologists. *J Nanobiotechnol* 2022;**20**:262.
107. Shaw S, Shit GC, Tripathi D. Impact of drug carrier shape, size, porosity and blood rheology on magnetic nanoparticle-based drug delivery in a microvessel. *Colloids Surf A Physicochem Eng Asp* 2022;**639**:128370.
108. Banerjee A, Qi J, Gogoi R, Wong J, Mitragotri S. Role of nanoparticle size, shape and surface chemistry in oral drug delivery. *J Control Release* 2016;**238**:176−85.
109. Jia W, Wang Y, Liu R, Yu X, Gao H. Shape transformable strategies for drug delivery. *Adv Funct Mater* 2021;**31**:202009765.
110. Hoshyar N, Gray S, Han H, Bao G. The effect of nanoparticle size on *in vivo* pharmacokinetics and cellular interaction. *Nanomedicine* 2016;**11**:673−92.
111. Sykes EA, Chen J, Zheng G, Chan WC. Investigating the impact of nanoparticle size on active and passive tumor targeting efficiency. *ACS Nano* 2014;**8**:5696−706.
112. Aldayel AM, Hufnagel S, O'Mary HL, Valdes SA, Alzhrani RF, Xu H, et al. Effect of nanoparticle size on their distribution and retention in chronic inflammation sites. *Discov Nano* 2023;**18**:105.
113. Bazak R, Houri M, Achy SEL, Hussein W, Refaat T. Passive targeting of nanoparticles to cancer: a comprehensive review of the literature. *Mol Clin Oncol* 2014;**2**:904−8.
114. Khalil IA, Faheem A, El-Tanani M. Targeted drug delivery to the spleen and its implications for the prevention and treatment of cancer. *Pharmaceutics* 2025;**17**:651.
115. Souza IDL, Saez V, Mansur CRE. Lipid nanoparticles containing coenzyme Q10 for topical applications: an overview of their characterization. *Colloids Surf B Biointerfaces* 2023;**230**:113491.
116. Shameli K, Kalali B, Moeini H, Kartouzian A. Lipid-based colloidal nanocarriers for site-specific drug delivery. *Colloids Interfaces* 2026; **10**:7.
117. Davis ME, Chen Z, Shin DM. Nanoparticle therapeutics: an emerging treatment modality for cancer. *Nat Rev Drug Discov* 2008; **7**:771−82.
118. Souri M, Golzaryan A, Soltani M. Charge-switchable nanoparticles to enhance tumor penetration and accumulation. *Eur J Pharm Biopharm* 2024;**199**:114310.
119. Guo Z, Sui J, Ma M, Hu J, Sun Y, Yang L, et al. pH-responsive charge switchable PEGylated ε-poly-L-lysine polymeric nanoparticles-assisted combination therapy for improving breast cancer treatment. *J Control Release* 2020;**326**:350−64.
120. Lee H, Park B, Lee J, Kang Y, Han M, Lee J, et al. Transcytosis-inducing multifunctional albumin nanomedicines with deep penetration ability for image-guided solid tumor treatment. *Small* 2023;**19**:2303668.
121. Wang Y, Cong Y, Cai M, Liang X, Wang L, Zhou D. Charge-conversional click polyprodrug nanomedicine for targeted and synergistic cancer therapy. *J Control Release* 2023;**356**:567−79.
122. Soo Choi H, Liu W, Misra P, Tanaka E, Zimmer JP, Itty Ipe B, et al. Renal clearance of quantum dots. *Nat Biotechnol* 2007;**25**:1165−70.
123. Albanese A, Tang PS, Chan WCW. The effect of nanoparticle size, shape, and surface chemistry on biological systems. *Annu Rev Biomed Eng* 2012;**14**:1−16.
124. Voke E, Arral ML, Squire HJ, Lin TJ, Zheng L, Coreas R, et al. Protein corona formed on lipid nanoparticles compromises delivery efficiency of mRNA cargo. *Nat Commun* 2025;**16**:8699.
125. Kaymaz SV, Nobar HM, Sarıgül H, Soylukan C, Akyüz L, Yüce M. Nanomaterial surface modification toolkit: principles, components, recipes, and applications. *Adv Colloid Interface Sci* 2023;**322**:103035.
126. Ly PD, Ly KN, Phan HL, Nguyen HHT, Duong VA, Nguyen HV. Recent advances in surface decoration of nanoparticles in drug delivery. *Front Nanotechnol* 2024;**6**:1456939.
127. Shreffler JW, Pullan JE, Dailey KM, Mallik S, Brooks AE. Overcoming hurdles in nanoparticle clinical translation: the influence of experimental design and surface modification. *Int J Mol Sci* 2019;**20**: 6056.
128. Fang Y, Xue J, Gao S, Lu A, Yang D, Jiang H, et al. Cleavable PEGylation: a strategy for overcoming the "PEG dilemma" in efficient drug delivery. *Drug Deliv* 2017;**24**:22−32.
129. Yetisgin AA, Cetinel S, Zuvin M, Kosar A, Kutlu O. Therapeutic nanoparticles and their targeted delivery applications. *Molecules* 2020;**25**:2193.
130. Sun K, Yuan L, Chen S, Sun Y, Wei D. Alendronate Pt^{IV} prodrug amphiphile for enhanced chemotherapy targeting and bone destruction inhibition in osteosarcoma. *Adv Healthcare Mater* 2024;**13**:2302746.
131. Yan J, Wei D, Zhao Z, Sun K, Sun Y. Osteosarcoma-targeting Pt^{IV} prodrug amphiphile for enhanced chemo-immunotherapy *via* Ca^{2+} trapping. *Acta Biomater* 2025;**193**:474−83.
132. Grzelczak M, Vermant J, Furst EM, Liz-Marzán LM. Directed self-assembly of nanoparticles. *ACS Nano* 2010;**4**:3591−605.
133. Wang C, Wang Z, Zhang X. Amphiphilic building blocks for self-assembly: from amphiphiles to supra-amphiphiles. *Acc Chem Res* 2012;**45**:608−18.
134. Esmaeili H, Mousavi SM, Hashemi SA, Lai CW, Chiang WH, Bahrani S. Application of biosurfactants in the removal of oil from emulsion. In: Inamuddin, Adetunji CO, editors. *Green sustainable process for chemical and environmental engineering and science*. Elsevier; 2021. p. 107−27.
135. Xing P, Zhao Y. Multifunctional nanoparticles self-assembled from small organic building blocks for biomedicine. *Adv Mater* 2016;**28**: 7304−39.

136. Xu L, Wang X, Liu Y, Yang G, Falconer RJ, Zhao CX. Lipid nanoparticles for drug delivery. *Adv NanoBiomed Res* 2022;**2**: 2100109.
137. Eygeris Y, Gupta M, Kim J, Sahay G. Chemistry of lipid nanoparticles for RNA delivery. *Acc Chem Res* 2022;**55**:2−12.
138. Takayama R, Inoue Y, Murata I, Kanamoto I. Characterization of nanoparticles using DSPE-PEG_{2000} and soluplus. *Colloids Interfaces* 2020;**4**:28.
139. Zhang X, Ning S, Fang F, Zhou C, Yang Z, Cao L, et al. Leveraging cisplatin-derived prodrugs as helper lipids in LNPs to boost the efficacy of cancer chemoimmunotherapy. *ACS Nano* 2026;**20**: 1448−61.
140. Tang L, Yin Y, Cao Y, Liu H, Qing G, Fu C, et al. Bioorthogonal chemistry-guided inhalable nanoprodrug to circumvent cisplatin resistance in orthotopic nonsmall cell lung cancer. *ACS Nano* 2024; **18**:32103−17.
141. Elsabahy M, Wooley KL. Design of polymeric nanoparticles for biomedical delivery applications. *Chem Soc Rev* 2012;**41**:2545−61.
142. Guerassimoff L, Ferrere M, Bossion A, Nicolas J. Stimuli-sensitive polymer prodrug nanocarriers by reversible-deactivation radical polymerization. *Chem Soc Rev* 2024;**53**:6511−67.
143. Yang J, Su T, Wang Q, Shi R, Ding J, Chen X. Glucose metabolism-targeted poly(amino acid) nanoformulation of oxaliplatin(IV)-aspirin prodrug for enhanced chemo-immunotherapy. *Adv Mater* 2025;**37**: 2419033.
144. Li X, Cai J, Zhang H, Sun S, Zhao S, Wang Z, et al. A trisulfide bond containing biodegradable polymer delivering Pt(IV) prodrugs to deplete glutathione and donate H_2S to boost chemotherapy and antitumor immunity. *ACS Nano* 2024;**18**:7852−67.
145. Nicolas J. Drug-initiated synthesis of polymer prodrugs: combining simplicity and efficacy in drug delivery. *Chem Mater* 2016;**28**: 1591−606.
146. Huang X, Brazel CS. On the importance and mechanisms of burst release in matrix-controlled drug delivery systems. *J Control Release* 2001;**73**:121−36.
147. Nicolas J, Mura S, Brambilla D, Mackiewicz N, Couvreur P. Design, functionalization strategies and biomedical applications of targeted biodegradable/biocompatible polymer-based nanocarriers for drug delivery. *Chem Soc Rev* 2013;**42**:1147−235.
148. Wei D, Huang Y, Wang B, Ma L, Karges J, Xiao H. Photo-reduction with NIR light of nucleus-targeting Pt^{IV} nanoparticles for combined tumor-targeted chemotherapy and photodynamic immunotherapy. *Angew Chem Int Ed Engl* 2022;**61**:e202201486.
149. Zheng YR, Suntharalingam K, Johnstone TC, Yoo H, Lin W, Brooks JG, et al. Pt(IV) prodrugs designed to bind non-covalently to human serum albumin for drug delivery. *J Am Chem Soc* 2014;**136**: 8790−8.
150. Xie P, Jin Q, Zhang L, Zhang H, Montesdeoca N, Karges J, et al. Endowing Pt(IV) with perfluorocarbon chains and human serum albumin encapsulation for highly effective antitumor chemoimmunotherapy. *ACS Nano* 2024;**18**:13683−95.
151. Wang W, Cai J, Wen J, Li X, Yu Y, Zhang L, et al. Boosting ferroptosis *via* abplatin(IV) for treatment of platinum-resistant recurrent ovarian cancer. *Nano Today* 2022;**44**:101459.
152. Hu Q-D, Tang G-P, Chu PK. Cyclodextrin-based host−guest supramolecular nanoparticles for delivery: from design to applications. *Acc Chem Res* 2014;**47**:2017−25.
153. Deng Y, Wang Y, Jia F, Liu W, Zhou D, Jin Q, et al. Tailoring supramolecular prodrug nanoassemblies for reactive nitrogen species-potentiated chemotherapy of liver cancer. *ACS Nano* 2021;**15**: 8663−75.
154. Parra-Nieto J, del Cid MAG, de Cárcer IA, Baeza A. Inorganic porous nanoparticles for drug delivery in antitumoral therapy. *Biotechnol J* 2021;**16**:2000150.
155. Adhikari C. Polymer nanoparticles-preparations, applications and future insights: a concise review. *Polym Technol Mater* 2021;**18**: 1996−2024.
156. Wei F, Ke L, Gao S, Karges J, Wang J, Chen Y, et al. *In situ* oxidative polymerization of platinum(IV) prodrugs in pore-confined spaces of $CaCO_3$ nanoparticles for cancer chemoimmunotherapy. *Chem Sci* 2023;**14**:7005−15.
157. Liu XM, Zhu ZZ, He XR, Zou YH, Chen Q, Wang XY, et al. NIR light and GSH dual-responsive upconversion nanoparticles loaded with multifunctional platinum(IV) prodrug and rgd peptide for precise cancer therapy. *ACS Appl Mater Interfaces* 2024;**16**:40753−66.
158. Wang X, Liu G, Pu X, Ren T, Zhang F, Shen M, et al. Combating cisplatin-resistant lung cancer using a coiled-coil lipopeptides modified membrane fused drug delivery system. *J Control Release* 2025;**379**:45−58.
159. Zhen J, Sun L, Ji L, Zhou S, Cui Y, Li Z. EDN1 facilitates cisplatin resistance of non-small cell lung cancer cells by regulating the TNF signaling pathway. *World J Surg Oncol* 2025;**23**:71.
160. Kelland LR. Preclinical perspectives on platinum resistance. *Drugs* 2000;**59**:37−8.
161. Song IS, Savaraj N, Siddik ZH, Liu P, Wei Y, Wu CJ, et al. Role of human copper transporter Ctr1 in the transport of platinum-based antitumor agents in cisplatin-sensitive and cisplatin-resistant cells. *Mol Cancer Ther* 2004;**3**:1543−9.
162. Hermann G, Heffeter P, Falta T, Berger W, Hann S, Koellensperger G. *In vitro* studies on cisplatin focusing on kinetic aspects of intracellular chemistry by LC−ICP−MS. *Metallomics* 2013;**5**:636.
163. Siddik ZH. Cisplatin: mode of cytotoxic action and molecular basis of resistance. *Oncogene* 2003;**22**:7265−79.
164. Kleih M, Böpple K, Dong M, Gaißler A, Heine S, Olayioye MA, et al. Direct impact of cisplatin on mitochondria induces ROS production that dictates cell fate of ovarian cancer cells. *Cell Death Dis* 2019;**10**:851−62.
165. Cullen KJ, Yang Z, Schumaker L, Guo Z. Mitochondria as a critical target of the chemotheraputic agent cisplatin in head and neck cancer. *J Bioenerg Biomembr* 2007;**39**:43−50.
166. Jin P, Jiang J, Zhou L, Huang Z, Nice EC, Huang C, et al. Mitochondrial adaptation in cancer drug resistance: prevalence, mechanisms, and management. *J Hematol Oncol* 2022;**15**:97.
167. Chválová K, Brabec V, Kašpárková J. Mechanism of the formation of DNA−protein cross-links by antitumor cisplatin. *Nucleic Acids Res* 2007;**35**:1812−21.
168. Cohen SM, Lippard SJ. Cisplatin: from DNA damage to cancer chemotherapy. *Prog Nucleic Acid Res Mol Biol* 2001;**67**:93−130.
169. Zhu S, Pabla N, Tang C, He L, Dong Z. DNA damage response in cisplatin-induced nephrotoxicity. *Arch Toxicol* 2015;**89**:2197−205.
170. Hemann MT, Lowe SW. The p53−Bcl-2 connection. *Cell Death Differ* 2006;**13**:1256−9.
171. Lopez J, Tait SWG. Mitochondrial apoptosis: killing cancer using the enemy within. *Br J Cancer* 2015;**112**:957−62.
172. Casares C, Ramírez-Camacho R, Trinidad A, Roldán A, Jorge E, García-Berrocal JR. Reactive oxygen species in apoptosis induced by cisplatin: review of physiopathological mechanisms in animal models. *Eur Arch Oto-Rhino-Laryngology* 2012;**269**:2455−9.
173. Jiang X, Wang X. Cytochrome *c*-mediated apoptosis. *Annu Rev Biochem* 2004;**73**:87−106.
174. Galluzzi L, Senovilla L, Vitale I, Michels J, Martins I, Kepp O, et al. Molecular mechanisms of cisplatin resistance. *Oncogene* 2012;**31**: 1869−83.
175. Holzer AK, Howell SB. The internalization and degradation of human copper transporter 1 following cisplatin exposure. *Cancer Res* 2006;**66**:10944−52.
176. Lee J, Petris MJ, Thiele DJ. Characterization of mouse embryonic cells deficient in the Ctr1 high affinity copper transporter. *J Biol Chem* 2002;**277**:40253−9.
177. Ren H, Wang Z, Chen Y, Liu Y, Zhang S, Zhang T, et al. SMYD2-OE promotes oxaliplatin resistance in colon cancer through MDR1/P-glycoprotein *via* MEK/ERK/AP1 pathway. *OncoTargets Ther* 2019; **12**:2585−94.

178. Samimi G, Katano K, Holzer AK, Safaei R, Howell SB. Modulation of the cellular pharmacology of cisplatin and its analogs by the copper exporters ATP7A and ATP7B. *Mol Pharmacol* 2004;**66**: 25−32.
179. Kalayda GV, Wagner CH, Buß I, Reedijk J, Jaehde U. Altered localisation of the copper efflux transporters ATP7A and ATP7B associated with cisplatin resistance in human ovarian carcinoma cells. *BMC Cancer* 2008;**8**:175.
180. Kuo MT, Chen HHW. Role of glutathione in the regulation of cisplatin resistance in cancer chemotherapy. *Met Based Drugs* 2010; **2010**:430939.
181. Lan D, Wang L, He R, Ma J, Bin Y, Chi X, et al. Exogenous glutathione contributes to cisplatin resistance in lung cancer A549 cells. *Am J Transl Res* 2018;**10**:1295−309.
182. Gillet LCJ, Schärer OD. Molecular mechanisms of mammalian global genome nucleotide excision repair. *Chem Rev* 2006;**106**: 253−76.
183. Caiola E, Salles D, Frapolli R, Lupi M, Rotella G, Ronchi A, et al. Base excision repair-mediated resistance to cisplatin in KRAS(G12C) mutant NSCLC cells. *Oncotarget* 2015;**6**:30072−87.
184. Nehmé A, Baskaran R, Aebi S, Nebel DFS, Cenni B, Wang JYJ, et al. Differential induction of c-Jun NH_2-terminal kinase and c-Abl kinase in DNA mismatch repair-proficient and -deficient cells exposed to cisplatin. *Cancer Res* 1997;**57**:3253−7.
185. Lin X, Howell SB. DNA mismatch repair and p53 function are major determinants of the rate of development of cisplatin resistance. *Mol Cancer Ther* 2006;**5**:1239−47.
186. Vaisman A, Varchenko M, Umar A, Kunkel TA, Risinger JI, Barrett JC, et al. The role of hMLH1, hMSH3, and hMSH6 defects in cisplatin and oxaliplatin resistance: correlation with replicative bypass of platinum−DNA adducts. *Cancer Res* 1998;**58**:3579−85.
187. Muller PAJ, Vousden KH. P53 mutations in cancer. *Nat Cell Biol* 2013;**15**:2−8.
188. Vazquez A, Bond EE, Levine AJ, Bond GL. The genetics of the p53 pathway, apoptosis and cancer therapy. *Nat Rev Drug Discov* 2008;**7**: 979−87.
189. Hientz K, Mohr A, Bhakta-Guha D, Efferth T. The role of p53 in cancer drug resistance and targeted chemotherapy. *Oncotarget* 2017; **8**:8921−46.
190. Mir R, Tortosa A, Martinez-Soler F, Vidal A, Condom E, Pérez-Perarnau A, et al. Mdm2 antagonists induce apoptosis and synergize with cisplatin overcoming chemoresistance in TP53 wild-type ovarian cancer cells. *Int J Cancer* 2013;**132**:1525−36.
191. Ogawara Y, Kishishita S, Obata T, Isazawa Y, Suzuki T, Tanaka K, et al. Akt enhances Mdm2-mediated ubiquitination and degradation of p53. *J Biol Chem* 2002;**277**:21843−50.
192. Kanwar JR, Kamalapuram SK, Kanwar RK. Targeting survivin in cancer: the cell-signalling perspective. *Drug Discov Today* 2011;**16**: 485−94.
193. Xing H, Weng D, Chen G, Tao W, Zhu T, Yang X, et al. Activation of fibronectin/PI-3K/Akt2 leads to chemoresistance to docetaxel by regulating survivin protein expression in ovarian and breast cancer cells. *Cancer Lett* 2008;**261**:108−19.
194. Cho HJ, Kim JK, Kim KD, Yoon HK, Cho MY, Park YP, et al. Upregulation of Bcl-2 is associated with cisplatin-resistance *via* inhibition of Bax translocation in human bladder cancer cells. *Cancer Lett* 2006;**237**:56−66.
195. Guo J, Chen S, Zhang Y, Liu J, Jiang L, Hu L, et al. Cholesterol metabolism: physiological regulation and diseases. *MedComm* 2024; **5**:e476.
196. Wang Y, Cai L, Li H, Chen H, Yang T, Tan Y, et al. Overcoming cancer resistance to platinum drugs by inhibiting cholesterol metabolism. *Angew Chem Int Ed Engl* 2023;**62**:e202309043.
197. Snaebjornsson MT, Janaki-Raman S, Schulze A. Greasing the wheels of the cancer machine: the role of lipid metabolism in cancer. *Cell Metab* 2020;**31**:62−76.
198. Yan A, Jia Z, Qiao C, Wang M, Ding X. Cholesterol metabolism in drug-resistant cancer. *Int J Oncol* 2020;**57**:1103−15.
199. Sun Q, Liu D, Cui W, Cheng H, Huang L, Zhang R, et al. Cholesterol mediated ferroptosis suppression reveals essential roles of coenzyme Q and squalene. *Commun Biol* 2023;**6**:1108.
200. de Dios C, Abadin X, Roca-Agujetas V, Jimenez-Martinez M, Morales A, Trullas R, et al. Inflammasome activation under high cholesterol load triggers a protective microglial phenotype while promoting neuronal pyroptosis. *Transl Neurodegener* 2023;**12**:10.
201. Qiu Y, Shi YN, Zhu N, Zhang S, Zhang CJ, Gu J, et al. A lipid perspective on regulated pyroptosis. *Int J Biol Sci* 2023;**19**:2333−48.
202. Guo X, Liang XJ, Liu JL, Li ZH, You Z, Zhao D, et al. Precise carrier-free Pt(IV)-nanobombs for apoptosis/ferroptosis synergistic tumor therapy: a new effective method to obtain good chemotherapy and low toxicity. *J Med Chem* 2025;**68**:387−404.
203. Hsu H, Chen M, Baskaran R, Lin Y, Day CH, Lin Y, et al. Oxaliplatin resistance in colorectal cancer cells is mediated *via* activation of ABCG2 to alleviate ER stress induced apoptosis. *J Cell Physiol* 2018;**233**:5458−67.
204. Hashemi M, Esbati N, Rashidi M, Gholami S, Raesi R, Bidoki SS, et al. Biological landscape and nanostructural view in development and reversal of oxaliplatin resistance in colorectal cancer. *Transl Oncol* 2024;**40**:101846.
205. Mandic A, Hansson J, Linder S, Shoshan MC. Cisplatin induces endoplasmic reticulum stress and nucleus-independent apoptotic signaling. *J Biol Chem* 2003;**278**:9100−6.
206. Tian J, Liu R, Qu Q. Role of endoplasmic reticulum stress on cisplatin resistance in ovarian carcinoma. *Oncol Lett* 2017;**13**: 1437−43.
207. Siwecka N, Rozpędek W, Pytel D, Wawrzynkiewicz A, Dziki A, Dziki Ł, et al. Dual role of endoplasmic reticulum stress-mediated unfolded protein response signaling pathway in carcinogenesis. *Int J Mol Sci* 2019;**20**:4354.
208. Tang Z, Du W, Xu F, Sun X, Chen W, Cui J, et al. Icariside II enhances cisplatin-induced apoptosis by promoting endoplasmic reticulum stress signalling in non-small cell lung cancer cells. *Int J Biol Sci* 2022;**18**:2060−74.
209. Sun F, Shen H, Liu Q, Chen Y, Guo W, Du W, et al. Powerful synergy of traditional Chinese medicine and aggregation-induced emission-active photosensitizer in photodynamic therapy. *ACS Nano* 2023;**17**: 18952−64.
210. Yuan X, Yu B, Wang Y, Jiang J, Liu L, Zhao H, et al. Involvement of endoplasmic reticulum stress in isoliquiritigenin-induced SKOV-3 cell apoptosis. *Recent Pat Anticancer Drug Discov* 2013;**8**:191−9.
211. Yang X, Qiu Y, Fang F, Cao Z, Fu H, Chen X, et al. Isoliquiritigenin-loaded platinum(IV) prodrug micelles induce sustained endoplasmic reticulum stress for promoting cisplatin chemosensitivity in ovarian cancer. *ACS Mater Lett* 2024;**6**:5275−84.
212. Goel S, DeCristo MJ, Watt AC, BrinJones H, Sceneay J, Li BB, et al. CDK4/6 inhibition triggers anti-tumour immunity. *Nature* 2017;**548**: 471−5.
213. Wei X, Yang M, Zou H, Shen S, Li Y, Chen L, et al. Poly(amino acid) nanoformulation of cyclin-dependent kinase 4 and 6 inhibitor for molecularly targeted immunotherapy in triple-negative breast cancer. *J Control Release* 2025;**380**:760−72.
214. Iyengar M, O'Hayer P, Cole A, Sebastian T, Yang K, Coffman L, et al. CDK4/6 inhibition as maintenance and combination therapy for high grade serous ovarian cancer. *Oncotarget* 2018;**9**:15658−72.
215. Zhu S, Li J, Sun H, Liang J, Qiu Z, Zhou X, et al. A biotin guided Pt^{IV} amphiphilic prodrug synergized with CDK4/6 inhibition for enhanced tumor targeted therapy. *Nanoscale* 2025;**17**:9907−13.
216. Braal CL, Jongbloed EM, Wilting SM, Mathijssen RHJ, Koolen SLW, Jager A. Inhibiting CDK4/6 in breast cancer with palbociclib, ribociclib, and abemaciclib: similarities and differences. *Drugs* 2021;**81**:317−31.
217. Maines MD. Heme oxygenase: function, multiplicity, regulatory mechanisms, and clinical applications. *FASEB J* 1988;**2**:2557−68.
218. Schumacher A, Zenclussen AC. Effects of heme oxygenase-1 on innate and adaptive immune responses promoting pregnancy success and allograft tolerance. *Front Pharmacol* 2015;**5**:288.

219. Mei J, Tian HX, Zhang XY, Chen YS, Wang LY, Zhang Z, et al. Heme oxygenase 1 (HO-1) is a drug target for reversing cisplatin resistance in non-small cell lung cancer. *J Adv Res* 2025;**80**: 1121−37.
220. Liu XM, Li Z, Wang XY, Ding BW, Wang JQ, Qiao X, et al. Self-assembled HO-1i-Pt(IV) nanomedicine targeting p38/MAPK and MDR pathways for cancer chemo-immunotherapy. *J Control Release* 2025;**379**:797−813.
221. de Visser KE, Joyce JA. The evolving tumor microenvironment: from cancer initiation to metastatic outgrowth. *Cancer Cell* 2023;**41**: 374−403.
222. Petrova V, Annicchiarico-Petruzzelli M, Melino G, Amelio I. The hypoxic tumour microenvironment. *Oncogenesis* 2018;**7**:10.
223. Bejarano L, Jordão MJC, Joyce JA. Therapeutic targeting of the tumor microenvironment. *Cancer Discov* 2021;**11**:933−59.
224. Anderson NM, Simon MC. The tumor microenvironment. *Curr Biol* 2020;**30**:R921−5.
225. Simón L, Sanhueza S, Gaete-Ramírez B, Varas-Godoy M, Quest AFG. Role of the pro-inflammatory tumor microenvironment in extracellular vesicle-mediated transfer of therapy resistance. *Front Oncol* 2022;**12**:897205.
226. Bristow RG, Hill RP. Hypoxia, DNA repair and genetic instability. *Nat Rev Cancer* 2008;**8**:180−92.
227. Chen Z, Han F, Du Y, Shi H, Zhou W. Hypoxic microenvironment in cancer: molecular mechanisms and therapeutic interventions. *Signal Transduct Target Ther* 2023;**8**:70.
228. Park K, Veena MS, Shin DS. Key players of the immunosuppressive tumor microenvironment and emerging therapeutic strategies. *Front Cell Dev Biol* 2022;**10**:830208.
229. Jiang R, Yang L, Liu X, Xu Y, Han L, Chen Y, et al. Genetically engineered macrophages reverse the immunosuppressive tumor microenvironment and improve immunotherapeutic efficacy in TNBC. *Mol Ther* 2025;**33**:3339−59.
230. Rohwer N, Zasada C, Kempa S, Cramer T. The growing complexity of HIF-1α's role in tumorigenesis: DNA repair and beyond. *Oncogene* 2013;**32**:3569−76.
231. Yong L, Tang S, Yu H, Zhang H, Zhang Y, Wan Y, et al. The role of hypoxia-inducible factor-1 alpha in multidrug-resistant breast cancer. *Front Oncol* 2022;**12**:964934.
232. Devarajan N, Manjunathan R, Ganesan SK. Tumor hypoxia: the major culprit behind cisplatin resistance in cancer patients. *Crit Rev Oncol Hematol* 2021;**162**:103327.
233. Sun K, Wei X, Han S, Sun Y, Xiao H, Wei D. Biotin receptor-targeting Pt^{IV} oxygen carrying prodrug amphiphile for alleviating tumor hypoxia induced immune chemotherapy suppression. *ACS Nano* 2025;**19**:13300−13.
234. Fan L, Zheng N, Peng F, Zhao Z, Fan D, Cai S, et al. Nitric oxide affects cisplatin cytotoxicity oppositely in A2780 and A2780-CDDP cells *via* the connexin32/gap junction. *Cancer Sci* 2020;**111**: 2779−88.
235. Karthika C, Sureshkumar R, Zehravi M, Akter R, Ali F, Ramproshad S, et al. Multidrug resistance of cancer cells and the vital role of P-glycoprotein. *Life* 2022;**12**:897.
236. Wink DA, Cook JA, Christodoulou D, Krishna MC, Pacelli R, Kim S, et al. Nitric oxide and some nitric oxide donor compounds enhance the cytotoxicity of cisplatin. *Nitric Oxide* 1997;**1**:88−94.
237. Turchi JJ. Nitric oxide and cisplatin resistance: NO easy answers. *Proc Natl Acad Sci USA* 2006;**103**:4337−8.
238. Dou Y, Zhao F, Li X, Guo Y. Monitoring nitric oxide-induced hypoxic tumor radiosensitization by radiation-activated nanoagents under BOLD/DWI imaging. *ACS Biomater Sci Eng* 2021;**7**: 5242−54.
239. He S, Zheng L, Qi C. Myeloid-derived suppressor cells (MDSCs) in the tumor microenvironment and their targeting in cancer therapy. *Mol Cancer* 2025;**24**:5.
240. Ni Y, Zhou X, Yang J, Shi H, Li H, Zhao X, et al. The role of tumor−stroma interactions in drug resistance within tumor microenvironment. *Front Cell Dev Biol* 2021;**9**:637675.
241. Sui H, Dongye S, Liu X, Xu X, Wang L, Jin CQ, et al. Immunotherapy of targeting MDSCs in tumor microenvironment. *Front Immunol* 2022;**13**:990463.
242. Li K, Shi H, Zhang B, Ou X, Ma Q, Chen Y, et al. Myeloid-derived suppressor cells as immunosuppressive regulators and therapeutic targets in cancer. *Signal Transduct Target Ther* 2021;**6**:362.
243. Rego EM, He LZ, Warrell RP, Wang ZG, Pandolfi PP. Retinoic acid (RA) and As_2O_3 treatment in transgenic models of acute promyelocytic leukemia (APL) unravel the distinct nature of the leukemogenic process induced by the PML-RARα and PLZF-RARα oncoproteins. *Proc Natl Acad Sci USA* 2000;**97**:10173−8.
244. Wang B, Zhou J, Li R, Tang D, Cao Z, Xu C, et al. Activating $CD8^+$ T cells by Pt(IV) prodrug-based nanomedicine and aPD-L1 antibody for enhanced cancer immunotherapy. *Adv Mater* 2024;**36**:2311640.
245. Bai X, Shao J, Duan T, Liu X, Wang M, Li X, et al. Exo-miR-1290-induced by COX-2 overexpression promotes cancer-associated fibroblasts activation and tumor progression by CUL3−Nrf2 pathway in lung adenocarcinoma. *Cell Commun Signal* 2023;**21**:242.
246. Suarez-Carmona M, Lesage J, Cataldo D, Gilles C. EMT and inflammation: inseparable actors of cancer progression. *Mol Oncol* 2017;**11**:805−23.
247. Singh A, Settleman J. EMT, cancer stem cells and drug resistance: an emerging axis of evil in the war on cancer. *Oncogene* 2010;**29**: 4741−51.
248. Wang H, Wang Z, Li Y, Lu T, Hu G. Silencing snail reverses epithelial−mesenchymal transition and increases radiosensitivity in hypopharyngeal carcinoma. *OncoTargets Ther* 2020;**13**:497−511.
249. Zhang M, Chen Y, Feng S, He Y, Liu Z, Zhang N, et al. Transferrin-modified carprofen platinum(IV) nanoparticles as antimetastasis agents with tumor targeting, inflammation inhibition, epithelial−mesenchymal transition suppression, and immune activation properties. *J Med Chem* 2024;**67**:16416−34.
250. Liberti MV, Locasale JW. The warburg effect: how does it benefit cancer cells?. *Trends Biochem Sci* 2016;**41**:211−8.
251. Pelicano H, Martin DS, Xu RH, Huang P. Glycolysis inhibition for anticancer treatment. *Oncogene* 2006;**25**:4633−46.
252. Zhang M, Xu J, Yang Z, Ding L, Han H, Ma M, et al. Glycolysis-inhibiting tumor cell-derived microparticles to enhance immunogenic cell death for synergistic cancer immunotherapy. *Biomaterials* 2026; **328**:123832.
253. Galluzzi L, Guilbaud E, Schmidt D, Kroemer G, Marincola FM. Targeting immunogenic cell stress and death for cancer therapy. *Nat Rev Drug Discov* 2024;**23**:445−60.
254. Ahmed A, Tait SWG. Targeting immunogenic cell death in cancer. *Mol Oncol* 2020;**14**:2994−3006.
255. Zitvogel L, Kepp O, Kroemer G. Immune parameters affecting the efficacy of chemotherapeutic regimens. *Nat Rev Clin Oncol* 2011;**8**: 151−60.
256. Galluzzi L, Senovilla L, Zitvogel L, Kroemer G. The secret ally: immunostimulation by anticancer drugs. *Nat Rev Drug Discov* 2012; **11**:215−33.
257. Amiri M, Molavi O, Sabetkam S, Jafari S, Montazersaheb S. Stimulators of immunogenic cell death for cancer therapy: focusing on natural compounds. *Cancer Cell Int* 2023;**23**:200.
258. Yadollahvandmiandoab R, Jalalizadeh M, Buosi K, Garcia-Perdomo HA, Reis LO. Immunogenic cell death role in urothelial cancer therapy. *Curr Oncol* 2022;**29**:6700−13.
259. Krysko DV, Garg AD, Kaczmarek A, Krysko O, Agostinis P, Vandenabeele P. Immunogenic cell death and DAMPs in cancer therapy. *Nat Rev Cancer* 2012;**12**:860−75.
260. Wang Q, Ju X, Wang J, Fan Y, Ren M, Zhang H. Immunogenic cell death in anticancer chemotherapy and its impact on clinical studies. *Cancer Lett* 2018;**438**:17−23.
261. He X, Xu C. Immune checkpoint signaling and cancer immunotherapy. *Cell Res* 2020;**30**:660−9.
262. Azimnasab-sorkhabi P, Soltani-asl M, Kfoury Junior JR. Cytotoxic T-lymphocyte-associated protein 4 (CTLA-4) as an undetermined tool in tumor cells. *Hum Cell* 2023;**36**:1225−32.

263. Kong X, Zhang J, Chen S, Wang X, Xi Q, Shen H, et al. Immune checkpoint inhibitors: breakthroughs in cancer treatment. *Cancer Biol Med* 2024;**21**:451−72.
264. Kim TK, Vandsemb EN, Herbst RS, Chen L. Adaptive immune resistance at the tumour site: mechanisms and therapeutic opportunities. *Nat Rev Drug Discov* 2022;**21**:529−40.
265. Patsoukis N, Wang Q, Strauss L, Boussiotis VA. Revisiting the PD-1 pathway. *Sci Adv* 2020;**6**:eabd2712.
266. Nakanishi J, Wada Y, Matsumoto K, Azuma M, Kikuchi K, Ueda S. Overexpression of B7-H1 (PD-L1) significantly associates with tumor grade and postoperative prognosis in human urothelial cancers. *Cancer Immunol Immunother* 2007;**56**:1173−82.
267. Thibaudin M, Fumet JD, Chibaudel B, Bennouna J, Borg C, Martin-Babau J, et al. First-line durvalumab and tremelimumab with chemotherapy in RAS-mutated metastatic colorectal cancer: a phase 1b/2 trial. *Nat Med* 2023;**29**:2087−98.
268. Park SJ, Ye W, Xiao R, Silvin C, Padget M, Hodge JW, et al. Cisplatin and oxaliplatin induce similar immunogenic changes in preclinical models of head and neck cancer. *Oral Oncol* 2019;**95**: 127−35.
269. Guo J, Yu Z, Das M, Huang L. Nano codelivery of oxaliplatin and folinic acid achieves synergistic chemo-immunotherapy with 5-fluorouracil for colorectal cancer and liver metastasis. *ACS Nano* 2020;**14**:5075−89.
270. Liu J, Li Z, Zhao D, Feng X, Wang C, Li D, et al. Immunogenic cell death-inducing chemotherapeutic nanoformulations potentiate combination chemoimmunotherapy. *Mater Des* 2021;**202**:109465.
271. Kroemer G, Galassi C, Zitvogel L, Galluzzi L. Immunogenic cell stress and death. *Nat Immunol* 2022;**23**:487−500.
272. Liu P, Chen J, Zhao L, Hollebecque A, Kepp O, Zitvogel L, et al. PD-1 blockade synergizes with oxaliplatin-based, but not cisplatin-based, chemotherapy of gastric cancer. *Oncoimmunology* 2022;**11**:2093518.
273. Voorwerk L, Slagter M, Horlings HM, Sikorska K, van de Vijver KK, de Maaker M, et al. Immune induction strategies in metastatic triple-negative breast cancer to enhance the sensitivity to PD-1 blockade: the TONIC trial. *Nat Med* 2019;**25**:920−8.
274. Zeng P-H, Yin W-J. The cGAS/STING signaling pathway: a crosstalk of infection, senescence and tumors. *Cell Cycle* 2023;**22**:38−56.
275. Cao L, Tian H, Fang M, Xu Z, Tang D, Chen J, et al. Activating cGAS−STING pathway with ROS-responsive nanoparticles delivering a hybrid prodrug for enhanced chemo-immunotherapy. *Biomaterials* 2022;**290**:121856.
276. Xiang D, Han X, Li J, Zhang J, Xiao H, Li T, et al. Combination of IDO inhibitors and platinum(IV) prodrugs reverses low immune responses to enhance cancer chemotherapy and immunotherapy for osteosarcoma. *Mater Today Bio* 2023;**20**:100675.
277. Wang C, Guan Y, Lv M, Zhang R, Guo Z, Wei X, et al. Manganese increases the sensitivity of the cGAS−STING pathway for double-stranded DNA and is required for the host defense against DNA viruses. *Immunity* 2018;**48**:675−87.e7.
278. Lv M, Chen M, Zhang R, Zhang W, Wang C, Zhang Y, et al. Manganese is critical for antitumor immune responses *via* cGAS−STING and improves the efficacy of clinical immunotherapy. *Cell Res* 2020;**30**:966−79.
279. Ming Q, Liu J, Lv Z, Wang T, Fan R, Zhang Y, et al. Manganese boosts natural killer cell function *via* cGAS−STING mediated UTX expression. *MedComm* 2024;**5**:e683.
280. Zhang X, Tang D, Xiao H, Li B, Shang K, Zhao D. Activating the cGAS−STING pathway by manganese-based nanoparticles combined with platinum-based nanoparticles for enhanced ovarian cancer immunotherapy. *ACS Nano* 2025;**19**:4346−65.
281. Do K, Doroshow JH, Kummar S. Wee1 kinase as a target for cancer therapy. *Cell Cycle* 2013;**12**:3348−53.
282. Matheson CJ, Backos DS, Reigan P. Targeting WEE1 kinase in cancer. *Trends Pharmacol Sci* 2016;**37**:872−81.
283. Wang W, Yang F, Zhang L, Wang M, Yin L, Dong X, et al. Targeting DNA damage and repair machinery *via* delivering WEE1 inhibitor and platinum (IV) prodrugs to stimulate STING pathway for maximizing chemo-immunotherapy in bladder cancer. *Adv Mater* 2024;**36**:2308762.
284. Chen C, Liu J, Lin X, Xiang A, Ye Q, Guo J, et al. Crosstalk between cancer-associated fibroblasts and regulated cell death in tumors: insights into apoptosis, autophagy, ferroptosis, and pyroptosis. *Cell Death Discov* 2024;**10**:189.
285. Yu P, Zhang X, Liu N, Tang L, Peng C, Chen X. Pyroptosis: mechanisms and diseases. *Signal Transduct Target Ther* 2021;**6**:128.
286. Zheng Y, Peng K, Cao Q, Mao Z. Metal complexes stimulating immunogenic pyroptosis as burgeoning antitumor strategy. *Angew Chem Int Ed Engl* 2025;**64**:e202507186.
287. Romero D. Dasatinib regulates immune cell function. *Nat Rev Clin Oncol* 2018;**15**:200.
288. Zhu SW, Ye M, Ma X, Wu ZZ, Wan SC, Yang SC, et al. pH-responsive nanoprodrugs combining a Src inhibitor and chemotherapy to potentiate antitumor immunity *via* pyroptosis in head and neck cancer. *Acta Biomater* 2022;**154**:497−509.
289. Zhu Y, Wang X, Feng L, Zhao R, Yu C, Liu Y, et al. Intermetallics triggering pyroptosis and disulfidptosis in cancer cells promote antitumor immunity. *Nat Commun* 2024;**15**:8696.
290. Yu B, Wang Y, Bing T, Tang Y, Huang J, Xiao H, et al. Platinum prodrug nanoparticles with COX-2 inhibition amplify pyroptosis for enhanced chemotherapy and immune activation of pancreatic cancer. *Adv Mater* 2024;**36**:2310456.
291. Ma T, Du J, Zhang Y, Wang Y, Wang B, Zhang T. GPX4-independent ferroptosis—a new strategy in disease's therapy. *Cell Death Discov* 2022;**8**:434.
292. Ursini F, Maiorino M. Lipid peroxidation and ferroptosis: the role of GSH and GPx4. *Free Radic Biol Med* 2020;**152**:175−85.
293. Pope LE, Dixon SJ. Regulation of ferroptosis by lipid metabolism. *Trends Cell Biol* 2023;**33**:1077−87.
294. Wiernicki B, Maschalidi S, Pinney J, Adjemian S, Vanden Berghe T, Ravichandran KS, et al. Cancer cells dying from ferroptosis impede dendritic cell-mediated anti-tumor immunity. *Nat Commun* 2022;**13**: 3676.
295. Stockwell BR, Friedmann Angeli JP, Bayir H, Bush AI, Conrad M, Dixon SJ, et al. Ferroptosis: a regulated cell death nexus linking metabolism, redox biology, and disease. *Cell* 2017;**171**:273−85.
296. Li J, Wang Q, Xia G, Adilijiang N, Li Y, Hou Z, et al. Recent advances in targeted drug delivery strategy for enhancing oncotherapy. *Pharmaceutics* 2023;**15**:2233.
297. Veselov VV, Nosyrev AE, Jicsinszky L, Alyautdin RN, Cravotto G. Targeted delivery methods for anticancer drugs. *Cancers (Basel)* 2022;**14**:622.
298. Hu Y, Song J, Feng A, Li J, Li M, Shi Y, et al. Recent advances in nanotechnology-based targeted delivery systems of active constituents in natural medicines for cancer treatment. *Molecules* 2023;**28**: 7767.
299. Xia D, Qian Q, Wang S, Dong X, Liu Y. Alendronate functionalized bone-targeting pomolic acid liposomes restore bone homeostasis for osteoporosis treatment. *Int J Nanomed* 2024;**19**:7983−96.
300. Cummings SR, Santora AC, Black DM, Russell RGG. History of alendronate. *Bone* 2020;**137**:115411.
301. Shen M, Wang Y, Bing T, Tang Y, Liu X, Yu Y. Alendronate triggered dual-cascade targeting prodrug nanoparticles for enhanced tumor penetration and STING activation of osteosarcoma. *Adv Funct Mater* 2023;**33**:2307013.
302. Park H, Yu S, Koo T. Gene editing in cancer therapy: overcoming drug resistance and enhancing precision medicine. *Cancer Gene Ther* 2025;**32**:1293−302.
303. Ran FA, Hsu PD, Wright J, Agarwala V, Scott DA, Zhang F. Genome engineering using the CRISPR-Cas9 system. *Nat Protoc* 2013;**8**: 2281−308.
304. Ma Y, Liao J, Cheng H, Yang Q, Yang H. Advanced gene therapy system for the treatment of solid tumour: a review. *Mater Today Bio* 2024;**27**:101138.
305. Yamaguchi H, Hung MC. Regulation and role of EZH2 in cancer. *Cancer Res Treat* 2014;**46**:209−22.

306. Zhang Q, Kuang G, He S, Liu S, Lu H, Li X, et al. Chain-shattering Pt(IV)-backboned polymeric nanoplatform for efficient CRISPR/Cas9 gene editing to enhance synergistic cancer therapy. *Nano Res* 2021;**14**:601−10.
307. Moazzam M, Zhang M, Hussain A, Yu X, Huang J, Huang Y. The landscape of nanoparticle-based siRNA delivery and therapeutic development. *Mol Ther* 2024;**32**:284−312.
308. Tian Z, Liang G, Cui K, Liang Y, Wang Q, Lv S, et al. Insight into the prospects for RNAi therapy of cancer. *Front Pharmacol* 2021;**12**: 644718.
309. Zhang Q, Kuang G, He S, Lu H, Cheng Y, Zhou D, et al. Photo-activatable prodrug-backboned polymeric nanoparticles for efficient light-controlled gene delivery and synergistic treatment of platinum-resistant ovarian cancer. *Nano Lett* 2020;**20**:3039−49.
310. Chen Y, Chen CY, Huang H, Luo Z, Mu Y, Li S, et al. Knocking down of Xkr8 enhances chemotherapy efficacy through modulating tumor immune microenvironment. *J Control Release* 2024;**370**: 479−89.
311. Wei D, Fan J, Yan J, Liu C, Cao J, Xu C, et al. Nuclear-targeting lipid Pt^{IV} prodrug amphiphile cooperates with siRNA for enhanced cancer immunochemotherapy by amplifying Pt−DNA adducts and reducing phosphatidylserine exposure. *J Am Chem Soc* 2024;**146**:1185−95.
312. Wei D, Yan J, Cao Z, Han S, Sun Y. Nucleus-targeting oxaplatin(IV) prodrug amphiphile for enhanced chemotherapy and immunotherapy. *J Control Release* 2024;**373**:216−23.
313. Yang Y, Mai Z, Zhang Y, Yu Z, Li W, Zhang Y, et al. A cascade targeted and mitochondrion-dysfunctional nanomedicine capable of overcoming drug resistance in hepatocellular carcinoma. *ACS Nano* 2023;**17**:1275−86.
314. Liu Y, Wang D, Liu H, Liu L, Li S, Zhou Z, et al. A clinically translatable ternary platinum(IV) prodrug for synergistically reversing drug resistance. *J Med Chem* 2023;**66**:4045−58.
315. Ka H, Park HJ, Jung HJ, Choi JW, Cho KS, Ha J, et al. Cinnamaldehyde induces apoptosis by ROS-mediated mitochondrial permeability transition in human promyelocytic leukemia HL-60 cells. *Cancer Lett* 2003;**196**:143−52.
316. Jia D, Park J, Jung K, Levine H, Kaipparettu B. Elucidating the metabolic plasticity of cancer: mitochondrial reprogramming and hybrid metabolic states. *Cells* 2018;**7**:21.
317. Du Y, Li Y, Li X, Jia C, Wang L, Wang Y, et al. Sequential enzyme activation of a "pro-staramine"-based nanomedicine to target tumor mitochondria. *Adv Funct Mater* 2020;**30**:1904697.
318. Lu H, Tong W, Jiang M, Liu H, Meng C, Wang K, et al. Mitochondria-targeted multifunctional nanoprodrugs by inhibiting metabolic reprogramming for combating cisplatin-resistant lung cancer. *ACS Nano* 2024;**18**:21156−70.
319. Yang J, Yang Z, Wang H, Chang Y, Xu J, Zhang X. A polymeric nanoparticle to co-deliver mitochondria-targeting peptides and Pt(IV) prodrug: toward high loading efficiency and combination efficacy. *Angew Chem Int Ed Engl* 2024;**63**:e202402291.
320. Han S, Al-Jamal KT. Combined facile synthesis, purification, and surface functionalization approach yields monodispersed gold nanorods for drug delivery applications. *Part Part Syst Charact* 2023; **40**:2300043.
321. Murugan C, Sharma V, Murugan RK, Malaimegu G, Sundaramurthy A. Two-dimensional cancer theranostic nanomaterials: synthesis, surface functionalization and applications in photothermal therapy. *J Control Release* 2019;**299**:1−20.
322. Yan R, Hu Y, Liu F, Wei S, Fang D, Shuhendler AJ, et al. Activatable NIR fluorescence/MRI bimodal probes for *in vivo* imaging by enzyme-mediated fluorogenic reaction and self-assembly. *J Am Chem Soc* 2019;**141**:10331−41.
323. Wen X, Zhang R, Hu Y, Wu L, Bai H, Song D, et al. Controlled sequential *in situ* self-assembly and disassembly of a fluorogenic cisplatin prodrug for cancer theranostics. *Nat Commun* 2023;**14**:800.
324. Yu Y, Wei D, Bing T, Wang Y, Liu C, Xiao H. A polyplatin with hands-holding near-infrared-II fluorophores and prodrugs at a precise ratio for tracking drug fate with realtime readout and treatment feedback. *Adv Mater* 2024;**36**:2402452.
325. Al Refaai KA, AlSawaftah NA, Abuwatfa W, Husseini GA. Drug release *via* ultrasound-activated nanocarriers for cancer treatment: a review. *Pharmaceutics* 2024;**16**:1383.
326. Pauling L, Coryell CD. The magnetic properties and structure of hemoglobin, oxyhemoglobin and carbonmonoxyhemoglobin. *Proc Natl Acad Sci U S A* 1936;**22**:210−6.
327. Shen M, Wang Y, Zhang L, Bing T, Li X, Zhu L, et al. Ultrasound-triggered cascade delivery *via* poly-oxaliplatin nanoparticles for immunotherapy. *Adv Funct Mater* 2025;**35**:2425565.
328. Wang J, Gong Q, Jiao L, Hao E. Research advances in BODIPY-assembled supramolecular photosensitizers for photodynamic therapy. *Coord Chem Rev* 2023;**496**:215367.
329. Zhang Y, Xu C, Yang X, Pu K. Photoactivatable protherapeutic nanomedicine for cancer. *Adv Mater* 2020;**32**:2002661.
330. Spector DV, Abramchuk DS, Bykusov VV, Zharova AO, Egorova ES, Voskresenskaya AS, et al. BODIPY: synthesis, modification, and applications in sensing and biomedicine. *Russ Chem Rev* 2024;**93**: RCR5136.
331. An Q, Xiang SR, Zou YQ. Recent progresses in combination cancer therapy using cyanine dye-based nanoparticles. *Pharm Sci Adv* 2024; **2**:100040.
332. Chu H, Cao T, Dai G, Liu B, Duan H, Kong C, et al. Recent advances in functionalized upconversion nanoparticles for light-activated tumor therapy. *RSC Adv* 2021;**11**:35472−88.
333. Overchuk M, Weersink RA, Wilson BC, Zheng G. Photodynamic and photothermal therapies: synergy opportunities for nanomedicine. *ACS Nano* 2023;**17**:7979−8003.
334. Shen J, Zhao L, Han G. Lanthanide-doped upconverting luminescent nanoparticle platforms for optical imaging-guided drug delivery and therapy. *Adv Drug Deliv Rev* 2013;**65**:744−55.
335. Tang D, Zhou H, Cui M, Liang G, Zhang H, Xiao H. NIR-II light accelerated prodrug reduction of Pt(IV)-incorporating pseudo semiconducting polymers for robust degradation and maximized photothermal/chemo-immunotherapy. *Adv Mater* 2023;**35**: 2300048.
336. Ding K, Wang L, Zhu J, He D, Huang Y, Zhang W, et al. Photo-enhanced chemotherapy performance in bladder cancer treatment *via* albumin coated AIE aggregates. *ACS Nano* 2022;**16**: 7535−46.
337. Wan S, Ye M, Yang Q, Zhang T, Zhang M, Ma X, et al. Diselenide-based dual-responsive prodrug as pyroptosis inducer potentiates cancer immunotherapy. *Adv Healthcare Mater* 2023;**12**:2202135.
338. Zhang Q, Lin J, Li J, Zhou Y, Bi Z, Yang H, et al. Mitochondrial-targeted multifunctional platinum-based nano "terminal-sensitive projectile" for enhanced cancer chemotherapy efficacy. *ACS Nano* 2025;**19**:8711−26.
339. Spector DV, Bykusov V, Zharova A, Kuzmichev I, Isaeva YA, Khaydukov EV, et al. Nanoformulation of the photoactive cisplatin prodrug for combined photothermal therapy and bioimaging. *ACS Appl Nano Mater* 2024;**7**:25603−18.
340. Yang K, Zhao S, Li B, Wang B, Lan M, Song X. Low temperature photothermal therapy: advances and perspectives. *Coord Chem Rev* 2022;**454**:214330.
341. Bykusov V, Kuzmichev I, Isaeva YA, Stepanov M, Akasov RA, Huang L, et al. Pt(IV)-BODIPY nanoparticles for photoinduced tumor ablation and NIR light-activated chemotherapy. *ACS Appl Nano Mater* 2026;**9**:1813−28.
342. Xiao X, Wang Y, Chen J, Qin P, Chen P, Zhou D, et al. Self-targeting platinum(IV) amphiphilic prodrug nano-assembly as radiosensitizer for synergistic and safe chemoradiotherapy of hepatocellular carcinoma. *Biomaterials* 2022;**289**:121793.
343. Wang Y, Wang L, Li T, Ouyang M, Xiong H, Zhou D. Bimetallic nanoparticles as cascade sensitizing amplifiers for low-dose and robust cancer radio-immunotherapy. *Acta Pharm Sin B* 2024;**14**: 1787−800.